Triaxial behaviour of ballast and the role of confining pressure under cyclic loading

Joanne Lackenby
University of Wollongong

TRIAXIAL BEHAVIOUR OF BALLAST AND THE ROLE OF CONFINING PRESSURE UNDER CYCLIC LOADING

A thesis submitted in fulfilment of the

requirements for the award of the degree

DOCTOR OF PHILOSOPHY

from

UNIVERSITY OF WOLLONGONG

by

JOANNE LACKENBY

BE Engineering (Environmental)

FACULTY OF ENGINEERING

2006

CERTIFICATION

I, Joanne Lackenby, declare that this thesis, submitted in fulfilment of the requirements for the award of Doctor of Philosophy, in the School of Civil, Mining and Environmental Engineering, University of Wollongong, is wholly my own work unless otherwise referenced or acknowledged. The document has not been submitted for qualifications at any other academic institution.

The following publications are related to the research work conducted in this study:

Indraratna, B., **Lackenby, J.**, and Christie, D., (2005). "Effect of Confining Pressure on the Degradation of Ballast under Cyclic Loading." *Géotechnique*, 55 (4), pp. 325–328.

Lackenby, J., Indraratna, B., McDowell, G., and Christie, D., (2006). "Triaxial Behaviour of Ballast and the Role of Confining Pressure under Cyclic Loading." Submitted to *Géotechnique* for review in September 2005.

Lackenby, J., and Premaratne, P., (2005). "Method of Noise Removal for the Calculation of Resilient Strain and Resilient Modulus." Chapter in "Mechanics of Ballasted Rail Tracks – A Geotechnical Prospective" by B. Indraratna and W. Salim, Taylor and Francis Group/ Balkema, The Netherlands.

Indraratna, B., Khabbaz, H., Salim, W., **Lackenby, J.**, and Christie, D., (2004). "Ballast Characteristics and the Effects of Geosynthetics on Rail Track

Deformation." *International Conference on Geosynthetics and Geoenvironmental Engineering*, *ICGGE,* Bombay, India, pp. 3-12.

Lackenby, J., and Indraratna, B. (2004). "The Effect of Confining Pressure on the Behaviour of Railway Ballast under Cyclic Loading." *Proceedings of the 6th Australia New Zealand Young Geotechnical Professionals Conference*, July, Gold Coast, Australia, pp. 115-120.

Joanne Lackenby

5 June, 2006

ABSTRACT

Traditional railway foundations or substructures, consisting of one or two granular layers overlying a subgrade or natural formation, have become increasingly overloaded in recent years due to the utilisation of faster and heavier trains. During this period, there has been little, if any, re-engineering of the substructure in Australia, resulting in maintenance cycles becoming more frequent and increasingly expensive. Finding economical and practical techniques for enhancing the stability and safety of the substructure, thereby ensuring a capacity for supporting further increases in load, is vital in securing the long-term viability of the railway industry.

The load bearing ballast is located directly below the sleepers and is responsible for limiting the stresses projected onto the weaker subgrade and preventing train-induced sleeper movement. Two significant ballast problems arising from increasing axle loads are differential settlement and degradation. It is thought that substructure enhancement can be attained and these problems largely curtailed through the manipulation of the level of effective confining pressure supporting the ballast layer.

To investigate this possibility, a series of large-scale, high-frequency, drained, cyclic triaxial tests were conducted to examine the deformation (permanent and resilient) and degradation response of railway ballast. It was identified that the level of lateral confining pressure should be considered as an important design parameter. Two of the major benefits arising from increased confinement are reduced lateral movement (spreading) and vertical settlement resulting in improved line and level, and superior track stiffness and associated enhancements in ride comfort for passengers. The major

drawback in the event of excessive confinement is unacceptable levels of particle breakage. The experimental results indicated, however, that insufficient confining pressure is as damaging in terms of particle breakdown as excessive pressure, and that minimal degradation will be achieved at some intermediate value. For maximum deviator stress magnitudes of 230, 500 and 750 kPa, 'optimum' breakage conditions were encountered within the confining pressure ranges 15 – 65, 25 – 95, and 50 – 140 kPa, respectively.

Practical methods of increasing the in-situ track confinement are suggested and evaluated in terms of ease of installation, effectiveness and cost. It is concluded that the more superior methods of achieving increased confining pressure are by reinforcing the ballast using geosynthetics, or by increasing the effective overburden pressure through increased shoulder and/or crib height or via the achievement of a higher initial ballast density (greater compaction).

ACKNOWLEDGMENTS

First and foremost, a big thank you to my supervisor Prof. Buddhima Indraratna for all his support, academic guidance, and enthusiasm towards my postgraduate studies at the University of Wollongong.

Grateful appreciation is also expressed to my co-supervisors, Dr. Hadi Khabbaz and Dr. Mohamed Shahin, for their assistance and constructive comments. I also wish to thank David Christie from the RailCRC for his technical input, and Dr. Prashan Premaratne of the Faculty of Informatics, University of Wollongong, for his help with the signal processing.

Without sponsorship from the RailCRC this research project would not have been possible. The financial support of the RailCRC, and the technical support and direction offered by the Theme 2 Project 6 steering committee is greatly appreciated.

Thanks to the technical staff at the University of Wollongong, Alan, Bob, Ian, Ian and Kenny, for keeping me sane in the laboratory and for letting me use their radio.

Thanks to my parents Margaret and Philip for all the free food donated to me when I didn't have time to go shopping, and for all their encouragement and moral support. Gratitude is also expressed to my friends and fellow students at UOW for keeping the study atmosphere enjoyable and pleasant.

Last but not least, a big thank you to my best friend and soul mate Melissa-Ann Dunn for all her encouragement and patience, for providing timely distractions and adventures in times of stress, and for actually volunteering to read this thesis.

TABLE OF CONTENTS

LIST OF FIGURES

LIST OF TABLES

LIST OF NOTATION

θ	bulk stress = $\sigma_1'+\sigma_2'+\sigma_3'$
ν	coefficient of lateral stress
ϕ	friction angle
ψ	ratio of cyclic deviator stress to peak static deviator stress
η	speed factor
δ	track condition descriptor
β	train loading state
α'	coefficient
β'	coefficient
γ'	coefficient
ϕ'	dynamic impact factor
$(\sigma_1'/\sigma_3')_p$	peak stress ratio
γ_0	coefficient
ε_1	axial strain after first loading cycle
γ_1	coefficient
σ_1'	major principal stress
$\sigma_1'-\sigma_3'$	deviator stress magnitude
σ_2'	intermediate effective stress
σ_3'	effective confining pressure
ε_a	axial strain
$\varepsilon_{a,rec}$	recoverable portion of axial strain
σ_d	magnitude of deviator stress
γ_b	specimen unit weight
$\psi_{failure}$	ψ ratio at failure during a stepwise cyclic test
ψ_{final}	ψ ratio at 20% axial strain during a stepwise cyclic test
ε_N	axial strain after a particular number of cycles
τ_{oct}	$= \sqrt{2}/3(\sigma_1'-\sigma_3')$ (axisymmetric conditions)
σ_{oct}	$= 1/3(\theta)$
Δq_{cyc}	difference between the maximum and minimum cyclic load
ε_r	radial strain

ΔS	change in total particle surface area
ε_s	shear strain
ε_v	volumetric strain
ΔW_k	difference between W_{ki} and W_{kf}
A	area between particle size distribution curves before and after loading
a	asperity diameter
A	material constant
a	regression coefficient
a′	settlement after one cycle
a_0	coefficient
B	material constant
b	regression coefficient
B	area between final particle size distribution and the arbitrary boundary of maximum breakage
b′	sleeper breadth
b_0	coefficient
BBI	ballast breakage index
B_g	breakage index
b_p	breakage potential
B_p	total breakage potential
b_{pl}	values of b_p after loading
b_{po}	values of b_p before loading
B_r	relative breakage
B_t	total breakage
C	regression coefficient
c′	coefficient
CSDZ	compressive stable degradation zone
C_u	coefficient of uniformity
D	particle diameter
D	regression coefficient
$d\varepsilon_a/dN$	rate of axial strain
d_1	diameter of largest particle retained on a particular sieve
d_2	diameter of smallest particle retained on a particular sieve

d_{95}	95% of the maximum sieve aperture d_{max}
DFT	discrete Fourier transform
d_h	horizontal distance between rail centres
DIF	dynamic impact factor
d_m	mean particle diameter
d_{max}	maximum sieve aperture
d_{min}	minimum sieve aperture
d_s	superelevation deficiency
DUDZ	dilatant unstable degradation zone
E	regression coefficient
e_0	initial void ratio
E_r	rail modulus
F	axial force
F	regression coefficient
g	distance between rail centres
G	gap grading
g	regression coefficient
G	regression coefficient
G_s	specific gravity
H	regression coefficient
h	regression coefficient
h	vertical distance from rail top to vehicle centre of mass
I_r	rail moment of inertia
k	regression coefficient
K_0	coefficient of earth pressure at rest
k_0	initial permeability
k_1	material constant
k_2	material constant
k_3	material constant
l	total sleeper length
L	effective sleeper length
M	moderate grading
m	regression coefficient
M_R	resilient modulus

n	ballast porosity
N	number of loading cycles
n	regression coefficient
n_1	regression coefficient
N_{int}	number of loading cycles per interval
ODZ	optimum degradation zone
P	static wheel load
p	regression constant
p′	mean effective stress
PSD	particle size distribution
Q	wheel load
$q_{max,cyc}/p'$	stress ratio
$q/p'_{failure}$	stress ratio at failure during a stepwise cyclic test
q/p'_{final}	stress ratio at 20% axial strain during a stepwise cyclic test
$q/p'_{peak,sta}$	peak stress ratio during a static test
$q_{max,cyc}$	maximum cyclic load
$q_{min,cyc}$	minimum cyclic load
$q_{peak,sta}$	static peak deviator stress
q_r	actual load transmitted to sleeper from static wheel
R	constant
R	ratio of cyclic deviator stress to static failure deviator stress
R^2	coefficient of determination
S	surface area
s	regression coefficient
SA	surface area
S_N	settlement after a particular number of cycles
S_w	specific surface area
t	probability of maximum allowable rail deflection not being exceeded
t	regression coefficient
t′	sleeper thickness
u	material constant
U	uniform grading
u′	track modulus

v	material constant
V	train speed
V′	volume
VU	very uniform grading
W_{kf}	percentage by weight retained on each sieve after loading
W_{ki}	percentage by weight retained on each sieve before loading
x	empirical coefficient
Y	coefficient
y_r	rail deflection

CHAPTER 1

INTRODUCTION

1.1 General Background

Australia has over 43000 km of broad, narrow, standard and dual gauge ballasted rail track (Figure 1.1, Commonwealth of Australia, 1999). The railway system plays a major role in hauling bulk commodities to ports, conveying passengers, and transporting freight along major corridors. In recent years, however, road transport has become more competitive in all areas of transportation. This is mainly due to improvements in road infrastructure and decreasing road transportation costs. These trends have increased the pressure on the railway industry to improve transportation efficiency by limiting maintenance and infrastructure expenses.

One area that has been identified by railway corporations as financially expensive is the maintenance of the track substructure (the ballast, subballast and subgrade layers). For instance, in New South Wales alone, millions of dollars are spent each year in quarrying the 800000 tonnes of coarse aggregate required to maintain the ballast profile (Mineral Resources, 2002). Over the 1992/3 financial year, 12 million dollars were spent on the purchase of ballast (Indraratna *et al*., 1997). Furthermore, considerable costs are accrued by the execution of track maintenance procedures (e.g. tamping, ballast cleaning). Track closures are not only financially expensive but also cause inconvenience and annoyance to passengers.

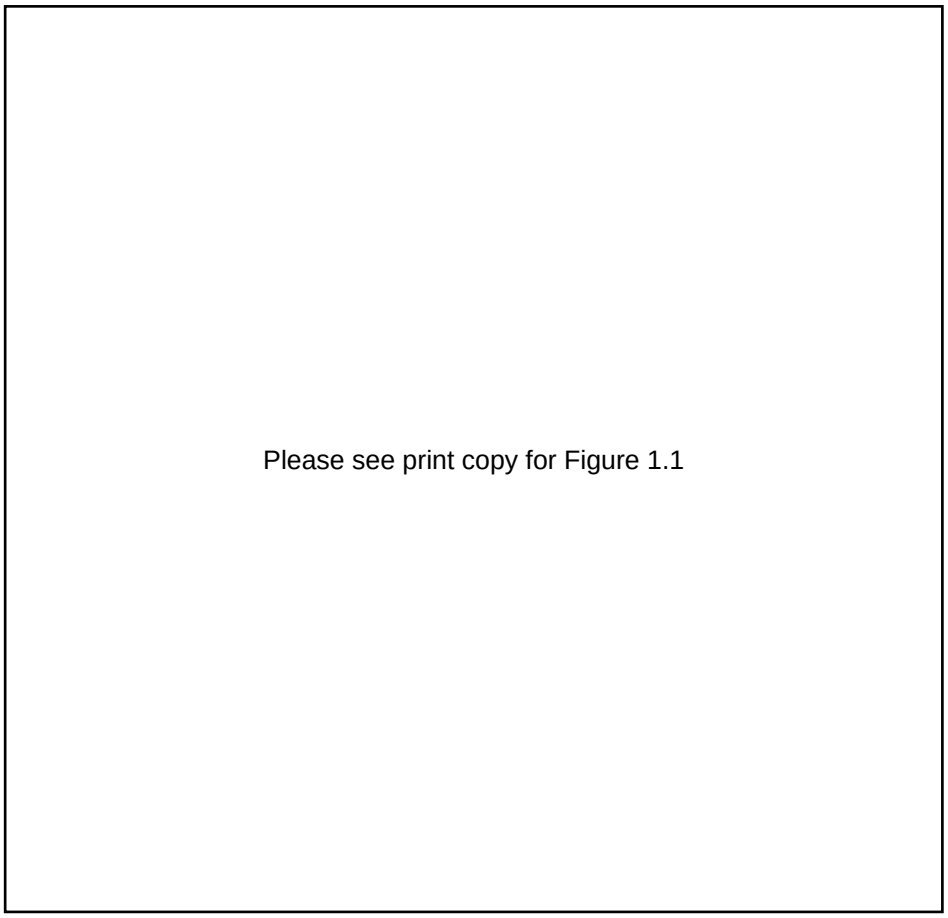

Figure 1.1 Australia's railway network (after Salim, 2004)

Track substructure maintenance costs are steadily increasing, and this is largely due to the utilisation of faster and heavier trains, coupled with a lack of substructure design alteration to counteract greater sleeper-ballast contact pressures. Increasing vertical cyclic loads in the absence of horizontal and vertical substructure strengthening provisions has resulted in decreasing maintenance cycles, increasing costs, and a reduction in rail track efficiency and reliability.

1.2 Statement of the Problem

Excessive settlement within the ballast, subballast and subgrade layers and associated track misalignment is a major source of the aforementioned increase in maintenance costs. It is anticipated that maintenance cycles can be lengthened (and costs reduced) if an improved understanding of the physical and mechanical characteristics of this region, in particular the ballast layer, is obtained. Ballast is typically comprised of relatively hard and strong, angular, gravel sized particles. Under the influence of cyclic train loading, ballast particles rearrange and attempt to attain a more stable configuration through the processes of vertical settlement, lateral spreading, and particle degradation. The ballast layer is most prone to settlement and transverse spreading for two reasons, a) it is loosened during maintenance (unlike the subballast and subgrade layers), and b) it is subjected to the highest stress ratios.

Vertical settlement is a major problem especially when it occurs non-uniformly or differentially along a short length of track (Gaskin and Raymond, 1976; Selig and Waters, 1994), ultimately culminating in elevated derailment risk, speed restrictions and poor ride quality. Lateral ballast spreading destabilises the track structure and decreases the magnitude of lateral resistance offered to trains. The scope and type of particle breakage depends to a large extent on the applied train axle load and the constituents of the parent rock. Even under low to moderate axle loads, breakage of sharp ballast corners can occur at interparticle contact points, resulting in a loss of particle angularity and significantly reduced track shear strength. Particle degradation can also increase the magnitude of track settlement and enhance ballast fouling prospects.

As indicated by Salim (2004), ballast degradation and associated track deformations are generally ignored in conventional rail track design. Parameters that are important in the design of alternate civil engineering structures, such as the degree of aggregate compaction (roadways), or the magnitude of pressure supporting the granular layers (retaining walls), also appear to have been given only modest attention. The cost of replacing ballast will continue to increase into the future unless railway foundations are re-engineered using innovative design concepts. Significant changes are required immediately to guard against excessive settlement and degradation. This study examines the deformation and degradation processes of ballast under cyclic loading with the aim of suggesting practical and pioneering techniques that could be utilised by railway corporations to enhance the performance of the track substructure. The possibility of modified in-situ confining pressure (increased ballast support) is considered in this thesis as a promising rail track design alteration.

1.3 Objectives and Scope of Research

The major objective of this thesis is to investigate the behavioural characteristics of railway ballast under repeated traffic loading at a cyclic frequency that simulates 'high-speed' train travel, namely 20 Hz. Most prior ballast studies have utilised frequencies significantly less than 10 Hz (and usually < 3 Hz). This study also aims to advance the current state of knowledge regarding the behaviour of coarse granular materials under drained, cyclic loading conditions, focusing on permanent deformation, stiffness response, and particle degradation analysis. Within the scope of this research, only one ballast aggregate type has been examined. The degradation analysis takes into account

breakage from mechanical processes only and excludes other influences such as the effects of weathering.

The specific objectives of this research study are summarised below:

(a) Experimental investigation of the effects of key parameters, namely confining pressure, deviator stress magnitude, and number of loading cycles, on fundamental ballast properties, including permanent deformation (axial and volumetric strain), resilient deformation (resilient modulus) and particle degradation.

(b) Development of empirical relationships linking confining pressure and deviatoric stress amplitude to the fundamental properties.

(c) Development of a particle degradation quantification method specific to railway ballast, considering currently available methods and ballast characteristics such as particle size distribution.

(d) Detection of 'optimum' in-situ ballast confining pressures through triaxial experiments.

(e) Identification of potential benefits and pitfalls associated with modifying the in-situ ballast confining pressure.

(f) Identification and recommendation of practical and cost effective methods that could suitably modify the level of in-situ ballast confining pressure.

1.4 Thesis Outline

This thesis is divided into 8 chapters including this Introduction. A summary of the remaining Chapters is given below.

Chapter 2 provides an overview of the current state of research regarding ballast behaviour under both static and cyclic loading. Emphasis is placed on the deformation (permanent and resilient) and degradation response of ballast and other granular materials under repeated loading conditions. The effect of confining pressure and induced lateral pressures on aggregate deformation is also examined in detail.

Chapter 3 describes the large-scale triaxial experiments conducted to evaluate the deformation and degradation behaviour of ballast under high-speed cyclic loading.

Presented in Chapter 4 are the permanent (axial and volumetric) and resilient (resilient modulus) strain results from the large-scale triaxial experiments. Included is a definition of specimen failure under constant amplitude loading, a comparison of static and cyclic triaxial behaviour, and an examination of the effect of specimen particle size distribution on ballast response. Empirical relationships are derived to associate the state of stress and number of cycles to axial strain and resilient modulus.

Chapter 5 provides the degradation results of the cyclic experiments, focussing on the effect of stress state on ballast breakdown. Also incorporated is an assessment of the differences observed between static and cyclic breakage behaviour, the influence of the number of loading cycles, the effect of aggregate grading, and other minor areas of

study such as the influence of coordination number, the particle sizes most vulnerable to breakage, and the impact of breakage type on track deformation behaviour.

Chapter 6 provides an account of the results obtained from stepwise (gradually increasing) loading experiments.

The implications associated with the experimental results from Chapters 4, 5 and 6 are expressed in Chapter 7, along with practical and cost effective techniques that could be employed to successfully enhance the performance of the substructure.

The conclusions of the study are presented in Chapter 8, together with recommendations for future research. A list of References and Appendices are located after Chapter 8.

CHAPTER 2

LITERATURE REVIEW

2.1 Introduction

Railway systems play a major role in hauling bulk commodities to ports, conveying passengers, and transporting freight along major corridors. In recent years, however, road transport has become more competitive, due in part to improvements in road infrastructure, but also the inconvenience and costs associated with train delays and routine track maintenance. Railway corporations have identified that maintaining the track substructure is particularly expensive, largely because of faster and heavier trains acting on a substructure configuration originally designed to support much lighter loads.

It is thought that substructure maintenance costs can be significantly reduced through an enhanced understanding of the physical and mechanical properties of the substructure region, in particular the ballast layer. This Chapter provides a current review of the permanent and resilient deformation response of railway ballast and other granular materials to diverse stress states.

2.2 Track Components – The Superstructure and Substructure

Traditional ballasted railway lines comprise a superstructure (rails, fastening system and sleepers) overlying a substructure (ballast, subballast and subgrade), as depicted in Figure 2.1. During train passage, wheel loads are transferred from the superstructure through the sleeper-ballast interface and into the substructure. The load (stress) imparted

onto each track component generally diminishes with decreasing proximity from the passing wheel. Although the superstructure is an integral part of the railway system, a detailed discussion of its roles and characteristics has been neglected in this Chapter. Instead, the focus is solely on the functions and characteristics of the ballast, capping (subballast), and subgrade (formation) layers.

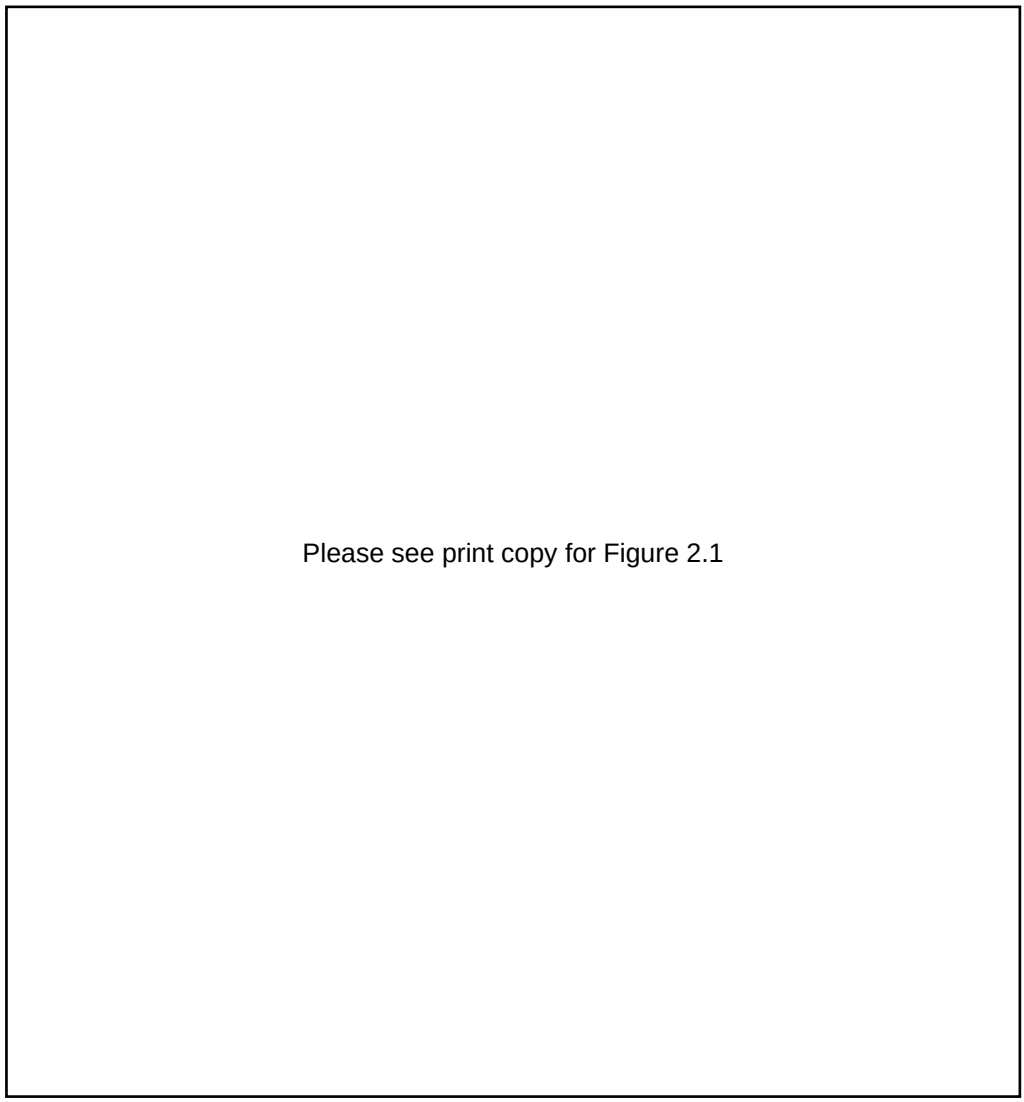

Figure 2.1 Superstructure and substructure components of a railway line, (a) lateral view, and (b) longitudinal view (after Selig and Waters, 1994)

2.2.1 The Ballast Layer

Ballast can be defined as a free draining coarse aggregate used as support for railway track (Standards Australia, 1996). It is composed of medium to coarse gravel sized aggregates with a small percentage of cobble sized particles (typically 20 – 60 mm). Ballast usually has igneous or well-cemented sedimentary origins. It is excavated in quarries by blasting and/or ripping, and then crushed and screened to produce fragments of appropriate size (Mineral Resources, 2002). Common ballast materials include dolomite, rheolite, gneiss, basalt, granite and quartzite, although many others are currently in use (Raymond, 1979). Traditionally, ballast has been considered high quality if comprised of crushed, angular, hard rock, has a uniform grading, is free from dirt and other contaminants, and is fracture and attrition resistant (Selig and Waters, 1994).

The desirable functions of railway ballast have been well documented (e.g. Hay, 1953; Doyle, 1980; Jeffs and Marich, 1987; Jeffs, 1989; Jeffs and Tew, 1991; Selig and Waters, 1994; Profillidis, 1995; Indraratna *et al*., 1998; Ionescu *et al*., 1998; Schmutz, 2000). In order to be successful, ballast must:

- transmit large sleeper-ballast contact pressures to the subgrade at significantly reduced levels,
- resist disturbing forces caused by wheel loads, and prevent excessive vertical, lateral, and longitudinal sleeper movement,
- provide adequate drainage and retard plant growth,
- assist with rail track maintenance procedures such as tamping and ballast cleaning, and

- provide the necessary dynamic resiliency, energy absorption, vibration attenuation, and noise absorption.

Figure 2.1 classifies ballast into four types depending on the function and in-track location. Crib ballast, located between the sleepers, is mainly responsible for providing longitudinal track stability against train braking and accelerating forces, thermal expansion and contraction, and rail wave action. Shoulder ballast is positioned at the ends of the sleepers and extends to the bottom of the ballast bed. Apart from providing limited confining pressure, the shoulder counteracts lateral wheel and rail buckling reaction forces. Top and bottom ballast (load bearing ballast) is usually about 300 mm deep and supports the sleeper vertically. According to Selig and Waters (1994), top ballast is compacted by tamping whereas the bottom ballast remains relatively undisturbed. Of particular importance to the long-term stability of railway track is the ability of the load bearing ballast to resist degradation and deformation caused by vertical dynamic wheel loads. Failure of the ballast layer to stabilise cyclic wheel loads, including impact loading induced by wheel flats and track irregularities such as dipped welds, can result in derailment and possible loss of human life.

At present, there is no world-wide standard governing the physical and durability characteristics of ballast. Instead, it is common for countries or individual railway organisations to develop specifications based on economic restrictions and the availability of aggregates. Table 2.1 summarises the recommended physical ballast criterion in Australia (Foun and Martin, 2002; Indraratna *et al*., 1997; Standards Australia, 1996), Canada (Gaskin and Raymond, 1976; Raymond, 1985) and the USA

(Gaskin and Raymond, 1976; Hay, 1953). Ballast particle sizes tend to be uniform in nature and Figure 2.2 shows typical distributions currently being used.

Table 2.1 Ballast specifications in Australia, Canada and the USA

Property	**Australia**	**Canada**	**USA**
	Value (%, unless otherwise stated)		
Crushing Value	< 25		
LAA*	< 25	< 20	< 40
MA**	< 5		
Abrasion Number	< 40		
Flakiness	< 30	< 25	
Misshapen Particle	< 30		
Sodium Sulphate Soundness	< 6	< 5	< 10
Magnesium Sulphate Soundness		< 10	
Soft and Friable Pieces		< 5	< 5
Fines (< No. 200 sieve size)		< 1	< 1
Clay Lumps		< 0.5	< 0.5
Unit Weight	> 1200 kg/m^3		> 1120 kg/m^3
Bulk Specific Gravity	> 2.5 (dimensionless)	> 2.6 (dimensionless)	
Freeze-thaw		< 3	
Sphericity		0.55 – 0.7 (dimensionless)	

*Los Angeles Abrasion, ** Mill Abrasion

2.2.2 The Subballast (Capping) Layer

A subballast layer (Figure 2.1) typically comprising of broadly graded sand-gravel mixtures, artificially stabilised soils, or geosynthetic membranes is often (but not always) positioned between the subgrade and ballast (Selig and Waters, 1994). The subballast layer is usually 150 mm thick (Profillidis, 1995; Selig and Waters, 1994) with

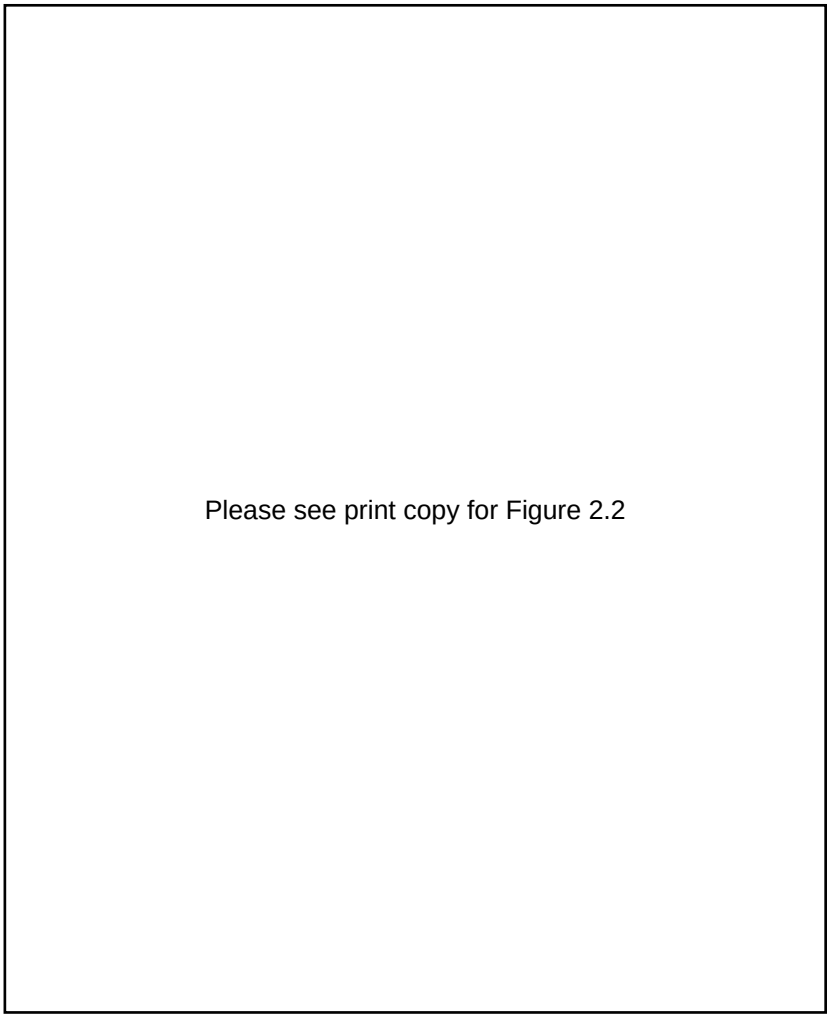

Figure 2.2 Ballast particle size distributions currently employed by railway organisations. (SRA – State Rail Authority of NSW (Australia), SNCF – Societe Nationale des Chemins de Fer (French railway enterprise), BR – British Rail, CFR – Compania Nationala de Cai Ferate (Romanian railway company), AREA – American Railway Engineering Association, CNR – Canadian National Railway, CP – Canadian Pacific).

depths in the USA as large as 300 mm (Raymond, 1978). The main roles of the subballast are to (Selig and Waters, 1994):

- minimise stresses on the subgrade by providing additional load distribution,

- provide a load bearing foundation beneath the ballast bed,
- increase overall track resiliency,
- prevent ballast particles penetrating the subgrade, and the subsequent formation of slurry, and
- assist in drainage by promoting water transfer away from the subgrade.

The permeability of the capping layer is an important consideration in track design. It must be appreciably smaller than the permeability of the ballast to ensure drainage via the shoulder, but sufficient to prevent water clogging and poor drainage in the subgrade. If additional granular track thickness is required due to large axle loads and/or poor local soil or environmental conditions, it is more common and economical to fix the ballast depth at a minimal value and increase the thickness of the capping layer as required (Shahu *et al*., 1999).

2.2.3 The Subgrade Layer

The subgrade (Figure 2.1) consists of naturally deposited soil, fill material, or a combination of the two. Its primary role is to provide a stable foundation that supplies resiliency to the track structure above. Subgrade characteristics substantially affect overall track stiffness (Selig and Waters, 1994), with stiffer subgrades reducing settlement and impact loading (Raymond, 1978), as well as promoting greater superstructure stability. Tracks possessing subgrades with low bearing capacity or poor drainage may require speed restrictions and/or load limitations (Zicha, 1989). In most cases, track problems associated with the subgrade (e.g. clay pumping) can be minimised or prevented if adequate drainage is provided.

2.3 Train Loading and Track Forces

2.3.1 Estimation of the Rail Seat Load

Due to a lack of theoretical knowledge regarding cyclic or dynamic loading transfer processes from train wheels into the substructure, empirical relationships based on static experimental and field measurements are often used to estimate sleeper-ballast contact pressures. Table 2.2 lists the variables that are known to influence ballast loading pressures. Traditional sleeper-ballast contact pressure calculation utilises a single axle load with the assumption that it acts over multiple sleepers due to rail stiffness (e.g. Figure 2.3). The actual load, q_r, transmitted from a static train wheel, P, to the rail seat can be calculated based on the simplified relationships shown in Table 2.3. In Australia, the static axle design load is 25 tonnes (Standards Australia, 1997a), translating to maximum rail seat loads ranging from 5 to 8.125 tonnes (49 to 80 kN).

Table 2.2 Variables that affect sleeper-ballast contact pressures (FIP, 1987; Jeffs and Tew, 1991; Standards Australia, 1997a)

Please see print copy for Table 2.2

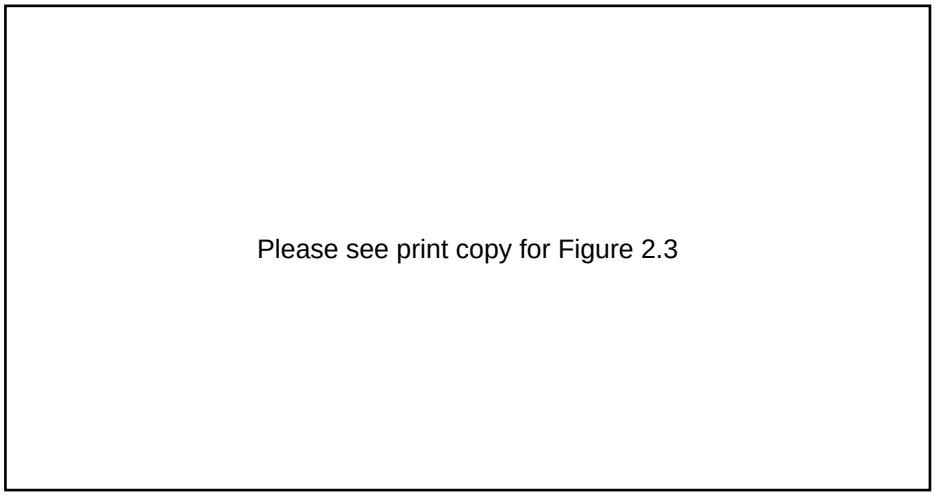

Figure 2.3 Typical in-track wheel load distribution (after Selig and Waters, 1994)

Table 2.3 Empirical relationships used to calculate the maximum rail seat load (adapted from Jeffs and Tew (1991) with additional data added)

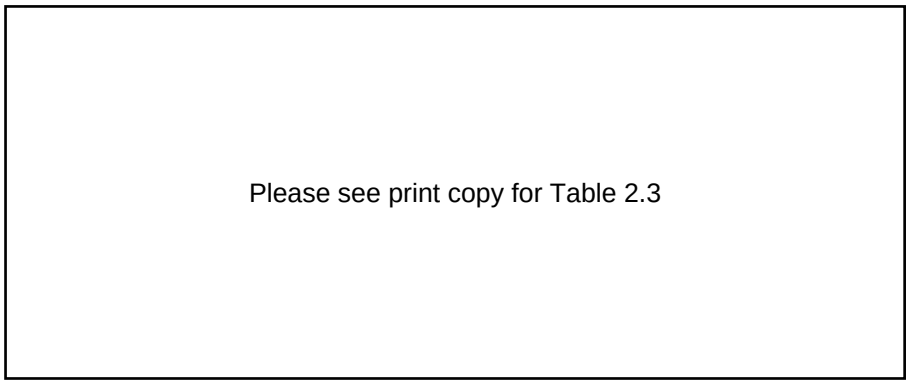

2.3.2 Dynamic Impact Factors

The rail seat load estimation method above fails to capture cyclic loading/unloading effects due to train movement. Standards Australia (1997a) states that the design load for sleepers must consider the following three factors:

a) the static axle load,

b) the effects of static loads travelling at speed, and

c) dynamic effects due to train, rail and track imperfections.

Sleepers are designed to withstand a load not less than 2.5 times the static design wheel load to prevent damage from impact and dynamic loading (Standards Australia, 1997a). In-track dynamic excitation results from wheel flats, rail joints, dipped welds, railhead corrugation, and bridge, grade crossing and transition effects. To account for these anomalies in relation to sleeper-ballast contact pressure, the rail seat load is multiplied by a dynamic impact factor ϕ'. While a significant number of these factors exist the versions supplied by ORE (1965) and Broadley *et al*. (1981) (Appendix A) are considered to be the most reliable because they are formulated and calibrated using actual field data. Impact factors typically range between 1.3 – 1.5 for good to average tracks but they can increase significantly in the event of extremely poor track and/or train conditions. Impact factors have been used by the railway industry for several decades, but analytical and numerical modelling has recently been suggested as a more realistic and accurate method for predicting train loading amplitudes on the substructure.

2.3.3 Effective Sleeper Contact Area

For new or freshly maintained tracks, load transmittance from sleeper to ballast occurs over an area located directly below the rail seat (Jeffs and Tew, 1991). With time or increasing traffic tonnage, the distribution of pressure becomes more uniform over the entire sleeper. Equations 2.1 (Clarke, 1957) and 2.2 (Schramm, 1961) are commonly used to calculate the effective sleeper length L (the length of sleeper carrying load). Equation 2.1 is applicable for timber sleepers and Equation 2.2 for timber, concrete, or steel sleepers. l is the total sleeper length, g is the distance between rail centres, and t' is the sleeper thickness. For standard lengths l (i.e. about 2500 – 2600 mm), Equation 2.1

can be simplified to $L = l/3$. The effective area of a sleeper can be computed by multiplying the effective length by the breadth b', and the sleeper-ballast contact pressure by dividing the dynamic load by the effective area.

$$L = (l - \mathrm{g})\left(1 - \frac{(l - \mathrm{g})}{125t'^{0.75}}\right) \tag{2.1}$$

$$L = l - \mathrm{g} \tag{2.2}$$

2.3.4 Maximum Allowable Ballast Pressure

The maximum allowable vertical sleeper-ballast contact pressure for a particular track section is a function of the ballast quality, type of sleeper, and subgrade, drainage and track condition. According to FIP (1987), most railway authorities allow 400 – 500 kPa of pressure on the ballast layer. Stresses exceeding this can cause excessive degradation and unsatisfactory track settlement. Alternatively, Standards Australia (1997a) states that pressure should not exceed 750 kPa for high-quality, abrasion-resistant ballast. The allowable pressure should be reduced accordingly if a lower quality material is used (Standards Australia, 1997a), however, no procedure for calculating the magnitude of this reduction is provided.

2.3.5 Estimates of Lateral Confining Pressure

Current ballast placement (maintenance) techniques generate a layer of granular material that is essentially self-supporting and free to spread laterally under cyclic train loading due to minimal resisting forces. Ishikawa and Sekine (2003) assert that in-situ confining pressure decreases laterally from the centre of the sleeper, and with reduced

depth. Raymond and Davies (1978) concluded that the lateral confining stress is unlikely to exceed 140 kPa, whereas Suiker (1997) insinuated that 10 – 90 kPa covers in-situ conditions. Selig and Alva-Hurtado (1982) estimated confining pressures to range between 21 and 83 kPa, although the method of attaining these values was not disclosed. The four main sources of in-situ lateral confining pressure are:

- sleeper-ballast interface resistance (friction),
- particle interlock due to high internal friction angle and surface roughness,
- overburden pressure from crib and shoulder ballast, and
- "locked-in" or residual stresses from maintenance procedures and train passage.

Large vertical train loads combined with relatively minor horizontal confining stresses can significantly rearrange ballast during cyclic loading. Baessler and Rucker (2003) showed that dynamic loading with minimal confinement can push ballast aside (lateral migration or flow), as illustrated in Figure 2.4. During field testing, Scott (1985) observed that rail settlement was significantly greater than subgrade settlement, and speculated that such behaviour was due to lateral migration of the ballast and subballast. Yoo and Selig (1979) documented that both lateral and longitudinal strains are generally extensional under traffic loading and vertical strains are generally smaller than horizontal strains. Lateral flow of particles can reduce the horizontal residual stresses that confine the layer, hence reducing the stability of the track (Selig and Waters, 1994). Figure 2.5 shows that an absence of lateral confinement can also contribute to superstructure problems such as track buckling.

Please see print copy for Figure 2.4

Figure 2.4 Lateral ballast spreading due to low ballast confinement (after Baessler and Ruecker, 2003)

Figure 2.5 Inadequate lateral confinement can contribute to track buckling

2.4 Track Substructure Problems

Neil (1976) classifies substructure failure into two categories, failure caused by a loss of strength and failure from soil slurry penetration (pumping track). Due to increased train speeds and loads in recent years several costly substructure problems have emerged, the most important being ballast degradation, differential track settlement, track fouling, clay pumping, and subgrade failure. Problems originating in the subgrade can largely be prevented if track drainage is sufficient and soil strength is reasonable. Figure 2.6 illustrates a number of tracks suffering from poor drainage. The problems of particular interest in this thesis, ballast degradation and differential track settlement, are more a function of stress state than degree of saturation.

Figure 2.6 Tracks suffering from inadequate drainage

2.4.1 Ballast Degradation

Although most degradation results from train loading (Gaskin and Raymond, 1976), transportation and handling, weathering, tamping and the use of compaction machines also breaks ballast down (Selig and Waters, 1994). Figure 2.7 illustrates a track suffering from excessive ballast breakage. As breakage progresses the particles become smaller which in turn fouls the ballast and inhibits track drainage. As a consequence of crushing at one location, local stress redistribution can lead to degradation at a new location (Sowers *et al*., 1965; Billam, 1971), producing differential settlement (Ionescu *et al*., 1998). In addition, breakage decreases particle angularity and diminishes the track shear strength. Ballast deterioration is a particular problem on high speed lines (Zicha, 1989). Because ballast particles are primarily angular most breakage is derived from corner degradation and attrition, although splitting is also observed. The processes and consequences of particle degradation will be examined in greater detail shortly.

Figure 2.7 Track suffering from ballast degradation

2.4.2 Differential Track Settlement

Track settlement is generally only a significant problem when it occurs non-uniformly, or differentially, along a short length (or breadth) of track as shown in Figure 2.8 (Gaskin and Raymond, 1976; Selig and Waters, 1996). Over 50% of the total deformation of railway lines (both differential and uniform) originates from the ballast layer (Suiker, 1997; Ionescu *et al*., 1998; Indraratna *et al*., 2001), with the remainder attributed to the subballast and subgrade. Between surface operations (e.g. tamping), or with good track drainage and a strong subgrade/subballast combination, the ballast layer displays the greatest degree of settlement (Selig and Waters, 1994). Figure 2.9 depicts the influence of the various substructure layers and tamping operations on settlement as a function of time. Settlement results from the reorientation and rearrangement of particles as they attempt to form a denser and more stable assembly. Train impact loads, inconsistent breakage, and localised lateral flow of ballast also contribute to differential settlement.

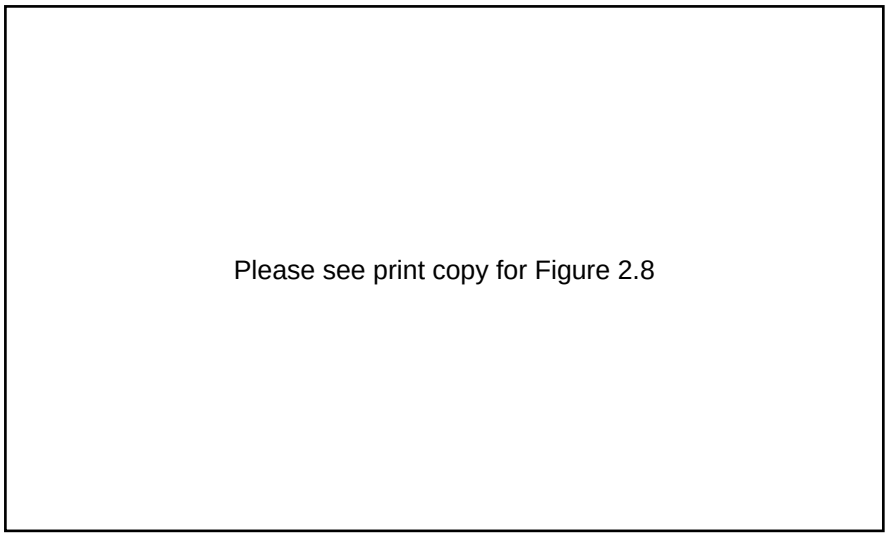

Figure 2.8 Track suffering from differential track settlement (after Suiker, 1997)

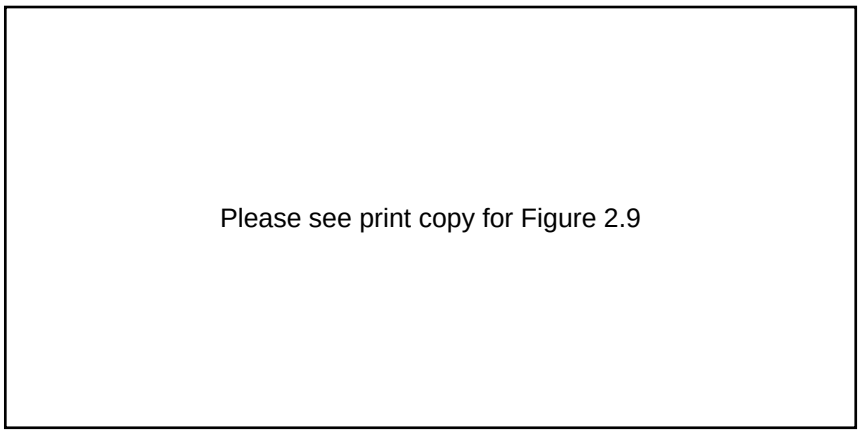

Figure 2.9 Contribution of ballast to track settlement, and the influence of tamping (after Brown and Selig, 1991)

Subgrade settlement evolves gradually and contributes more significantly to long term track performance (Figure 2.9). Subgrade differential settlement is accredited to non-uniform soil strength distribution and inconsistent soil deviator stresses. The pumping of slurry (clay pumping) from the subgrade into the subballast and ballast layers can also cause vertical and/or horizontal track misalignment.

2.4.3 Track Fouling

Ballast is designed to be free draining but when this is wholly or partially impeded due to void blockage by fine particles (sand sized or smaller), the ballast is said to be "fouled". Figure 2.10 illustrates the various sources of fouling. Ballast breakdown has been identified as the most significant source of fouling, contributing at least 50% (Chrismer, 1985; Chrismer and Read, 1994; Selig and Waters, 1994; Indraratna *et al*., 1997; 1998). Selig and Waters (1994) recognise clay pumping and the infiltration of foreign materials as the other major contributors. Foreign material penetrating into the ballast from the surface can include objects delivered with the ballast, dropped from trains, or wind and water blown matter. In Australia, Queensland Rail states that coal dropped from freight trains is responsible for 70 – 95% of the fouling of its lines (Feldman and Nissen, 2002).

Fouling can either assist or inhibit ballast performance depending on the extent and size of the fouling particles. Diminished performance occurs when the fouling material is silt or clay sized (less than 0.063 mm), in which case 100% replacement of ballast may be necessary (Selig and Waters, 1994). If the fouling material is sand sized, the strength, stability, and stiffness can be improved (Raymond, 1979; Selig and Waters, 1994). However, with time, these particles will ultimately decrease the void ratio and drainage capacity. Unlike fouling from clay and silt particles, 100% replacement should not be necessary, and maintenance costs are significantly reduced.

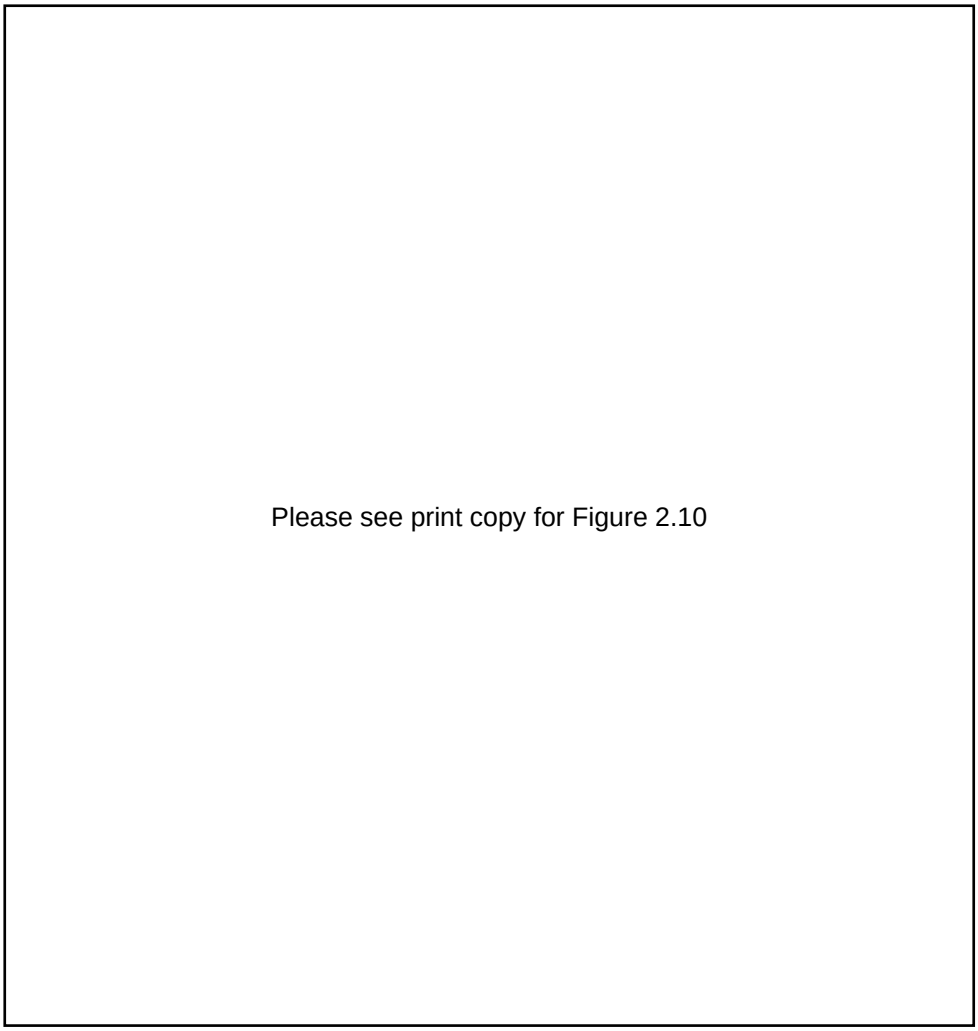

Figure 2.10 Sources of ballast fouling (after Selig and Waters, 1994)

2.5 Effect of Loading Characteristics on Permanent Deformation under Cyclic Loading

When ballast and other granular materials are subjected to cyclic loading, various micromechanical processes take place that affect the overall macroscopic behaviour. Granular materials are said to 'deform' when the loading regime rearranges the particles and 'degrade' when particles are broken into smaller pieces or fragments. Particle degradation is, therefore, a type of deformation. This section reviews the deformation

behaviour of granular materials under cyclic loading and examines the influence of loading amplitude, frequency, stress path, stress history and response of the material to the number of cycles.

2.5.1 Deformation Mechanisms in Granular Materials

Slip, sliding, rotation and rolling are four micro-mechanical processes that affect the global deformation of the ballast layer (or a granular assembly). Slip is defined as the relative motion of particles in contact under an applied load produced by sliding and/or rolling (Liao *et al*., 1995). Slipping (or sliding) occurs when the surface friction is overcome and the contact point arrangement is altered (i.e. different location and number of contact points). The strain resulting from slip is irreversible upon removal of the applied load, preventing a return to the original configuration (Harris, 1992). Cundall *et al*. (1982) observed that sliding and slip is rarely observed in highly stressed particles in granular assemblies, but is common in relatively unloaded regions.

Rolling and rotation are closely related, with rolling defined as the actual deformation taking place at the contact, and rotation as movement with respect to a reference axis (Iwashita and Oda, 1998). Particle rotation is imperative in the formation of shear bands in granular materials, and both rolling and sliding control dilatancy inside such shear bands (Iwashita and Oda, 1998; 2000). Moreover, Bardet and Proubet (1991) found that particles have minimal rotation outside shear bands. Since rock particles have a rough surface texture and contacts are often surfaces instead of points, surface resistance can greatly affect particle rolling and rotation (Iwashita and Oda, 2000; 2001). Ng and

Dobry (1994) conducted numerical simulations of sand and observed higher shear strength and stiffness, and stronger dilation when particle rotation was prevented.

Slip, sliding, rotation and rolling occur on a microscopic scale, but the macroscopic effect is an increase in settlement and a subsequent increase in compaction.

2.5.2 Effect of Maximum Cyclic Load

It is acknowledged that the maximum applied deviatoric stress has a significant influence on the permanent deformation characteristics of granular materials under cyclic loading (e.g. Luo, 1973; Brown, 1974; Brown *et al*., 1975; Raymond and Williams, 1978; Alva-Hurtado, 1980; Stewart, 1986; Jeffs and Marich, 1987; Li and Selig, 1996; Indraratna *et al*., 2000; 2001; Mohajeri and Towhata, 2003). When a specimen is subjected to multiple magnitudes of loading, the largest load has the greatest effect on the degree of settlement (Shenton, 1985; Stewart, 1986; Diyaljee, 1987; Selig and Waters, 1994). Any load less than half the maximum is insignificant in determining the overall plastic deformation (ORE, 1974; Shenton, 1985; Diyaljee, 1987). ORE (1970) established that a small number of high amplitude loads are much more important than a large number of minor loads in establishing track deterioration. Selig and Waters (1994) maintain that the largest load is the most significant, even at an occurrence of 1 in 1000.

In relation to volumetric strain accumulation, Kempfert *et al*. (2003) witnessed increased volumetric compression for specimens with greater deviatoric load using cyclic triaxial resonant column tests. Similarly, Raymond and Williams (1978) and

Olowokere (1975) showed that volumetric strain increases with deviator stress magnitude (Figure 2.11). Chang and Whitman (1988) observed three distinct volumetric straining behaviours during cyclic loading: a) soil densification with accumulating shear strain and number of cycles when the applied load is relatively small (below the critical state line), b) soil dilation with accumulating shear strain and number of cycles when the load is significantly large (above the critical state line), and c) no volume change but an accumulation of shear strain with number of cycles when the applied load coincides with the critical state line.

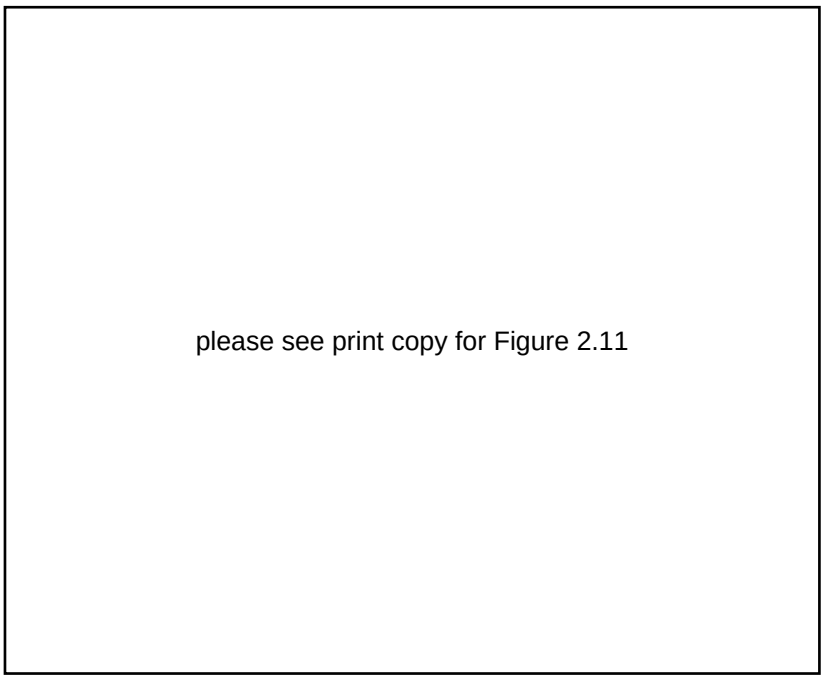

Figure 2.11 Effect of deviator stress magnitude on axial and volumetric strain (after Olowokere, 1975)

The magnitude of cyclic deviator stress required to cause failure as a function of the static peak strength has been investigated by several researchers. Lashine (1971) witnessed specimen failure when the applied cyclic shear stress exceeded 75-80% of the undrained shear strength of the material. Brown *et al*. (1975) recognised 90% undrained shear strength as the failure threshold. Brown and Selig (1991) found that little plastic

strain developed in granular materials when the peak stress ratio was kept below a certain limit, with 70% being established as appropriate in most cases. Boyce *et al*. (1976) also suggested 70% as a threshold stress to prevent the unstable accumulation of permanent deformation.

2.5.3 Effect of Minimum Cyclic Load

The minimum cyclic loading magnitude is important in characterising the settlement behaviour of granular materials. Shenton (1974), Jeffs and Marich (1987) and Jeffs (1989) found that complete unloading of ballast causes a substantial increase in settlement, which was attributed to greater ballast movement and impact loading (Jeffs and Marich, 1987). Baessler and Rucker (2003) showed that ballast settlement increased whenever the minimum load was lowered temporarily. They concluded that reducing the minimum load by a certain degree produces a larger increase in settlement than would occur with a similar increase in maximum load.

2.5.4 Frequency

Suiker (1997) studied the effect of saturation on granular response and determined that loading frequency concerns only saturated materials due to the flow of pore water. When ballast is fouled, drainage can be prevented and viscous effects may become important. Eisenmann *et al*. (1994), however, stated that settlement is significantly influenced by high train speeds.

2.5.5 Effect of Loading Path and Stress History

The load imposed on the track substructure is complex due to multiple wheel spacings, varying support conditions along different sections, and random paths of force generated within the ballast bed (Jeffs and Marich, 1987). These complexities make it extremely difficult to accurately reproduce substructure loading patterns in the laboratory. In an attempt to overcome these difficulties, a number of past studies utilised multiple stress amplitudes and stress paths to examine the behaviour of granular materials. The most comprehensive study was conducted by Stewart (1986) who performed a series of cyclic triaxial tests on well-graded railroad ballast. The tests involved full unloading, partial unloading and mixed loading conditions, in addition to constant and variable load amplitudes. Stewart (1986) found that the order of applied stresses did not affect the final permanent strain, providing equivalency in the number of cycles at each stress level (in agreement with Brown and Selig (1991) and Selig and Waters (1994)). However, a substantial number of other researchers (e.g. Marsal, 1967; Knutson, 1976; Shenton, 1974; Brown and Hyde, 1975; Bowling, 1980) believe that permanent deformation will be greatest when the biggest load is applied first. Progressively increasing the load (prestressing) can reduce the rate and magnitude of plastic deformation and amplify the stress required to initiate failure (Diyaljee, 1987).

2.5.6 Effect of Number of Cycles

Collins and Boulbibane (2000) and Sabine *et al*. (2002) have defined four types of material response under cyclic loading, a) purely elastic, b) elastic shakedown, c) plastic shakedown, and d) incremental collapse or ratcheting, as illustrated in Figure 2.12. If

the loading magnitude is adequately small, no permanent strains will be induced and the material response will be purely elastic. For loads exceeding the elastic limit, the material will initially display permanent deformation, before the material either elastically or plastically 'shakesdown', and there is no further accumulation of permanent strain with increasing cycle number. The fourth material response, incremental collapse or ratchetting, symbolises the continuing accumulation of permanent strain with each successive loading cycle until the material 'fails'.

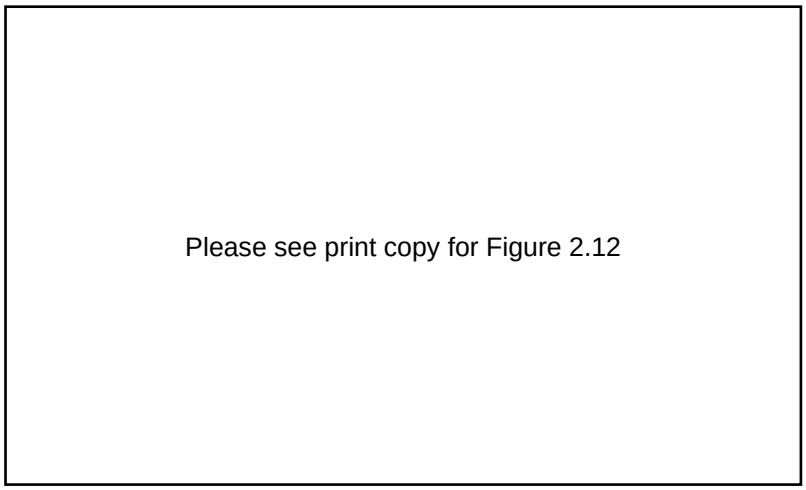

Figure 2.12 Material responses under cyclic loading (after Collins and Boulbibane, 2000)

It is well established that settlement or vertical strain accumulates approximately logarithmically with the number of cycles N (Barksdale, 1972a; Shenton, 1974; 1985; Olowokere, 1975; Raymond and Williams, 1978; Lentz and Baladi, 1981; Brown and Selig, 1991; Frost *et al*., 2004). Raymond and Williams (1978) and Olowokere (1975) witnessed a similar response for volumetric strain (Figure 2.11). The final permanent vertical strain is a function of the strain resulting from the first cycle, and the number of cycles (Alva-Hurtado and Selig, 1981; Stewart, 1986). Profillidis (1995) indicated that the first cyclic load causes the greatest amount of plastic strain and the rate of

deformation decreases with each subsequent cycle until a stable condition is attained, which concurs with Raymond and Williams (1978), Diyaljee (1987) and Mohajeri and Towhata (2003), amongst others. The number of cycles required to achieve such stability differs between researchers. For example, 10000 cycles (Brown, 1974; Uzan, 1999) has been quoted, along with 100000 cycles (Raymond and Williams, 1978; Shin *et al*., 2002) and over one million cycles (Brown *et al*., 1975).

Equations 2.3, 2.4 and 2.5 are commonly employed to estimate axial strain ε_N or settlement S_N as a function of the number of cycles N. ORE (1970) developed Equation 2.3 to approximate ballast deformation behaviour based on the strain resulting from the first cycle ε_1, where c′ is a coefficient often equal to 0.2. Li and Selig (1996) identify Equation 2.4 as the most widely used model, where a′ is the settlement after one cycle, and x is an empirical coefficient. Equation 2.5 connects ε_N to N and the deviator stress magnitude $(\sigma_1-\sigma_3)$ (ORE, 1970). In this relationship, n is the ballast porosity, and Y is a coefficient depending on the applied stress level (varies from 1 to 3).

$$\varepsilon_N = \varepsilon_1(1+c'log N) \quad (2.3)$$

$$S_N = a'N^x \quad (2.4)$$

$$\varepsilon_N = 0.082(100n-38.2)(\sigma_1-\sigma_3)^Y(1+0.2log N) \quad (2.5)$$

2.6 Degradation Behaviour of Single Rocks and Granular Materials under Static and Cyclic Loading

The mechanical response of a granular material (i.e. stress-strain characteristics, shear strength, drainage capability etc.) to a particular loading regime is largely dependent on

the ability of individual particles to remain intact, i.e. to retain initial size and shape. If particle integrity is not preserved, the risk of massive deformation and failure is substantially increased. A thorough appreciation of the degradation performance of single rock specimens (rock cores) and granular materials under a variety of loading conditions and the identification of critical factors affecting particle breakage is vital in characterising the overall strength and stability of the aggregate. These issues have been treated below, and various breakage quantification methods for granular materials are discussed in Appendix B.

2.6.1 Degradation Mechanisms of Single Rock Particles

The behaviour of single cylindrical rock cores, or rocks of arbitrary shape, loaded between two flat plates (uniaxial or diametric) has been studied in some detail (e.g. Hobbs, 1963; Sammis and Ashby, 1986; Singh, 1988; Wong *et al*., 1996; Eberhardt *et al*., 1999; Tang *et al*., 2000; 2001; Fang and Harrison, 2002). Particle fracture strength under these conditions depends predominantly on the parent rock strength, grain geometry, prevalence of flaws, number of loading contacts, and loading direction. Perhaps the most critical finding in relation to single-rock degradation relates to fracture initiation. It has been documented that fractures are activated through existing internal flaws that act as stress concentrators, with the size of the flaw an important factor in determining the likelihood of breakage. Grady and Kipp (1987) and Ray *et al*. (1999) noticed that the rate of loading significantly affected the size of the fragmented pieces. When strain (loading) rates are slow, only a small number of flaws or cracks become active, resulting in comparatively large fragments, but if the load is applied more

rapidly, a greater stress level can be achieved before crack coalescence occurs, leading to smaller fragments.

Of particular importance to this thesis is the effect of confining pressure on rock behaviour. Tang *et al*. (2001) identified that a brittle-ductile failure transition exists that is characterised by the level of confinement around the specimen. Sammis and Ashby (1986) and Fang and Harrison (2002) conducted compression tests on rock cores and found that confining pressure has a significant effect on the induced failure mechanisms, as illustrated in Figure 2.13. Greater lateral constraint increases the stiffness and maximum breakage strength. At low confining pressure (Figures 2.13a and 2.13d), brittle rock failure is instigated by splitting parallel to the major principal stress σ_1' (tensile failure). Moderate confining pressures (Figure 2.13b) produce shear fault (band) formation inclined to σ_1'. Specimens subjected to high confinement display more than one failure surface, and deformation is comprised of many short, homogenously distributed micro-fractures (compressive failure). Brittle materials such as rocks can exhibit plastic or ductile characteristics at high confining pressures where a greater amount of energy is required to cause crushing. Tensile type failures produce coarse fragments and compressive or shear failures tend to produce finer fragments, with the degree of fineness increasing with the magnitude of lateral support (Tang *et al*., 2001).

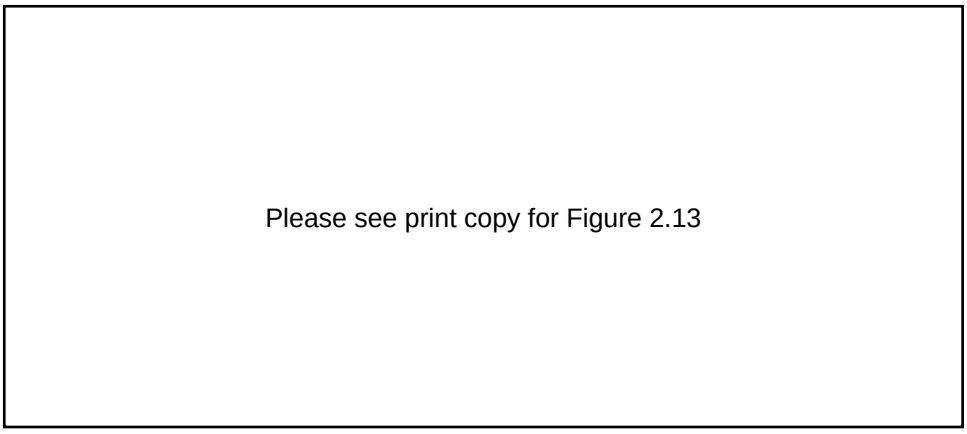

Figure 2.13 Failure modes of brittle rock cylinders under axial compression σ_1' as a function of confining pressure σ_3', (a) Low σ_3', (b) intermediate σ_3', (c) high σ_3', and (d) low σ_3' (after Sammis and Ashby, 1986)

2.6.2 Degradation Mechanisms of Granular Materials

Studying confined or unconfined single-particle loading provides a useful introductory description of the fundamental mechanisms of particle degradation. However, unlike single rock specimens, particles contained within granular assemblies interact with at least four neighbours (Bernal and Mason, 1960; Jenkins *et al*., 1989) leading to considerably more complex loading paths. Contact forces between particles are random in intensity and direction, with the magnitude depending on the size and shape of grains, and the arrangement and number of contact points (Marsal, 1973). In addition, Oda (1972), Cundall *et al*. (1982) and Kou *et al*. (2001) ascertained that the deviatoric force is not carried uniformly by all particles, but instead observed that the major (axial) stress is transmitted mainly through chain or column like structures aligned in the direction of the major principal stress, further complicating the loading configuration. They found that particles participating in these vertical force columns are highly stressed, whereas all remaining particles carry little or no load. Obviously, particles in

the highly stressed zones are more likely to experience degradation. A further difficulty arises from variations in particle strength within the assembly. It has been acknowledged that when the particle tensile strength range is relatively restricted, local crushing causes stress redistribution and particle rearrangement that produces further crushing in the near vicinity (Sowers *et al*., 1965; Liu *et al*., 1993). If, however, the range of tensile strengths is large, stress concentrations caused by fractured grains do not significantly influence which grains break next, and grain fracture is essentially random (Liu *et al*., 1993). Properly understanding the breakage of particles within a granular assembly is a multifaceted problem dependent on a large number of particle, aggregate, and loading variables.

Particle breakage is related to both interparticle contact area (Raymond, 1977) and contact forces (Feng, 1984). In the field environment, particle degradation can result from excessive loading amplitudes (physical breakage) or from weathering (chemical breakage). Lees and Kennedy (1975) recognised that the degradation of granular materials can occur in three ways:

a) breakage of angular corners or projections,

b) grinding or attrition of asperities, and

c) splitting of particles into two or more approximately equal parts.

Previous experimental and numerical investigations examining the deformation and degradation response of granular materials subjected to increasing (static) stress levels have suggested the existence of four characteristic stages of behaviour. Similar studies for cyclic loading scenarios are rare, highlighting the urgent need for further exploration in this area. However, Ionescu *et al*. (1998) briefly outlined four phases (different to the

static phases) that demonstrate granular behaviour under constant cyclic stress amplitudes. The deformation and degradation processes for both static and cyclic loading are presented below.

2.6.3 Deformation and Degradation Phases under Monotonic (Static) Loading

Hagerty *et al*. (1993) and McDowell and Bolton (1998) have identified four phases of deformation (Table 2.4) that characterise the behaviour of granular assemblies under gradually increasing (static) stress intensities. When an initially low stress level (deviatoric or all-round) is applied, processes such as sliding and rolling cause particle rearrangement and a subsequent increase in specimen density. These deformation processes continue into Phase 2, however, stress magnitudes are now sufficiently large for particle breakage to commence. Breakage initially results from the transmission of loads through protruding points (sharp edges), but splitting ensues once the stresses become large enough. Splitting usually occurs in the larger, weaker particles through planes of weakness such as microfissures and cracks that form during blasting and crushing (Marsal, 1967).

Table 2.4 Phases of deformation and degradation under gradually increasing loads

Phase	Stress level	Sources of Densification
1	Low	Slipping, rolling, sliding
2	High	Slipping, rolling, sliding, breakage
3	Higher	Breakage
4	Highest	Nil (equilibrium condition)

The high degree of compaction achieved during Phase 2 prevents further densification from non-destructive mechanisms. Instead, Phase 3 involves densification from particle crushing only. McDowell and Bolton (1998) illustrated that a fractal distribution of

particle sizes can evolve during this phase if breakage is the consequence of particle splitting. By the end of Phase 3, only the smallest particles are vulnerable to crushing. All breakage ceases and equilibrium is established once the comminution limit for small particles is achieved (Oldecop and Alonso, 2001) (Phase 4), and the coordination number (number of interparticle contact points) is maximised.

2.6.4 Deformation and Degradation Phases under Constant Amplitude Cyclic Loading

Few studies have attempted to describe the degradation of granular materials as a function of the number of cycles N (at constant or increasing stress magnitude). According to Ionescu *et al*. (1998), the breakdown of particles does not commence until at least 100000 loading cycles have been completed (Table 2.5). Ionescu *et al*. (1998) subjected railway ballast to cyclic loading and determined that rapid and considerable dynamic packing and sliding of particles occurs during the initial 20000 cycles (stabilisation stage), resulting in significant settlement and the formation of a relatively compact aggregate compared to the initial arrangement. A consolidation phase lasting around 100000 cycles involving minor ballast settlement follows the stabilisation phase, leading to a further increase in particle packing. Phase 3 behaviour is typified by the commencement of edge (corner) and irregularity degradation, and Phase 4 by the splitting of relatively weak particles. Equilibrium was not established as breakage was considered to continue indefinitely but at a decreasing rate with increasing number of loading cycles.

Table 2.5 Phases of deformation and degradation under constant amplitude cyclic loading (data from Ionescu *et al*., 1998)

Please see print copy for Table 2.5

2.7 Factors Affecting the Degradation of Granular Materials

Chrismer (1985) acknowledged grain hardness, toughness, shape, and weathering resistance as the most important variables affecting particle degradation. Alternatively, Hardin (1985) considers crushing to be mainly dependent on the particle size distribution, particle shape, effective stress state and stress path, void ratio, hardness and moisture content. Instead of evaluating in-track performance, standard laboratory tests are used to determine the suitability of rock aggregates as ballast (Chrismer, 1985; Indraratna *et al*., 1998). Therefore, aggregates that successfully fulfil laboratory requirements may not be suitable for actual field application, and vice-versa. The factors that affect grain breakage can be broken into three categories as shown in Table 2.6 (Hay, 1953; Sowers, 1965; Gaskin and Raymond, 1976; Raymond, 1979; Raymond and Diyaljee, 1979; Barton and Kjaernsli, 1981; Janardhanam and Desai, 1983; Hardin, 1985; Chrismer, 1985; Jeffs and Marich, 1987; Jeffs, 1989; Selig and Waters, 1994; Lade *et al*., 1996; Indraratna *et al*., 1997; 1998; 2000; 2001; Ionescu *et al*., 1998). Only the following aspects will be considered here:

- particle shape, size and grading,
- loading magnitude, type and number of loading cycles, and

- confining pressure.

Table 2.6 Factors affecting particle breakage in granular materials

Aggregate Properties	Particle Properties	Loading Properties
Specific gravity	Soundness	Loading pattern/magnitude
Hardness	Particle shape	Confining pressure
Weathering resistance	Particle size	In-track depth
Mineralogical composition	Particle size distribution	Train speed/frequency
Toughness	Surface roughness	Ballast thickness
Internal bonding		Initial density
Grain size		Degree of saturation
		Number of cycles

2.7.1 Particle Shape, Size and Grading

Previous research has demonstrated that more spherical particles do not break as frequently as those with increased angularity or irregularity (Lee and Farhoomand, 1967; Hardin, 1985; Selig and Waters, 1994; McDowell *et al*., 1996; Tang *et al*., 2001). This is because rounder particles have a more regular stress distribution with less sharp corners and edges (Tang *et al*., 2001).

There are two conflicting views regarding the effect of particle size on degradation:

1) Larger particles are more affected by breakage (Lee and Farhoomand, 1967; Raymond, 1979; Hardin, 1985; Chrismer, 1985; Jeffs 1989; Lade *et al*., 1996; Indraratna *et al*., 1998; 2000; 2001; Ionescu *et al*., 1998; Eberhardt *et al*., 1999).
2) Smaller particles are more affected by breakage (Billam, 1971; Al-Hussaini 1983; McDowell *et al*., 1996; McDowell and Bolton, 1998; Tsoungui *et al*., 1999).

Lade *et al*. (1996) conducted high pressure triaxial tests on dense Cambria sand and concluded that crushing increases with particle size due to a higher prevalence of flaws (microfractures) and a greater probability of internal defects. Hardin (1985) agrees with this assertion and also identifies that the normal contact forces on a soil element increase with particle size. Smaller particles require more energy to fracture (Brown *et al*., 1996) and are statistically stronger (McDowell and Harireche, 2002). In addition, smaller particles are often less angular and are hence subjected to less stress concentrations.

Due to difficulties associated with an in-depth study of breakage mechanisms using experimental apparatus, numerical modelling techniques are often utilised (e.g. McDowell *et al*., 1996; McDowell and Bolton, 1998; Tsoungui *et al*., 1999). According to McDowell and Bolton (1998) there are two opposing forces affecting the likelihood of breakage, particle size and coordination number (number of contact points). Numerical simulations have illustrated that smaller particles fracture more readily due to a limited coordination number and poor load distribution. The number of interparticle contacts increases with particle size providing a superior loading distribution and a decreased probability of fracture.

With railway ballast the evidence clearly suggests that larger particles are degraded by cyclic train loads. Indraratna *et al*. (2000 and 2001) found that latite basalt grains of 55 mm or greater are most involved in breakage, with particles less than 10 mm largely unaffected, whereas Indraratna *et al*. (1998) stated that grain sizes between 26.5 – 53 mm are most prone to degradation.

It is commonly acknowledged that the degree of particle breakage decreases as the particle size distribution becomes broader or more well graded (C_u increases) (Lee and Farhoomand, 1967; Marsal, 1967; Lees and Kennedy, 1975; Loret, 1982; Lade *et al*., 1996; Daouadji *et al*., 2001). For example, Daouadji *et al*. (2001) investigated the effect of grading on sand particle rupture and found that poorly graded aggregates exhibited enhanced grain crushing. The reduced degradation magnitude associated with well graded material is attributed to a superior distribution of intergranular forces and lower contact stresses related to increased coordination number (Lade *et al*., 1996; Daouadji *et al*., 2001).

2.7.2 Loading Magnitude, Type and Number of Loading Cycles

The stress state (or stress path) is the most critical factor affecting degradation in granular materials. Breakage increases with the magnitude of shear or mean principal stress (e.g. Lee and Farhoomand, 1967; Marsal, 1973; Raymond and Williams, 1978; Hardin, 1985; Lade *et al*., 1996; Indraratna *et al*., 1998; Tang *et al*., 2001; Hyodo *et al*., 2002). Degradation can occur at low stress levels due to the random nature and intensity of local contact forces within the assembly (Marsal, 1973; Indraratna *et al*., 1998), or after a large number of cycles by the process of fatigue (Ray *et al*., 1999; Goder *et al*., 2002).

Lade *et al*. (1996) conducted drained and undrained triaxial tests and witnessed considerably more degradation in the drained tests due to greater effective stresses. Hyodo *et al*. (2002), however, still observed substantial breakage during undrained

cyclic shearing even though the effective stresses were continually decreasing. Al-Hussaini (1983) and Hyodo *et al*. (2002) found that the crushing magnitude during the consolidation phase of triaxial testing was insignificant compared to the shearing phase. In the latter study, breakage during undrained shear at a confining pressure of 3 MPa far exceeded breakage in specimens isotropically consolidated to 10 MPa. Furthermore, breakage is considerably more advanced in triaxial compression than extension tests (Lade *et al*., 1996). Finally, Billam (1971), Lade *et al*. (1996) and Tang *et al*. (2001) demonstrated that degradation becomes constant at high pressure due to 'saturation' (or surrounding) of the remaining large particles by small particles. 'Saturation' allows the formation of a dense mass that is able to resist shearing without further crushing.

The effect of the number of cycles N on degradation has not been studied in great detail. Miura and O′Hara (1979) conducted drained triaxial tests on decomposed granite and determined that the rate of breakage is rapid during the first 200 cycles, but lessens with continued cycling (Figure 2.14). Goder *et al*. (2002) compressed three materials and identified that a significant degree of breakage occurs in the first cycle (N = 1), and that the amount of damage accumulates with N (e.g. Figure 2.15). Raymond and Williams (1978) also witnessed considerable breakdown of ballast specimens during the first cycle but explained that limited breakage is expected beyond the initial cycle unless the aggregate is poor or many millions of cycles are applied.

2.7.3 Confining Pressure

The magnitude of particle degradation under static triaxial loading increases with the effective confining pressure σ_3' as shown in Figure 2.16 (Lee and Farhoomand, 1967;

Lee and Seed, 1967; Marsal, 1967; Al-Hussaini, 1983; Lade *et al*., 1996; Indraratna *et al*., 1998; 2001). This behaviour is believed to be due to suppressed dilation at higher pressures (Indraratna *et al*., 1998; 2001; Coop *et al*., 2004) and larger deviatoric loads. Ueng and Chen (2000) also identified that the rate of energy consumed by particle breakage increases with the confining pressure.

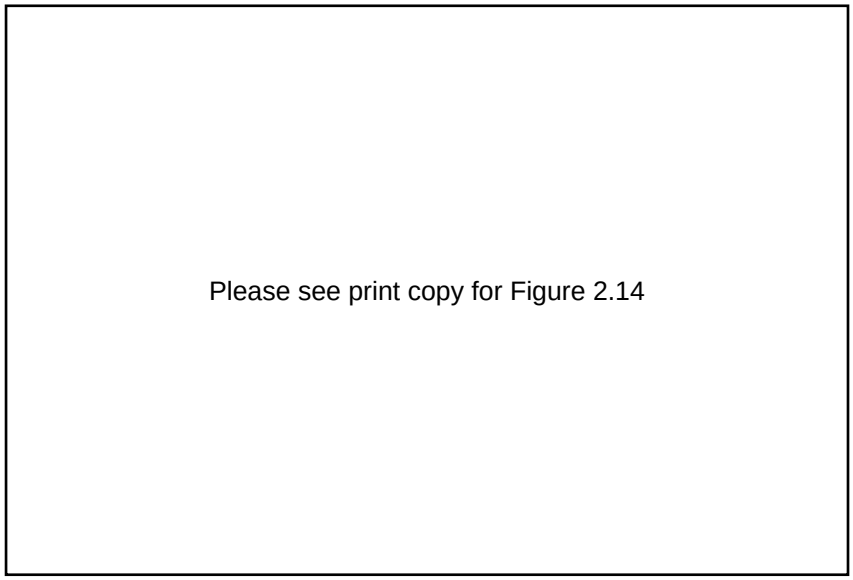

Figure 2.14 Relationship between breakage (increase in surface area) and number of cycles (after Miura and O′Hara, 1979)

There are limited studies which examine the effect of confining pressure σ_3' on breakage under cyclic loading. Raymond and Williams (1978) conducted drained compression and extension tests on Coteau dolomite ballast at σ_3' of 51.7 and 206.8 kPa, and concluded that the magnitude of σ_3' has no significant influence on the degree of degradation. Breakage was measured by computing the percentage of particles passing the No. 4 sieve, and the results are reproduced in Figure 2.17. In all cases except the R = 0.5 and σ_3' = 206.8 kPa specimen (where R is the ratio of cyclic to static peak deviator stress), Figure 2.17 indicates increasing breakage with σ_3'. Hyodo *et al*. (2002) conducted undrained two-way cyclic shear tests on silica sand for σ_3' = 0.1, 3 and

5 MPa, and observed no significant breakage for $\sigma_3' = 0.1$ MPa. However, breakage was found to increase with cyclic stress ratio and σ_3' according to Figure 2.18. Therefore, it appears that increased breakage is associated with larger σ_3', although this deduction is far from conclusive.

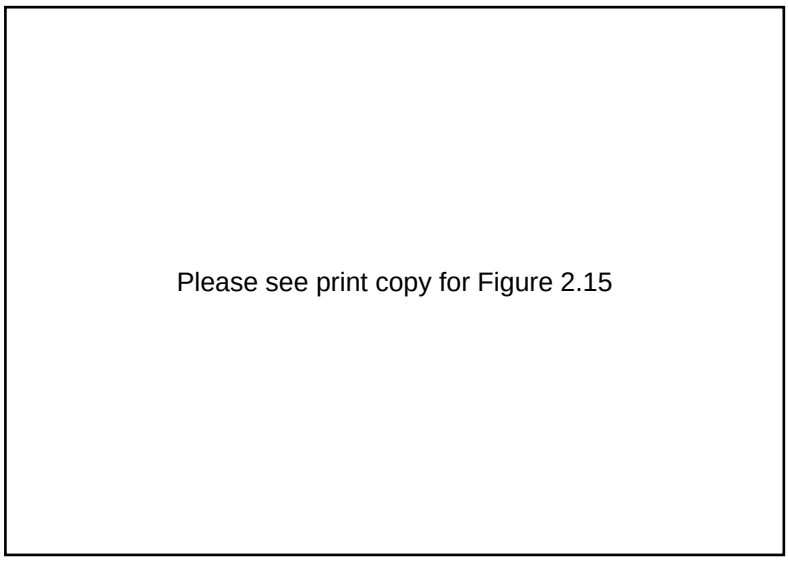

Figure 2.15 Effect of number of cycles on percentage of broken particles for potassium sulphate (after Goder *et al*., 2002)

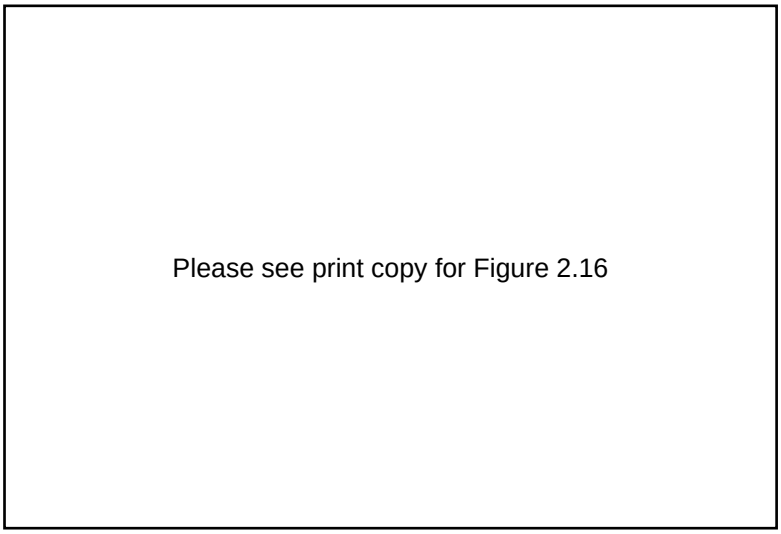

Figure 2.16 Effect of confining pressure on the breakage of dense Cambria sand during drained high pressure triaxial tests (after Lade *et al*., 1996)

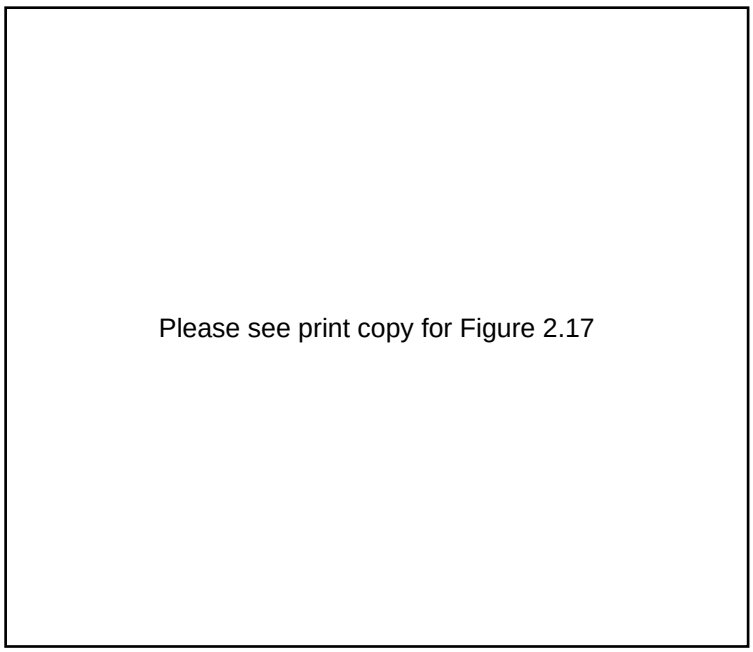

Figure 2.17 Effect of confining pressure on breakage of dolomite ballast during cyclic loading tests (after Raymond and Williams, 1978)

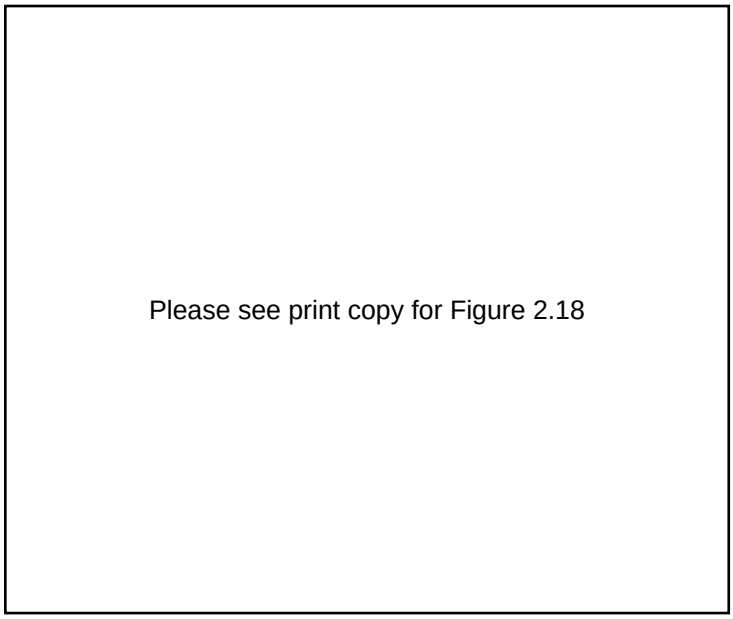

Figure 2.18 Effect of applied cyclic stress ratio and confining pressure on breakage of silica sand (after Hyodo *et al*., 2002)

2.8 Lateral Pressures Induced in Granular Materials

During the lifetime of a railway line, the ballast layer is subjected to compaction and tamping stresses (during initial construction and maintenance), and cyclic train loading. Prior to traffic loading, there are two major sources of lateral pressure in the ballast layer, geostatic (overburden) stresses and compaction stresses (Seed and Duncan, 1986). Both stress types can act inwards (i.e. as a confining stress) or outwards (i.e. as a destabilising stress). Traffic induced lateral stresses act to destabilise confining pressures. A major design parameter for the substructure is the magnitude of vertical deviator stress, however, the effect of loading on the transient and residual horizontal stresses within the ballast layer have not been studied intensely. The magnitude of lateral stress may have a significant effect on the behaviour of the entire track system. Excessive lateral destabilising stresses and subsequent ballast movement (spreading) can relieve the induced pressures that confine the layer, and the track will be prone to unacceptable levels of settlement.

When granular materials are compacted the resulting increase in horizontal stress depends on the loading amplitude and boundary conditions. Removing the compaction load releases most of the vertical pressure but only a percentage of this pressure dissipates horizontally, resulting in horizontal pressures substantially greater than pre-compaction levels (Duncan *et al*., 1991). Seed and Duncan (1986) state that as much as 40 - 90% of the peak horizontal stress may remain as residual stress in granular materials after removal of the compaction load, particularly near the surface of the granular material (Duncan *et al*., 1991).

During traffic loading, lateral stresses are reintroduced with each successive axle load, which can rearrange the particles at shallow depths (Seed and Duncan, 1986). The magnitude of confining stress offered by the shoulder ballast (in conjunction with other confinement sources) should be large enough to prevent lateral spreading of load bearing ballast and prevent differential track settlement, loss of shear strength and degradation.

2.8.1 Horizontal Stress Accumulation During Compaction

Earl (1997) studied the compactive nature of soil (sandy loam and clay soil) by conducting plate shrinkage and confined compression tests. During this investigation three distinct phases of behaviour were observed, as illustrated in Figure 2.19a: 1) initial compaction of soil at constant lateral stress, 2) continuing compaction with increasing lateral stress, and 3) compaction and lateral soil movement. Figure 2.19b demonstrates the coefficient of earth pressure at rest K_0 (ratio of lateral to axial stress) as a function of axial pressure for confined and unconfined conditions. In Figure 2.19b, K_0 falls during Phase 1 and increases with lateral stress in Phase 2. Once Phase 3 is encountered, K_0 behaviour is dependent on the boundary conditions. For the confined condition, K_0 remains approximately constant with increasing axial strain, but for unconfined specimens, the lateral stress generated exceeds the confining ability of the soil, leading to lateral soil movement and a subsequent decrease in K_0.

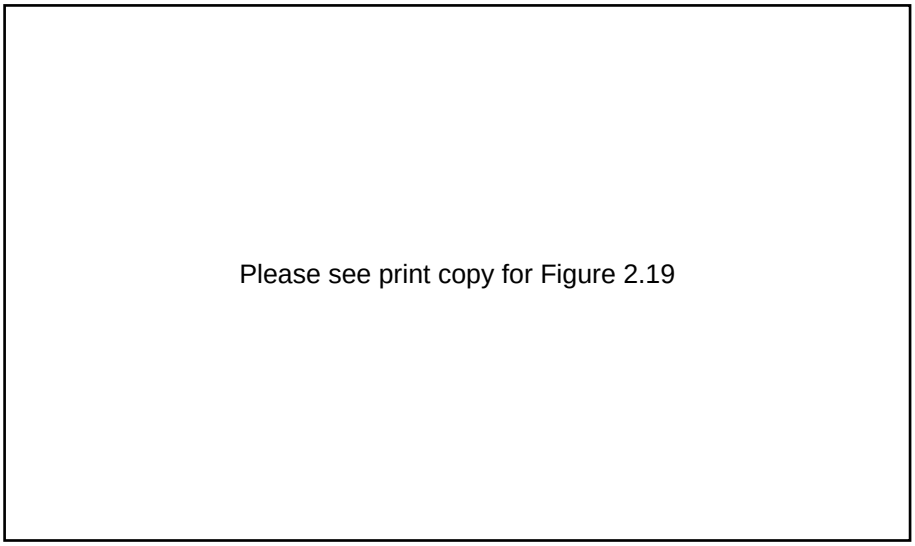

Figure 2.19 Behaviour of soil during plate shrinkage and confined compression tests, (a) Phases of deformation, and (b) Effect of axial pressure on induced lateral stresses (after Earl, 1997)

2.8.2 Horizontal Stress Accumulation During Traffic Loading

Sawicki and Swidzinski (1995) subjected granular materials to cyclic oedometer compaction testing and measured the resulting vertical strains and lateral stresses. Figure 2.20 presents typical data illustrating the effect of the number of cycles N and amplitude of maximum vertical stress on the magnitude of residual lateral stress. Figure 2.20 indicates that the lateral stress is significantly affected by the level of vertical stress, and increases at a decreasing rate with N. The magnitude of residual horizontal stress is significantly smaller than the magnitude of vertical deviator stress. For example, for a maximum deviator stress of 842 kPa, the residual lateral stress after 10 cycles is approximately 55 kPa, or 6.5% of the deviator stress. This percentage increases to 15.5% when the deviator stress is reduced to 211 kPa.

The boundary conditions for oedometer tests and in-situ railway ballast are significantly different. Whilst the granular materials under investigation in Sawicki and Swidzinski (1995) were restrained by a solid boundary, railway ballast is virtually free to spread laterally (dilation). Therefore, the peak and residual lateral stresses are expected to be significantly reduced in the track environment due to this lack of containment (confining pressure).

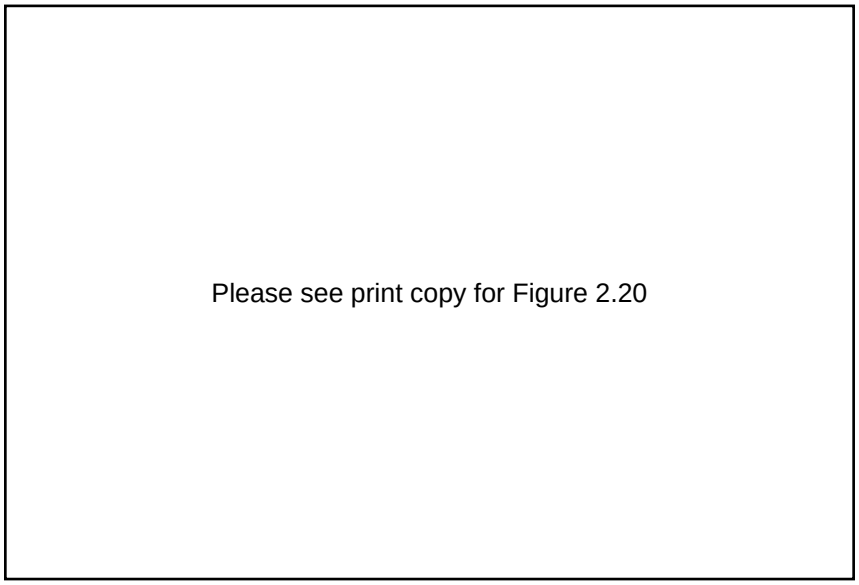

Figure 2.20 Effect of maximum vertical stress amplitude and number of cycles on residual lateral stresses (after Sawicki and Swidzinski, 1995)

Freeman and Harr (2004) placed instruments on two sections of test pavement and measured the coefficient of lateral stress ν (the ratio of horizontal to vertical stress) for common pavement materials. In concept ν is similar to the earth pressure coefficient but captures the entire elastic-plastic range. Using the central limit theorem of probability and back analysis, they found that under a uniformly distributed square load, the maximum vertical stress exerted on the material decreases as ν increases, implying superior load distribution with increasing ν. This situation is depicted in Figure 2.21 for

a depth of 0.3 m. They also concluded that materials with higher ν display more rapid stress attenuation. Generally, fine grained materials were found to have higher ν than coarser materials which was attributed to the cohesive nature of the fine soils. Typical ν values for sand and crushed limestone are quoted as approximately 0.15, and for clays this value climbs to about 0.42. Like K_0, ν is possibly related to the internal friction angle of the particles, but this aspect has not been reported by Freeman and Harr (2004).

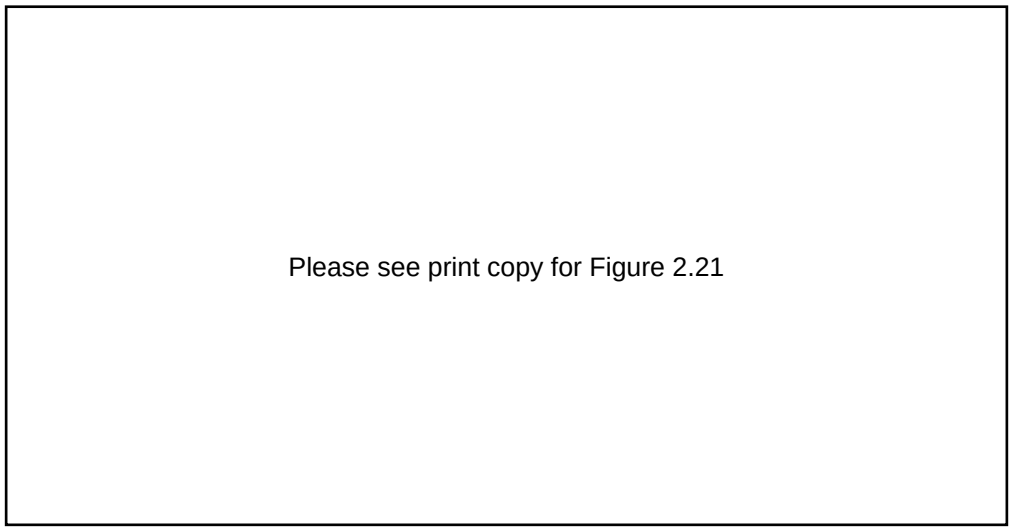

Figure 2.21 Effect of horizontal to vertical stress ratio ν on lateral pressure with lateral distance from the loading plate (after Freeman and Harr, 2004)

Norman and Selig (1983) measured the change in horizontal stress of ballast under repeated loading, and the major findings are illustrated in Figure 2.22. Initially the horizontal stresses are small, in this case approximately 1.5 kPa, with the exact value dependant on the compactive effort. After applying the first load the horizontal stress increases to approximately 60 kPa, and then drops to about 18 kPa when unloaded. The evolution of the residual (unloaded) and transient (loaded) horizontal stresses converge to an almost steady state condition after about 1000 cycles. Assuming the shoulder

ballast does not displace laterally, this method provides a reasonable estimation of horizontal track stresses.

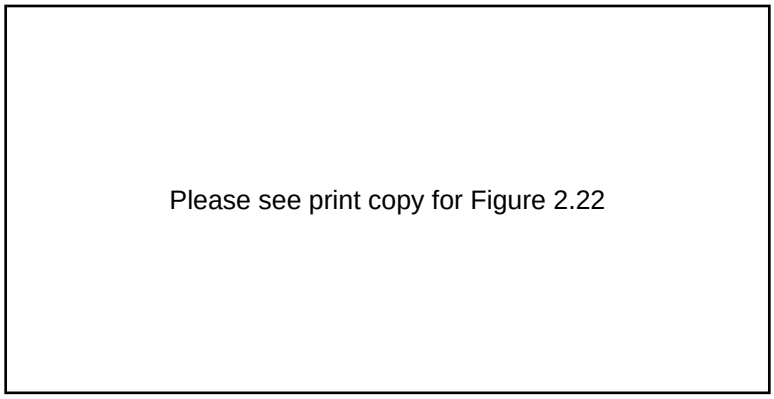

Figure 2.22 Effect of number of cycles on horizontal stresses in ballast (after Norman and Selig, 1983)

2.9 Effect of Confining Pressure on Permanent Deformation Behaviour of Granular Materials

2.9.1 Static Loading Behaviour

The effect of confining pressure σ_3' on the static or monotonic behaviour of granular materials, particularly sand and rockfill, has been examined by a large number of researchers (e.g. Bishop, 1966; Vesic and Clough, 1968; Marsal, 1967; 1973; Billam, 1971; Ponce and Bell, 1971; Marachi *et al*., 1972; Raymond and Davies, 1978; Penman, 1978; Miura and O′Hara, 1979; Charles and Watts, 1980; Barton and Kjaernsli, 1981; Al-Hussaini, 1983; Jeffs, 1989; Indraratna *et al*., 1993; 1998; 2000; 2001; Yamamuro and Lade, 1996; Mirghasemi *et al*., 1997; Sitharam, 1999; Maeda and Miura, 1999; Kato *et al*., 2003). Ballast needs to be tested at relatively low σ_3' to mimic in-situ conditions (Indraratna *et al*., 2001). Unfortunately much of the research listed above is

not always applicable to railway ballast due to large discrepancies in the confining pressures and loading paths applied (Schultze, 1961; Raymond *et al*., 1976; Alva-Hurtado and Selig, 1981; Jeffs and Marich, 1987; Indraratna *et al*., 1998). Nevertheless, it is well established that under static loading as σ_3' increases:

a) the volumetric strain changes from dilation to compression. Particle movement and rearrangement is largely restrained at higher confining pressure, thus limiting the scope for lateral straining and dilation,

b) the axial strain at failure increases and behaviour becomes increasingly ductile,

c) the peak stress ratio at failure $(\sigma_1'/\sigma_3')_p$ decreases due to particle breakage,

d) the internal friction angle ϕ (strength) decreases because of reduced interparticle friction, particle crushing, and the inability of specimens to dilate,

e) the peak deviator stress increases due to the limited horizontal particle displacement and subsequent increase in load carrying capacity. In addition, the stress required to attain a particular strain increases with σ_3',

f) the degradation of particles increases because of the suppression of dilation and increased magnitudes of deviator stress, and

g) the specimen stiffness (modulus) increases.

2.9.2 Cyclic Loading Behaviour

Remarkably, few studies have examined the effect of confining pressure σ_3' on the behaviour of granular materials under drained cyclic loading, indicating a fundamental requirement for further research in this area. Boominathan and Hari (2002) considered the effect of σ_3' on the behaviour of fly ash under cyclic loading and found that

resistance to liquefaction increases with σ_3'. The shear stiffness (Borden *et al*., 1996; Li and Ding, 2002; Tanaka, 2003) and resilient modulus (e.g. Hicks, 1970; Allen, 1973) of specimens have also been shown to increase with σ_3'. Shahnazari and Towhata (2002) identified that specimens with higher confinement have superior strength and exhibit greater resistance to deformation. Mohajeri and Towhata (2003) conducted drained shear experiments on sand, silty sand and loam, and concluded that specimens with lower vertical σ_3' displayed larger increments of shear and volumetric strain.

Raymond and Williams (1978) found that the volumetric strain increases with cell pressure during drained cyclic loading and that any increase in σ_3' improves material stability. Suiker *et al*. (2005) subjected subballast specimens to cyclic loading and recognised that the volumetric strain increases with σ_3'. Lastly, Brown (1974) conducted triaxial tests on crushed granite and ascertained that the permanent axial strain increases with decreasing σ_3' (Figure 2.23). Similarly, Barksdale (1972b), Selig and Alva-Hurtado (1982), Khedr (1985), Stewart (1986) and Uzan (1999) demonstrated that for a given deviator stress, the permanent deformation increases significantly as σ_3' decreases.

2.10 Resilient Behaviour of Granular Materials

The resilient modulus M_R is a stress-strain relationship that describes the long-term elastic behaviour of materials under repetitive traffic loading (Ozel and Mohajerani, 2001). When a granular material is subjected to cyclic loading the resulting deformation is comprised of permanent (non-recoverable) and resilient (recoverable) components, as illustrated in Figure 2.24. M_R can be calculated according to Equation 2.6, where σ_d is

the magnitude of deviator stress, and $\varepsilon_{a,rec}$ the recoverable axial strain. An increasing M_R signifies increasing stiffness. After a significant number of cycles, most deformation is essentially elastic (the material has undergone 'shakedown'), hence the use of recoverable strain to portray the long-term response to cyclic loading (Zaman *et al*., 1994).

$$M_R = \sigma_d / \varepsilon_{a,rec} \qquad (2.6)$$

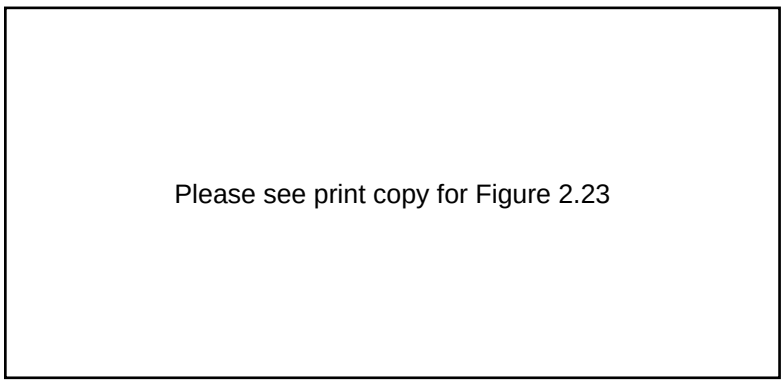

Figure 2.23 Effect of confining pressure on the permanent strain behaviour of crushed granite (after Brown, 1974)

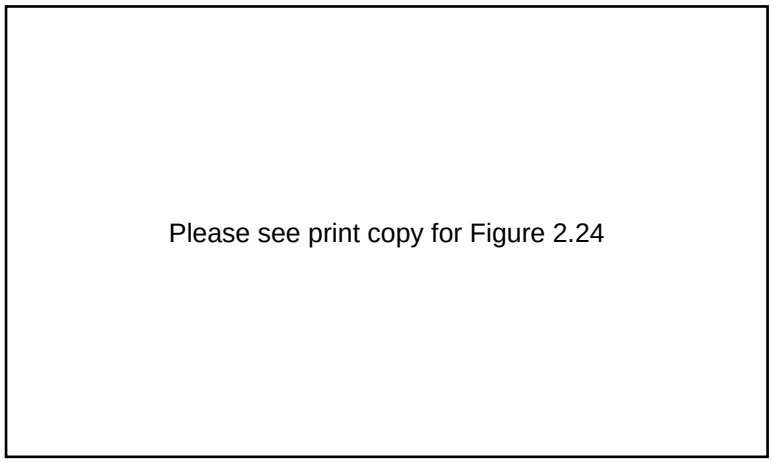

Figure 2.24 Permanent and resilient deformation components of granular materials under cyclic loading (after Selig and Alva-Hurtado, 1982)

2.10.1 Factors Affecting the Resilient Deformation of Granular Materials

Table 2.7 outlines the material, loading and environmental parameters that influence the M_R response of granular materials. The parameters that are considered most significant for this study are:

- aggregate type and geometry (shape and texture),
- aggregate grading and size,
- stress history and stress sequence,
- number of loading cycles, and
- stress state.

Table 2.7 Factors affecting the resilient modulus of granular materials

Material Parameters	Loading Parameters	Environmental Parameters
Aggregate type and geometry	Loading frequency and pulse duration	Temperature
Aggregate grading and size	Stress history and stress sequence	
Fines content or degree of fouling	Number of loading cycles	
Degree of saturation or moisture content	Stress-state - confining pressure and deviator stress magnitude	
Dry density	Compaction method and effort	

2.10.2 Aggregate Type and Geometry (Shape and Texture)

Zaman *et al*. (1994) subjected six materials (three limestones, sandstone, granite and rhyolite) to cyclic loading and found that the type of aggregate significantly influenced the resilient response, with M_R values for the various materials differing by 20 – 50%. Hicks (1970) studied the effect of surface texture (roughness) and particle shape by

loading crushed and partially crushed materials. M_R was found to be enhanced when the particle shape became more angular and the texture rougher. This finding has since been verified elsewhere (Hicks and Monismith, 1971; Allen and Thompson, 1974; Yoder and Witczak, 1975; Barksdale and Itani, 1989).

2.10.3 Aggregate Grading and Size

The effect of grading on M_R has been deemed insignificant or minor compared to other influences (most notably the stress state or confining pressure) by a number of researchers (Hicks, 1970; Knutson and Thompson, 1977; Rada and Witczak, 1981; Thom and Brown, 1987; 1988; Zaman *et al*., 1994). For example, Zaman *et al*. (1994) witnessed an insignificant change (< 10%) in M_R when the coefficient of uniformity C_u was increased from 43.3 to 65.6. Thom and Brown (1988) studied the effect of grading on the shear stiffness of crushed, dolomitic limestone and identified that uniform specimens are marginally stiffer. Alternatively, Knutson and Thompson (1977) determined that well graded ballast has a slightly higher M_R than the standard (more uniform) No. 4 and No. 5 ballast gradations. In contrast to these studies, Janardhanam and Desai (1983), Thompson (1989) and Sweere (1990) have all documented grading as having a significant influence on M_R.

Janardhanam and Desai (1983) performed true triaxial tests on railway ballast to study the effect of particle size on M_R as a function of different confining pressures. They ascertained that M_R increases with grain size, and at low confining pressures (< 20 psi), an almost linear relationship between M_R and mean grain size was obtained (Figure 2.25). A similar trend was observed by Bosserman (1981) for in-situ railway ballast.

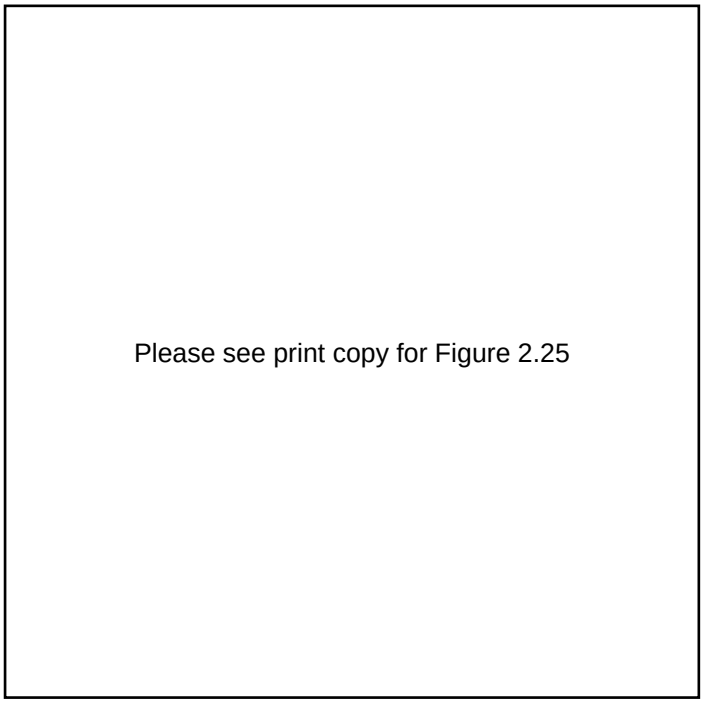

Figure 2.25 Relationship between resilient modulus and mean grain size (after Janardhanam and Desai, 1983)

2.10.4 Placement Density

The majority of research indicates that M_R increases with increasing density (e.g. Coffman *et al*., 1964; Hicks, 1970; Hicks and Monismith, 1971; Allen and Thompson, 1974; Yoder and Witczak, 1975; Lee *et al*., 1995). More recent studies, however, such as those by Thom and Brown (1987 and 1988), Brown and Selig (1991) and Zaman *et al*. (1994) report only a minor density dependency. Allen and Thompson (1974) identified that density effects are more significant at lower bulk stress, and Hicks (1970) concluded that density is more imperative for partially crushed rather than crushed materials.

2.10.5 Stress History and Stress Sequence

Past studies suggest that a single specimen can be used to measure the resilient response for multiple loading paths and stress sequences, providing the failure stress state is not approached (Hicks, 1970; Allen, 1973; Kalcheff and Hicks, 1973; Allen and Thompson, 1974; Yoder and Witczak, 1975; Brown and Hyde, 1975; Knutson and Thompson, 1977; Rowshanzamir, 1995). For example, Rowshanzamir (1995) conducted true triaxial tests on well graded crushed basalt and established that the loading sequence does not affect resiliency. Similarly, Raad and Figueroa (1980) determined that soils maintain their complete M_R characteristics even after large permanent deformations (Figure 2.26). Conversely, Dehlen (1969) reported that M_R can be affected by stress history as a consequence of progressive densification, particle rearrangement, and the development and dissipation of excess pore water pressure. Boyce *et al*. (1976) conducted cyclic loading tests on crushed rock and found that excessive permanent deformation can also influence the magnitude of resilient strain.

2.10.6 Number of Loading Cycles

Yoder and Witczak (1975) and Khedr (1985) established that the number of cycles N has little, if any, significant affect on the magnitude of M_R (Figure 2.27). Alva-Hurtado (1980) and Brown and Selig (1991), nonetheless, identified that providing the material characteristics do not change significantly, the resilient modulus will increase approximately logarithmically with N, as shown in Figure 2.28. There is disagreement regarding the number of cycles required to attain a stable resilient state. Brown (1974) conducted drained triaxial tests on crushed granite and determined that equilibrium

materialises after approximately 10000 cycles whereas other researchers believe as few as 100 cycles are required to achieve stable M_R readings (Dehlen, 1969; Hicks, 1970; Allen, 1973; Allen and Thompson, 1974; Khedr, 1985).

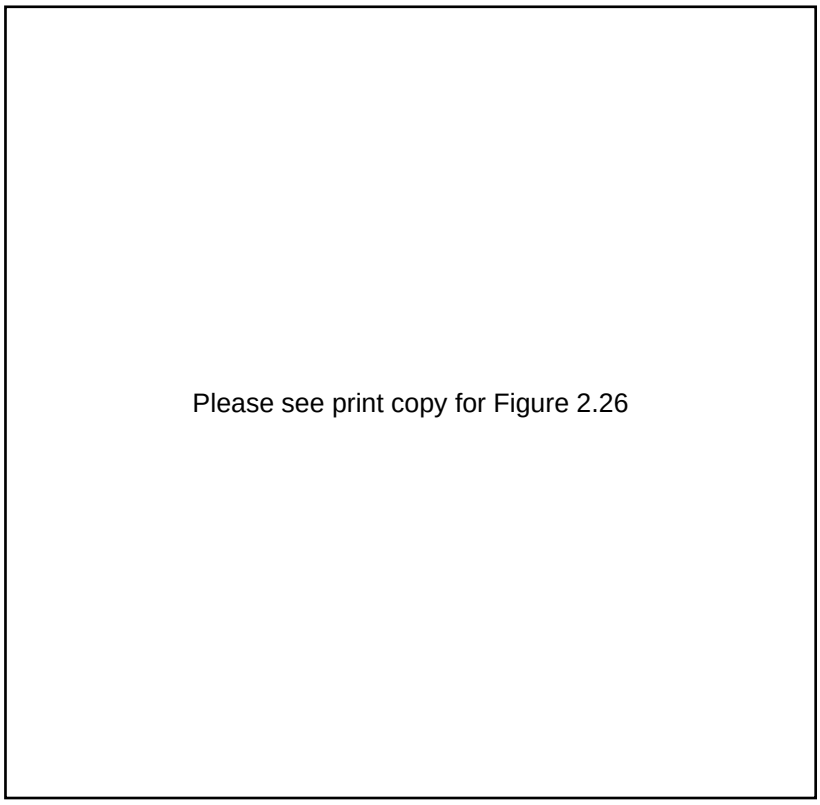

Figure 2.26 Effect of large-scale permanent deformation on the resilient response of granular materials (after Raad and Figueroa, 1980)

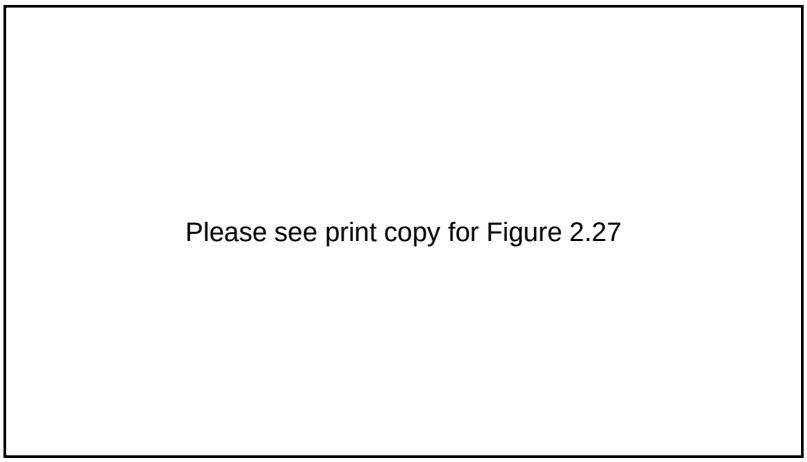

Figure 2.27 Evolution of resilient modulus with number of cycles (after Khedr, 1985)

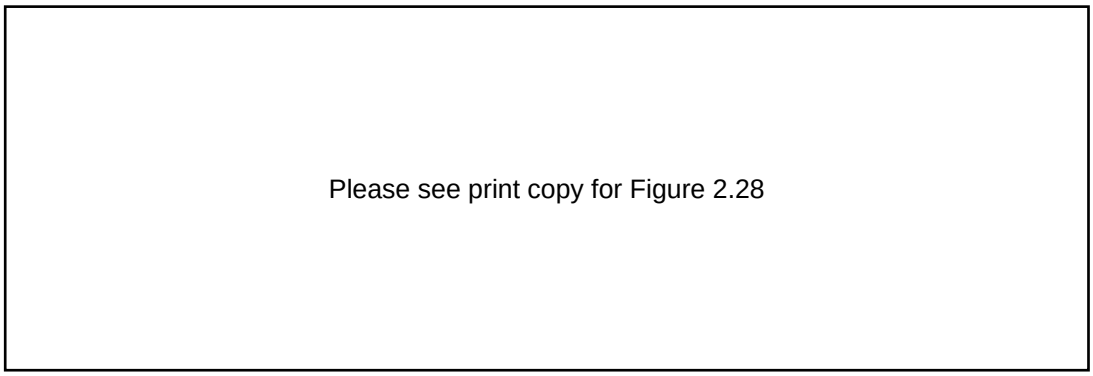

Figure 2.28 Effect of deviator stress and number of cycles on the evolution of resilient modulus (after Brown and Selig, 1991)

2.10.7 State of Stress

Researchers concur that the predominant factor affecting M_R is the magnitude of σ_3' or bulk stress (= $\sigma_1'+\sigma_2'+\sigma_3'$), and it has been established without exception that M_R increases with increasing σ_3' (e.g. Hicks, 1970; Allen, 1973; Allen and Thompson, 1974; Knutson and Thompson, 1977; Khedr, 1985; Jorenby and Hicks, 1986; Sweere, 1990; Zaman *et al*., 1994; Rowshanzamir, 1995; Zeghal, 2004). For instance, Allen and Thompson (1974) recorded a 400% increase in M_R for a crushed limestone aggregate when the bulk stress was increased from 69 to 552 kPa.

The effect of deviator stress on M_R is somewhat uncertain. Zeghal (2004) conducted numerical simulations on assemblies of circular particles and concluded that the magnitude of deviator stress is only significant at low σ_3' (Figure 2.29a). This is in agreement with Trollope *et al*. (1962), Hicks and Monismith (1971), and Chou (1977). In contrast, Brown (1974) showed deviator stress to be significant at low and high values of σ_3', but not at intermediate values (Figure 2.29b). Alternatively, Khedr (1985) established that M_R increases with dynamic deviator stress, in accordance with Seed *et al*. (1967) and Allen (1973).

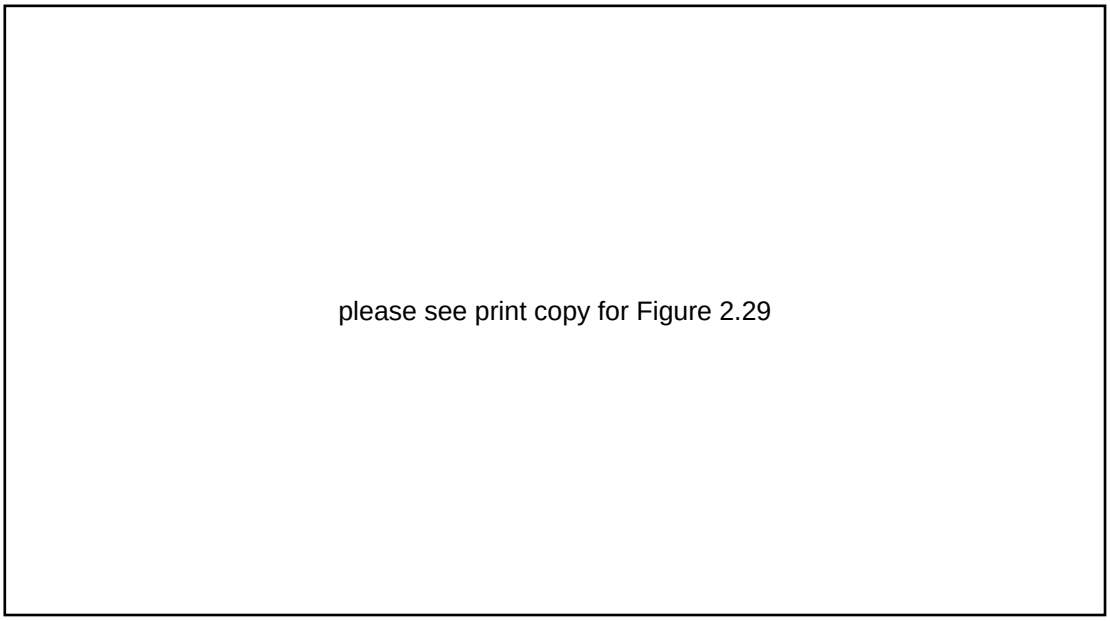

Figure 2.29 Effect of deviator stress and confining pressure on resilient modulus, (a) after Zeghal (2004), and (b) after Brown (1974)

2.10.8 Resilient Modulus Relationships

Table 2.8 summarises numerous non-linear models developed to relate the magnitude of resilient modulus M_R to the state of stress. These models can be divided into two categories, single stress and multi-stress parameter models, based on the number of incorporated stress terms (i.e. σ_3', deviator stress, or bulk stress). The most frequently used relationship in Table 2.8 is known as the 'K-θ' model (Seed *et al*., 1967). Whilst this equation is simple to apply, it has a number of disadvantages including:

1) it assumes M_R is independent of the deviator stress (Hicks, 1970; Shackel, 1973b),
2) it cannot adequately describe the change in M_R with stress state (Uzan, 1985), and
3) it is dimensionally unsatisfactory, k_2 is dimensionless and k_1 has dimensions of MPa (Nataatmadja, 1989).

Table 2.8 Non-linear models relating resilient modulus to stress state

Please see print copy for Table 2.8

Numerous studies (e.g. Shackel, 1973a; Brown, 1974; Uzan, 1985; Nataatmadja and Tan, 2001) have demonstrated that the resilient response of granular materials depends on the magnitude of deviator stress and the bulk stress or confining pressure. For this reason, multi-stress parameter models were developed that independently incorporate both the axial and lateral stress states. The multi-stress models outlined in Table 2.8 were formulated based on experimental data obtained by each researcher, and are therefore capable of reproducing and/or estimating M_R under limited testing environments. Rhee (1991) collected published data and conducted a statistical analysis to determine the applicability of various models, and proclaimed the Uzan (1985)

equation (Table 2.8) as superior due to its empirical validation and theoretical basis. This model, however, has three material constants and for this reason is less than ideal.

2.10.9 Effects of In-Situ Ballast Resilient Modulus

The track modulus u′ (Equation 2.7), defined as the pressure per unit length of rail required to cause unit track deflection, is commonly used to evaluate the track quality and stiffness characteristics. In Equation 2.7, Q is the wheel load, y_r the rail deflection, E_r the rail modulus, and I_r the rail moment of inertia. The resiliency of rail track components affects track vibration, noise radiation, and contact forces between the wheel and rail (Wu and Thompson, 1999). The resilient modulus of the ballast layer contributes to the overall track stiffness, and greater stiffness is known to be beneficial in terms of reducing the energy required for train movement, reducing ballast wear, and providing superior load spreading abilities. Other sources of resiliency include the subgrade and rail pads. Passenger comfort will suffer if the track modulus is too low, but excessive track modulus can lead to increased rates of vehicle and track component deterioration (Selig and Alva-Hurtado, 1982; Brown and Selig, 1991).

$$u' = \frac{1}{4}\sqrt[3]{\left(\frac{Q}{y_r}\right)^4 \frac{1}{E_r I_r}} \qquad (2.7)$$

Increasing the granular layer stiffness (ballast and/or capping resilient modulus) is an effective technique for reducing the stresses projected onto the subgrade (Figure 2.30). Table 2.9 provides typical M_R values for in-situ ballast and subgrade materials, and Figure 2.31 emphasises the effect of bulk stress on M_R for each substructure stratum.

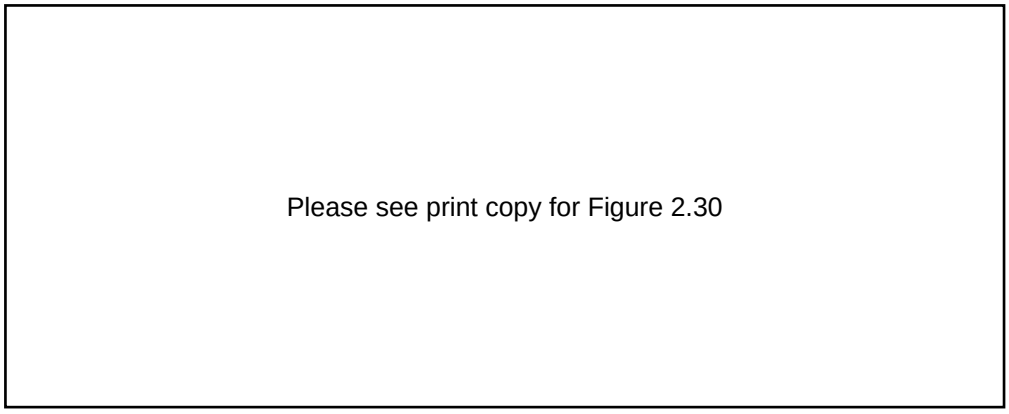

Figure 2.30 Effect of increased granular layer stiffness on deviator stress levels in the subgrade (after Brown and Selig, 1991)

Table 2.9 Typical ballast and subgrade resilient modulus values for railway lines (after Li and Selig, 1998)

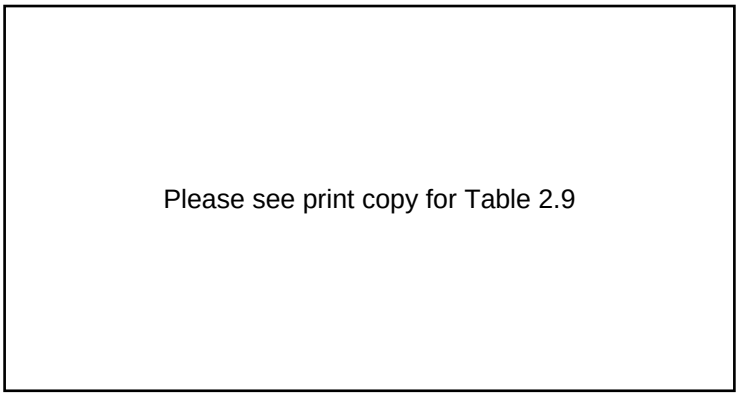

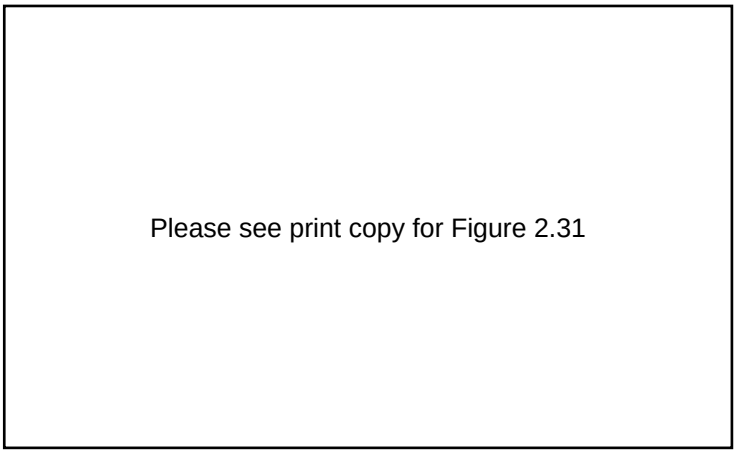

Figure 2.31 Effect of bulk stress on resilient modulus of granite ballast, subballast and subgrade (after Selig and Alva-Hurtado, 1982).

CHAPTER 3

LABORATORY PROCEDURES

3.1 Introduction

The deformation and degradation response of railway ballast under cyclic compression loading has been investigated using a series of large-scale triaxial experiments. Ballast specimens were subjected to a range of loading magnitudes to simulate the in-situ sleeper-ballast contact pressures currently existing in Australia. Details regarding the large-scale equipment, testing material, specimen preparation methods, testing procedure, and data analysis processes are presented below.

3.2 Large Scale Triaxial Apparatus

The testing of coarse aggregates in conventional apparatus can give misleading results due to the disparity between particle and equipment size. As the ratio of specimen to maximum particle size approaches six, equipment size effects can be ignored (Marachi *et al*., 1972; Indraratna *et al*., 1998). Due to the substantial physical dimensions associated with ballast, a large-scale triaxial apparatus was designed and built at the University of Wollongong (Figures 3.1a and 3.1b). Originally intended for static or monotonic loading, the apparatus was recently upgraded with a dynamic actuator to allow the simulation of high-speed cyclic train loading. Details on the dynamic actuator can be found in Appendix C. The triaxial apparatus can incorporate specimens 300 mm in diameter and 600 mm high, and consists of five main parts:

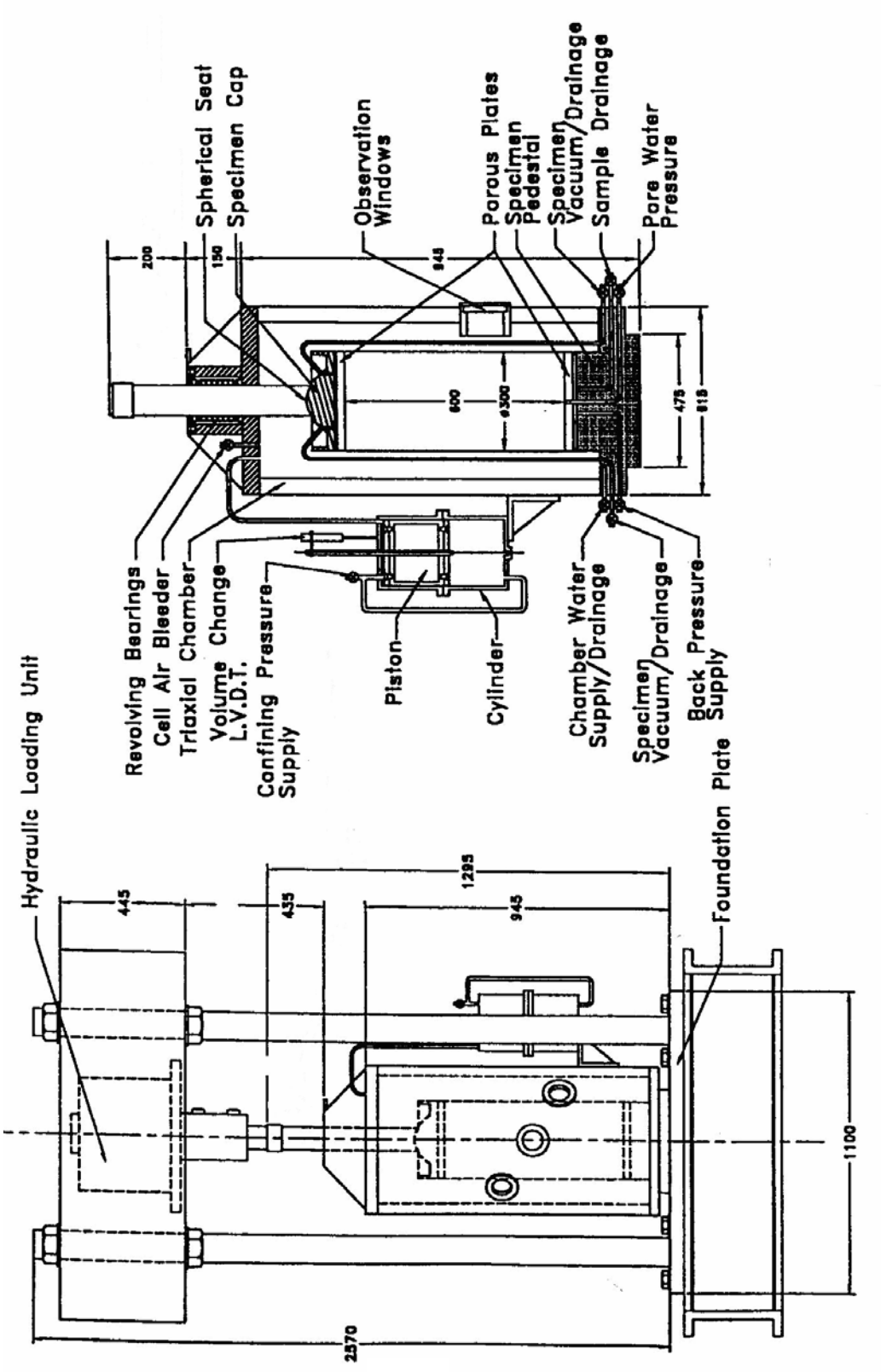

(a)

Figure 3.1 Large-scale triaxial apparatus, (a) Schematic (continued over page)

(b)

Figure 3.1 Large-scale triaxial apparatus (continued), (b) Photograph

1) A triaxial chamber surrounding the membrane and enclosed ballast sample (Figure 3.2a),

2) A high frequency test rig (dynamic actuator, Figure 3.2b),

3) A confining pressure system (Figure 3.2c) utilising both compressed air and water,

4) A back pressure system (a head of water), and

5) A volume change measurement device (Figure 3.2d).

Further details on the triaxial apparatus can be found in Indraratna (1996) and Indraratna *et al*. (1998).

3.3 Characteristics of the Testing Material

Current standards for railway ballast (e.g. Standards Australia, 1996) specify the physical and durability requirements of the parent rock, but do not evaluate performance under in-situ track conditions (Chrismer, 1985; Indraratna et al., 1998). Igneous material has been shown to be particularly suitable for use on railway tracks because of its relatively high compressive strength, particle hardness, and resistance to weathering (Salim, 2004). In the current study, all test specimens were comprised of fresh latite basalt, a quarried igneous aggregate commonly used as railway ballast in New South Wales, Australia. Latite basalt is a dark coloured volcanic (igneous) rock containing the main minerals feldspar, plagioclase and augite and its physical and durability attributes are shown in Table 3.1. Figure 3.3 illustrates the appearance and shape of the testing material. Table 3.2 and Figure 3.4 demonstrate the particle size distribution utilised in the present study to examine the effects of confining pressure and deviator stress magnitude, which is representative of current industry practice (Standards Australia, 1996). In addition to these tests, four different gradations were used to investigate the effects of particle size distribution (PSD) on ballast behaviour, and these are depicted in Figure 3.5 and Table 3.3. A maximum particle size of 53 mm was chosen to ensure a satisfactorily high specimen to particle size ratio of 5.7 for most tests, however the more well graded specimens in Table 3.3 did contain particles up to 63 mm in diameter.

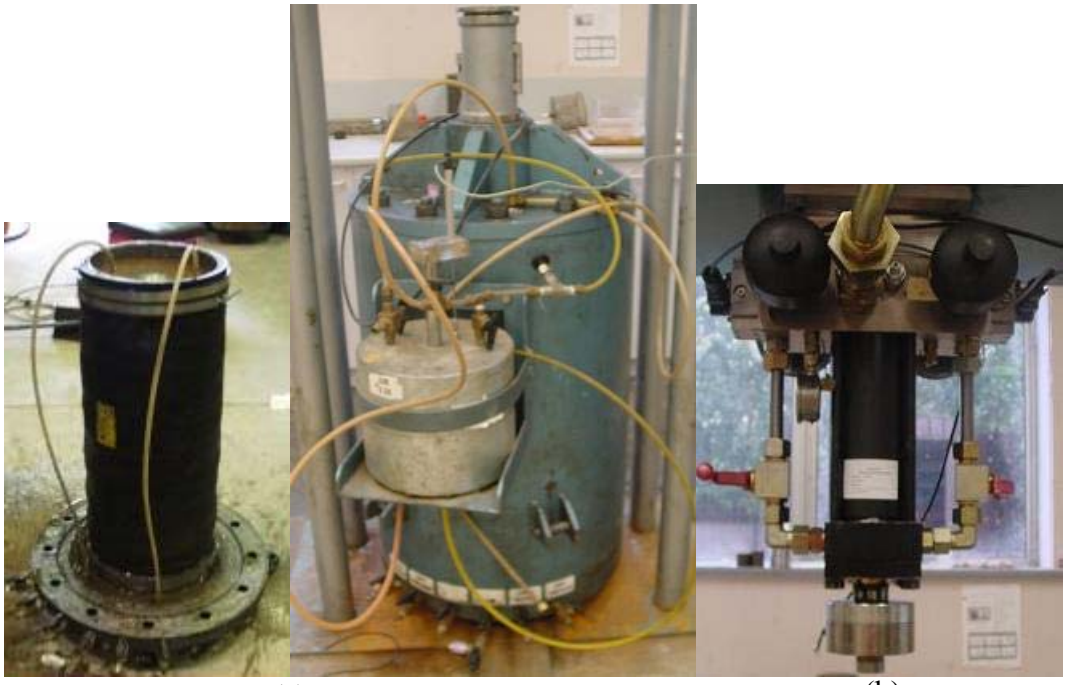

(a) (b)

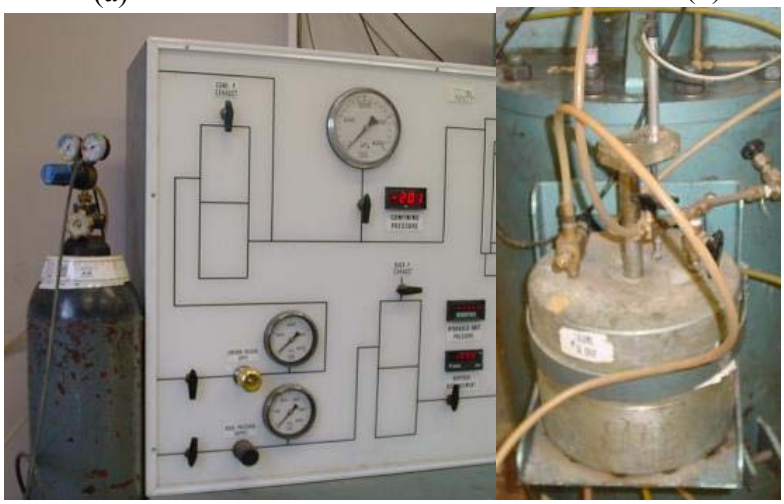

(c) (d)

Figure 3.2 Additional details of the testing apparatus, (a) The triaxial chamber and membrane, (b) The dynamic actuator, (c) The confining pressure system, and (d) The volume change measurement device

Table 3.1 Physical and durability characteristics of latite basalt (after Indraratna *et al*., 1998 and Salim and Indraratna, 2002)

Please see print copy for Table 3.1

Figure 3.3 Physical appearance of latite basalt

Table 3.2 Particle size distribution used in most tests, and industry practice upper and lower bounds (Standards Australia, 1996)

Please see print copy for Table 3.2

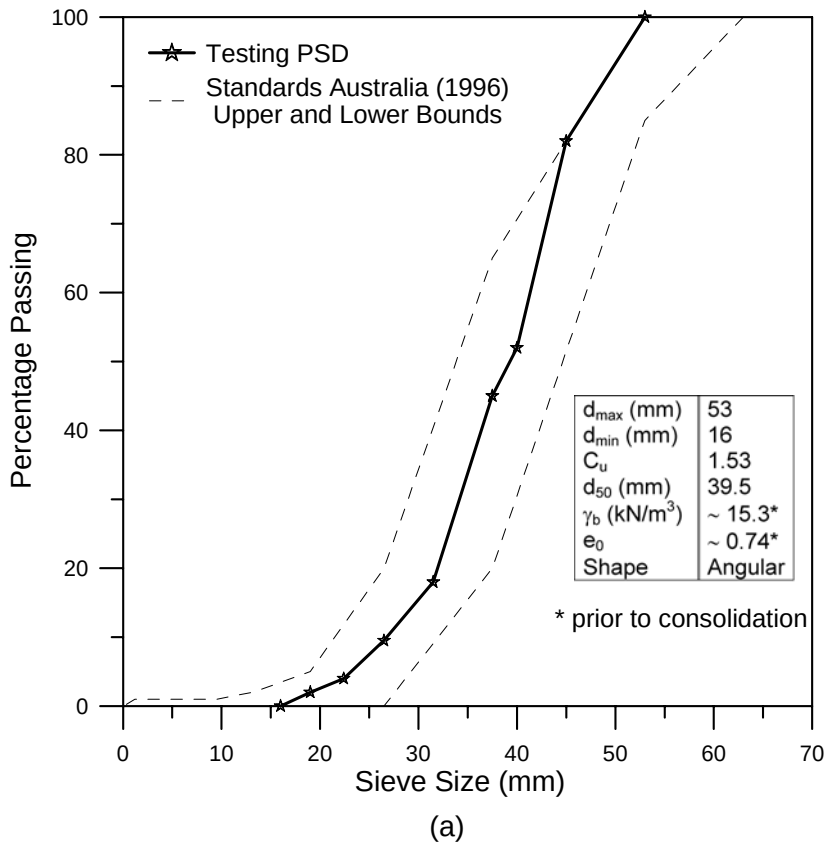

(a)

Figure 3.4 Specimen particle size distribution, and current industry distributions

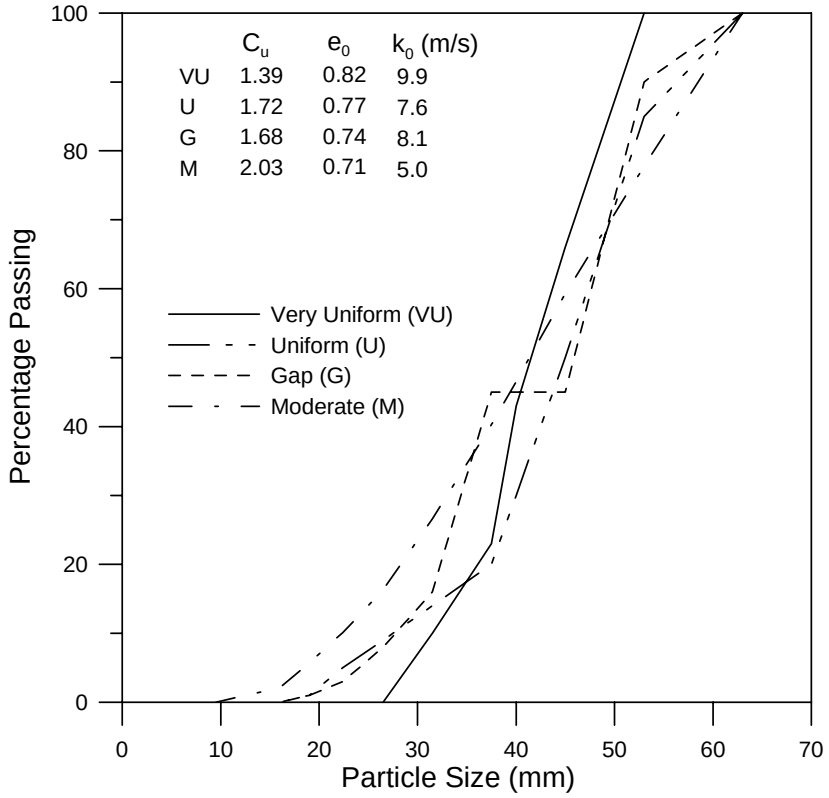

Figure 3.5 Particle size distributions used to investigate the effect of grading

Table 3.3 Particle size distributions used to examine the effects of grading

Sieve Size (mm)	Very Uniform C_u = 1.39	Uniform C_u = 1.72	Gap C_u = 1.68	Moderate C_u = 2.03
	Percentage Passing			
63	-	100	100	100
53	100	85	90	78
45	66	50	45	59
40	43	30	45	47
37.5	23	20	45	40
31.5	10	14	16	27
26.5	0	9	8	16
22.4	-	5	3	10
19	-	1	1	6
16	-	0	0	2
9.5	-	-	-	0

3.4 Preparation of Ballast Specimens and Testing Procedure

The latite basalt was washed using a high-pressure hose to remove any dust and clay adhering to the surface of the particles and then sorted into the required distribution by utilising at least two passes through a set of 13 standard sieves (aperture size 63 – 2.36 mm). Two passes were found to be necessary to guarantee the accuracy of the initial distribution and the integrity of the breakage results. Upon drying, the correct weight of each size in accordance with Figure 3.4 (or Figure 3.5) was mixed to ensure a reasonable degree of sample homogeneity. Following the preparation of the aggregate, a 5 mm thick rubber membrane (Figure 3.2a) was secured to the cell base using steel hose clamps to preclude water leakage during testing. The membrane had to be thick enough to prevent piercing by sharp particles.

The preliminary experiments conducted considered the effect of particle size distribution (PSD) on ballast behaviour. These specimens were compacted in ten layers for approximately sixty seconds per layer within a split cylindrical mould using a jackhammer with a specially attached fitting and rubber pad to minimise particle breakage. It was identified, however, that this compaction duration was excessive and caused a noteworthy degree of breakdown. It is thought, however, that this occurrence would not affect the qualitative analysis of the effect of PSD on ballast degradation behaviour, providing the compaction time is equivalent for each PSD specimen. It is well known that graded aggregates can be compacted to higher densities than uniform specimens. Therefore, in order to mimic field conditions as closely as possible, PSD specimens were compacted to equivalent heights and specimens varied in initial density and void ratio (see Figure 3.5).

Subsequently, the ballast for all other experiments was compacted in eight layers for approximately 25 seconds per layer. In order to prevent over-compaction of the lower layers, the depth of each layer was gradually decreased (i.e. the bottom layer was the thickest and the top layer the thinnest) with the compaction time remaining constant for each layer. This method is similar to the under-compaction concept of Ladd (1978) and Budiman and Wibowo (1993), and results in a relatively uniform initial specimen density and minimal breakage associated with high contact stresses at the base of the triaxial chamber. The degree of breakage caused by compaction was measured by subjecting some samples to 'compaction only' (i.e. no cyclic shearing was conducted). It was confirmed that the method of compaction (8 layers at 25 sec/layer) caused insignificant degradation compared to cyclic shearing, illustrating the importance of compaction duration on particle breakage. Following compaction, specimens had initial void ratios and bulk unit weights of approximately 0.72 – 0.76 and 15.3 kN/m^3, respectively, and these values simulate those expected for heavy haul tracks.

All ballast specimens were saturated using a small back pressure and allowed to settle overnight with sample saturation ensured (B > 0.96) immediately prior to shearing. During the application of σ_3', changes in specimen volume and void ratio *e* were recorded, and typical changes in *e* during consolidation ranged from 0.05 at smaller σ_3', to 0.2 when σ_3' = 240 kPa. An initial static load was applied to each specimen at a rate of 1 mm/sec to a stress amplitude equal to the average of the minimum and maximum cyclic deviator stress. Loading frequencies up to 20 Hz were utilised in the experiments to simulate high speed train loading, nevertheless, a conditioning phase at 1 Hz loading frequency was necessary at the commencement of the loading regime (during rapid

vertical deformation) to prevent impact loading and loss of actuator contact with the specimen, and to allow adequate dissipation of excess pore water pressure. Assuming a minimum 2 m spacing between axles, 20 Hz corresponds to a train speed of 144 km/hr. The cyclic load was alternated between two compressive stress states, $q_{min,cyc}$ (= $\sigma_1'_{min}$ - σ_3') and $q_{max,cyc}$ (= $\sigma_1'_{max}$ - σ_3'), where σ_1' and σ_3' are the major and minor effective stresses, as indicated in Figure 3.6. A $q_{min,cyc}$ value of about 45 kPa was used in each test to represent the vertical stress caused by superstructure components in the unloaded condition, and also to prevent a loss of actuator-specimen contact as discussed above. The maximum deviator stress $q_{max,cyc}$ defines the magnitude of cyclic loading. Loading continued until the desired number of cycles was completed, or the maximum vertical deformation of the apparatus was obtained (about 25% axial strain). In addition to the single amplitude tests, a number of stepwise (gradually increasing) loading tests were conducted. All experiments were isotropically consolidated, saturated, drained, cyclic, one-way compression tests. Following cyclic shearing, the specimens were dried and the breakage magnitude evaluated following a repeat of the sieving procedure. Membrane corrections were calculated using the ASTM (2002) method assuming an axial strain of 20%, a membrane thickness of 5 mm and a membrane elastic stiffness of 1100 kPa, resulting in a required correction for deviator stress of 15 kPa. This value was deemed insignificant for most specimens (< 3% error), with the remaining specimens adjusted as required.

3.5 Deviatoric Load Calculation Method

As described in Section 2.3 (Chapter 2), determining the magnitude of a 'typical' sleeper-ballast contact pressure resulting from a 'standard' train axle load relies on some

fairly significant simplifications regarding impact and velocity forces. Calculation methods are entirely empirical in nature (e.g. the dynamic impact factor ϕ' computation procedures in Appendix A, or estimated load percentages per sleeper) and offer only rough estimates for complex transfer processes. Nevertheless, the dynamic impact factor approach was utilised for the initial experiments conducted as outlined in Table 3.4. For instance, the $q_{max,cyc}$ = 230 kPa experiments were originally designed to represent a 25 tonne axle load with no vertical excitation ($\phi' = 0$) based on a number of simplifying criteria. Similarly, $q_{max,cyc}$ = 300 kPa (particle size distribution) tests involved a 25 tonne axle load multiplied by a ϕ' value of 1.3 to represent a 'good' track (according to Section 2.3.2, Chapter 2).

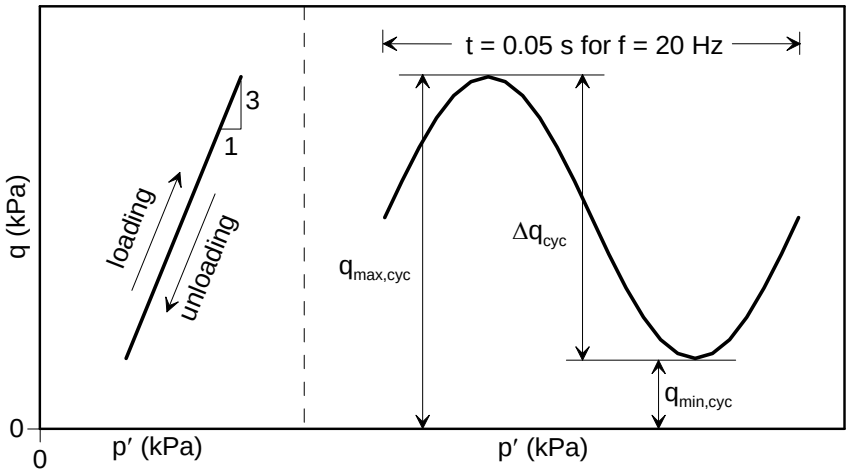

Figure 3.6 Cyclic stress state and loading path in the current tests

Due to the large degrees of uncertainty associated with current sleeper-ballast contact pressure estimations, instead of using the ϕ' procedure to calculate $q_{max,cyc}$ in all remaining tests, stress values were selected based on allowable pressures specified by various researchers in Section 2.3.4 (Chapter 2). Using this approach, a certain $q_{max,cyc}$

value, say 500 kPa, could represent different tonnages, each with a particular (and varying) dynamic impact factor.

Table 3.4 Summary of triaxial tests

$q_{max,cyc}$ (kPa)	σ_3' (kPa)	Number of Cycles	Frequency (Hz)	$q_{max,cyc}/p'$	Other
300	45	500000	20	2.07	C_u = 1.39, see Figure 3.5
〃	〃	〃	〃	〃	C_u = 1.72, see Figure 3.5
〃	〃	〃	〃	〃	C_u = 1.68, see Figure 3.5
〃	〃	〃	〃	〃	C_u = 2.03, see Figure 3.5
230	1	500000	20	2.96	C_u = 1.53, see Figure 3.4
〃	8	〃	〃	2.72	〃
〃	30	〃	〃	2.16	〃
〃	60	〃	〃	1.68	〃
〃	120	〃	〃	1.17	〃
〃	240	〃	〃	0.73	〃
500	3	500000	20	2.95	〃
〃	10	〃	〃	2.83	〃
〃	20	〃	〃	2.68	〃
〃	30	〃	〃	2.54	〃
〃	45	〃	〃	2.36	〃
〃	60	〃	〃	2.21	〃
〃	90	〃	〃	1.95	〃
〃	120	〃	〃	1.74	〃
〃	180	〃	〃	1.44	〃
〃	240	〃	〃	1.23	〃
750	120	2	20	2.03	〃
〃	〃	1000	〃	2.03	〃
〃	〃	10000	〃	2.03	〃
〃	〃	25000	〃	2.03	〃
〃	〃	500000	〃	2.03	〃
〃	〃	2000000	〃	2.03	〃
〃	240	500000	20	1.53	〃
〃	60	〃	〃	2.42	〃
〃	30	500000	〃	2.68	〃
1000	120	500000	〃	2.21	〃
1250	120	500000	〃	2.33	〃
increasing	120	141000	20	--	5000 cycles/interval
increasing	120	295000	〃	--	10000 cycles/interval
increasing	60	101030	〃	--	5000 cycles/interval

3.6 Data Analysis Methods

3.6.1 Permanent Strain (Axial and Volumetric)

The permanent axial deformation was measured using a position transducer within the actuator interfaced with a datataker (datalogger). During shearing, the actuator never losses contact with the specimen (unloads), therefore the downward movement of the actuator replicates the specimen deformation. A 20 mm change in the actuator position would, for example, correspond to a 20 mm decrease in the specimen height. This system performs the same task as an externally mounted linear variable differential transducer (LVDT).

A volume change device (Figure 3.2d) was utilised to measure the specimen volumetric strain. A piston within the device responds to water entering the (dilating) specimen or leaving the (compressing) specimen, and an LVDT and datataker record the piston movement. 1mm of piston movement corresponds to a 34.5 cm^3 loss (or gain) in specimen volume. Radial strain ε_r and shear strain ε_s can be calculated using 3.1 and 3.2, respectively, where ε_a and ε_v are the major principal strain and volumetric strain (positive in compression), respectively. Additionally, Equation 3.3 defines the mean effective stress p′. Under drained loading conditions, a typical stress path has a slope of 3 (Figure 3.6). An increase in σ_3' produces a shift in the stress path towards a higher value of p′, and increasing $q_{max,cyc}$ (or decreasing $q_{min,cyc}$) simply lengthens the stress path. Both confining pressure and back pressure variations were recorded using transducers at the base of the specimen, and the relatively small stress distribution attributed to specimen self-weight has been incorporated in the effective stresses.

$$\varepsilon_r = (\varepsilon_v - \varepsilon_a)/2 \quad (3.1)$$

$$\varepsilon_s = 2/3(\varepsilon_a - \varepsilon_r) \quad (3.2)$$

$$p' = 1/3\ (\sigma_1 + 2\sigma_3') \quad (3.3)$$

Axial and volumetric straining behaviour during the cyclic triaxial tests is compared to monotonic test results on latite basalt by Indraratna *et al*. (1998) and Salim (2004) in order to evaluate the differences in behaviour.

3.6.2 Breakage Quantification

Various particle breakage indices have been proposed to quantify the degree of particle breakage in granular materials (Appendix B), and in general these techniques are based on: a) the increase in percent passing a single sieve size, or b) changes to the entire particle size distribution. One breakage index that utilises the latter technique is the surface area method (e.g. Miura and O′Hara, 1979). Whilst this method is highly successful for some aggregates it requires an assumption of particle shape, which is difficult for highly angular aggregates such as ballast. Therefore, ballast breakage analysis is better suited to a method based solely on sieve analysis where no assumptions are necessary.

Previous triaxial testing on ballast has shown that particle degradation causes a shift in the initial particle size distribution towards smaller particle sizes, with the maximum size unchanged before and after loading (e.g. Indraratna *et al*., 1998). This shift in the distribution curve traces out an area *A* (Figure 3.7). The greater the breakage the larger

the shift in the gradation curve from its original position, thus the greater the value of *A*. In conventional particle size distribution curves, the horizontal axis (particle sizes) is expressed on a log scale, mainly because of the high range of grain sizes (from microns to cm) that need to be considered, for example in well graded soils. However, ballast is uniform and has a narrow range of particle sizes and C_u values, allowing a linear scale to be used for the horizontal axis. This greatly simplifies the calculation of Area *A*, and results in *A* having units of mm.

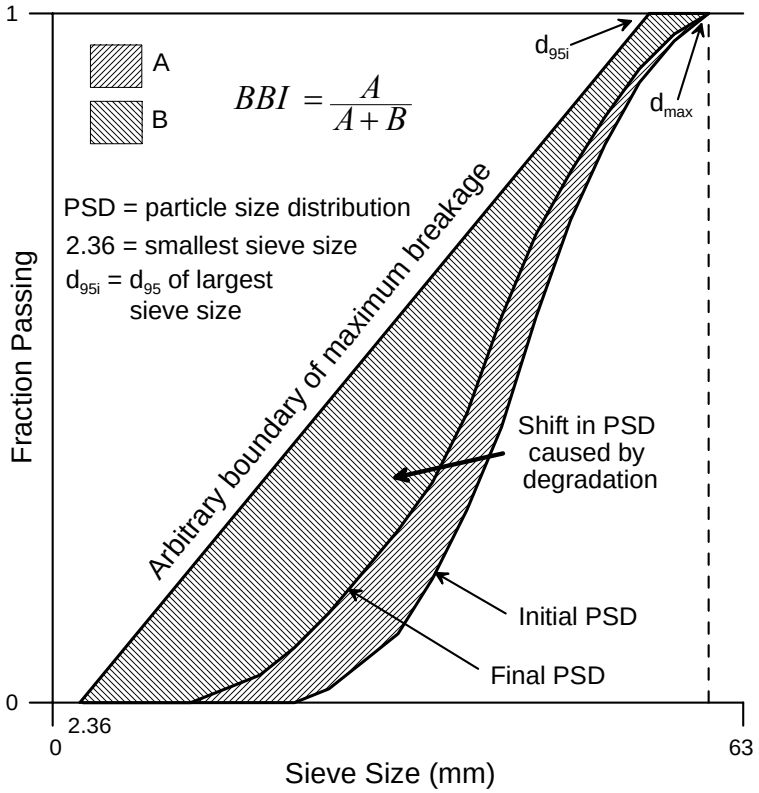

Figure 3.7 Evaluation of the Ballast Breakage Index (BBI)

Hardin (1985) defined the upper breakage limit for sands by a breakage potential B_p after assuming that high pressure loading can reduce all particles to silt sized particles (see Appendix B). Whilst it is theoretically possible for the same to be achieved with ballast, the considerably lower stresses encountered during train loading prevent total particle annihilation from occurring. Therefore, instead of defining the breakage

potential by a single minute particle size, in reality it is more appropriate to consider an arbitrary boundary of maximum breakage (Figure 3.7). This boundary is governed by the availability of the smallest sieve size (2.36 mm in this case) and signifies a practical upper limit for ballast breakage, extending from d_{95} of the maximum sieve aperture d_{max} to the smallest sieve aperture d_{min}. The Ballast Breakage Index (*BBI*) (Equation 3.4) is therefore proposed as a suitable method for representing ballast degradation. *A* is the area as defined previously, and *B* is the potential breakage or the area between the arbitrary boundary of maximum breakage and the final particle size distribution (Figure 3.7).

It is important to note, however, that the use of d_{95} may not be suitable for ballasts that do not have the traditional uniform gradation with C_u of approximately 1.5 - 1.6. For ballast gradings that are either more broadly graded or have only a small percentage of the largest particle size, it may be possible for the PSD curve to actually intersect the $d_{95} - d_{min}$ boundary. In the event of this scenario, an alternative maximum sieve size aperture such as (say) d_{85} can be employed, as the upper constraint of the boundary is arbitrary and has no physical significance. In this thesis, d_{95} has been utilised for all tests. BBI has a lower limit of 0 (no breakage) and an upper limit of 1. BBI is qualitatively similar to the relative breakage B_r of Hardin (1985) and both methods give comparable breakage trends.

$$BBI = \frac{A}{A+B} \tag{3.4}$$

It is also important to note that both BBI and B_r are only suitable when a single particle size distribution is being examined. If various gradations are under investigation, the

denominator ($A + B$) in Equation 3.4 differs for each distribution, making a comparison of the different gradings difficult. The area A or an alternative breakage quantification method such as B_g (Marsal, 1973, Appendix B) may provide a better assessment of the effects of particle size distribution on particle degradation. In this thesis, a variety of breakage quantification methods have been employed to represent the degree of degradation for the specimens with different PSD.

3.6.3 Resilient Modulus

Bursts of data (1000 readings in 1.7 seconds, sampling frequency 590 Hz) were collected by the dynamic actuator control program GOUI (see Appendix C) to evaluate the resilient modulus M_R. The bursts were sampled over two channels, load (later converted to stress) and actuator position (recoverable or resilient strain). M_R is calculated according to Equation 3.5, where Δq_{cyc} is the magnitude of deviator stress as defined in Figure 3.6, and $\varepsilon_{a,rec}$ is the recoverable portion of axial strain (Figure 2.24).

$$M_R = \Delta q_{cyc} / \varepsilon_{a,rec} \qquad (3.5)$$

It was identified during each burst that electrical noise was interfering with the return signal, resulting in misleading M_R values. A method devised to remove this noise, hence allowing the proper determination of M_R can be found in Appendix D.

3.7 Summary of Cylindrical Triaxial Experiments

A total of 34 cyclic triaxial tests (Table 3.4) were conducted to investigate the effects of confining pressure (σ_3'), cyclic deviator stress magnitude ($q_{max,cyc}$), grading (PSD) and the number of cycles (N) on the permanent (plastic) strain, resilient modulus, and breakage of ballast. Some of the tests were repeated to verify the reliability of data. The levels of $q_{max,cyc}$ utilised are typical of the stresses currently permitted in tracks (Standards Australia, 1997a), with $q_{max,cyc}$ amplitudes > 750 kPa included to represent the higher axle loads of freight trains planned in the near future.

CHAPTER 4

PERMANENT AND RESILIENT STRAIN BEHAVIOUR OF BALLAST UNDER CYCLIC LOADING

4.1 Introduction

This Chapter presents and discusses the permanent and resilient strain deformation behaviour of railway ballast resulting from a series of drained, constant confining pressure, high frequency, cyclic, one-way compression triaxial tests. The main areas of investigation are the effects of confining pressure and deviator stress magnitude on permanent (axial and volumetric) and resilient strain behaviour as a function of the number of loading cycles N. The effect of the aggregate particle size distribution (PSD) is also investigated. All experiments were conducted at 20 Hz loading frequency. Previous static test results for latite basalt supplied by Salim (2004) and Indraratna *et al*. (1998) form the basis of a comparison between the static and cyclic response. Experimental data in relation to breakage and degradation behaviour can be found in Chapter 5, and Chapter 6 details the results of variable amplitude tests.

This Chapter begins with a definition of specimen failure under constant amplitude cyclic loading, which is important in characterising ballast response and identifying the loading conditions that are likely to cause detrimental in-situ performance. The effects of confining pressure and deviator stress magnitude on the axial and volumetric strain of specimens is investigated next, followed by a comparison of the behaviour of ballast under static and cyclic loading, and the effects of grading. The Chapter concludes with a consideration of the long-term elastic response (resilient modulus) of ballast.

4.2 Specimen 'Failure' under Constant Amplitude Cyclic Loading

During static triaxial testing of ballast it is customary for loading to continue until a certain predetermined value of axial strain ε_a has been obtained, for example 20%. Specimen failure is defined at the peak deviator stress $q_{peak,sta} = (\sigma_1' - \sigma_3')_{peak}$, and this value corresponds to the maximum load carrying capacity of the specimen. The magnitude of $q_{peak,sta}$ is dependent on specimen loading conditions, in particular the effective confining pressure σ_3', the applied strain rate, and drainage characteristics. Unlike small-grained materials such as sand, no distinct failure plane or shear band is observed in large granular specimens. Instead, failure is usually accompanied by specimen 'bulging' (Indraratna *et al*., 1998).

Identifying a location of specimen 'failure' during cyclic loading, which may be signified by a loss of bearing capacity or some other mechanism, is fundamental in appreciating the strength limitations of materials exposed to repeated loading environments. During drained, stress controlled, cyclic loading at high frequency and constant deviator stress magnitude $q_{max,cyc}$ (Figure 3.6), the onset of 'failure' is somewhat difficult to ascertain due to the absence of a peak stress or a characteristic location of material weakening or softening. Past research has identified that specimen settlement is most significant during the initial loading cycles (e.g. Alva-Hurtado and Selig, 1981; Jeffs and Marich, 1987; Anderson and Key, 2000; Dahlberg, 2001). If the strength of the material is exceeded during this period (i.e. during the first cycle for constant $q_{max,cyc}$) then rapid axial strain ε_a and large expansive radial strains ε_r would result. The strength will continue to be exceeded temporarily with each successive loading cycle until the accumulative axial strain becomes extensive and the specimen

'fails'. The situation is vastly dissimilar to undrained loading where the build-up of excess pore water pressure and the subsequent commencement of liquefaction is the precursor to specimen failure. Two methods that could suitably define specimen failure under drained cyclic loading include:

1) Relating the rate of strain accumulation $d\varepsilon_a/dN$ to some constant C that characterises stable and unstable (failing) behaviour, such that failure occurs when $d\varepsilon_a/dN \geq C$, or
2) Utilising an arbitrary level of unacceptable strain accumulation, say 20 – 25%.

Any estimation of a constant C would be difficult because a material may still perform satisfactorily in the long-term following high initial rates of strain. Failure of large ballast specimens under drained repeated loading appears to be more appropriately defined by an arbitrary level of axial strain accumulation, and $\varepsilon_a \geq 25\%$ has been chosen as the failure criterion for the ballast specimens. In the current study, $\varepsilon_a \approx 25\%$ corresponds to the maximum vertical displacement of the testing rig and therefore represents the upper limits of specimen deformation. Taking into consideration rail track design, a 25% axial strain in the ballast layer translates to a 75 mm loss in track geometry for the standard 300 mm ballast thickness. In the absence of failure the magnitude of ε_a achieved at the end of a fixed number of cycles N is dependent on the amplitudes of both $q_{max,cyc}$ and σ_3', and the breakage resistance of the particles.

It is important to note that 'failure' ($\varepsilon_a \geq 25\%$) under constant amplitude cyclic loading does not necessary imply a loss of specimen strength. Even after considerable vertical deformation specimens may still support the applied cyclic loads, and have thus not

'failed' in the traditional sense (i.e. loss of load bearing capacity). Even though the ballast layer may still be structurally sound after a significant degree of settlement, problems such as poor catenary/train contact or clearance issues can arise. Large-scale vertical track movement should therefore be avoided and the employment of an arbitrary level of strain accumulation is justified as a suitable failure criterion. The following section examines the effects of σ_3', $q_{max,cyc}$, and N on the axial strain ε_a response of railway ballast.

4.3 Permanent Axial (Shear) Strain Response

The axial strain ε_a response of selected specimens as a function of the number of loading cycles N is shown in Figure 4.1. The data relating to all specimens has been excluded here (and in some later sections of this chapter) for increased clarity. As anticipated, Figure 4.1 indicates decreasing ε_a with increasing σ_3'. When the magnitude of $q_{max,cyc}$ (or stress ratio $q_{max,cyc}/p'$) is sufficiently large, ε_a will continue to accumulate with N until $\varepsilon_a \geq 25\%$ (e.g. the specimen with $q_{max,cyc}$ = 750 kPa and σ_3' = 30 kPa in Figure 4.1). Stable conditions (shakedown) occur when ε_a remains below 25% during the initial few thousand cycles, albeit after significant deformation in the case of specimens with relatively small σ_3' and large $q_{max,cyc}$. In concurrence with previous studies (Brown, 1974; Raymond and Ismail, 2003) less than 10000 loading cycles are required for the stabilisation of permanent ε_a. A simple method of estimating the number of cycles necessary to attain shakedown is to plot the rate of axial strain $d\varepsilon_a/dN$ against N and discern the point at which $d\varepsilon_a/dN$ becomes negligibly small (approaches zero). An example of this technique is illustrated in Figure 4.2 for $q_{max,cyc}$ = 750 kPa and a selection of σ_3' values. The rate of ε_a accumulation is greatest during the initial cycles,

and becomes relatively insignificant after only 1000 loading cycles. In agreement with Figure 4.1, $d\varepsilon_a/dN$ is greater for smaller σ_3' in Figure 4.2. Figure 4.3 plots the influence of $q_{max,cyc}$ on ε_a, and clearly for a given σ_3' the degree of deformation increases with the loading amplitude.

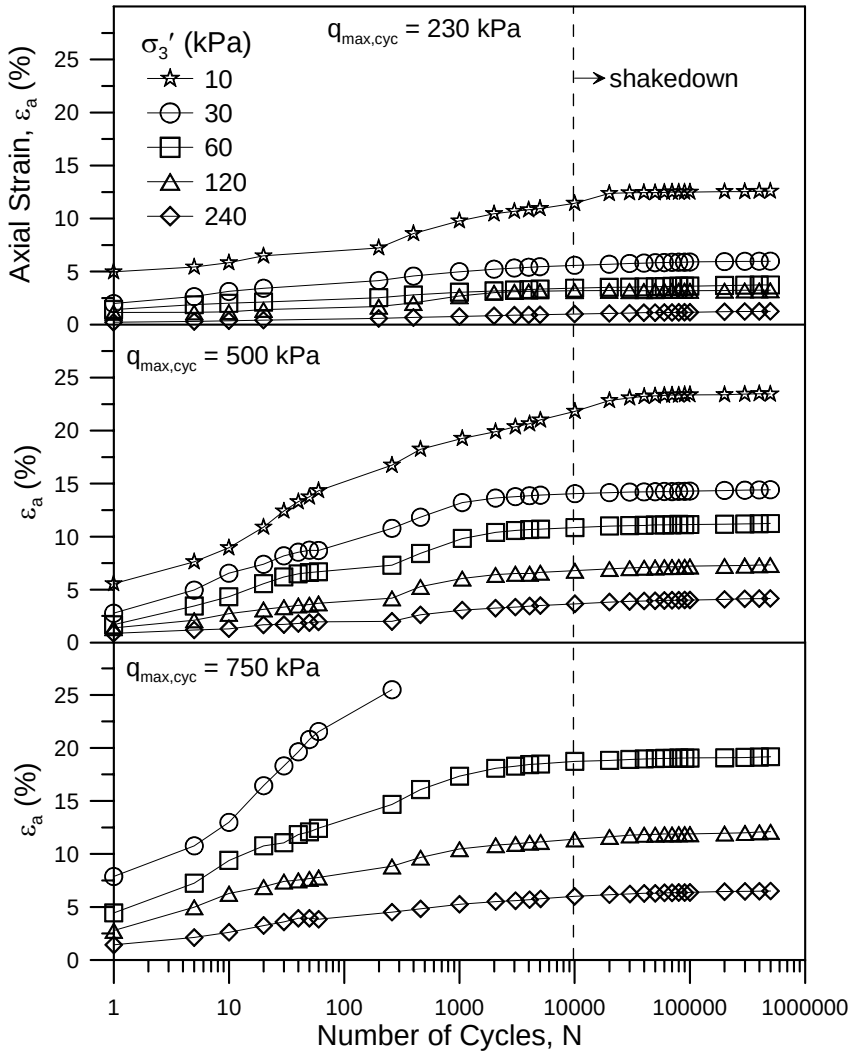

Figure 4.1 Axial strain ε_a as a function of the number of cycles N

The effect of confining pressure σ_3' on ε_a is best evaluated by plotting the final values of ε_a obtained at the completion of 500000 loading cycles. Figure 4.4 highlights the dependence of ε_a on both σ_3' and $q_{max,cyc}$. σ_3' and ε_a can be related by a simple power

relationship according to Equation 4.1, where *a* and *b* are the regression coefficients tabulated in Table 4.1.

$$\varepsilon_a\,(\%) = a\sigma_3'^{-b} \qquad (4.1)$$

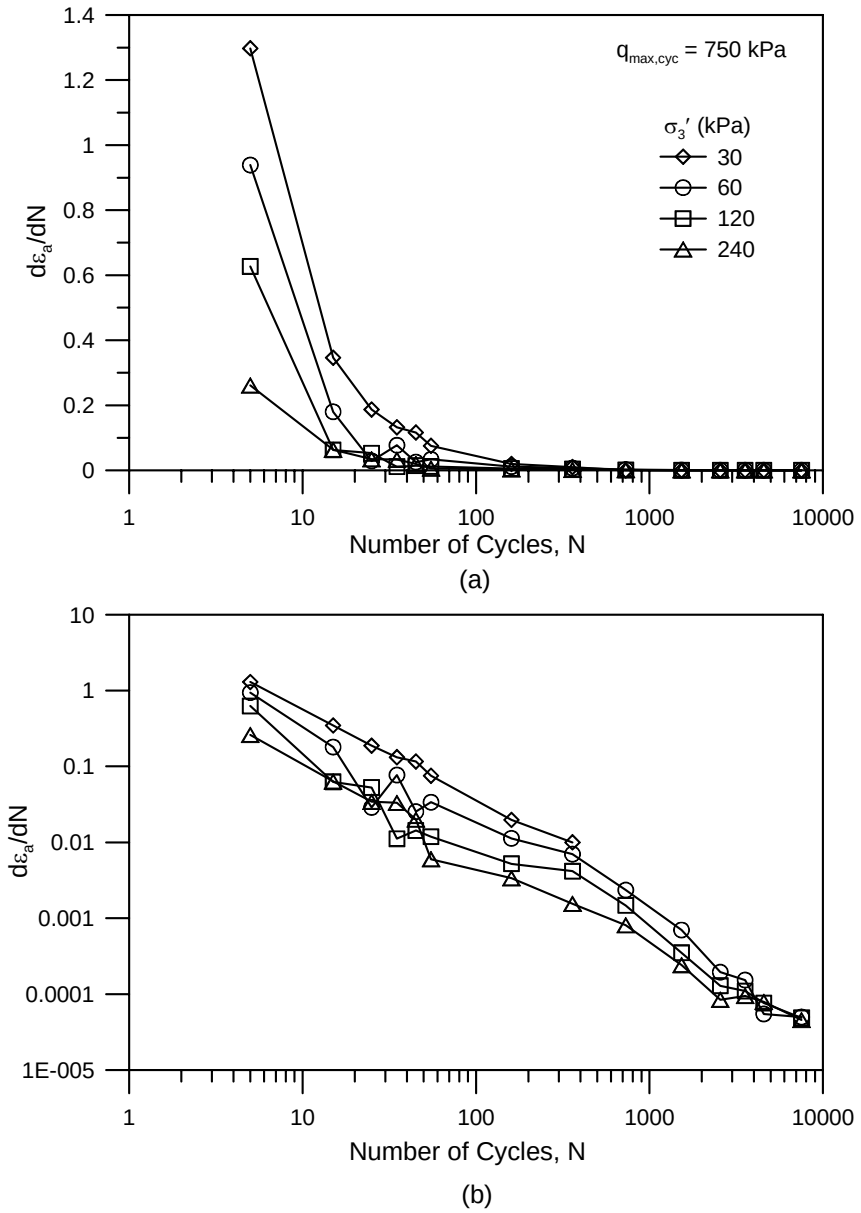

Figure 4.2 Rate of axial strain ε_a accumulation $d\varepsilon_a/dN$, (a) natural scale, and (b) logarithmic scale, for $q_{max,cyc}$ = 750 kPa and selected confining pressures σ_3'

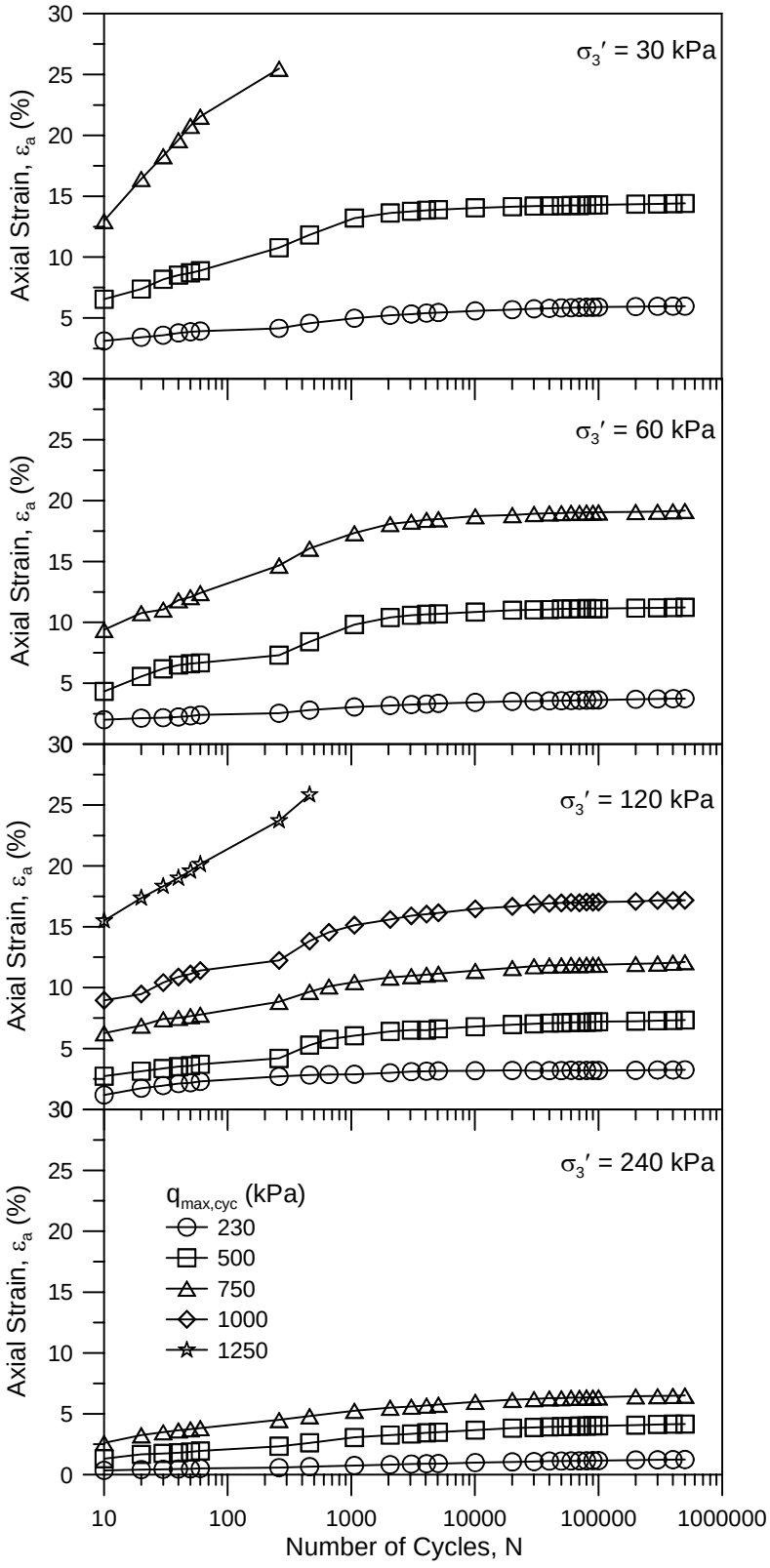

Figure 4.3 Effect of deviator stress magnitude $q_{max,cyc}$ on axial strain ε_a for σ_3' = 30, 60, 120 and 240 kPa

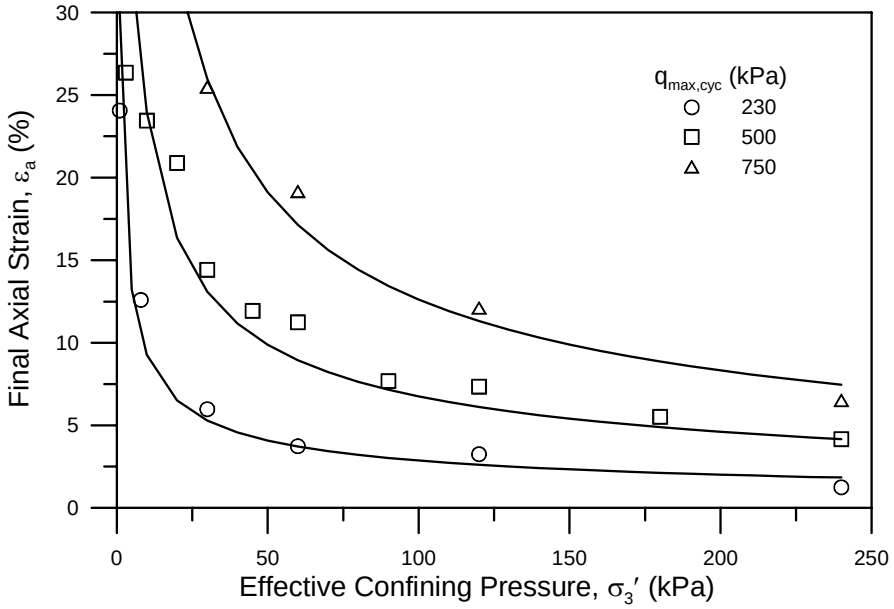

Figure 4.4 Axial strain ε_a values at the end of 500000 cycles

Whilst Equation 4.1 associates ε_a to σ_3', it is more imperative to find a relationship between all variables under consideration, namely, ε_a, σ_3', $q_{max,cyc}$ and N. Considering only the specimens that achieved shakedown, Equation 4.2 provides such a relationship:

$$\varepsilon_a\,(\%) = \frac{C q_{max,cyc}}{\sigma_3'^{\,D}} \tag{4.2}$$

Equation 4.2 contains two coefficients (*C* and *D*) that are both a function of the number of cycles N. The values of *C* and *D* fluctuate with evolving N according to Table 4.2 and Figures 4.5 and 4.6. It is interesting to note that R^2 values (between the measured and predicted values of M_R based on Equation 4.2) increase with N in Table 4.2, leading to the possibility of $R^2 \rightarrow 1$ when N reaches several millions of cycles.

Table 4.1 Regression coefficients from Equation 4.1 for the effect of confining pressure σ_3' on axial strain ε_a

$q_{max,cyc}$ (kPa)	*a*	*b*
230	30	0.51
500	85	0.55
750	200	0.60

Table 4.2 Values of coefficients *C* and *D* and the coefficient of determination R^2 with evolving N

N	*C*	*D*	R^2
10	0.0724	-0.5378	0.85
20	0.08	-0.5249	0.85
200	0.1073	-0.531	0.85
400	0.1183	-0.5208	0.86
1000	0.1296	-0.5134	0.87
2000	0.1381	-0.5156	0.88
3000	0.1392	-0.5123	0.88
4000	0.1398	-0.5104	0.88
5000	0.1404	-0.5091	0.89
10000	0.1418	-0.5049	0.89
20000	0.1459	-0.5061	0.90
30000	0.146	-0.5042	0.90
40000	0.1454	-0.5016	0.91
50000	0.1455	-0.5013	0.91
60000	0.1452	-0.5000	0.91
70000	0.1454	-0.4999	0.91
80000	0.1452	-0.4992	0.91
90000	0.1449	-0.4984	0.91
100000	0.145	-0.4983	0.91
200000	0.1443	-0.4951	0.91
300000	0.144	-0.4936	0.92
400000	0.1438	-0.4915	0.92
500000	0.1435	-0.4915	0.92

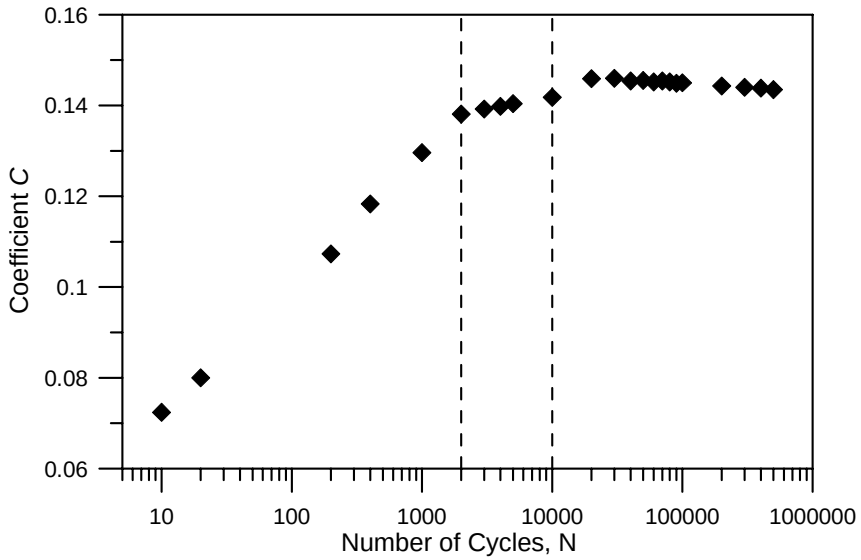

Figure 4.5 Relationship between coefficient *C* and the number of cycles N

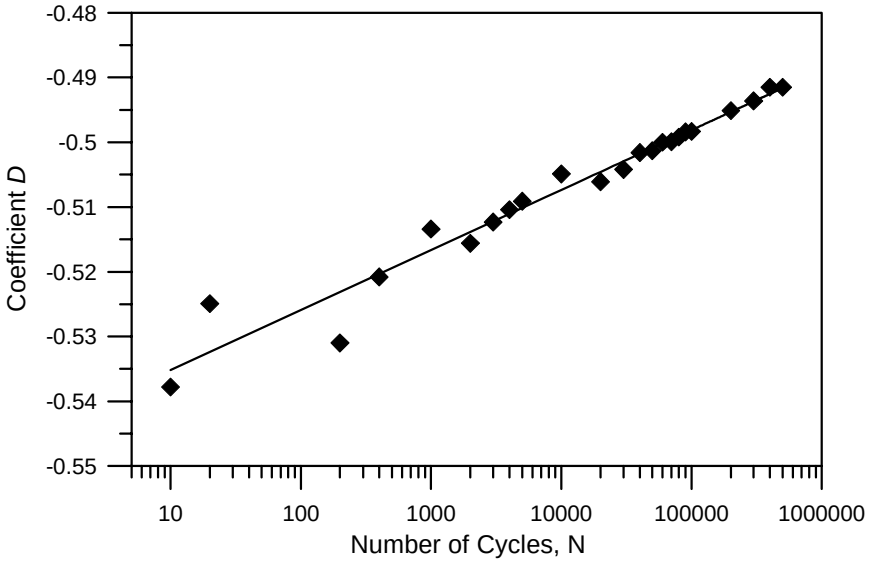

Figure 4.6 Relationship between coefficient *D* and the number of cycles N

It was established in Figure 4.1 that ε_a shakedown in the current study occurs within 10000 cycles. Figure 4.5 shows that the relationship between *C* and N can be broken into three distinct regions. When ε_a rates are greatest (within the first 2000 cycles), the relationship between coefficient *C* and N can be expressed as:

$$C = 0.0125\ln(N) + 0.0428 \text{ for } N \leq 2000;\ R^2 > 0.99 \quad (4.3)$$

Similarly, as N increases in Figure 4.5,

$$C = 0.0022\ln(N) + 0.1219 \text{ for } 2000 < N \leq 10000;\ R^2 > 0.99 \quad (4.4)$$

$$C = -0.0008\ln(N) + 0.1539 \text{ for } N > 10000;\ R^2 = 0.97 \quad (4.5)$$

Figure 4.6 shows the relationship between *D* and N, and these two parameters can be correlated by ($R^2 > 0.96$):

$$D = 0.004\ln(N) - 0.5444 \text{ for all N} \quad (4.6)$$

The reliability of Equation 4.2 depends on the accuracy of the predicted and measured data. As the power relationships for each N relating ε_a to $q_{max,cyc}/\sigma_3'$ have average R^2 values (0.85 – 0.92), significant variation between the measured and predicted ε_a is expected for some of the specimens. Figures 4.7, 4.8 and 4.9 plot the consistency between the measured and predicted values of ε_a for $q_{max,cyc}$ = 230, 500 and 750 kPa, respectively. There are considerable differences for several of the specimens, however, it is believed that Equation 4.2 still provides a satisfactory link between the various parameters under investigation.

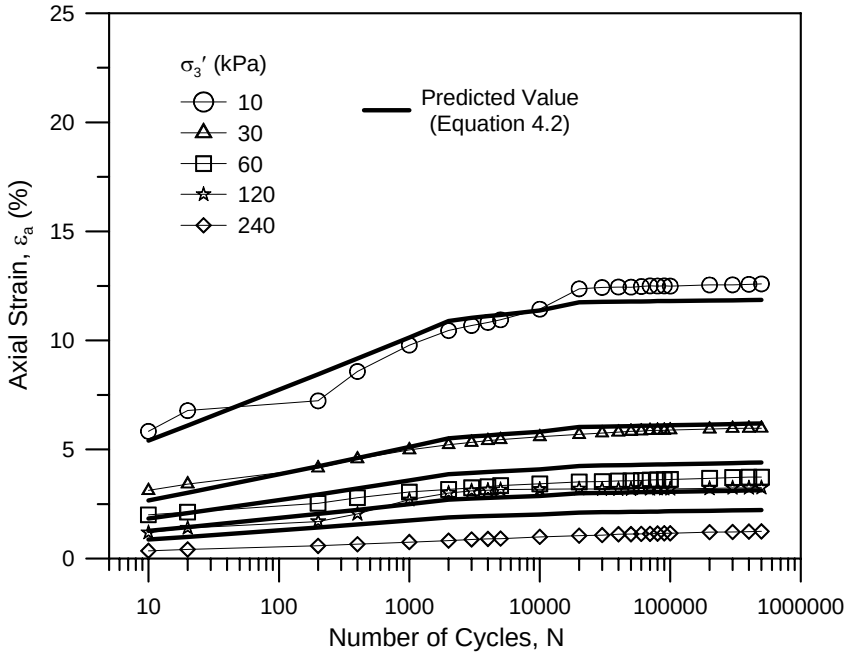

Figure 4.7 Correlation between the measured (lines with symbols) and predicted (solid lines) axial strain ε_a values for selected specimens for maximum deviator stress $q_{max,cyc}$ = 230 kPa

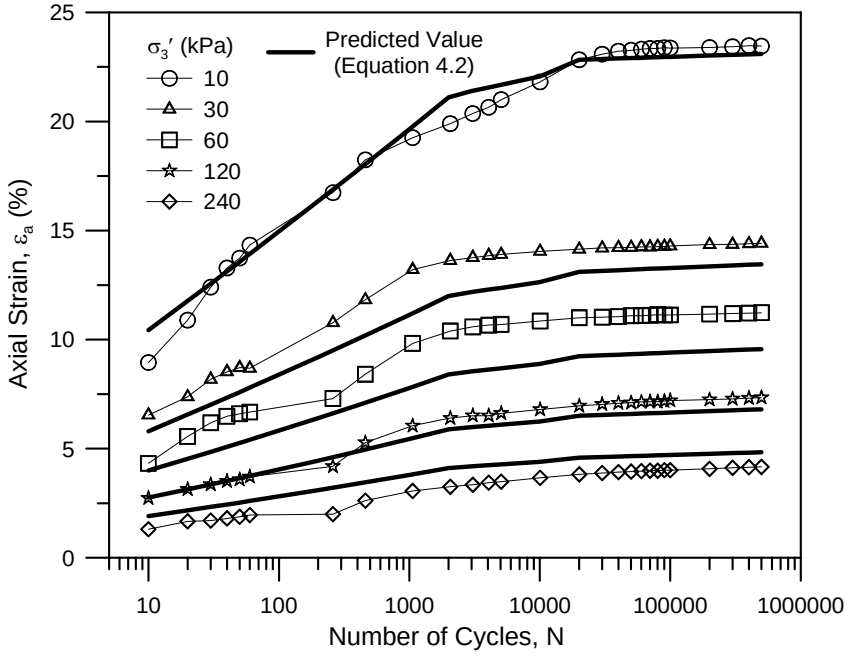

Figure 4.8 Correlation between the measured (lines with symbols) and predicted (solid lines) axial strain ε_a values for selected specimens for maximum deviator stress $q_{max,cyc}$ = 500 kPa

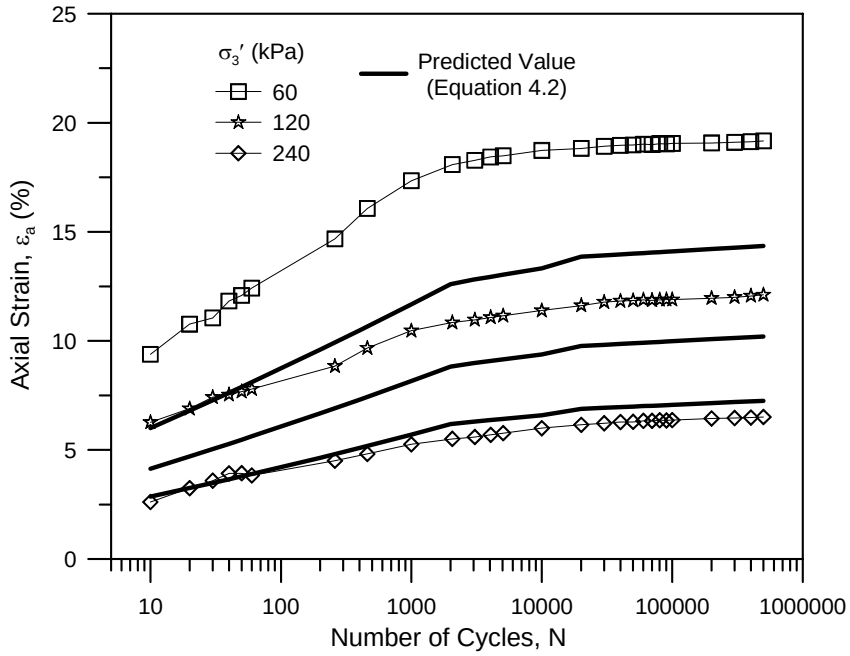

Figure 4.9 Correlation between the measured (lines with symbols) and predicted (solid lines) axial strain ε_a values for selected specimens for maximum deviator stress $q_{max,cyc}$ = 750 kPa

Finally, the correlation between axial strain ε_a and shear strain ε_s (Equation 3.2) under drained cyclic loading conditions is demonstrated in Figure 4.10. Only modest differences in the magnitudes of ε_a and ε_s can be observed, particularly at low σ_3', hence it appears that the two terms can be used interchangeably to describe the vertical deformation behaviour of ballast under these particular loading conditions.

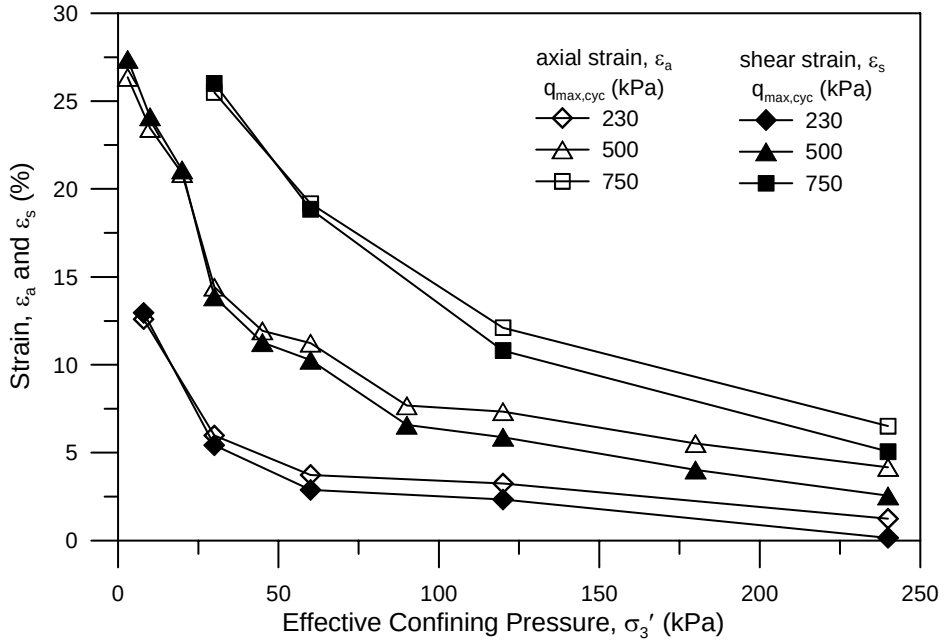

Figure 4.10 Effect of confining pressure σ_3' on axial strain ε_a and shear strain ε_s under drained cyclic loading conditions

4.4 Permanent Volumetric Strain Response

Reorientation and rearrangement of particles during cyclic loading generates a denser (compressing) or looser (dilating) packing assembly. Figure 4.11 illustrates that specimens subjected to low σ_3' exhibit dilative behaviour, whilst compression is observed for specimens with larger σ_3'. Compressive volumetric strain ε_v in specimens with sufficient σ_3' continues to develop approximately logarithmically with increasing N as depicted in Figure 4.11 for selected specimens. The degree of specimen contraction for a particular $q_{max,cyc}$ increases with σ_3' as the magnitude of expansive (negative) radial strain ε_r declines. Dilation in poorly confined specimens occurs primarily within the first 3000 cycles of loading and results from the excessive radial strains that occur in conjunction with large $q_{max,cyc}/p'$. It is interesting to note that as N

becomes large (> 100000 cycles) it is possible for the once dilating specimens to start displaying contractive behaviour, such as the $q_{max,cyc}$ = 500 kPa and σ_3' = 10 kPa specimen in Figure 4.11. This behaviour is partially attributable to the small (inward) lateral force provided by the confining fluid that continues to push against the specimen well after ε_a shakedown has occurred, thus contributing to specimen compression.

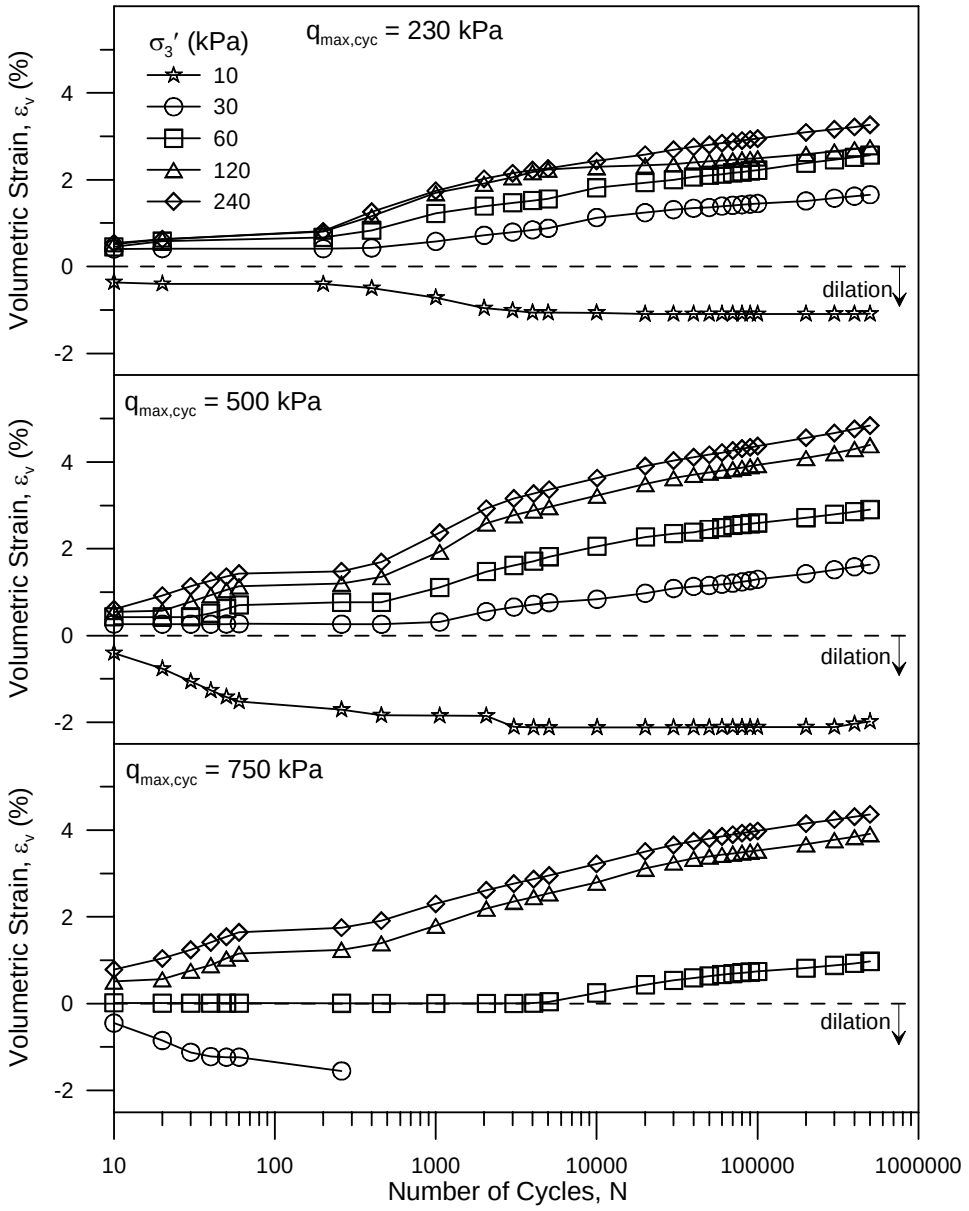

Figure 4.11 Effect of confining pressure σ_3' and number of cycles N on volumetric strain ε_v behaviour of selected specimens of latite basalt

The effect of deviator stress magnitude $q_{max,cyc}$ on ε_v is depicted in Figure 4.12. No definitive relationship between $q_{max,cyc}$ and ε_v can be observed, and this finding is more clearly portrayed in Figure 4.13 where the final values of ε_v after 500000 cycles are plotted against σ_3'. An explanation of this behaviour is provided in Section 4.5.

4.5 Comparison between Static (Monotonic) and Cyclic Behaviour of Latite Basalt

When considering the behaviour of granular materials under cyclic loading it is useful to compare the magnitude of loading $q_{max,cyc}$ to the peak deviator stress at failure $q_{peak,sta}$ obtained from static triaxial tests. The ratio $\psi = q_{max,cyc}/q_{peak,sta}$ is hence defined for this purpose, with a ψ value greater than one implying that the maximum cyclic loading amplitude exceeds the peak strength of a specimen monotonically sheared at the same σ_3'. The static data was obtained from the works of Indraratna *et al*. (1998) and Salim (2004). Figure 4.14 demonstrates that a bilinear relationship can accurately relate $q_{peak,sta}$ to σ_3' for latite basalt. The static ε_v behaviour at $q_{peak,sta}$ and $\varepsilon_a = 20\%$ is also depicted in Figure 4.14 and serves as a useful comparison to the cyclic ε_v response. Figure 4.15 exhibits the large range of ψ values employed in the cyclic triaxial tests (from approximately 0.2 to 2.60). It is important to note that there were some slight differences in the gradings used in the current study and those employed by Indraratna *et al*. (1998) and Salim (2004) for static loading. It is believed that these differences have only a minor or insignificant effect on the calculated ψ values, and hence have been ignored in the analysis.

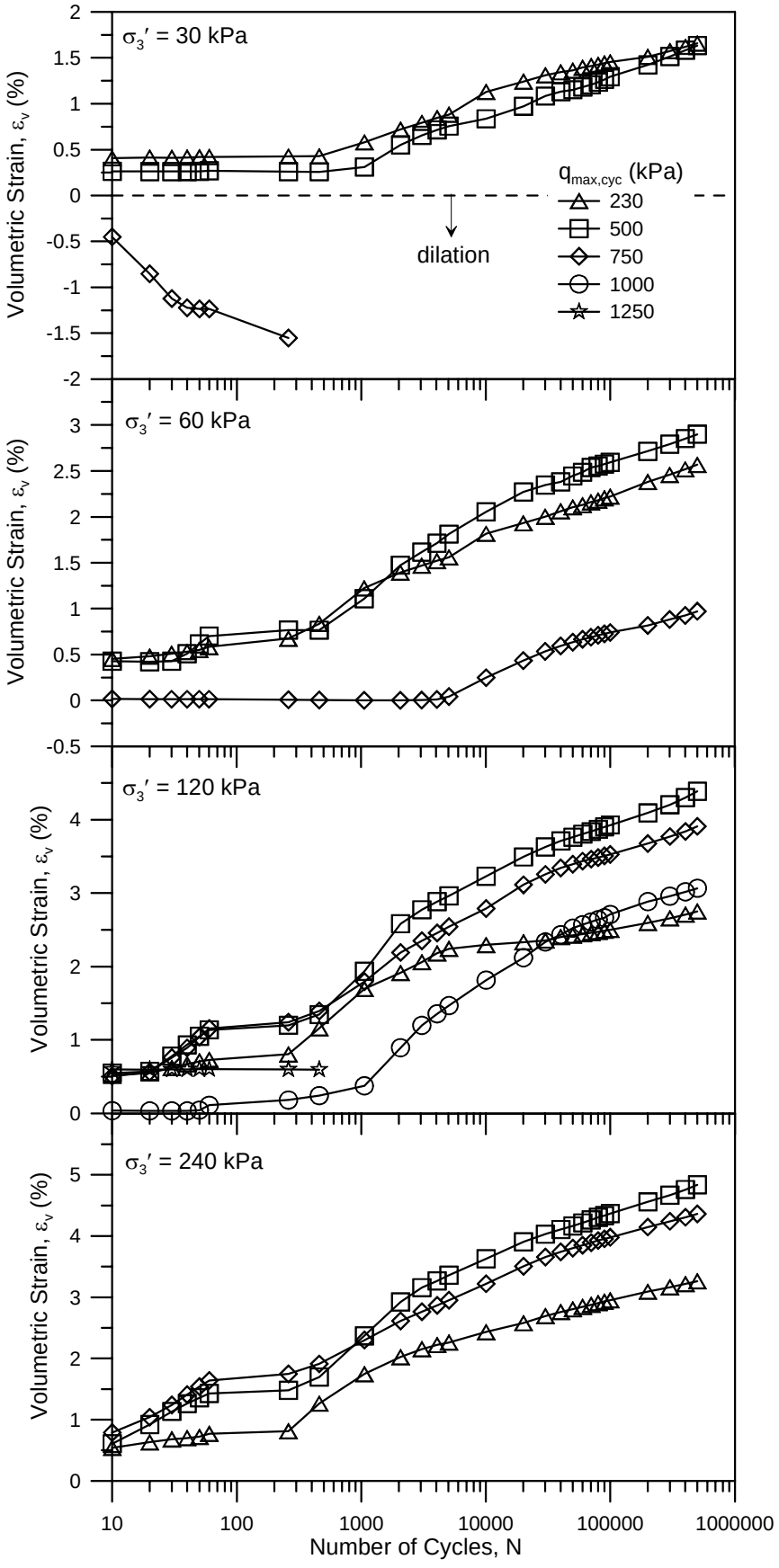

Figure 4.12 Effect of deviator stress magnitude $q_{max,cyc}$ on volumetric strain ε_v behaviour

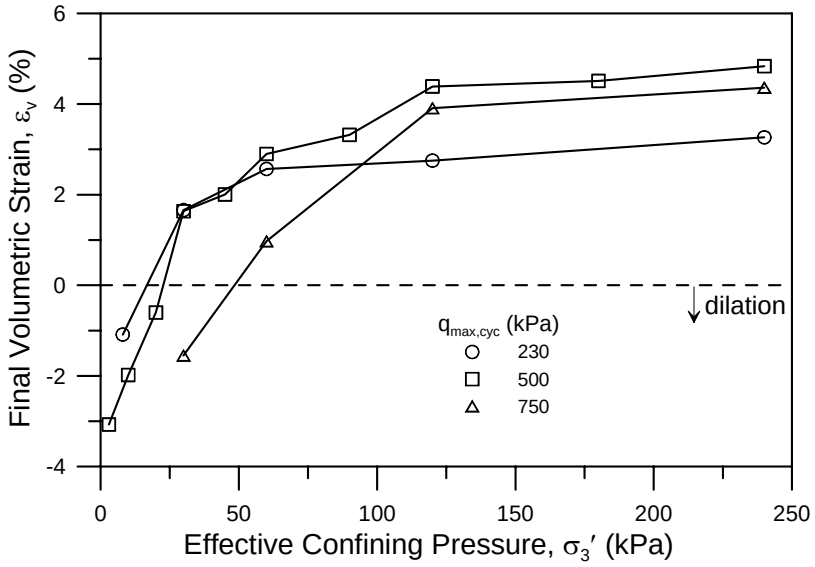

Figure 4.13 Final volumetric strain ε_v values after 500000 cycles

Please see print copy for Figure 4.14

Figure 4.14 Effect of confining pressure σ_3' on the static peak deviator stress at failure $q_{peak,sta}$ for latite basalt, and the volumetric strain ε_v at $q_{peak,sta}$ and ε_a = 20% (data from Indraratna *et al*., 1998 and Salim, 2004)

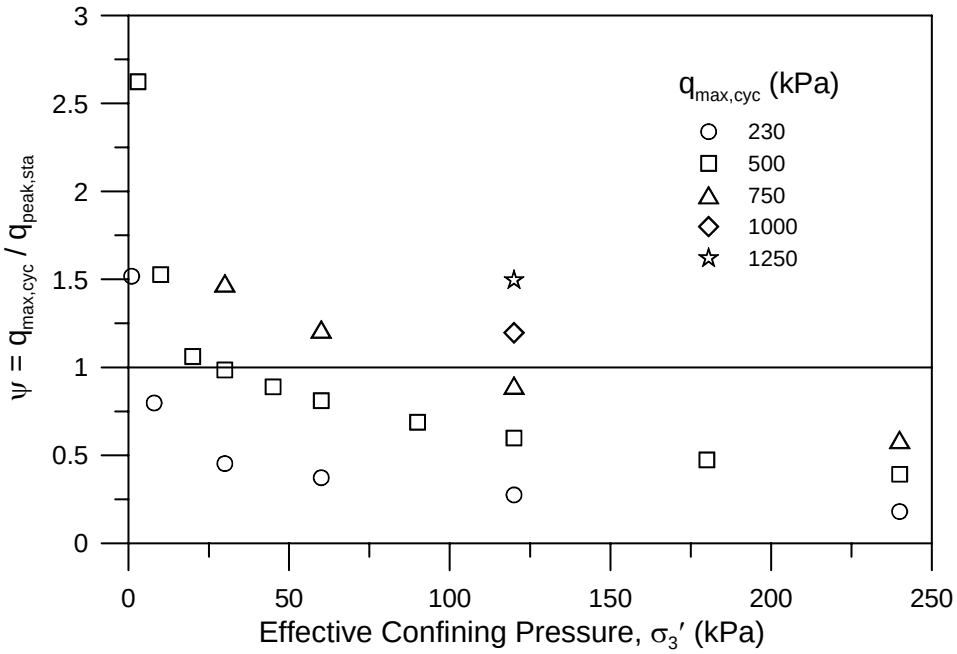

Figure 4.15 ψ values for the current cyclic triaxial tests

Figure 4.16 depicts the axial, radial and volumetric strains after 500000 cycles as a function of $q_{max,cyc}$. For a constant σ_3', greater $q_{max,cyc}$ generates larger axial (Figure 4.16a) and radial (Figure 4.16b) strains, as discussed previously. Figure 4.16c illustrates that volumetric straining tendencies are dependent on both ψ and σ_3', and that ε_v becomes more dilative with increasing $q_{max,cyc}/p'$. Raymond and Williams (1978) subjected specimens of Coteau dolomite ballast to ψ ratios of 0.25, 0.5 and 0.75, and witnessed increasing ε_v with ψ for σ_3' = 206.8 kPa (Figure 4.17), which indicates that maximum specimen compression occurs when ψ > 0.75. Negligible difference in ε_v was encountered for ψ = 0.5 and 0.75 when σ_3' was decreased to 51.7 kPa. Tests by Olowokere (1975) (Figure 2.11) also reveal increasing ε_v with ψ for ψ ≤ 0.75. In the current study, specimens display compressive behaviour when ψ < 0.5, and the magnitude of compression increases with $q_{max,cyc}$ and σ_3'. However, as ψ rises beyond 0.5, ε_v peaks and then starts to decline as ψ = 1 is approached (Figure 4.16c) suggesting

a point of maximum compression at $\psi \approx 0.75$. With continued increases in $q_{max,cyc}$ specimen compression declines, until $\psi >> 1$ and all specimens eventually dilate upon loading. The $q_{max,cyc}$ required to initiate maximum compression increases with σ_3'. For the condition $\psi > 1$, Figure 4.16c illustrates that the likelihood of dilative behaviour becomes greater with decreasing σ_3', but that specimens can still display compressional tendencies. Compared to static loading (Figure 4.14), cyclically loaded specimens demonstrate a significantly higher propensity for rapid initial compression, although this effect may diminish with increasing specimen density. Suiker *et al*. (2005) showed that granular materials display a strong tendency to compact under cyclic loading, even as ψ approaches 1, and a similar behaviour is observed in the current study.

Given ψ or $q_{max,cyc}$, it is possible to predict the final ε_a for latite basalt using Figure 4.18. Irrespective of the applied stresses, the variation of ε_a is confined within a narrow band when plotted against ψ for $\psi \leq 2$. A best fit median equation for the data shown in Figure 4.18 can be represented by Equation 4.8. For a good positive regression ($R^2 > 0.98$), *E* and *F* are material constants equal to -3 and 18, respectively.

$$\varepsilon_a\,(\%) = E + F\psi \qquad (4.8)$$

A comparison of the permanent straining behaviour of ballast under static and cyclic loading is provided in Figure 4.19 (static) and Figure 4.20 (cyclic). In accordance with other granular materials, ballast specimens under static triaxial loading at low σ_3' will initially compress slightly before dilating even at small ε_a (Figure 4.19). As the magnitude of σ_3' increases the incidence of dilation diminishes until specimens display

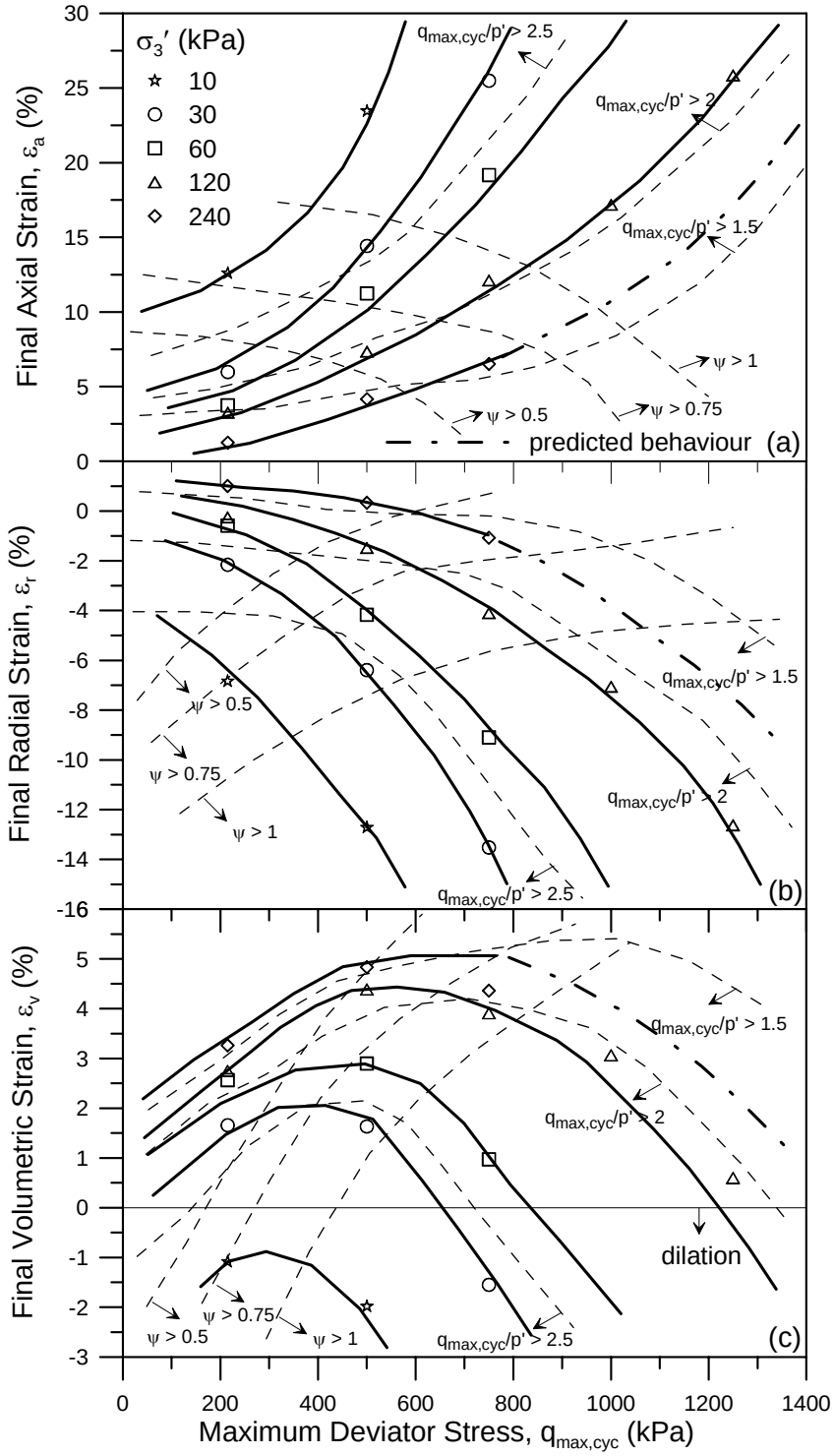

Figure 4.16 Final strain values after 500000 cycles and ψ and $q_{max,cyc}/p'$ contours as a function of $q_{max,cyc}$ for: (a) Axial strain ε_a, (b) Radial strain ε_r, and (c) Volumetric strain ε_v

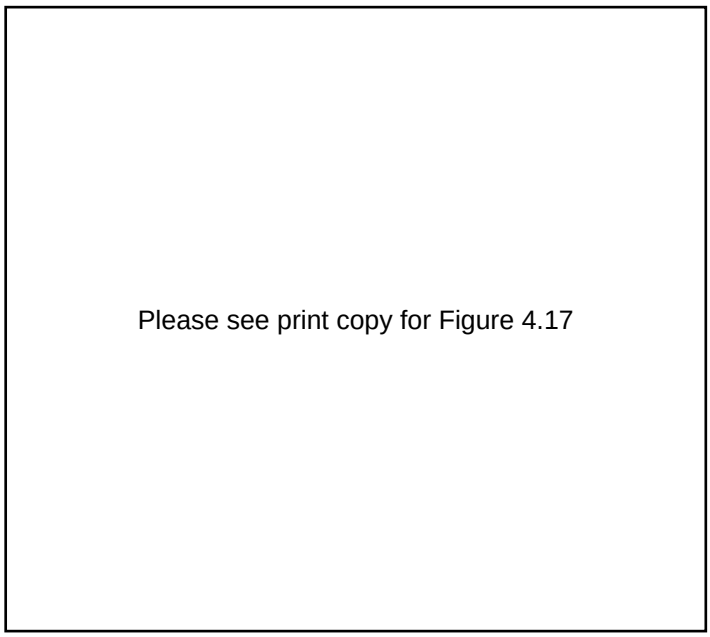

Figure 4.17 Effect of ψ (= X) on axial ε_a and volumetric ε_v strain behaviour of Coteau dolomite ballast (after Raymond and Williams, 1978)

only contractive behaviour up to large ε_a. The behaviour of cyclically loaded specimens (Figure 4.20) at low σ_3' is characterised by large ε_a and slightly compressive or dilative behaviour. With increasing σ_3' the magnitude of volumetric compression increases as ε_r decreases. Unlike static loading, cyclically loaded specimens that compress during the initial cycles will continue to compress indefinitely providing the deviator stress magnitude remains unchanged. The effect of stepwise loading (wherein the axial strain is forced to 20% by a gradually increasing cyclic load) on ε_a and ε_v is discussed in Chapter 6.

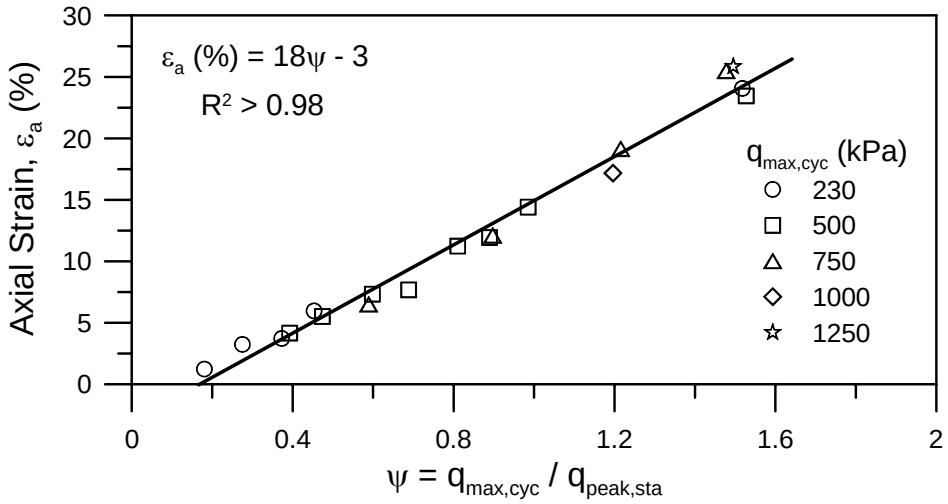

Figure 4.18 Prediction of axial strain ε_a based on the ratio ψ

Please see print copy for Figure 4.19

Figure 4.19 Axial ε_a versus volumetric ε_v strain behaviour for monotonic loading of latite basalt (data replotted from Indraratna *et al*., 1998)

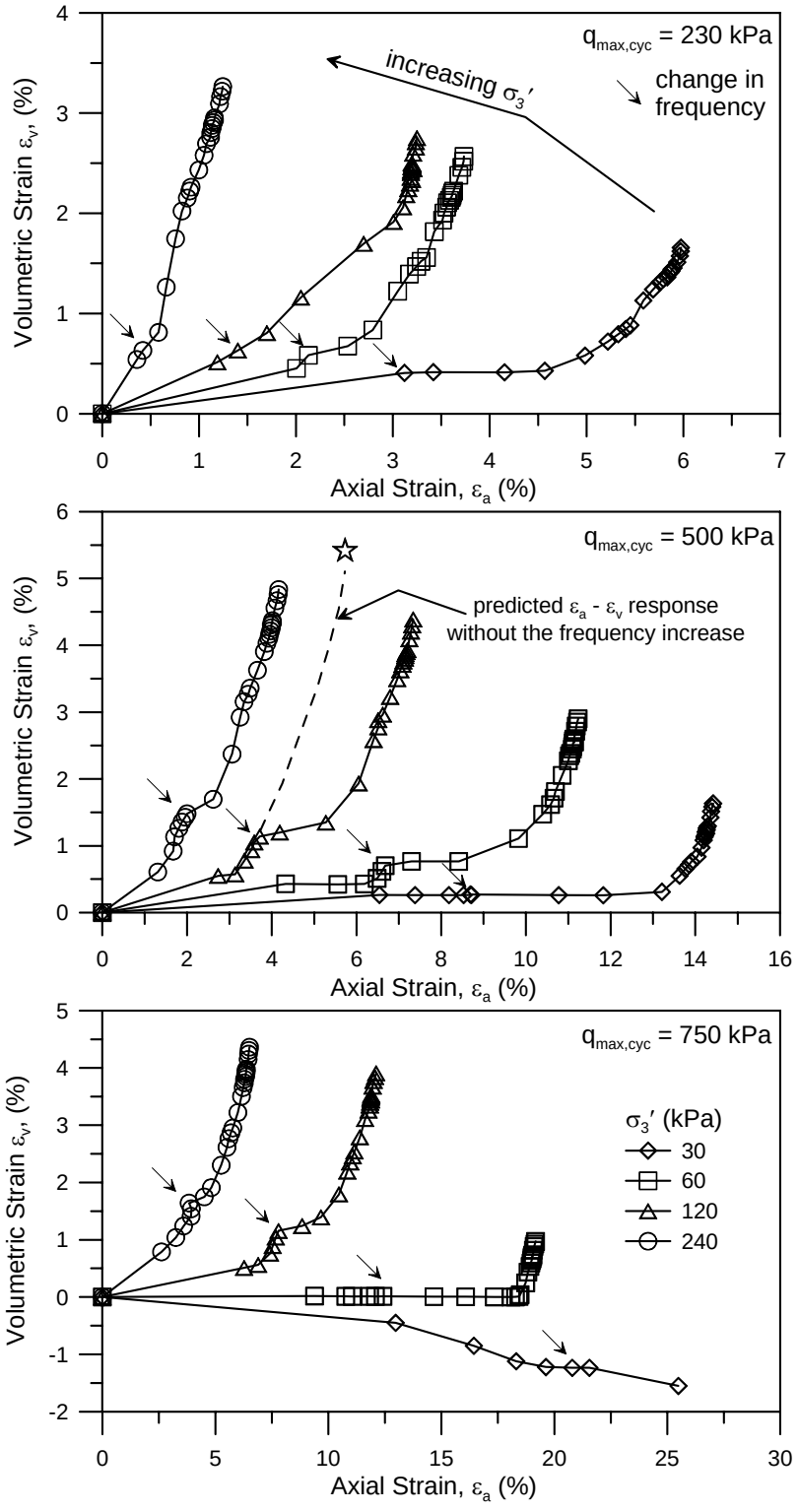

Figure 4.20 Axial ε_a versus volumetric ε_v strain behaviour for cyclic loading of latite basalt

One last significant feature regarding Figure 4.20 is the shape of each ε_a vs ε_v curve. As outlined in Chapter 3, the triaxial experiments involved an initial loading phase at a reduced frequency (typically 1 Hz) before the application of the final testing frequency for the remaining cycles. In Figure 4.20 the change in frequency is marked with an arrow, and in some cases the arrow corresponds to a definite change in the slope of the curve. Taking the $q_{max,cyc}$ = 500 kPa, σ_3' = 120 kPa specimen as an example, at about ε_a = 3.75% the frequency is increased from 1 to 20 Hz, and there is a subsequent jump in the measured ε_a. However, ε_v remains approximately constant during this period because the rapid increase in ε_r reduces the compressing capacity of the specimen. Without the frequency change the specimen would have shaken down at a lesser ε_a (the predicted ε_a – ε_v path is marked with a dotted line and star) as the rate of ε_a accumulation had already started to stabilise during the 1 Hz loading phase. This suggests that greater loading frequencies are likely to cause greater permanent ε_a deformation. In addition to Figure 4.16, Figure 4.20 also depicts the greater prevalence of compression in cyclically loaded specimens when compared to Figure 4.19.

4.6 Effect of Particle Size Distribution on Straining Behaviour

The effect of specimen particle size distribution (PSD) on axial and volumetric straining behaviour is depicted in Figures 4.21 and 4.22, respectively. Figure 4.21 identifies that the very uniform and uniform specimens display the greatest degree of ε_a, which is largely due to their looser inherent states (lower initial densities and higher void ratios) prior to cyclic shear. Accompanying the large ε_a for poorly graded specimens is greater volumetric compression (Figure 4.22). Although not explicitly plotted, there is very little difference in the measured ε_r for the four specimens, signifying that the main

source of variation in volumetric strain can be attributed to the extent of ε_a rather than ε_r.

4.7 Resilient Deformation Response (Resilient Modulus)

The effect of σ_3' and $q_{max,cyc}$ on the resilient modulus M_R was assessed by recording bursts of resilient (recoverable) strain and deviator stress data at numerous cycles N throughout each test. In the current study M_R is calculated according to Equation 3.5, where $\varepsilon_{a,rec}$ is the recoverable portion of axial strain, and Δq_{cyc} is the difference between $q_{max,cyc}$ and $q_{min,cyc}$ as shown earlier in Figure 3.6 (Chapter 3).

4.7.1 Resilient Strain Behaviour

Resilient strain $\varepsilon_{a,rec}$ data for each specimen was recorded using the program GOUI (Appendix C) and then filtered using signal processing (Appendix D) to produce an accurate and reliable depiction of the recoverable strain behaviour of ballast under high-speed cyclic loading. Figure 4.23 illustrates the effect of σ_3' and N on the magnitude of resilient strain for $q_{max,cyc}$ = 230, 500, and 750 kPa. With increasing σ_3' the reduced degree of deformation occurring during each loading-unloading cycle is exemplified by a reduction in $\varepsilon_{a,rec}$. As loading progresses, the magnitude of $\varepsilon_{a,rec}$ decreases with each successive loading cycle N. Beyond about 100000 cycles, however, there is a noticeable drop in the rate of $\varepsilon_{a,rec}$ deterioration, particularly at higher $q_{max,cyc}$ amplitudes, indicating the approach of stable long-term elastic conditions. Figures 4.24 and 4.25

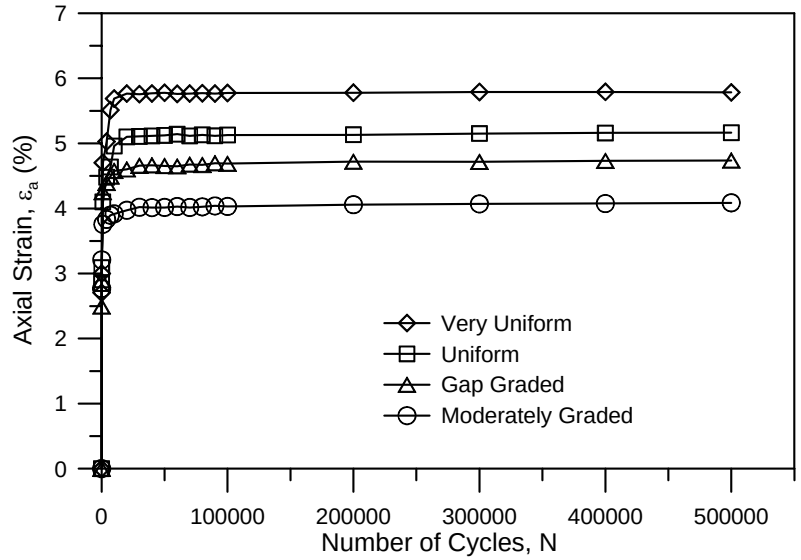

Figure 4.21 Effect of specimen particle size distribution on axial strain ε_a behaviour

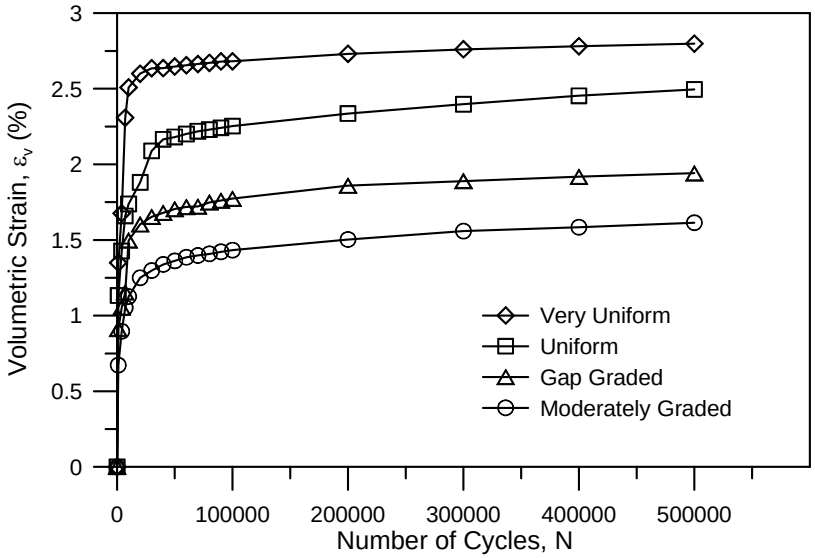

Figure 4.22 Effect of specimen particle size distribution on volumetric strain ε_v behaviour

depict the effect of $q_{max,cyc}$ on $\varepsilon_{a,rec}$ response. Figure 4.24 plots $\varepsilon_{a,rec}$ against N for σ_3' = 60 and 240 kPa, whilst Figure 4.25 portrays the final $\varepsilon_{a,rec}$ values after 500000 cycles for selected specimens as a function of σ_3'. Both figures clearly show that the magnitude of $\varepsilon_{a,rec}$ increases with $q_{max,cyc}$ (Δq_{cyc}).

4.7.2 Resilient Modulus

The effect of σ_3' and N on the resilient modulus M_R is illustrated in Figure 4.26. Evidently M_R increases with σ_3' and this finding is well reported in the literature (e.g. Hicks, 1970; Allen, 1973). The magnitudes of the measured M_R values correspond well with those supplied by Knutson and Thompson (1977), Alva-Hurtado and Selig (1981) and Selig and Alva-Hurtado (1982) for ballast under similar stress conditions. Previous research (e.g. Allen and Thompson, 1974; Khedr, 1985) acknowledged that M_R is independent of N after the completion of a small number of stress repetitions (typically less than 1000 cycles). However, Figure 4.26 predicts a continuing increase in M_R with N, although little change is observed beyond 100000 cycles in concurrence with Figure 4.23. It is customary during the resilient modulus testing of smaller-grained materials (less than 19 mm diameter) to apply a period of preconditioning to the specimen before the measurement of M_R under an assortment of stress conditions. Preconditioning is performed to permit the bedding of the end caps of the triaxial apparatus into the specimen, and to allow the stabilisation of the resilient strain (Standards Australia, 1995). The preconditioning stress utilised depends on the planned testing loads, and an example of such stress levels for granular unbound pavement materials is shown in Table 4.3. No testing procedures for materials with particle sizes greater than 19 mm currently exist. This fact combined with the desire to examine other parameters such as

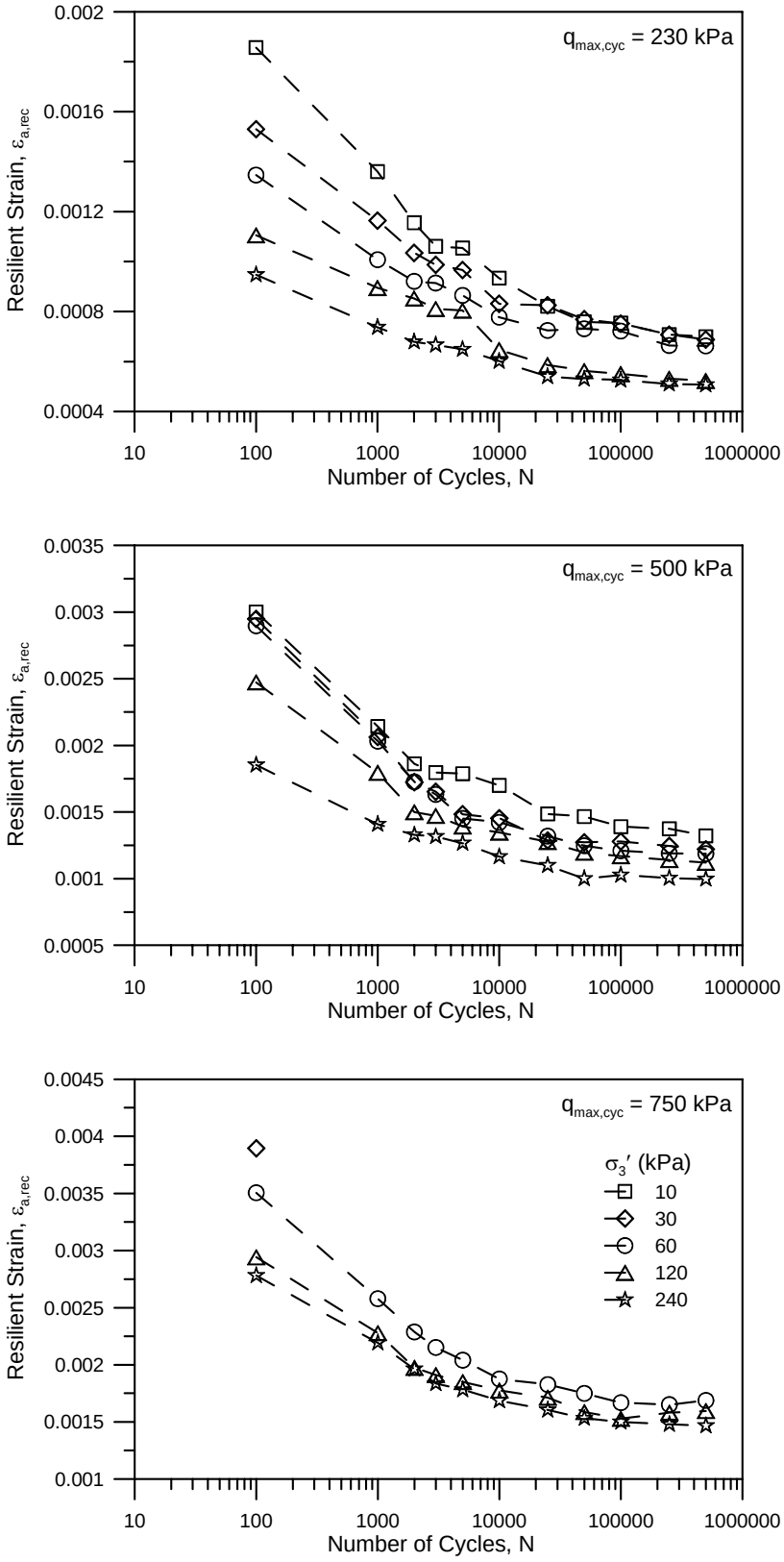

Figure 4.23 Effect of confining pressure σ_3' and the number of cycles N on the resilient (recoverable) strain $\varepsilon_{a,rec}$ for selected specimens

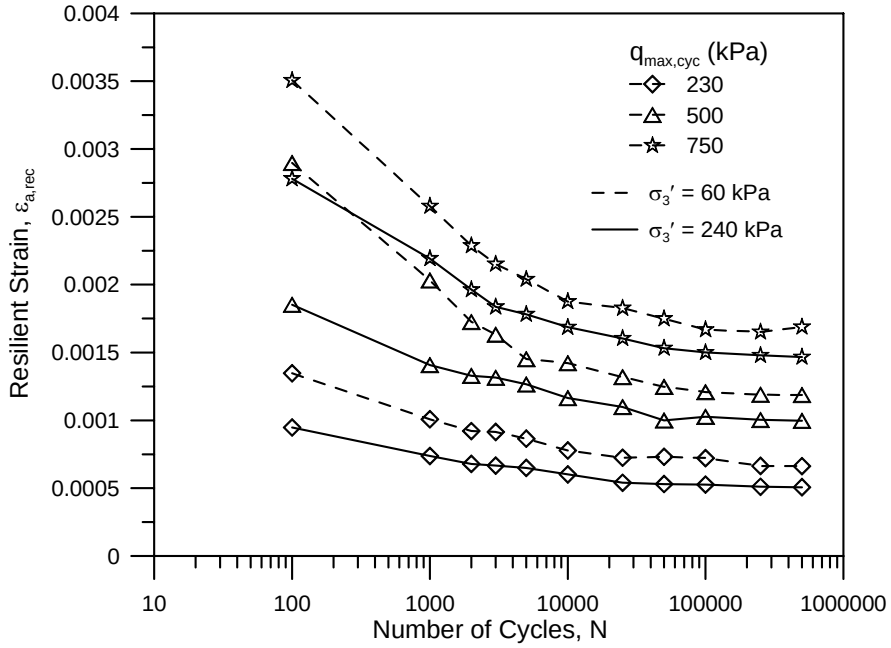

Figure 4.24 Effect of deviator stress magnitude $q_{max,cyc}$ (Δq_{cyc}) on the resilient strain $\varepsilon_{a,rec}$

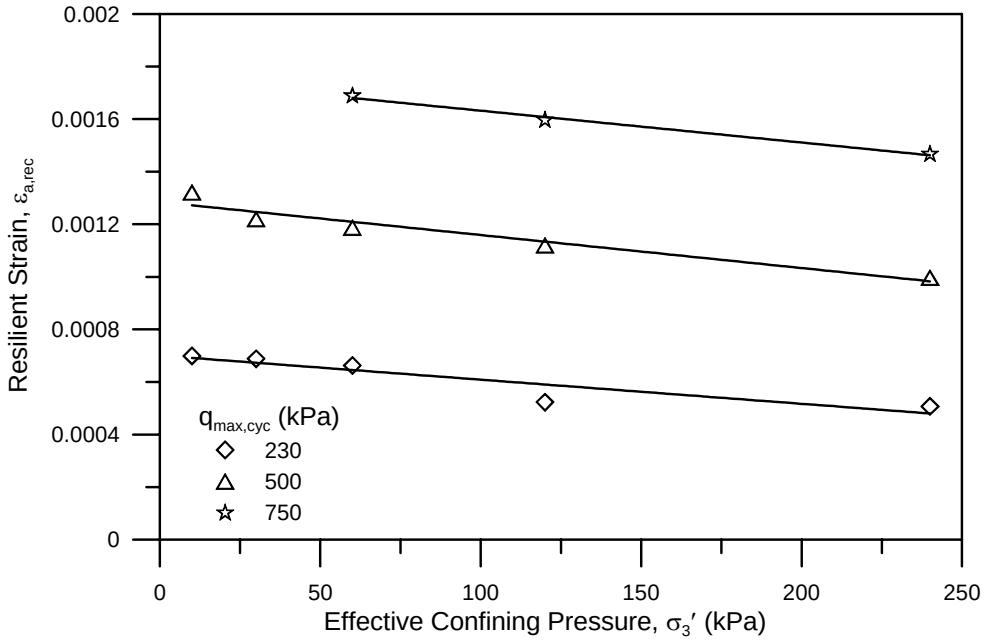

Figure 4.25 Final resilient strain $\varepsilon_{a,rec}$ after 500000 cycles as a function of the effective confining pressure σ_3'

permanent strain and particle degradation prevented the incorporation of a preconditioning phase in the current study, and this could be a contributing factor to the witnessed continual increase in M_R with N.

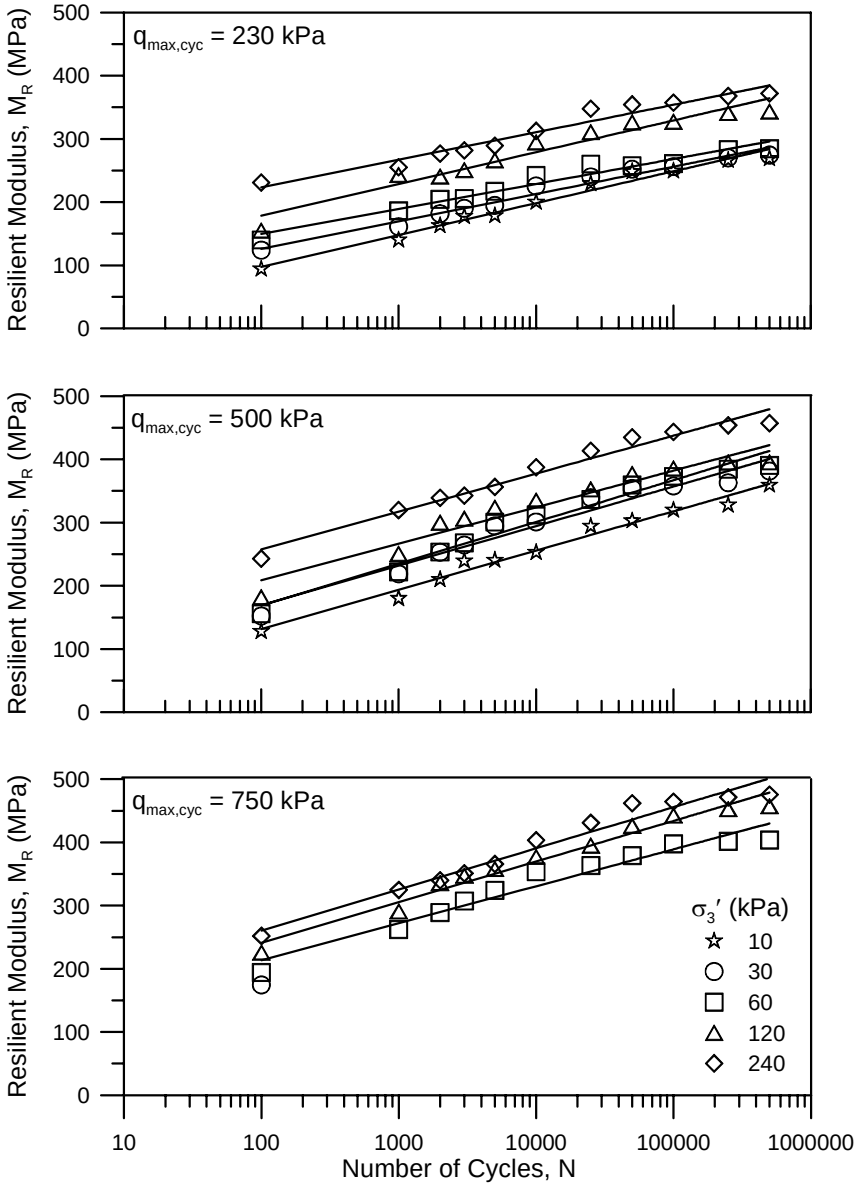

Figure 4.26 Effect of confining pressure σ_3' and the number of cycles N on the resilient modulus M_R for selected specimens

Selig and Alva-Hurtado (1982) recognised that a reduction in $\varepsilon_{a,rec}$ with each successive cycle and subsequent increase in M_R can be attributed, at least partly, to densification from cumulative ε_v. As ε_v increases indefinitely with N (Figure 4.11) leading to a reduction in void ratio and thus increased specimen stiffness, the progression of M_R with N in Figure 4.26 is warranted. Both ε_v and M_R display an approximately logarithmic relationship with N (particularly within the initial 100000 cycles) indicating a possible link between ε_v and the expected magnitude of M_R for a particular $q_{max,cyc}$ and σ_3'. In order to investigate this possibility, the curve fitting method outlined in John (1998) (Appendix E) was employed to find a suitable relationship between ε_v and M_R. After extensive analysis of a number of different models it was found that for each compressing specimen, the magnitude of M_R could be estimated from ε_v based on Equation 4.10, where *g* and *h* are regression coefficients with σ_3' entered in MPa and ε_v as the accumulated percentage. The constants *g* and *h*, the squared error, and the coefficient of correlation R^2 for the measured and predicted M_R magnitudes are tabulated in Table 4.4, and an example calculation is provided in Appendix E. An estimate of *g* and *h* based on σ_3' can be obtained from Figures 4.27 and 4.28, respectively.

$$M_R = g\,\sigma_3'\,\varepsilon_v\,N^h \qquad (4.10)$$

The effect of deviator stress magnitude $q_{max,cyc}$ (or Δq_{cyc}) on M_R is depicted in Figure 4.29 as a function of N, and in Figure 4.30 as a function of σ_3'. In agreement with some of the studies outlined in Chapter 2.10.7, the magnitude of M_R increases with the loading amplitude, although as $q_{max,cyc}$ increases the difference in obtained M_R becomes less significant for a given σ_3'.

Table 4.3 Example of the stress levels required for preconditioning of granular unbound pavement materials (after Standards Australia, 1995)

Please see print copy for Table 4.3

Table 4.4 Results of the curve fitting procedure for the relationship between volumetric strain ε_v and resilient modulus M_R

$q_{max,cyc}$ = 230 kPa				
σ_3' (kPa)	*g*	*h*	R^2	$\sum error^2$
30	13892	-0.073	0.99	1030
60	3850	-0.057	0.99	1225
120	1179	-0.0086	0.90	4761
240	876	-0.049	0.73	12326
$q_{max,cyc}$ = 500 kPa				
σ_3' (kPa)	*g*	*h*	R^2	$\sum error^2$
30	37336	-0.121	0.91	5478
45	8738	-0.055	0.98	992
60	4165	-0.049	0.98	1493
90	1859	-0.016	0.97	2109
120	1407	-0.049	0.97	1759
180	961	-0.048	0.92	4718
240	697	-0.045	0.91	5083
$q_{max,cyc}$ = 750 kPa				
σ_3' (kPa)	*g*	*h*	R^2	$\sum error^2$
120	922	-0.051	0.97	2013
240	716	-0.034	0.99	700

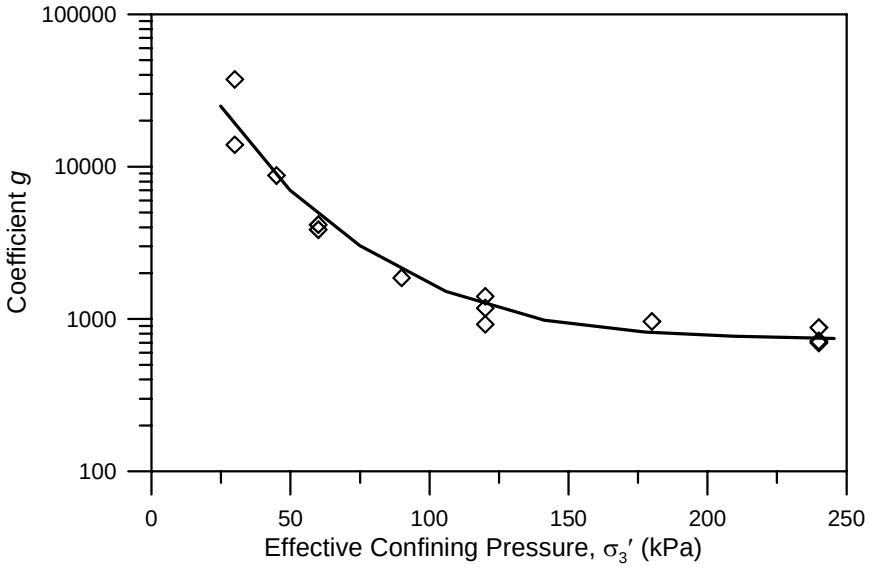

Figure 4.27 Estimation of the coefficient *g* in Equation 4.10

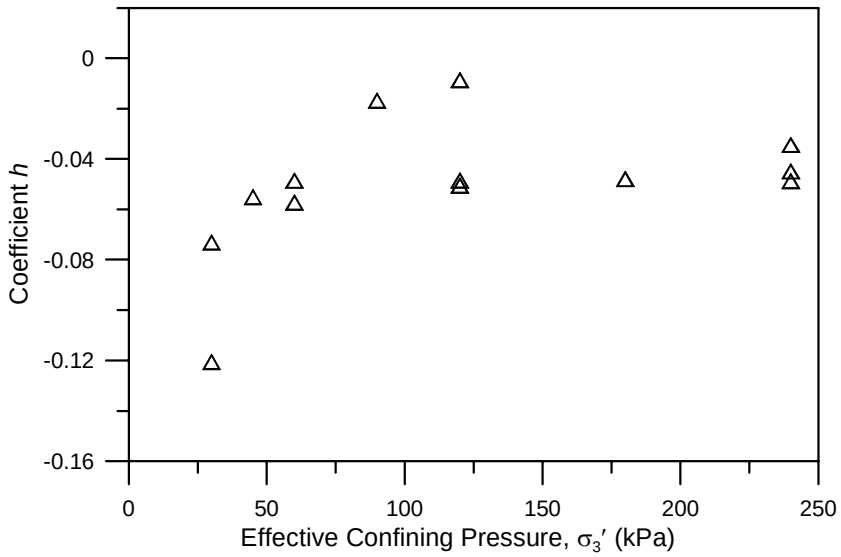

Figure 4.28 Estimation of the coefficient *h* in Equation 4.10

It has been suggested (e.g. Suiker *et al*., 2005) that specimens that are subjected to cyclic loading and then monotonically sheared to failure demonstrate increased strength and stiffness characteristics compared to specimens experiencing static loading only. Cyclic loading can generate an increase in specimen density, and associated increases in stiffness and strength can be significant, especially if the material has high compaction tendencies (Suiker *et al*., 2005). Whilst this procedure was not carried out here (due to detrimental effects on other parameters under investigation), it is expected that latite basalt would also exhibit increased strength following cyclic loading, providing the extent of permanent axial strain during the cyclic loading phase is not excessive. This theme will be investigated further in Chapter 6.

4.7.3 Accuracy of Existing Resilient Modulus Relationships

A significant number of relationships connecting the magnitude of M_R to the relevant stress condition have been devised in the past, and many of these are listed in Table 2.8.

In order to evaluate which models can most adequately predict the stiffness characteristics of railway ballast under high-speed drained cyclic loading, data from the $q_{max,cyc}$ = 230 kPa and 500 kPa tests was entered into the multi-stress parameter models shown in Table 4.5. In the models, *k*, *n*, and *m* are regression coefficients, θ is the bulk stress, τ_{oct} is the octahedral shear stress, σ_{oct} is the octahedral normal stress, σ_d is the deviator stress, and *R* is equal to $p\psi^3$ where *p* is a constant and ψ is as defined previously. The correlation (or lack of) between the measured and estimated M_R values were calculated and compared using the coefficient of correlation R^2 and the sum of the squared errors $\sum error^2$ (Appendix E) at various numbers of cycles N. The parameters *k*, *m*, *n*, and the R^2 and $\sum error^2$ values for each of the respective models are shown in Tables 4.6 – 4.9. Overall, the most satisfactory model appears to be that proposed by Elliott and David (1989) (average $\sum error^2$ for all tests = 873, R^2 = 0.93), followed by Shackel (1973b) ($\sum error^2$ = 1405, R^2 = 0.88).

4.7.4 Empirical Resilient Modulus Relationship

In order to establish an empirical equation relating the four parameters resilient modulus M_R, number of cycles N, maximum deviator stress $q_{max,cyc}$ and effective confining pressure σ_3', the model suggested by Brown *et al*. (1975) (Equation 4.11) was further extended to account for the change in M_R with N. The Brown *et al*. (1975) model was selected due to its simplicity and multi-stress parameter feature.

$$M_R = G\left(\frac{q_{max,cyc}}{\sigma_3'}\right)^H \qquad (4.11)$$

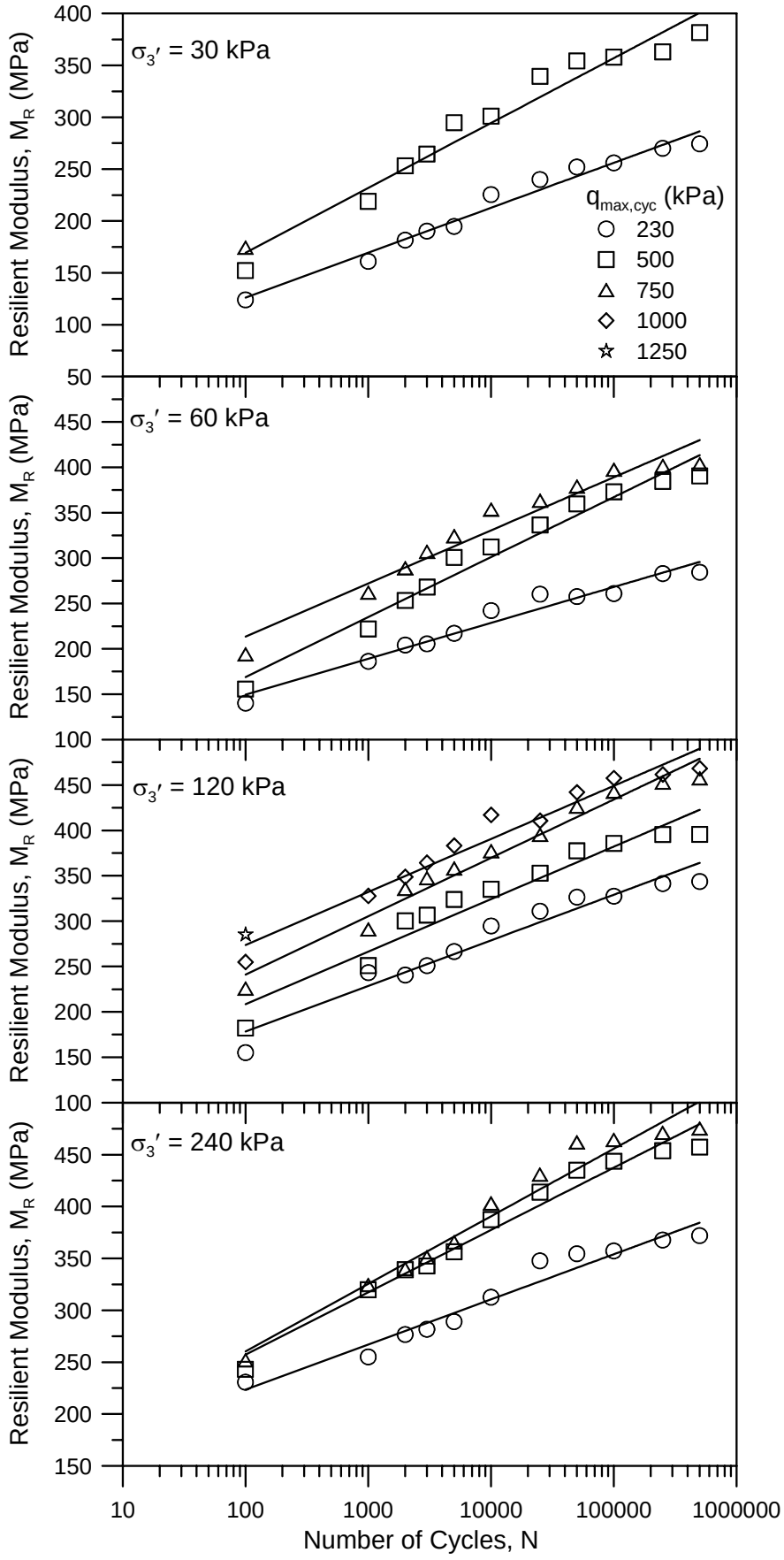

Figure 4.29 Effect of deviator stress magnitude $q_{max,cyc}$ (Δq_{cyc}) on the resilient modulus M_R as a function of the number of loading cycles N

As M_R evolves with N (e.g. Figure 4.26), it is possible to relate the coefficients *G* and *H* to the number of cycles N. For instance, for $q_{max,cyc}$ = 500 kPa there are nine experiments each with different σ_3' (ranging from 10 to 240 kPa, see Table 3.4). *G* and *H* values can be obtained for these nine experiments for each N according to the example given in Table 4.10. Tables 4.11 – 4.13 illustrate the *G* and *H* values for each respective $q_{max,cyc}$, and Figures 4.31 and 4.32 illustrate the effect of N on *G* and *H*. Note that there is some variation in *H* in Figure 4.32 for $q_{max,cyc}$ = 750 kPa, and this is attributed to the relative lack of data obtained for this deviator stress amplitude (data was obtained from three experiments only). The relationships between *G*, *H* and N are approximately logarithmic, with the lines of best fit provided in Table 4.14.

In summary, resilient modulus of ballast can be related to the confining pressure, deviator stress magnitude and number of cycles by Equation 4.11, where coefficients *G* and *H* are a function of N as shown in Table 4.14 and Figures 4.31 and 4.32.

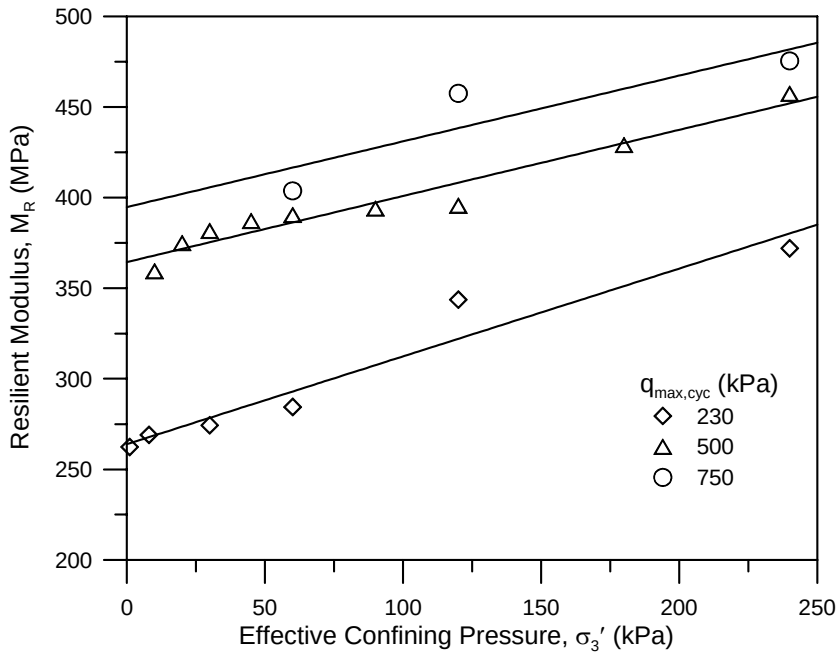

Figure 4.30 Final resilient modulus M_R values after 500000 cycles as a function of the effective confining pressure σ_3'

Table 4.5 Models tested for suitability for use in predicting resilient modulus M_R response during high speed drained cyclic loading of ballast

Reference	Model
Uzan (1985)	$M_R = k\theta^n(\sigma_d)^m$
Brown *et al*. (1975)	$M_R = k\left(\frac{\sigma_d}{\sigma_3}\right)^n$
Shackel (1973b)	$M_R = k\left[\frac{(\tau_{oct})^n}{(\sigma_{oct})^m}\right]$
Elliott and David (1989)	$M_R = \frac{k\theta^n}{10^R}$

Table 4.6 Results of the evaluation of the Uzan (1985) model

Please see print copy for Table 4.6

Table 4.7 Results of the evaluation of the Brown *et al*. (1975) model

Please see print copy for Table 4.7

Table 4.8 Results of the evaluation of the Shackel (1973b) model

Please see print copy for Table 4.8

Table 4.9 Results of the evaluation of the Elliott and David (1989) model

Please see print copy for Table 4.9

Table 4.10 Example of calculated coefficients *G* and *H* for $q_{max,cyc}$ = 500 kPa at 2000 loading cycles

σ_3' (kPa)	N	M_R (MPa) (measured)	M_R (MPa) (predicted)	$\sum error^2$
10	2000	210	204	36
20	2000	226	227	1
30	2000	253	242	129
45	2000	246	258	137
60	2000	253	269	251
90	2000	294	287	47
120	2000	300	300	0
180	2000	318	319	1
240	2000	339	334	29
			$\sum$	631
	G	373.9		
	H	-0.155		

Table 4.11 *G* and *H* values for $q_{max,cyc}$ = 230 kPa

N	*G*	*H*
100	208.0	-0.249
1000	255.0	-0.188
2000	261.7	-0.141
3000	265.9	-0.125
5000	276.0	-0.122
10000	305.5	-0.125
25000	324.4	-0.101
50000	327.1	-0.079
100000	329.2	-0.077
250000	343.2	-0.071
500000	345.5	-0.069

Table 4.12 *G* and *H* values for $q_{max,cyc}$ = 500 kPa

N	*G*	*H*
100	267.9	-0.201
1000	343.4	-0.176
2000	373.9	-0.155
3000	369.0	-0.124
5000	387.8	-0.114
10000	426.4	-0.129
25000	439.4	-0.108
50000	465.4	-0.108
100000	467.4	-0.097
250000	478.0	-0.096
500000	466.5	-0.070

Table 4.13 *G* and *H* values for $q_{max,cyc}$ = 750 kPa

N	*G*	*H*
100	313.0	-0.186
1000	386.8	-0.155
2000	394.2	-0.112
3000	397.0	-0.093
5000	407.6	-0.085
10000	449.0	-0.095
25000	495.8	-0.123
50000	545.3	-0.141
100000	531.0	-0.110
250000	541.7	-0.112
500000	548.5	-0.115

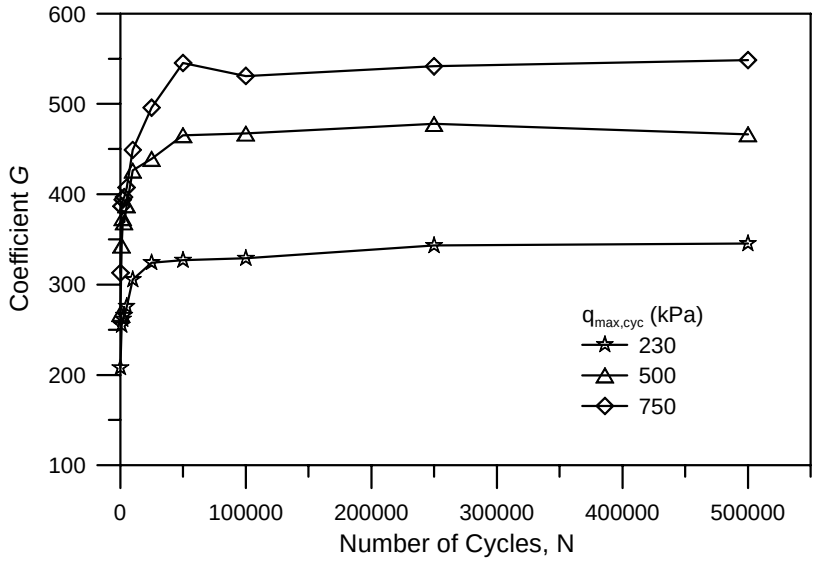

Figure 4.31 Relationship between coefficient *G* and the number of cycles N

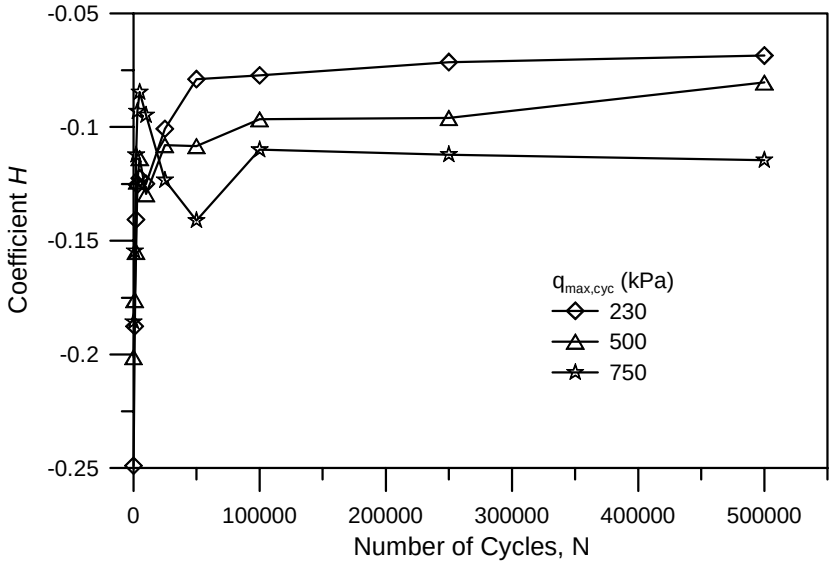

Figure 4.32 Relationship between coefficient *H* and the number of cycles N

Table 4.14 Relationships between deviator stress, coefficient *G* and N, and deviator stress, coefficient *H* and N

$q_{max,cyc}$ (kPa)	coefficient *G*
230	*G* = 16.946Ln(N) + 136.21
500	*G* = 24.877Ln(N) + 175.12
750	*G* = 30.87Ln(N) + 166.79
$q_{max,cyc}$ (kPa)	coefficient *H*
230	*H* = 0.0205Ln(N) - 0.3138
500	*H* = 0.0141Ln(N) - 0.2575
750	*H* = 0.0053Ln(N) - 0.1701

4.8 Chapter Summary

This Chapter described the permanent and resilient deformation behaviour of railway ballast under drained high-speed cyclic loading. After justifying the use of an arbitrary level of axial strain accumulation as the indicator of specimen failure, it was identified that the magnitude of axial strain is a function of both the deviator stress magnitude and

the effective confining pressure. Volumetric strain was shown to become increasingly compressive with increasing confining pressure. Unlike axial strain that exhibits shakedown within the initial 10000 loading cycles, volumetric strain continues to evolve indefinitely with increasing N. The influence of loading amplitude on the magnitude of volumetric strain suggests that maximum specimen compression can be achieved at approximately $\psi = 0.75$, where ψ is the ratio of the maximum cyclic deviator stress to the static peak strength. It was elucidated that cyclically loaded specimens display a much greater tendency for volumetric compression than statically loaded specimens, and that increased frequency may result in a significantly greater degree of permanent axial deformation.

The resilient strain magnitude was shown to increase with increasing loading amplitude and decreasing confining pressure. Similar to past studies, the resilient modulus increased with the level of confinement. A significant deviation from previous works occurred, however, when it was established that the resilient modulus increases indefinitely with the number of loading cycles in a similar way to the volumetric strain. A relationship between resilient modulus and volumetric strain as a function of the number of loading cycles was consequently established. It was expressed that the resilient modulus model devised by Elliott and David (1989) appears to provide a better fit to the measured data than other scrutinised multi-stress models. Lastly, an additional relationship was derived that can successfully correlate the resilient modulus to two stress states (confining pressure and deviator stress magnitude) as well as the number of cycles.

Chapter 5 investigates the breakage or degradation behaviour of latite basalt.

CHAPTER 5

BALLAST DEGRADATION UNDER CYCLIC LOADING

5.1 Introduction

This Chapter explores the degradation or breakage behaviour of railway ballast under drained cyclic loading by utilising the new breakage quantification method BBI (ballast breakage index, see Section 3.6.2, Chapter 3). The chapter begins with a brief summary of the effect of confining pressure on ballast degradation under static triaxial loading conditions. The influence of the number of loading cycles on degradation is examined next, followed by the effects of stress state (confining pressure and deviator stress magnitude) and particle size distribution. The chapter concludes with some additional details regarding degradation under cyclic loading and a summary of how ballast breakdown affects in-situ track performance.

It is expected that the degradation behaviour of particles under static and cyclic loading differs significantly, however, only a few studies have attempted to quantify breakage under cyclic loading. As explained previously in Section 2.6.2 (Chapter 2), Lees and Kennedy (1975) recognised that the degradation of granular materials can occur in three ways: a) the breakage of angular corners or projections, b) the grinding or attrition of asperities, and c) the splitting of particles into two or more approximately equal parts. As a result of the degradation process ballast particles become smaller. In the case of extreme particle breakage, even drainage can be impeded as observed in some ‘fouled’ rail tracks prior to maintenance. Moreover, as the particles become less angular, the shear strength is reduced. The study of ballast degradation under cyclic loading is

therefore extremely important in ensuring the integrity of the railway substructure and the track configuration as a whole.

5.2 Review of Ballast Degradation under Static Loading

Before examining the effects of confining pressure σ_3' and deviator stress magnitude $q_{max,cyc}$ on ballast degradation under cyclic loading, it is important to acknowledge the influence of σ_3' on particle breakage during drained monotonic triaxial shear. This subject has been considered extensively in the past (e.g. Marsal, 1973; Lade *et al*., 1996; Ueng and Chen, 2000; Indraratna and Salim, 2002), and results indicate that breakage can become significant at high σ_3'. The increasing levels of degradation associated with increasing σ_3' has been mainly attributed to the inability of aggregates to dilate under high levels of confinement. In addition, at elevated σ_3' larger deviatoric loads are required to instigate specimen failure, thus resulting in greater macroscopic stress concentrations acting on the specimen (and hence greater microscopic stresses on individual particles) and consequently increased breakage. Degradation under static loading commences with the rupture of angular corners and sharp asperities as particles attempt to rearrange to form a more stable configuration. As the deviatoric load increases, the splitting of the larger, weaker, more angular particles is expected. In summary, it is well established that the breakage magnitude increases with the effective confining pressure under monotonic triaxial loading conditions.

5.3 Effect of the Number of Loading Cycles on Ballast Degradation

The effect of the number of loading cycles N on ballast degradation was examined by subjecting six specimens to N = 2, 1000, 10000, 25000, 500000, and 2000000 loading cycles, respectively. The stress state $q_{max,cyc}$ = 750 kPa and σ_3' = 120 kPa at a 20 Hz cyclic frequency (see Table 3.4) was utilised for each specimen, except for the specimen with N = 2 that experienced only 1 Hz loading. Before detailing the results of the experiments, Figure 5.1 provides a review of the new ballast breakage index BBI (Equation 3.4). As explained in Chapter 3, as the degree of particle breakage increases the final particle size distribution (PSD) curve shifts further towards the smaller particle size region on a traditional PSD plot. The area *A* between the initial and final PSD increases resulting in a greater BBI value. The relative breakage B_r quantification technique introduced by Hardin (1985) would produce similar trends to BBI in relation to the effects of N, σ_3' and $q_{max,cyc}$ on breakage, however plots of B_r have been neglected from the current analysis.

The effect of N on axial strain ε_a, volumetric strain ε_v, radial strain ε_r, BBI and resilient modulus M_R for the six experiments is illustrated in Figures 5.2a – 5.2e, respectively. A reasonable degree of correlation exists between the various experiments, verifying the repeatability of the cyclic triaxial tests. As Figure 5.2d illustrates, particles fail (break or degrade) not only at the beginning of loading when ε_a rates are greatest, but also by fatigue as N increases. Data from Figures 5.2b and 5.2d at the conclusion of the each respective N are plotted in Figure 5.3a as a function of N. Evidently, both ε_v (in agreement with Section 4.4, Chapter 4) and BBI increase approximately logarithmically with N, particularly beyond about 1000 cycles in the case of BBI. The data from Figure

5.3a is replotted in Figure 5.3b as ε_v against BBI for N ≥ 1000. For N in the order of 1000 cycles or less, the particles are still undergoing initial shakedown, but for N ≥ 10000 a 'stabilising' stage is obtained where the relationship between ln ε_v and BBI is linear as shown in Figure 5.3b. Therefore, breakage can be represented as a function of volumetric strain according to:

$$\varepsilon_v(\%) = se^{t(BBI)} \tag{5.1}$$

In Equation 5.1, ε_v is the volumetric strain, and *s* and *t* are empirical constants (for latite basalt *s* = 1.73 and *t* = 10.0 with $R^2 > 0.98$). The rate of degradation, therefore, appears to be closely correlated to the rate of volumetric strain for compressing specimens under drained cyclic loading conditions.

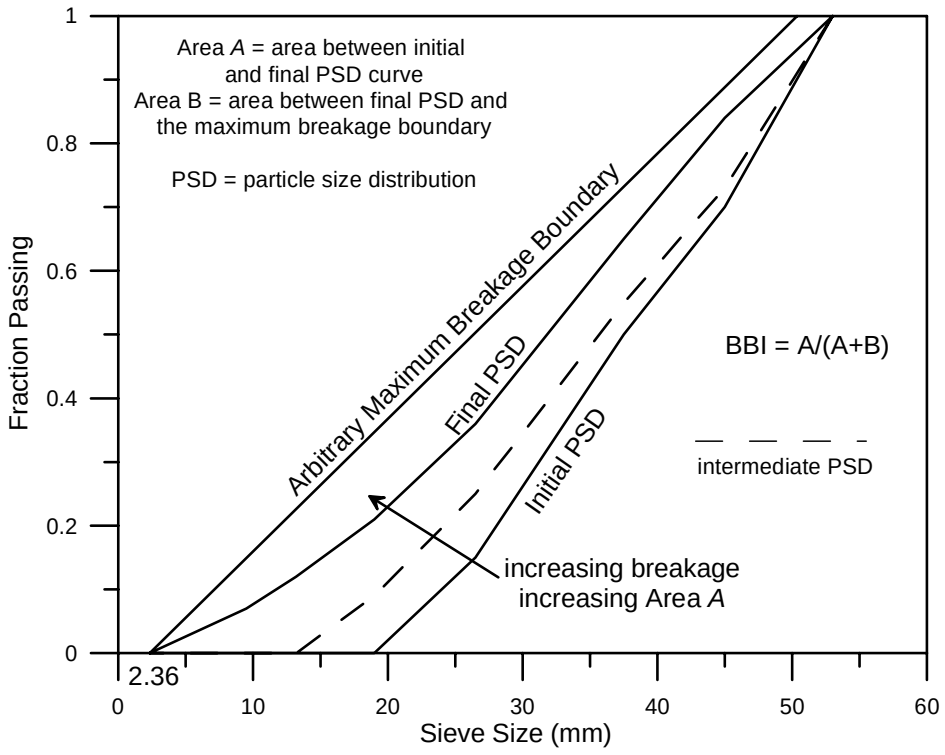

Figure 5.1 Review of the method of calculation of the ballast breakage index BBI

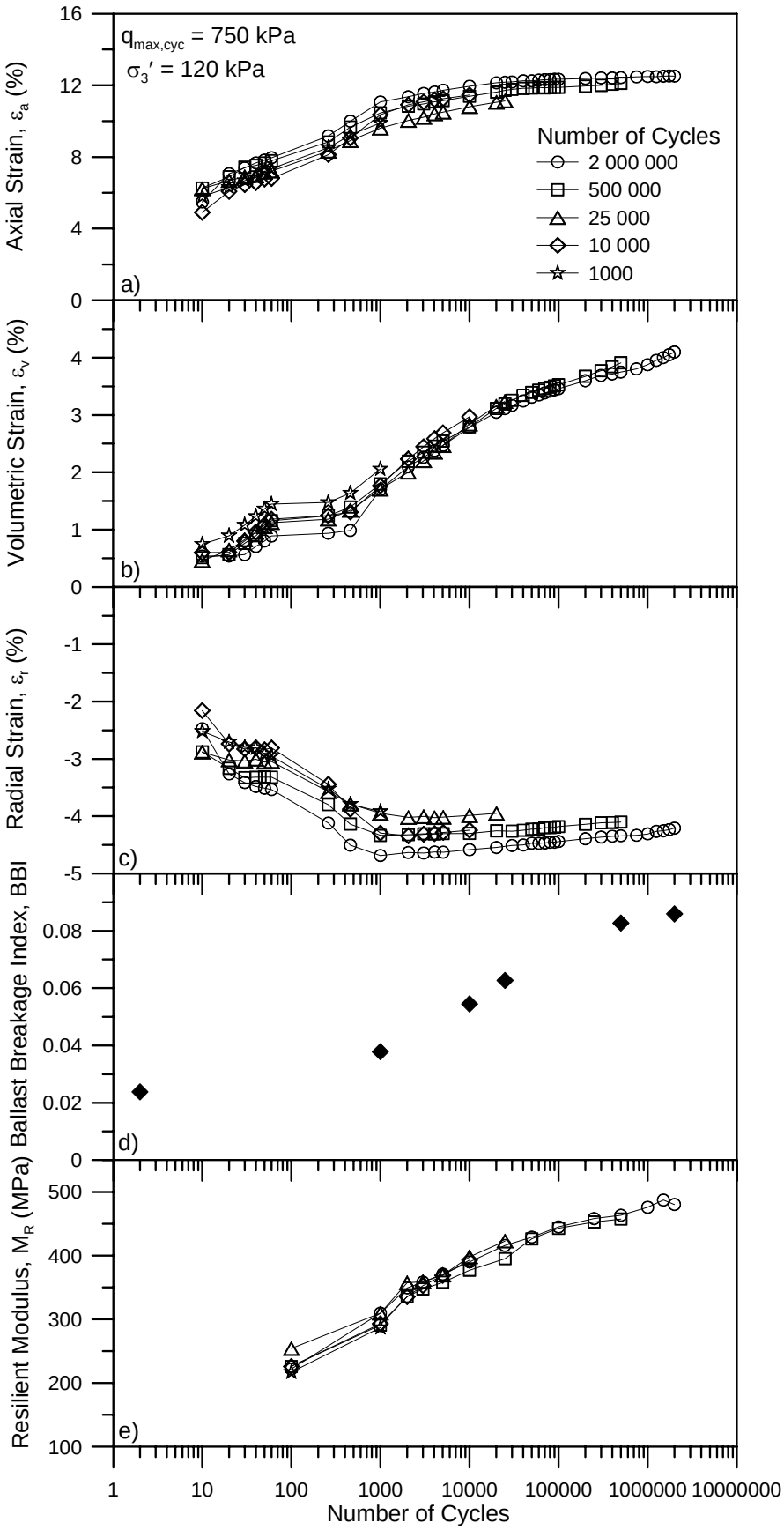

Figure 5.2 Effect of the number of loading cycles N on (a) Axial strain ε_a (b) Volumetric strain ε_v (c) Radial strain ε_r (d) Ballast breakage index BBI, and (e) Resilient modulus M_R

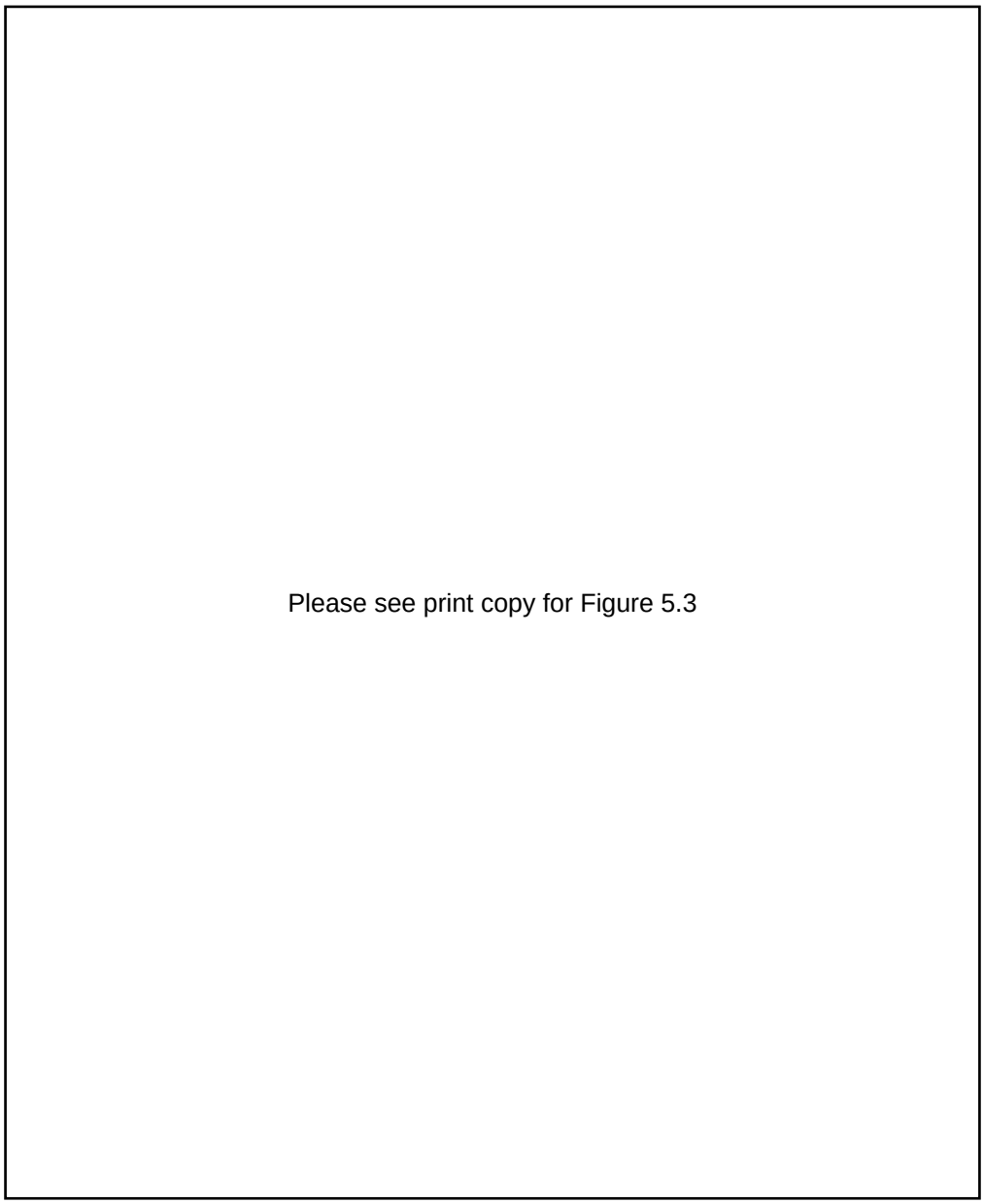

Figure 5.3 Relationships between volumetric strain ε_v, BBI and N, (a) ε_v and BBI as a function of N, and (b) BBI as a function of ε_v (after Indraratna *et al*., 2005)

Miura and O′Hara (1979) have also published data detailing the effect of the number of cycles N on particle degradation. The triaxial experiments were conducted on decomposed granite soil and were limited to a maximum N of 500 cycles. The volumetric strain ε_v and breakage data is depicted in Figure 5.4a as a function of N, where breakage is expressed by the change in total particle surface area (ΔSA), measured in cm^2/cm^3. They determined that the rates of breakage and ε_v develop rapidly during the first 100 - 200 cycles and gradually diminish thereafter. Figure 5.4b shows the measured and predicted values of ε_v based on Equation 5.1. In this case s = 0.413, t = 0.069 and BBI has been replaced by ΔSA. There is some similarity between the measured and predicted values, indicating that Equation 5.1 may be applicable in estimating the breakage magnitude based on the evolution of ε_v for other materials, providing the coefficients s and t are known. The main cause of the lack of correlation in Figure 5.4b is the ΔSA data point at N = 100 which is lower than expected. This highlights the sensitivity of Equation 5.1 to the measured breakage response. Further research is still required, however, to validate Equation 5.1 for other types of aggregates and for different breakage indices.

5.4 Effect of Stress State (Confining Pressure and Deviator Stress Magnitude) on Ballast Degradation under Cyclic Loading

The effect of confining pressure σ_3' on the breakage of ballast is illustrated in Figure 5.5 for three $q_{max,cyc}$ amplitudes of 230, 500 and 750 kPa. Clearly, there is no direct linear relationship between the magnitude of breakage and σ_3' as is often the case under monotonic triaxial shearing. Figure 5.5 shows that for the range of σ_3' considered (1 – 240 kPa), degradation is most significant at the extremities of the range i.e. at low and

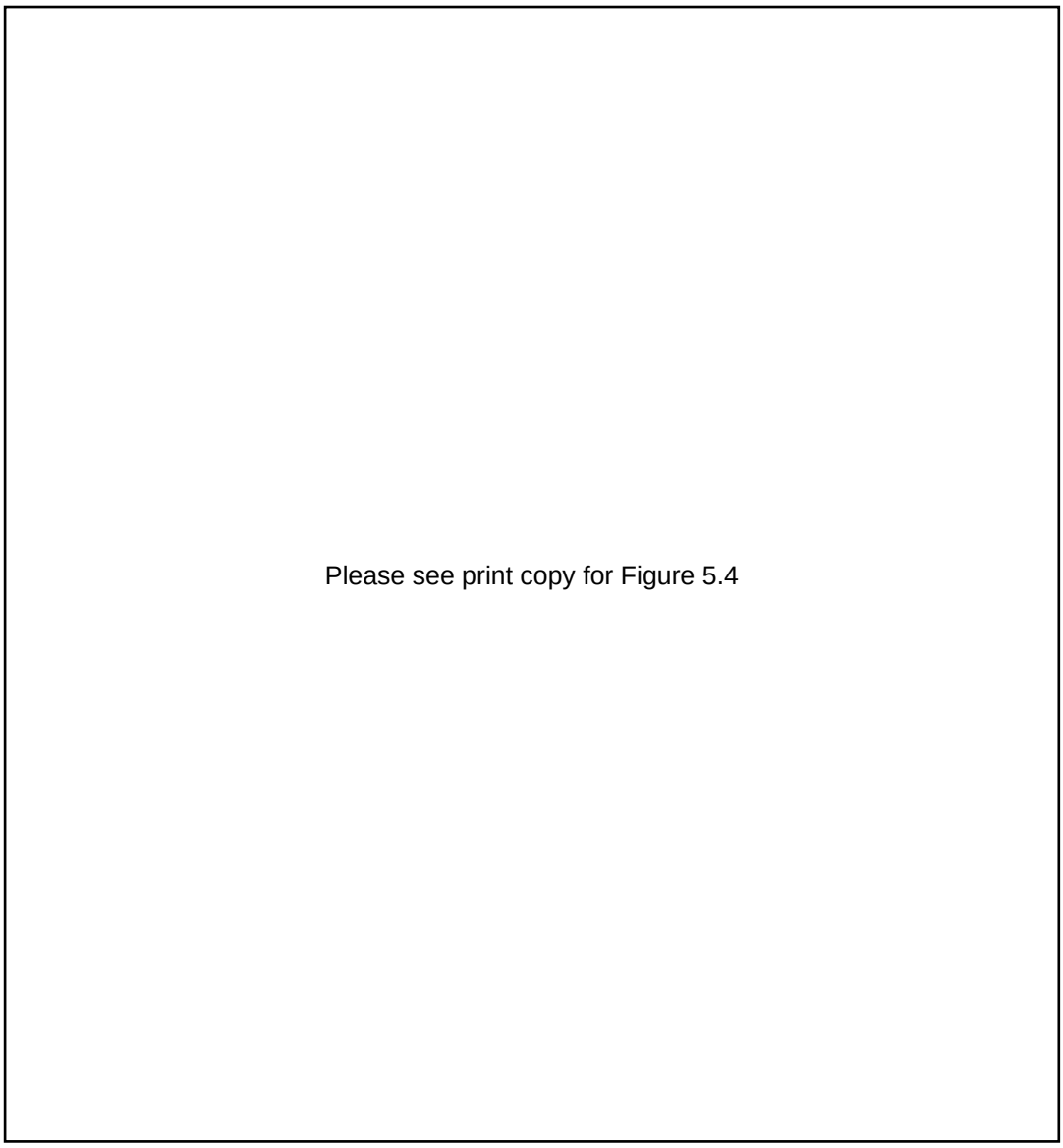

Figure 5.4 Effect of the number of loading cycles N on the change in surface area ΔSA for a decomposed granite soil (data replotted from Miura and O′Hara, 1979)

high σ_3'. At some intermediate value of σ_3' minimal breakage is obtained. Based on this observation, the breakage behaviour under cyclic loading has been categorised into three distinct zones that are delimited by specific σ_3' values and dependent on the $q_{max,cyc}$ amplitude. The zones have consequently been named the dilatant unstable degradation zone (DUDZ, occurring at low σ_3'), the optimum degradation zone (ODZ, intermediate σ_3'), and the compressive stable degradation zone (CSDZ, high σ_3') based on the corresponding volumetric strain behaviour. An explanation of each zone,

including the influences of σ_3', $q_{max,cyc}$ and the specimen straining and micromechanical response, is presented below.

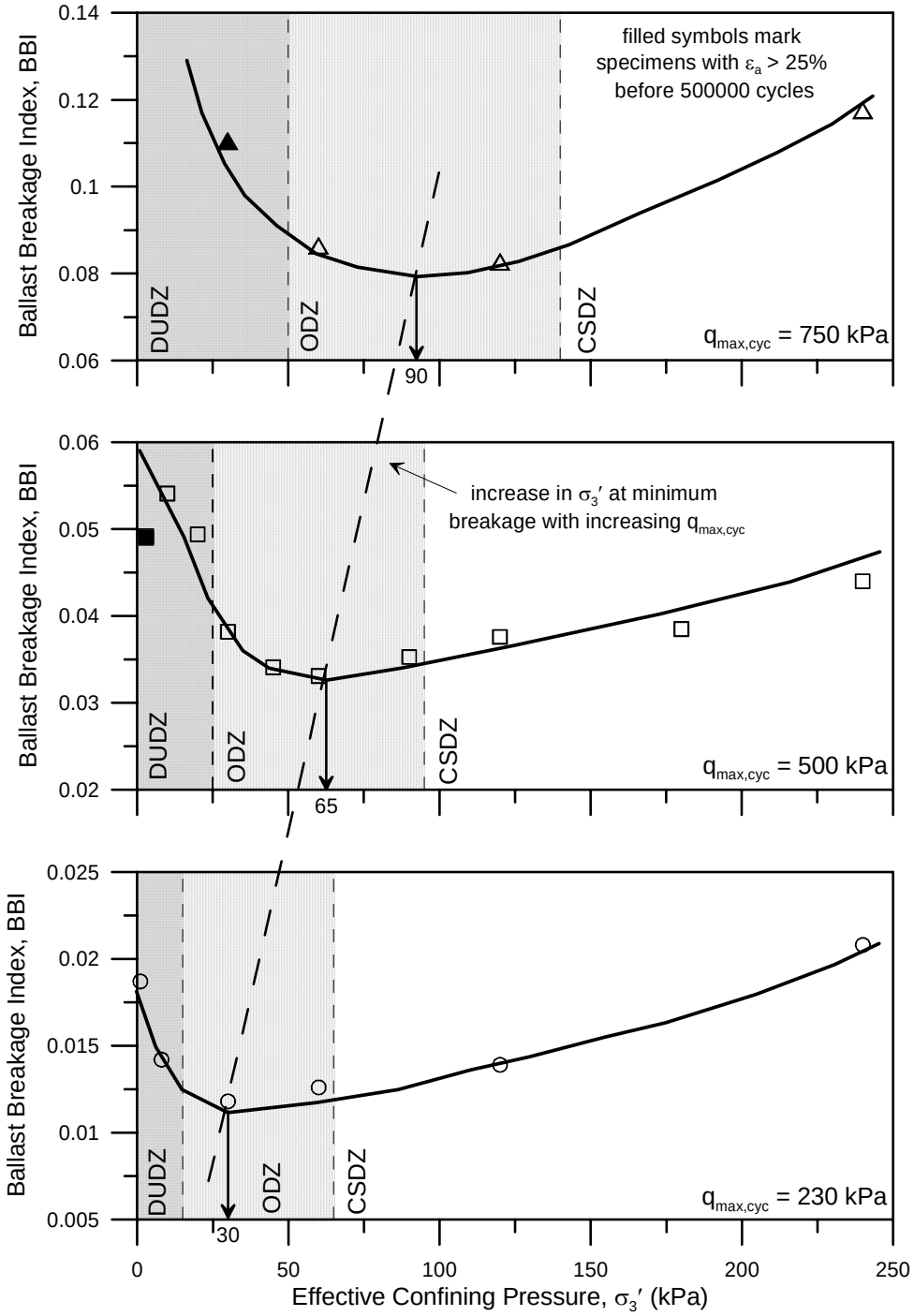

Figure 5.5 Effect of confining pressure σ_3' and maximum deviator stress $q_{max,cyc}$ on the ballast breakage index BBI

5.4.1 The Dilatant Unstable Degradation Zone (DUDZ)

Specimens that are subjected to low σ_3' and experience overall volumetric dilation during cyclic loading caused by rapid and considerable axial and expansive radial strains are characterised in the DUDZ. Indraratna *et al*. (1998) observed similar straining behaviour for the same material during static triaxial loading at small σ_3'. The specimens experiencing dilation (and the loads necessary to cause dilation) were illustrated earlier in Figure 4.13. Preliminary investigations using $q_{max,cyc}$ = 230 and 500 kPa initially established the upper bound of the DUDZ at σ_3' = 30 kPa (Indraratna *et al*., 2005). However, instead of utilising a single σ_3' to define the DUDZ - ODZ boundary, the addition of the $q_{max,cyc}$ = 750 kPa data revealed that the transition depends primarily on the magnitude of $q_{max,cyc}$ as illustrated in Figure 5.5. For relatively minor $q_{max,cyc}$ such as 230 kPa, the range of σ_3' defining the DUDZ is comparatively small because the deviator stress amplitude is insufficient to cause dilation, the main requirement for DUDZ behaviour. As the deviator stress $q_{max,cyc}$ increases for a given σ_3' the propensity for dilation becomes much greater, thus the DUDZ σ_3' range increases. The DUDZ boundaries for each respective $q_{max,cyc}$ are listed in Table 5.1 and can be determined from Figure 4.13 at ε_v = 0. Table 5.2 provides an estimate of the $q_{max,cyc}/p'$ range for each degradation zone, and from this table DUDZ behaviour typically occurs when $q_{max,cyc}/p' > 2.5$. This stress ratio value may vary depending on the aggregate under consideration.

Table 5.1 Upper confining pressure σ_3' bounds of the DUDZ and ODZ for each respective deviator stress magnitude $q_{max,cyc}$

	DUDZ	**ODZ**
$q_{max,cyc}$ (kPa)	σ_3' upper bound (kPa)	
230	15	65
500	25	95
750	50	140

Table 5.2 $q_{max,cyc}/p'$ ratios for the DUDZ, ODZ and CSDZ degradation zones

	$\mathbf{q_{max,cyc}/p'}$
DUDZ	> 2.5
ODZ	1.7 – 2.5
CSDZ	< 1.7

It is believed that specimens subjected to DUDZ conditions have poorly established particle contacts with relatively small particle-to-particle contact areas, allowing for significant relative movements (rolling, sliding etc) between particles. As a result of large shear forces and excessive axial and radial strains, particle breakage primarily results from the shearing and attrition of angular projections due to the considerable degrees of particle movement and rearrangement. Very little particle splitting is observed in the DUDZ due to ineffectual particle contacts.

Oda (1972) and Cundall *et al*. (1982) ascertained that the deviatoric force is not carried uniformly by all particles within a granular assembly, but is instead transmitted mainly through chain or column like structures aligned in the direction of the major principal stress. They found that particles participating in these vertical force columns were highly stressed, whereas all remaining particles carried little or no load. Consider, for

example, a DUDZ ballast specimen with major principal stress σ_1' equal to 780 kPa (macroscopic $q_{max,cyc}$ = 750 kPa, σ_3' = 30 kPa) with diameter 300 mm. This translates to an axial force F of 55 kN. This might be distributed over (say) 4 ballast columns, so that the induced characteristic stress (defined as F/D^2) on a ballast particle of diameter D = 40 mm would be about 8.5 MPa. This stress is insufficient to cause the splitting of an intact (flawless) particle based on the particle strengths given by Lim *et al*. (2005). However, if the characteristic stress F/a^2 induced in a small angular projection of size a in a deforming ballast column is considered, it is very likely to fracture. In the DUDZ, the cyclic forces propagate mainly through the weak and vulnerable corners as particles reorientate in order to sustain deformations, thus resulting in extensive degradation of the angular projections and the redistribution of inhomogeneous stresses within the particle assembly.

Degradation in the DUDZ is considered to be the most significant of the three zones, with breakage predominantly occurring at the onset of loading when the axial strain and dilation rates are at a maximum. Not only is breakage excessive in the DUDZ, but axial straining or settlement can also approach undesirable levels.

Figure 5.6 identifies that most specimens in the DUDZ were subjected to ψ values > 1 (where $\psi = q_{max,cyc}/q_{peak,sta}$ as defined in Chapter 4). Therefore, it appears that the three main rudimentary requirements for DUDZ behaviour are a small σ_3' (the magnitude of which is related to $q_{max,cyc}$), $\psi > 1$ and overall specimen dilation. Undoubtedly, DUDZ conditions should be avoided on railway tracks as much as possible, and this can be achieved by ensuring an adequate degree of lateral ballast support.

5.4.2 The Optimum Degradation Zone (ODZ)

Similar to the DUDZ, the range of σ_3' defining the ODZ is influenced by the applied $q_{max,cyc}$ as indicated in Figure 5.5. In the ODZ, the small increase in σ_3' is sufficient to cause an optimum internal stress distribution with increased inter-particle contact areas, resulting in significantly reduced breakage, lower axial strains, and overall specimen compression. The greater σ_3' for a given cyclic deviatoric amplitude provides improved horizontal contact stresses that diminish the induced tensile stresses within particles. The reduction in particle rearrangement lessens the risk of breakage associated with stress concentrations at the angular protrusions. In the DUDZ, excessive particle reorientation can lead to the degradation of the weak particle contacts. However, in the ODZ contact points are more secure and the vertical force chains outlined previously are expected to be more stable (better established) under the influence of cyclic loading. In addition, the coordination number (number of interparticle contacts) is expected to be slightly increased due to the reversal of ε_v behaviour (from dilative to compressive) (see Figure 4.13).

From Figure 5.6 it can be perceived that ODZ specimens generally have ψ values ranging from about 0.4 up to 1.2, and $q_{max,cyc}/p'$ values of about 1.7 – 2.5 (Table 5.2). Increasing the magnitude of $q_{max,cyc}$ also results in a wider ODZ zone (Table 5.1). With reduced settlement and degradation in the ODZ, rail tracks would benefit from slightly increased lateral confining pressure. The practical ways of increasing track confinement will be described and discussed in Chapter 7.

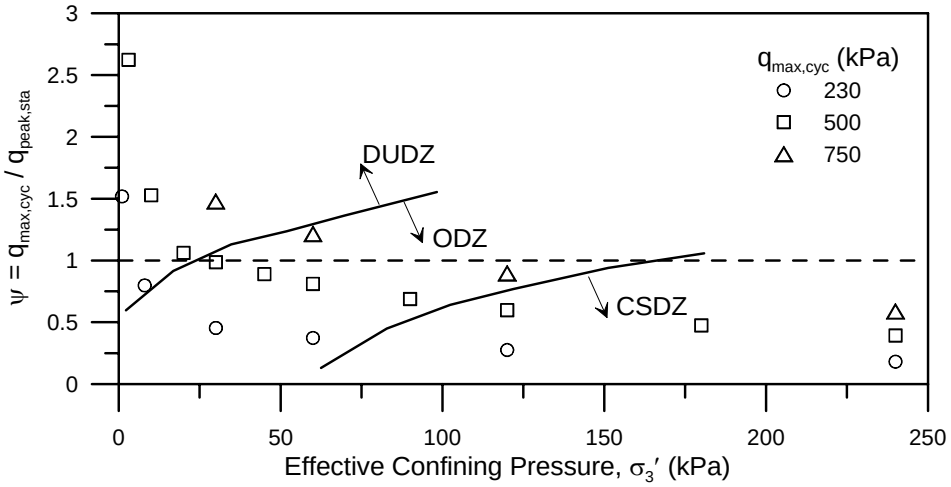

Figure 5.6 Relationship between ψ (= $q_{max,cyc}/q_{peak,sta}$) and confining pressure σ_3', and the location of the breakage zones DUDZ, ODZ and CSDZ

5.4.3 The Compressive Stable Degradation Zone (CSDZ)

Figure 5.5 illustrates that the CSDZ is characterised by the larger σ_3' values. In this zone, particle movement and dilation is largely suppressed due to the considerable levels of confinement. The moderate degree of σ_3' in the ODZ lessened the induced tensile stresses within particles, but in the CSDZ increasing levels of σ_3' force the centres of particles closer together into a denser arrangement introducing highly stressed but relatively secure contact points. The σ_3' boundary between the ODZ and CSDZ can be defined by a 'flattening out' of ε_v in Figure 4.13. The most significant difference between the ODZ and CSDZ is the reduced mobility of particles and subsequent decrease in the radial strain magnitude. Although corner degradation is still the foremost kind of breakage, some particle splitting also takes place in the CSDZ. The lack of interparticle sliding and rolling permits the splitting of the larger, more vulnerable particles through planes of weakness such as microcracks and other flaws. The vertical force chains are likely to be less parallel with the direction of the major principal stress

and more isotropic in the CSDZ due to lateral resistance from surrounding particles. It is expected that more particles within the CSDZ specimens will be directly affected by loading compared to the other zones. It is anticipated that upon initial loading angular projection breakage will still occur as a result of axial straining (similar to ODZ behaviour), but as the number of cycles increases fatigue of particles will also initiate particle splitting. Irrespective of the lower ψ and $q_{max,cyc}/p'$ ratios in the CSDZ, breakage is more significant in this zone compared to the ODZ because of the particle splitting. From Table 5.2 it can be seen that the stress ratio $q_{max,cyc}/p'$ is typically less than 1.7 for CSDZ specimens.

5.4.4 Effect of Deviator Stress Magnitude on Ballast Breakage

Evidently the extent of particle breakage increases with $q_{max,cyc}$ in Figure 5.5. To illustrate this finding more clearly, Figure 5.7 plots $q_{max,cyc}$ against BBI for selected values of σ_3'. It appears that the relationship between breakage and loading stress is approximately exponential, i.e. an increase in $q_{max,cyc}$ causes an exponential increase in the magnitude of degradation. Limiting train axle loads is therefore imperative in preventing excessive ballast breakdown.

5.4.5 Summary of the Degradation Zones

In essence, Figure 5.5 illustrates that the confining pressure necessary to achieve minimum breakage increases with the loading amplitude. Alternatively, if railway organisations were to increase train axle loads, an increased level of ballast confinement would be required to minimise the extent of ballast degradation.

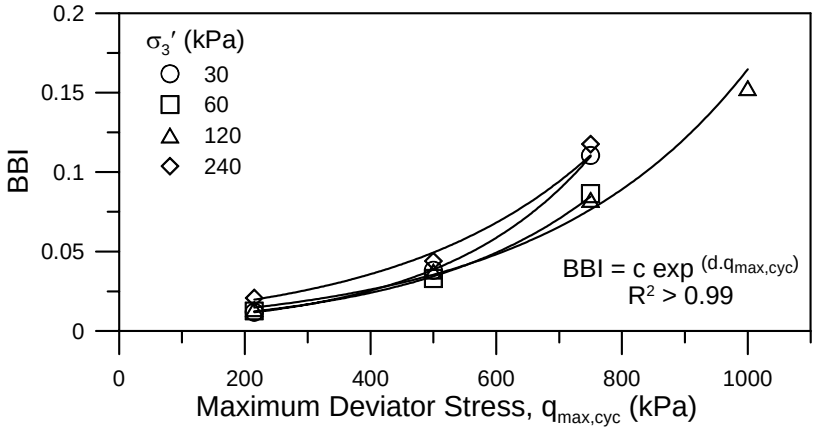

Figure 5.7 Effect of maximum cyclic deviator stress $q_{max,cyc}$ on the ballast breakage index BBI

A summary of the three breakage zones (the DUDZ, ODZ and CSDZ) is presented in Tables 5.3 and 5.4. Table 5.3 provides a pictorial outline of the zones including details of the types of breakage and the anticipated magnitude of particle rearrangement/movement. Table 5.4 relates the zones to the expected axial and volumetric straining behaviour, the resilient modulus and the quality of the interparticle contacts.

5.4.6 Expected Breakage Behaviour at Elevated Confining Pressures

As suggested by Lade *et al*. (1996) and Salim and Indraratna (2004), it is expected that if testing were continued to levels of confinement well beyond the range considered in the current study (i.e. in the MPa range) an alternative breakage behaviour would prevail. At higher confining pressures, the formation of a substantial volume of fines may bring about the attainment of a stable packing arrangement with an optimum internal load distribution. Because of the significant fines content it would then become increasingly more difficult to initiate further degradation. Subsequently, the extent of breakage may plateau with supplementary increases in σ_3', a process termed 'saturation'

by Tsoungui *et al*. (1999). This behaviour is demonstrated conceptually in Figure 5.8. Such magnitudes of confining pressure are well beyond the range encountered on typical railway tracks.

Table 5.3 Expected types of degradation for the three breakage zones, the DUDZ, ODZ and CSDZ, for a typical ballast section

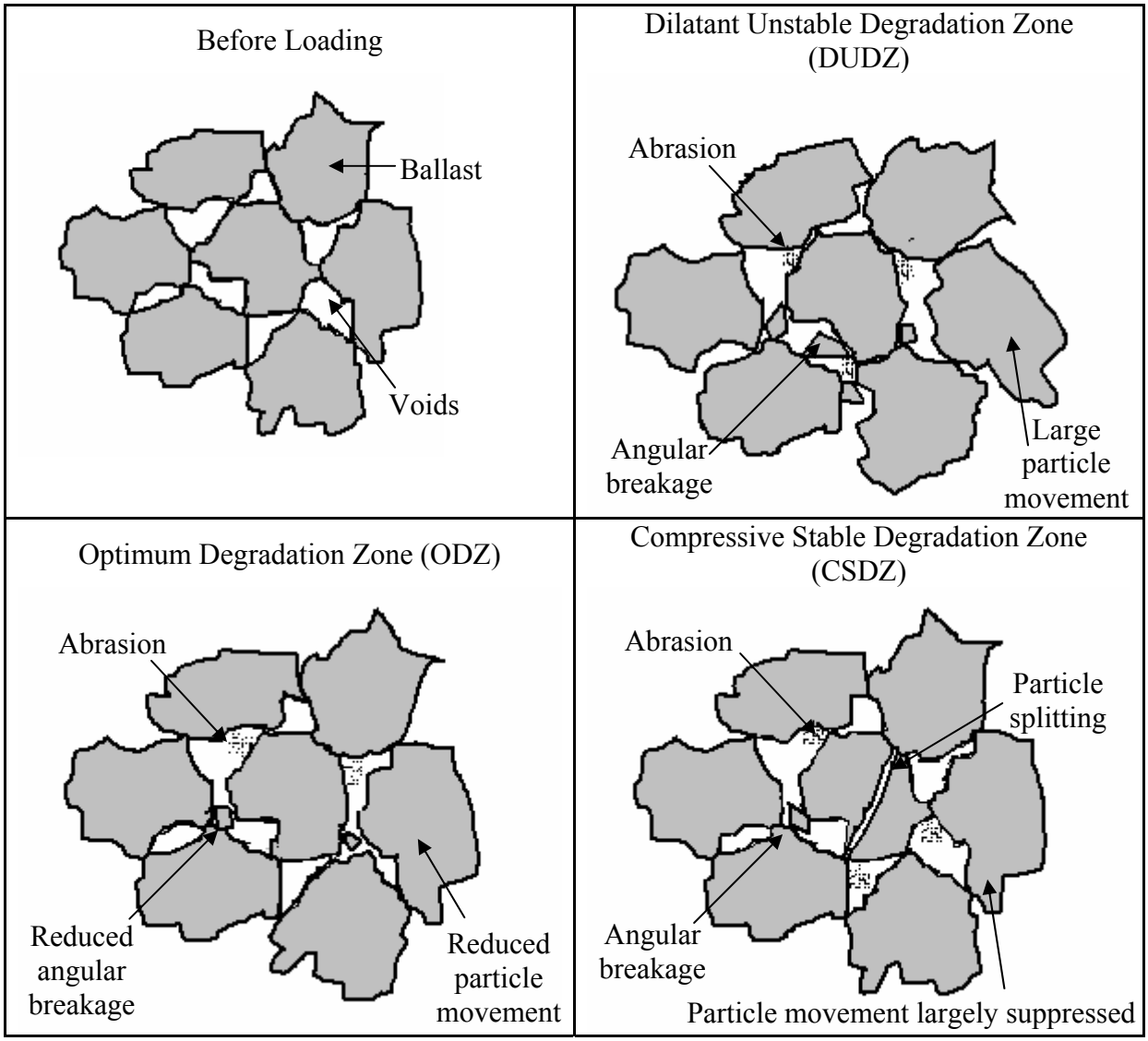

Table 5.4 Relationship between the degradation zones and other investigated parameters

	DUDZ	**ODZ**	**CSDZ**
Axial Strain	Rapid and extensive	Significant	Low
Volumetric Strain	Dilative	Slightly compressive	More compressive
Resilient modulus	Lowest	Higher	Highest
Types of breakage	Corner, abrasion	Corner, abrasion	Corner, abrasion, splitting
$q_{max,cyc}/p'$	> 2.5	1.7 - 2.5	< 1.7
ψ	> 0.75	0.4 – 1.2	< 0.75
Interparticle contact quality	Poor	Reasonable	Good

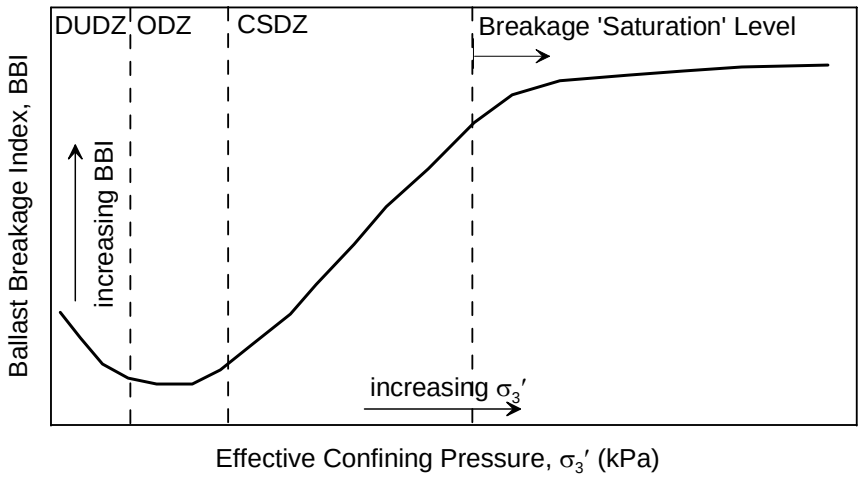

Figure 5.8 Predicted breakage behaviour BBI at confining pressures beyond the range considered in the current study (conceptual only)

5.5 Effect of Aggregate Particle Size Distribution on Breakage

Figure 5.9 illustrates the effect of specimen particle size distribution on the degradation behaviour of ballast using four different breakage quantification indices, the Area *A* (Section 3.6.2, Chapter 3), B_r (Hardin, 1985, Appendix B), B_g (Marsal, 1973), and BBI. Clearly, the various breakage indices produce different trends in relation to the effect of

specimen C_u on breakage. Both B_r and BBI indicate that the uniformly graded specimen suffered the most particle breakdown, whereas Area *A* and B_g designate the very uniform specimen as most prone to breakage. As explained in Section 3.6.2 (Chapter 3), B_r and BBI rely on a potential for degradation (the area between the PSD under consideration and a line of maximum breakage) that is different for each particular PSD, thus these methods do not provide a suitable means of comparison between multiple gradations. Instead, Area *A* and B_g are more suitable for this type of analysis. With this in mind, Figure 5.9 indicates that as the particle uniformity coefficient C_u increases (the specimens become more well graded) the tendency for particle degradation decreases, except in the case of the gap graded specimen. This specimen contained no particles in the size range 37.5 – 45 mm, and with these large particles removed the measured degradation was lower than expected based solely on the C_u value. The better graded specimens have a higher initial specimen density and associated higher coordination number because of void occupation by the finer sizes, contributing to superior interparticle load distribution and a smaller degree of degradation. In conclusion, decreased particle degradation can be expected if the ballast C_u is increased (i.e. the distribution is made more broadly graded through the incorporation of finer particles into the ballast array), or if the more 'vulnerable' sizes are removed.

5.6 Other Characteristics of Ballast Breakage

This section raises a number of issues that are useful in understanding the degradation response of railway ballast. The section commences with an investigation of the influence of coordination number on breakage and is followed by an examination of the

particle sizes that are most vulnerable to breakage. The section concludes with a discussion of the effects of breakage on resilient modulus.

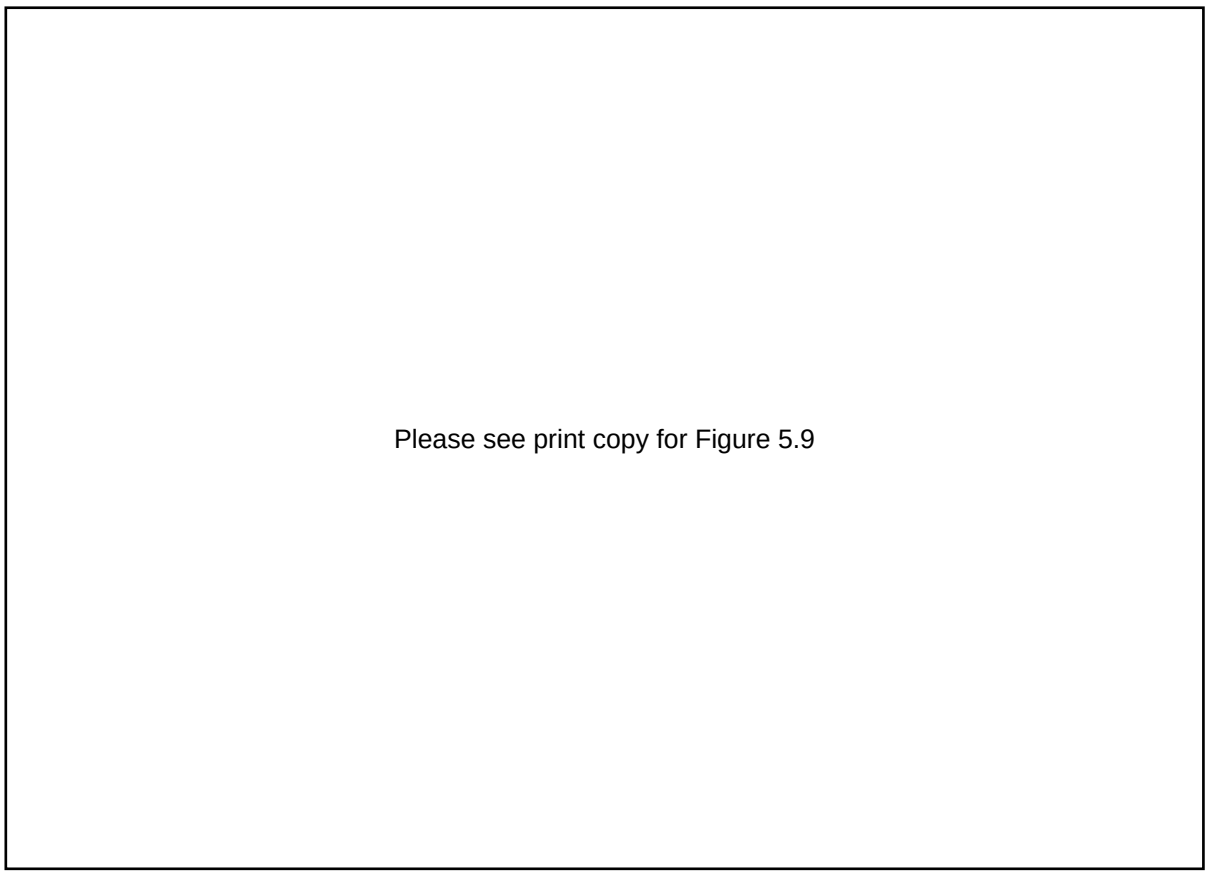

Figure 5.9 Effect of aggregate particle size distribution (C_u, coefficient of uniformity) on breakage using (a) Area *A*, (b) B_r (Hardin, 1985), (c) B_g (Marsal, 1973), and (d) BBI (Indraratna *et al*., 2005)

5.6.1 Influence of Coordination Number on Ballast Breakage

It has been established that the fracture probability of a particle subjected to compressional forces within a granular media is a function of the applied stresses ($q_{max,cyc}$ and σ_3'), the particle size, and the coordination number, i.e. the number of particle contacts (McDowell *et al*., 1996; McDowell and Bolton, 1998). McDowell and

Bolton (1998) examined the tensile splitting characteristics of particles and acknowledged that particle survival is reliant on two opposing factors, particle size and coordination number. However, they noted that high coordination numbers were less helpful for angular particles as these particles may fail in bending. In the current study, it was determined both visually and by sieve analysis that most ballast degradation was not the direct result of particle splitting, but is instead a consequence of corner and asperity breakage. Coordination number is, therefore, only pertinent when splitting is the predominant mode of fracture, and the extent of particle angularity is much more important in determining the likelihood of breakage. Typical examples of ballast splitting (in this case from the CSDZ) and corner degradation (from the DUDZ) are illustrated in Figure 5.10.

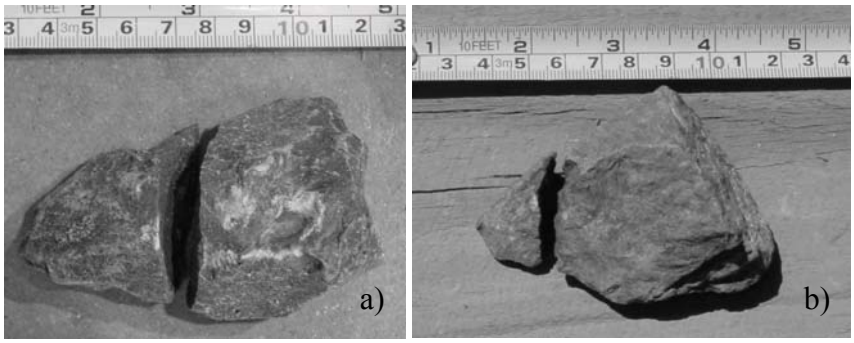

Figure 5.10 Examples of ballast breakage, (a) particle splitting in the CSDZ, and (b) corner degradation from the DUDZ

5.6.2 Particle Sizes Most Vulnerable to Degradation

Some studies of granular materials (e.g. Hardin, 1985; Lade *et al*., 1996; Indraratna *et al*., 1998) have recognised that the larger particles within an aggregate are more susceptible to degradation simply because of the greater prevalence of flaws such as microcracks within their volume. Other studies state that the smaller particles have a

higher chance of fracture due to the small number of particle contacts and the associated inferior intra-particle load distribution (e.g. McDowell *et al*., 1996; Tsoungui *et al*., 1999). Using sieving analysis, it is possible to determine if there has been a loss in mass of the largest size (i.e. the largest particles have suffered some degradation) but it is not possible to identify whether the smaller particles have also been broken. To determine categorically which ballast particle sizes are most prone to degradation one may require that each fraction be painted a different colour and the extent of change of each coloured fraction evaluated following loading. Whilst this procedure was not performed in the current study, it is anticipated that most breakage occurred amongst the bigger particles. This behaviour is anticipated because of the existence of a greater number of critical flaws within these particles, and the prevalence of corner breakage and asperity wear. In addition, the angular to very angular ballast particle shape suggests that the coordination number (which can be significant for larger particles) is of minor importance as discussed in Section 5.6.1. It is therefore expected that the larger particles are generally the most prone to degradation under cyclic loading.

5.6.3 Effect of Breakage on Resilient Modulus

From the breakage results displayed in Figures 5.2 and 5.5 there is no evidence to suggest that particle breakage has a significant effect on the magnitude of resilient modulus. However, the material used in the current study (latite basalt) is relatively strong in terms of breakage strength compared to other railway aggregates, and a weaker material may exhibit a reduced resilient modulus associated with large-scale particle breakdown. In the event of insignificant (minor) degradation, it is speculated that the measured resilient modulus might be slightly greater than for a test displaying

considerable breakage. It is important to note that standard laboratory triaxial tests do not simulate the effects of ballast fouling (caused by breakage and/or other factors such as clay pumping), which in the long term could bring about a reduction in the resiliency of the ballast and track structure.

5.6.4 Influence of Breakage Type on Track Behaviour

It is anticipated that immediately following track maintenance or the establishment of a new railway line, in-situ ballast breakage would initially consist of angular corner or projection breakage. This type of breakage would influence early track settlement behaviour. Particles would begin to display splitting characteristics under the following circumstances, a) once the ballast density reaches a critical value, or b) at the start of loading in the case of weak particles with pre-existing critical flaws. Particle splitting is more responsible for the long term safety and stability of the track structure. The grinding or attrition of asperities occurs during all stages of track life and contributes to ballast fouling and reduced drainage.

5.7 Chapter Summary

This chapter examined the effects of confining pressure, deviator stress magnitude and the number of cycles on ballast degradation under drained cyclic loading. A brief summary of the static triaxial degradation response of ballast was presented at the beginning of the Chapter, and this outline provided a useful comparison to the cyclic response. It was revealed that cyclic degradation has an approximate logarithmic relationship with the number of loading cycles, similar to the volumetric strain in

Chapter 4. The two parameters were consequently connected by a simple equation and then supplementary data provided by an alternate researcher was used to verify the reliability of the relationship.

Following the investigation regarding the number of cycles, it was identified that the degradation response can be broken into three distinct regions based on the magnitude of confining pressure. These zones were subsequently termed the dilatant unstable degradation zone (DUDZ, occurring at low σ_3'), the optimum degradation zone (ODZ, intermediate σ_3') and the compressive stable degradation zone (CSDZ, high σ_3'). The range of confining pressures defining each zone was found to be dependent on the cyclic loading amplitude. DUDZ specimens with small σ_3' were shown to be the most vulnerable to unacceptable levels of particle breakdown. These specimens also suffered from rapid and excessive axial strains and overall dilation. It was consequently concluded that DUDZ conditions should be prevented in track. It was acknowledged that there is a direct connection between minimised breakage and the amplitudes of confining pressure and deviator stress. In the event of increased train axle loads and/or speeds, the ballast confining pressure would also need to be increased for minimal ballast degradation to be ensured.

The Chapter also briefly examined the influences of aggregate particle size distribution and coordination number on breakage, the particle sizes most prone to breakage, and the effect of breakage on the measured resilient modulus.

The next Chapter details the results of variable amplitude (stepwise) experiments on the straining, breakage and resilient response of latite basalt.

CHAPTER 6

BEHAVIOUR OF BALLAST UNDER STEPWISE (VARIABLE AMPLITUDE) LOADING

6.1 Introduction

In the preceding chapters an arbitrary value of strain accumulation (ε_a > 25%) was considered to define specimen failure under constant deviator stress cyclic loading. Failure occurred rapidly within 500 cycles, usually not allowing sufficient time for the evaluation of the entire specimen response during or just after the onset of failure. To overcome this limitation, three triaxial tests (see Table 3.4, Chapter 3) were conducted wherein the cyclic deviator stress $q_{max,cyc}$ was increased in a stepwise fashion (variable amplitude loading) until $\varepsilon_a \geq 20\%$ (to correspond to the static triaxial testing conditions of Indraratna *et al*., 1998 and Salim, 2004). The results of these experiments and the divergences in behaviour from the static loading case are described in this Chapter.

6.2 Method of Load Application

The number of loading cycles per interval N_{int} was arbitrarily set equal to 5000 for two of the tests (σ_3' = 60 and 120 kPa), and to 10000 for the final experiment (σ_3' = 120 kPa). It was thought that a minimum of 5000 cycles per interval would be adequate to allow the attainment of stable conditions i.e. shakedown of the axial strain ε_a and significant volumetric strain ε_v accumulation. The minimum cyclic load was set equal to 3 kN (~ 45 kPa) and each step in the loading regime involved an increase in $q_{max,cyc}$ of about 45 kPa, with loading continued until $\varepsilon_a \geq 20\%$. Whilst this type of stepwise

loading is not exactly the same for real track environments, it is still useful in comparing static and cyclic behaviour, and for examining the failure characteristics of specimens under cyclic loading. In addition, the resilient modulus M_R was measured regularly to provide a thorough account of the elastic response.

6.3 Ballast Response to Stepwise Loading

Figure 6.1 depicts the loading regime, axial strain ε_a, volumetric strain ε_v, radial strain ε_r, and resilient modulus M_R response for the $\sigma_3' = 60$ and 120 kPa specimens with $N_{int} = 5000$. During stepwise cyclic loading, 'failure' is no longer defined by an arbitrary axial strain. Instead, Figure 6.1 illustrates that a sudden increase in ε_a and ε_r accompanied by a post-peak reduction in M_R can be considered as the onset of failure (marked with a black dot). Before the commencement of failure, specimen behaviour is characterised by a stabilising zone followed by a period of destabilisation. In Figure 6.1b, ε_a increases steadily with increasing N or $q_{max,cyc}$ (stabilising zone), until the cyclic failure load is approached (destabilising zone), at which point vertical deformation increases rapidly until $\varepsilon_a \geq 20\%$ (failure zone). In the case of the $\sigma_3' = 120$ kPa specimen, localised instabilities at about 110000 cycles correspond to rapid ε_a growth, however, specimen adaptation to the loading environment ensures the prevailing shakedown conditions by 120000 cycles. Failure is not instantaneous under stepwise loading, but instead complete deformation appears to take about 10000 cycles.

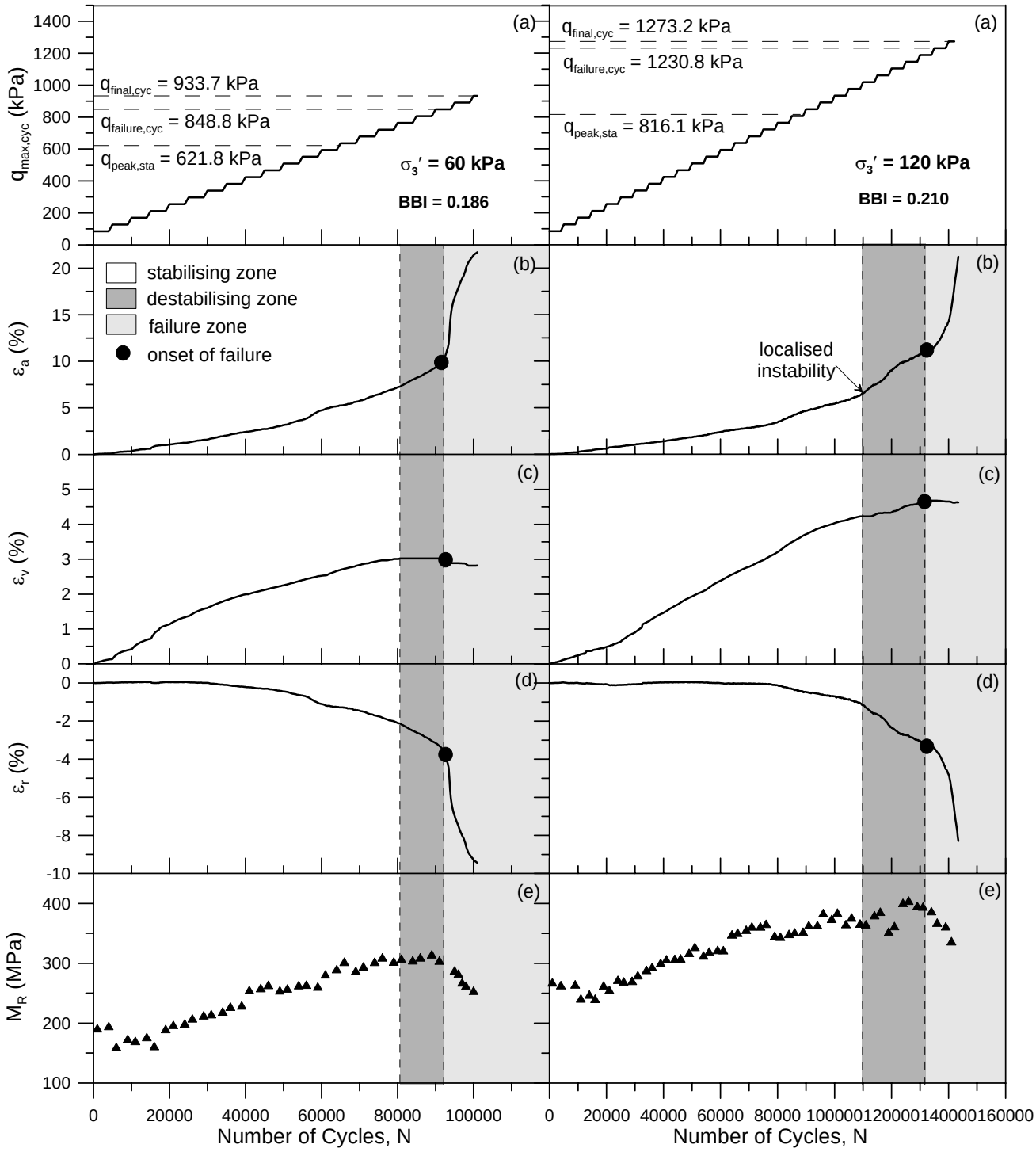

Figure 6.1 Behaviour of ballast under stepwise loading for σ_3' = 60 and 120 kPa and N_{int} = 5000, (a) loading magnitude $q_{max,cyc}$, (b) axial strain ε_a, (c) volumetric strain ε_v, (d) radial strain ε_r, and (e) resilient modulus M_R

In compliance with previous tests in Chapter 4, low to moderate $q_{max,cyc}$ amplitudes produce compressive behaviour (Figure 6.1c, stabilising zone) and dilation commences once outward radial strains increase significantly (Figure 6.1d) in the failure zone.

During the stabilising stage of stepwise loading M_R increases as the specimen stiffens (Figure 6.1e) but once failure is imminent M_R peaks and then starts to decrease. The decline in M_R within the failure zone is considerable but not catastrophic, as a substantial proportion of the increased stiffness from the stabilising zone is still retained (post-peak). The formation of local instabilities (Figure 6.1b) can result in a minor drop in M_R, but this drop is fully recoverable providing the rate of ε_a accumulation remains controlled (i.e. failure is prevented). Previous research by Raad and Figueroa (1980) determined that soils maintain their complete M_R characteristics even after the occurrence of large permanent deformations (Figure 2.26, Chapter 2). It is conceivable, however, that rapid failure of ballast in-situ should affect the resilient modulus of the track significantly as illustrated in Figure 6.1e. As the magnitude of permanent ε_a increases during failure, it is expected that the degree of recoverable strain would increase accordingly, thus resulting in decreased M_R. Lastly, Figure 6.1a shows that the degree of breakage (BBI) increases with the level of confinement.

6.4 Effect of the Number of Cycles per Interval on Ballast Response

Figure 6.2 plots the effect of the number of loading cycles per interval N_{int} on the ballast response for $\sigma_3' = 120$ kPa and $N_{int} = 5000$ and 10000. The major difference between the two tests in Figure 6.2 is the magnitude of ε_v achieved, the greater the number of cycles/interval, the greater the degree of volumetric compression. The quantity of

ballast degradation (BBI) also increases with N_{int}. There appears to be no significant difference in the magnitudes of peak M_R obtained or the magnitude of $q_{max,cyc}$ required to instigate failure. Similar to Figure 6.1, when the ε_a rate increases in the destabilising and failure zones, there is a corresponding drop in M_R and the tendency for ε_v to become more dilative.

6.5 Comparison between Static and Cyclic Loading Response

Tables 6.1 – 6.3 depict various q/p' and ψ values for the current cyclic stepwise tests, with the ψ value calculated based on data taken from Indraratna *et al*. (1998) and Salim (2004). These tables show that specimens under cyclic loading fail at a value of $q_{max,cyc}$ ($q/p'_{failure}$) significantly greater than $q_{peak,sta}$ ($q/p'_{peak,sta}$). Cyclic loading can enhance the stiffness, density and peak strength of specimens, particularly if the material has high compaction tendencies (Suiker *et al*., 2005). For example, in the current N_{int} = 5000 tests, ψ at failure is equal to 1.37 and 1.51 for σ_3' = 60 and 120 kPa, respectively, signifying significant material strength development caused by cyclic loading in the stabilising zone. This demonstrates that specimens that are cyclically loaded or preconditioned prior to static load implementation should be able to sustain higher loading magnitudes. Compared to the magnitude of dilation observed during static triaxial testing (Figures 4.14 and 4.19) the extent of dilation under stepwise cyclic loading is relatively insignificant, highlighting (in accordance with results from Chapter 4) the greater compressional tendencies of cyclically loaded specimens. Dilation during stepwise loading is marginal and occurs only within the failure zone.

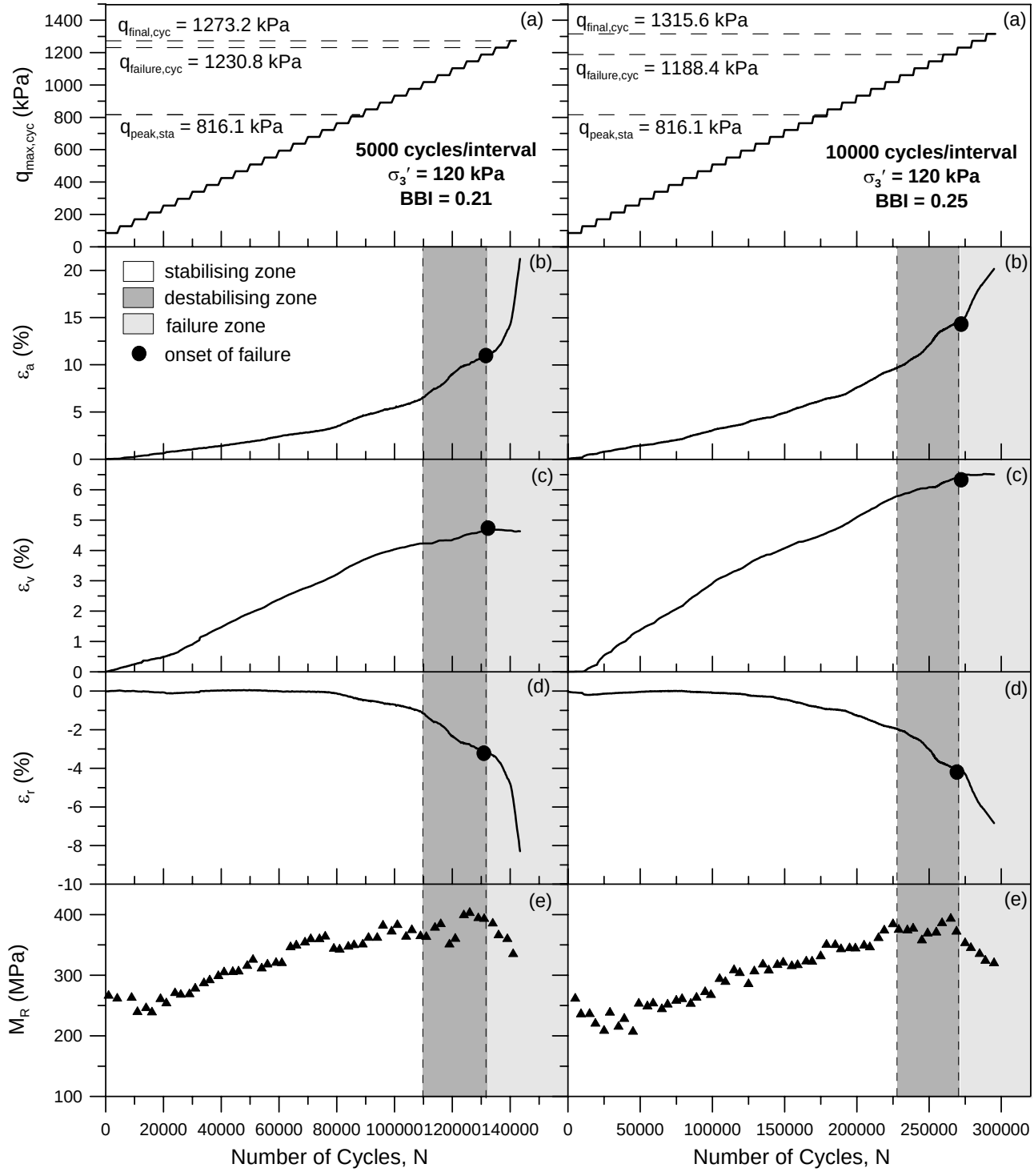

Figure 6.2 Effect of the number of cycles/interval on the behaviour of ballast for σ_3' = 120 kPa and N_{int} = 5000 and 10000 (a) loading magnitude $q_{max,cyc}$, (b) axial strain ε_a, (c) volumetric strain ε_v, (d) radial strain ε_r, and (e) resilient modulus M_R

Table 6.1 Various ψ and q/p' ratios for the $\sigma_3' = 60$ kPa and $N_{int} = 5000$ specimen

Ratio	Value
$q/p'_{peak,sta}$	2.33
$q/p'_{failure}$	2.48
q/p'_{final}	2.52
$\psi_{failure}$	1.37
ψ_{final}	1.50

Table 6.2 Various ψ and q/p' ratios for the $\sigma_3' = 120$ kPa and $N_{int} = 5000$ specimen

Ratio	Value
$q/p'_{peak,sta}$	2.08
$q/p'_{failure}$	2.32
q/p'_{final}	2.34
$\psi_{failure}$	1.51
ψ_{final}	1.56

Table 6.3 Various ψ and q/p' ratios for the $\sigma_3' = 120$ kPa and $N_{int} = 10000$ specimen

Ratio	Value
$q/p'_{peak,sta}$	2.08
$q/p'_{failure}$	2.30
q/p'_{final}	2.36
$\psi_{failure}$	1.46
ψ_{final}	1.61

6.6 Chapter Summary

This chapter investigated the response of three specimens subjected to gradually increasing cyclic loading amplitudes. Unlike repeated loading under constant deviator stress magnitude, when the load is progressively increased failure can be defined by a rapid increase in axial strain rate and a corresponding decrease in the resilient modulus, instead of by some arbitrary value of axial strain accumulation. As the loading magnitude increases, behaviour is characterised by a stabilising zone followed by a phase of destabilisation before failure commences and the specimen experiences extensive deformation. Once failure commences, there is a definite and significant drop in resilient modulus associated with rapid axial strain. When the number of cycles per loading interval is increased, there is a marked difference in the degree of volumetric compression achieved, but the magnitudes of deviator stress required to cause failure and the peak resilient modulus appear to be largely unaffected. Lastly, it was identified that specimens loaded with a gradually increasing cyclic load can accrue increased strength and stiffness. In agreement with previous chapters, stepwise loading is much more likely to cause compressive than dilative specimen volumetric behaviour.

The next chapter deals with the practical methods and implications of altering the in-situ ballast confining pressure.

CHAPTER 7

PRACTICAL METHODS AND IMPLICATIONS OF ALTERING THE IN-SITU EFFECTIVE BALLAST CONFINING PRESSURE

7.1 Introduction

Chapters 4 and 5 investigated thoroughly the influences of deviator stress magnitude (axle load), effective confining pressure and the number of loading cycles on the fundamental deformation and degradation behaviour of railway ballast under cyclic loading. It was acknowledged that the behaviour or response of ballast during triaxial testing is mostly dependent on the loading conditions (state of stress). As competition between road and rail transportation becomes more intensive, it is expected that train axle loads will continue to increase into the future. Increasing train loads without providing a practical alteration to the substructure design could have disastrous ramifications in terms of maintenance costs and potential derailments. Now that a detailed know-how of ballast response to high-speed cyclic loading has been achieved in the laboratory, it is necessary to identify and suggest practical and cost-effective techniques that may prove suitable for future improved rail track design. This Chapter introduces the concept of effective ballast confining pressure as a mechanism for providing the additional support required to counteract increasing axle loads. Two critical questions still remain to be answered, and these form the basis of this Chapter:

1) What will be achieved by modifying the in-situ ballast confining pressure, and
2) How can the in-situ ballast confining pressure be modified?

The Chapter is divided into three sections. Firstly, a brief summary of the results obtained in previous chapters with consideration given to the constant deviatoric stress experiments is provided. Following this, the possible benefits and pitfalls associated with the manipulation of the in-situ ballast confining pressure are identified and discussed. The Chapter concludes with a contemplation of several practical methods that could be employed to improve the confining characteristics of the ballast layer.

7.2 Summary of Experimental Findings

Figures 7.1 and 7.2 provide a conceptual summary of the experimental findings from Chapters 4 and 5. When the effective confining pressure σ_3' is increased and all remaining variables are kept constant (Figure 7.1), the triaxial experiments revealed a substantial drop in the magnitudes of axial strain ε_a (settlement) and radial expansion ε_r due to the larger degree of lateral support offered to specimens. A power relationship between ε_a and σ_3' was found to be suitable when an equivalent number of cycles N was considered. Increasing σ_3' also resulted in greater volumetric compression ε_v and a larger resilient modulus M_R, the latter being well documented in the literature. Particle breakage BBI was established to be most significant at low and high σ_3'. The σ_3' corresponding to minimised breakage was identified to be dependent on the magnitude of deviatoric load $q_{max,cyc}$.

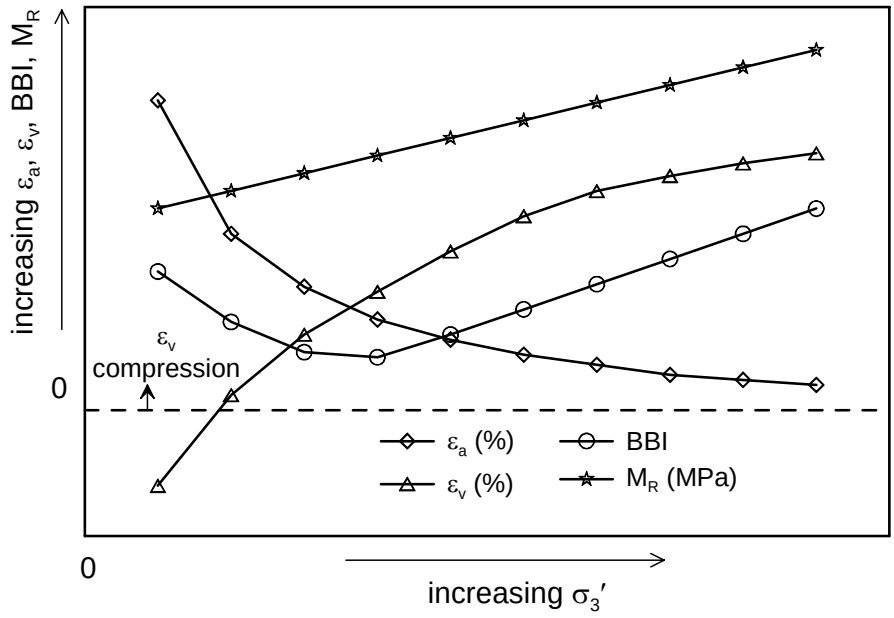

Figure 7.1 Conceptual diagram illustrating the effect of increasing confining pressure σ_3' on axial strain ε_a, volumetric strain ε_v, ballast breakage BBI, and resilient modulus M_R

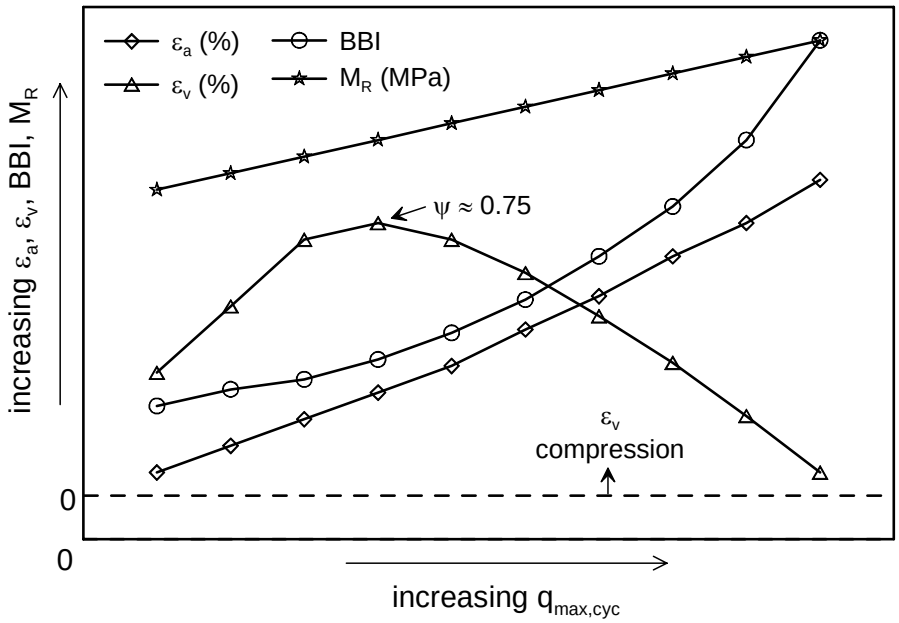

Figure 7.2 Conceptual diagram illustrating the effect of increasing deviator stress magnitude $q_{max,cyc}$ on axial strain ε_a, volumetric strain ε_v, ballast breakage BBI, and resilient modulus M_R

When $q_{max,cyc}$ is increased and all remaining variables kept constant (Figure 7.2), ε_a was recognised to increase approximately linearly. Increasing volumetric compression was observed with increasing $q_{max,cyc}$ until a ψ ratio of about 0.75 was achieved (where ψ is the quotient of $q_{max,cyc}$ and the static peak strength at failure $q_{peak,sta}$). Beyond $\psi \sim 0.75$, ε_v behaviour became gradually more dilative. Both M_R and BBI were shown to accelerate with increasing $q_{max,cyc}$ (Figure 7.2).

It was stated in Section 2.3.5 (Chapter 2) that the current in-situ ballast confining pressures are thought to be contained within the range 10 – 140 kPa. Lateral pressures are smallest after routine track maintenance due to the loosening of ballast and loss of sleeper seating (Profillidis, 1995). In the experimental analysis, σ_3' values up to 240 kPa were considered, and significantly different behaviours were encountered at low and high σ_3'. It is consequently expected that behaviour would also differ significantly in the field if a range of σ_3' of 10 to 140 kPa was utilised. The actual levels of in-situ lateral pressure have never been physically measured, so it is difficult to categorically determine whether values are closer to 10 or 140 kPa. However, track maintenance and construction procedures (e.g. a lack of extensive ballast compaction and poor sleeper-ballast friction), together with significant degrees of ballast breakdown and settlement, suggests the occupation of a region towards the smaller σ_3' values. Confining pressure on the load bearing ballast is a combination of overburden pressure, frictional properties (angle of internal friction and sleeper friction), and residual compaction stresses. Altering the level of confining pressure by manipulating one or more of these sources may prove very useful in future years in the development of safer and more stable tracks.

7.3 Consequences of Altering the In-Situ Effective Confining Pressure

From a foundation design perspective, there are three options concerning the magnitude of in-situ lateral ballast confining pressure. The first involves making no confinement modifications, and the possible repercussions of this have been described in Chapter 1. The main benefits and pitfalls associated with altering (increasing or decreasing) the level of effective track confinement on the behaviour of the ballast layer and the entire track structure are summarised in Table 7.1 and discussed in detail below.

Table 7.1 Benefits and pitfalls associated with increasing or decreasing the effective lateral in-situ ballast confining pressure

Effects of Decreasing the Lateral Confining Pressure		**Effects of Increasing the Lateral Confining Pressure**	
Benefits	**Pitfalls**	**Benefits**	**Pitfalls**
Less material required (cheaper ballast costs)	Increased ballast spreading leading to increased sleeper movement (lateral and vertical)	Reduced ballast spreading leading to reduced sleeper movement (lateral and vertical)	Increased costs associated with supplying additional confinement
	Potential for increased breakage	Increased track stability and stiffness (resilient modulus)	Potential for increased particle degradation
	Potential for track dilation	Improved track line and level and decreased requirement for tamping	Potential for increased ballast costs
	Increase in track maintenance costs	Smoother and more comfortable ride for passengers	

7.3.1 Track Response Corresponding to a Decrease in Lateral Confinement

It is apparent from the laboratory data that decreasing the confining pressure acting on the load bearing ballast would bring about increased lateral ballast spreading and settlement, and a subsequent increase in sleeper movement. This movement would be particularly evident on track curves (bends) where outward tangential train forces would cause transverse sleeper sliding in the event of deficient inward forces applied by the substructure. As the results from Chapters 4 and 5 indicated, low confining pressures would increase the potential for track dilation and hence excessive ballast degradation. In the DUDZ (dilatant unstable degradation zone, Section 5.4.1, Chapter 5) the lower the confining pressure σ_3' the greater the expected ballast degradation. In addition, less ballast confinement would result in greater maintenance costs associated with correction of line and level and ballast replacement due to particle breakdown.

Clearly, reducing the level of σ_3' supporting the load bearing ballast would have devastating effects on the cyclic response of the track structure and should therefore be avoided.

7.3.2 Track Response Corresponding to an Increase in Lateral Confinement

The benefits and pitfalls associated with increasing the ballast confining pressure are listed in Table 7.1. Evidently there are a substantial number of potential benefits connected with increased confinement. For instance, it is expected that increased lateral σ_3' will enhance the load spreading capabilities of the ballast layer which in turn will decrease the degree of vertical settlement, thus leading to a reduced requirement for

track tamping due to improved line and level. In addition, greater lateral confinement will produce superior track stiffness (resilient modulus) that will improve the ride characteristics for passengers. Routine maintenance costs are also expected to decrease due to a vast reduction in sleeper movement and track misalignment. Greater σ_3' on track bends will also allow faster train speeds owing to a decreased risk of lateral (outwards) sleeper travel.

On the downside, there would be increased construction costs associated with the actual application of additional inward pressures onto the ballast layer. Furthermore, as detailed in Chapter 5 for CSDZ specimens (compressive stable degradation zone, Section 5.4.3) excessive confinement without adequate particle rearrangement can cause particle splitting and unacceptable levels of degradation. This highlights the essential requirement of employing high quality aggregates (parent rock varieties that are both hard and tough) in conjunction with greater σ_3' to limit excessive particle breakdown. Premium ballast may largely eliminate the increased risks of excessive breakdown at larger σ_3'.

Chapter 5 acknowledged that enhancing the degree of confinement is imperative in minimising the extent of degradation in the event of increased axle loads. If the maximum deviatoric load $q_{max,cyc}$ is increased, there must be a corresponding increase in the magnitude of lateral confinement if ballast breakage is to be minimised. This concept is depicted in Figure 5.5 and Table 5.1. In addition, increases in deviatoric load are expected to cause greater ballast damage (in terms of settlements, lateral spreading and particle breakdown). Therefore, the larger the axle load the greater the confining pressure necessary to prevent substandard track performance.

7.4 Methods of Increasing the Effective In-Situ Confining Pressure

It was well established in Section 7.3 that only increases in the ballast confining pressure would be applicable to railway lines because of the loss of track stability and excessive deformation associated with decreasing the level of confinement. Several practical methods of increasing the ballast restraint have been suggested (e.g. Raymond and Williams, 1994; Indraratna *et al*., 2004), and the following four are detailed in this section:

a) Lateral constraints,

b) Geosynthetics,

c) Sleeper-ballast friction, and

d) Overburden pressure.

Each option is investigated in terms of the extent of benefit, associated costs, and suitability for in-situ use. Laboratory and field testing results for each method obtained from various researchers are also explored and discussed.

7.4.1 Lateral Restraints

One method of improving the lateral track resistance is by placing restraining barriers at the extremities of the sleepers or shoulder ballast to prevent outward ballast spreading and associated sleeper movement. An example of this technique is illustrated in Figure 7.3. Profillidis (1995) maintains that an increase in lateral resistance of around 170% can be achieved if concrete posts are placed against the sleeper ends, demonstrating the considerable advantages that can be realised in terms of lateral stability. It is identified, however, that this method (as well as the placement of restraining barriers against the

ballast shoulder) is relatively expensive and can also hinder maintenance procedures such as tamping and ballast cleaning.

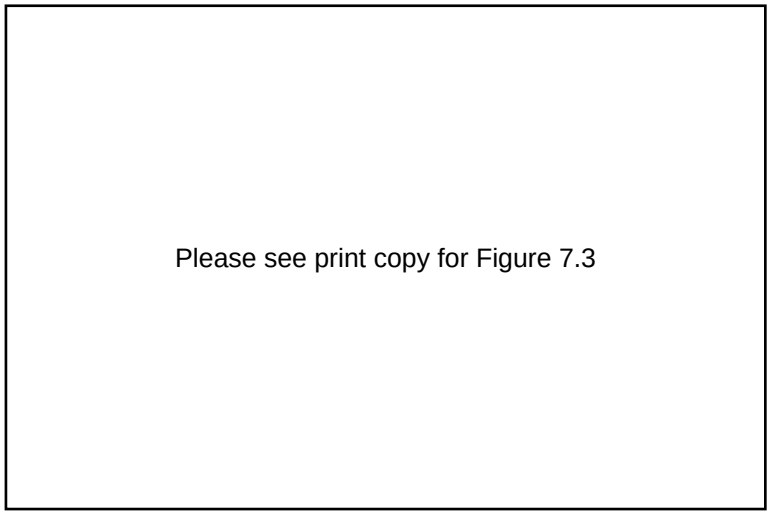

Figure 7.3 Increasing the lateral confining pressure using intermittent lateral restraints (after Indraratna *et al*., 2004)

7.4.2 Geosynthetics

Since the beginning of the 1970's geosynthetics have become increasingly utilised in railway substructures with the sole purpose of improving the performance characteristics of (in particular) problematic tracks (Raymond, 1999; Haeri *et al*., 2000; Lieberenz and Weisemann, 2002). An example of in-situ geosynthetic installation is depicted in Figure 7.4. Although there are many varieties of geosynthetics, the most commonly used types are geotextiles and geogrids. Geosynthetics have four common applications:

- Reinforcement of the granular or fine grained layers (geogrids or geotextiles),
- Drainage facilitation (geotextiles),
- Separation of the ballast/subballast layers from the subgrade (geotextiles), and
- Filtration of fine grained subgrade materials (geotextiles).

The main areas of concern in this section are the suitability of geosynthetics for improving the confining properties (reinforcing) of the load bearing ballast, the extent of potential improvements offered by geosynthetics, and suitable design criteria for in-situ placement.

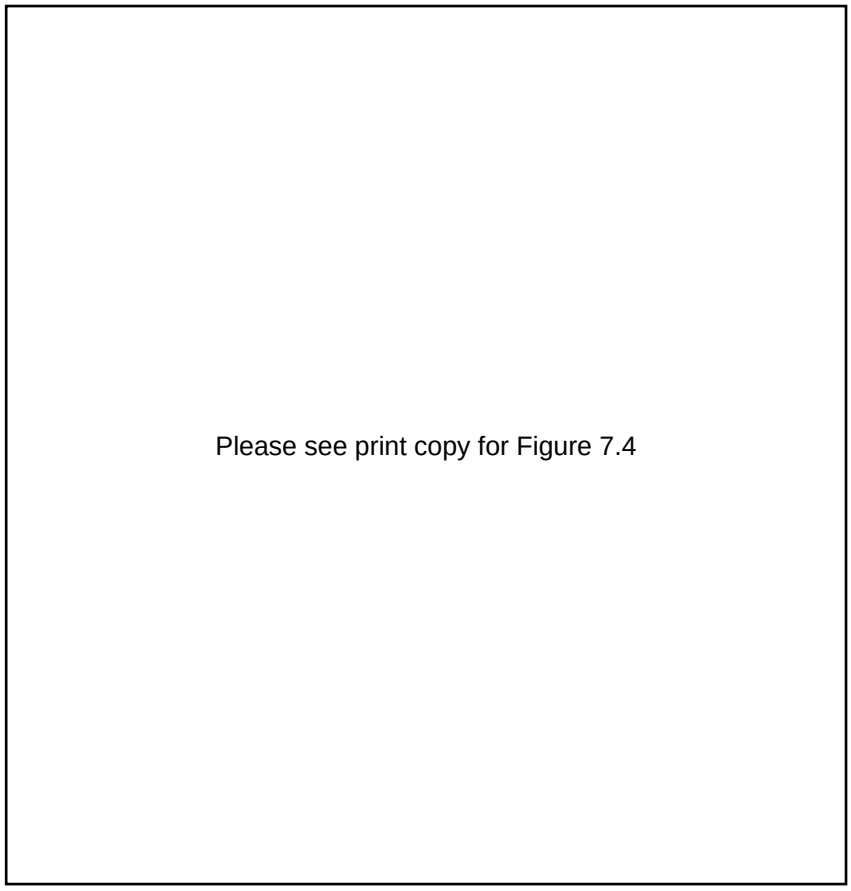

Figure 7.4 In-track installation of geosynthetics (after Selig and Waters, 1996)

A substantial number of researchers have investigated the reinforcing attributes of geosynthetics in the railway substructure. Many of these studies were based on laboratory testing (e.g. Raymond, 1992; 2002; Indraratna *et al*., 2002; Shin *et al*., 2002; Indraratna and Salim, 2003; Raymond and Ismail, 2003). Others, however, involved full scale field trials (e.g. Raymond, 1999; Profillidis, 2000; Li, 2000; Ashpiz *et al*., 2002; Lieberenz and Weisemann, 2002; Buonanno *et al*., 2003). Most studies utilised geogrids

as the reinforcing agent, although geotextiles have also been studied in some depth. As indicated by Indraratna *et al*. (2002), the extent of reinforcing success depends to a large degree on the type of geosynthetic employed.

7.4.2.1 Confinement Mechanisms Offered by Geosynthetics

Ghosh and Madhav (1994) provide details regarding the support mechanisms of a single layer of geosynthetic reinforcement and the development of confining pressure increase within a granular soil. They recognise that when a soil is loaded it attempts to spread laterally, but because of the contact between the soil and reinforcing agent tension forces develop within the reinforcement, leading to the mobilisation of internal shear stresses. The difference in extensibility between the soil and geosynthetic strip causes the mobilisation of stresses at the soil-reinforcement interface, and as the amount of strain increases there is a gradual increase in level of confinement. The amount of soil improvement is dependent on the magnitude of shear stress mobilised at the interface (Ashmawy *et al*., 1999). These shear stresses (tension forces) thus act as a confining agent by preventing the soil from spreading. The extent of the forces and strains transferred into the reinforcement depends on several factors including:

- the degree of soil-reinforcement friction,
- the degree of soil-reinforcement interlock,
- geosynthetic bearing (in the case of geogrids), and
- geosynthetic adhesion (in the case of undrained soft clays).

Ghosh and Madhav (1994) identify that tensile forces are maximum at the centre of a footing (or sleeper), and that the maximum increase in effective confining pressure will therefore be directly below the sleeper.

7.4.2.2 Optimum Operational Environments

The use of geosynthetic materials for reinforcement purposes has been shown to be particularly useful under certain conditions. For example, Ghosh and Madhav (1994) state that the confinement effect will be greatest when the granular material under consideration has a high initial stiffness. Raymond (2002), however, affirms greater usefulness when the foundation soil is in a loose condition. It is well established that geosynthetic performance improves as the effective confining pressure decreases (El-Naggar *et al*., 1997; Haeri *et al*., 2000; Moghaddas-Nejad and Small, 2003). In fact, at a higher σ_3' a greater deviator stress is required to mobilise the geosynthetic (Moghaddas-Nejad and Small, 2003). Raymond and Ismail (2003) revealed that geosynthetics become more useful at high axle loads and as the number of cycles increases. These characteristics make the use of geosynthetics particularly valuable on railway lines where the extent of intrinsic lateral containment within the substructure is limited (low σ_3') and the axle loads are continuing to increase.

7.4.2.3 Benefits to the Track Substructure

Apart from decreased lateral spreading, a number of other geosynthetic benefits have been identified, and these are listed below.

1) Geosynthetics have been shown to increase the bearing capacity and strength of railway structures and soils (McGown, 1976; Raymond, 1992; El-Naggar *et al*., 1997; Ashmawy *et al*., 1999; Haeri *et al*., 2000; Raymond and Ismail, 2003).

2) Geosynthetics can reduce the stress levels acting on the lower substructure layers by promoting enhanced load distribution (Brown and Selig, 1991; Jain and Kesheav, 1999; Shin *et al*., 2002). For example, Jain and Kesheav (1999) placed a double layer of geogrid beneath a railway section and measured a 30% reduction in the induced stress 0.9 m below the track when compared to identical loading without reinforcement.

3) Settlement has been shown to be significantly reduced by the incorporation of geosynthetics (Raymond, 1992; 2002; Ghosh and Madhav, 1994; Moghaddas-Nejad and Small, 1996; 2003; Indraratna *et al*., 2002; Indraratna and Salim, 2003; Raymond and Ismail, 2003). This is mainly due to the restriction in lateral spreading and increased soil stiffness. As an example, Raymond (2002) established that a geoweb placed within the ballast was successful in reducing the vertical settlement by between 13 - 30%. This resulted in a reduction in track maintenance costs. Also, Salim (2004) identified that including a layer of geosynthetics at the ballast/subballast interface significantly reduced the rate of wet recycled ballast settlement, as illustrated in Figure 7.5.

4) Reinforcing ballast and other granular materials has been demonstrated to decrease the degree of material breakdown and increase the aggregate life (Raymond, 2002; Indraratna *et al*., 2002; Indraratna and Salim, 2003). For instance, Indraratna and Salim (2003) recorded about a 45% decrease in ballast degradation when a woven geotextile was placed at the ballast/subballast interface.

5) Reinforcement can reduce aggregate dilation due to enhanced confinement (Haeri *et al*., 2000).

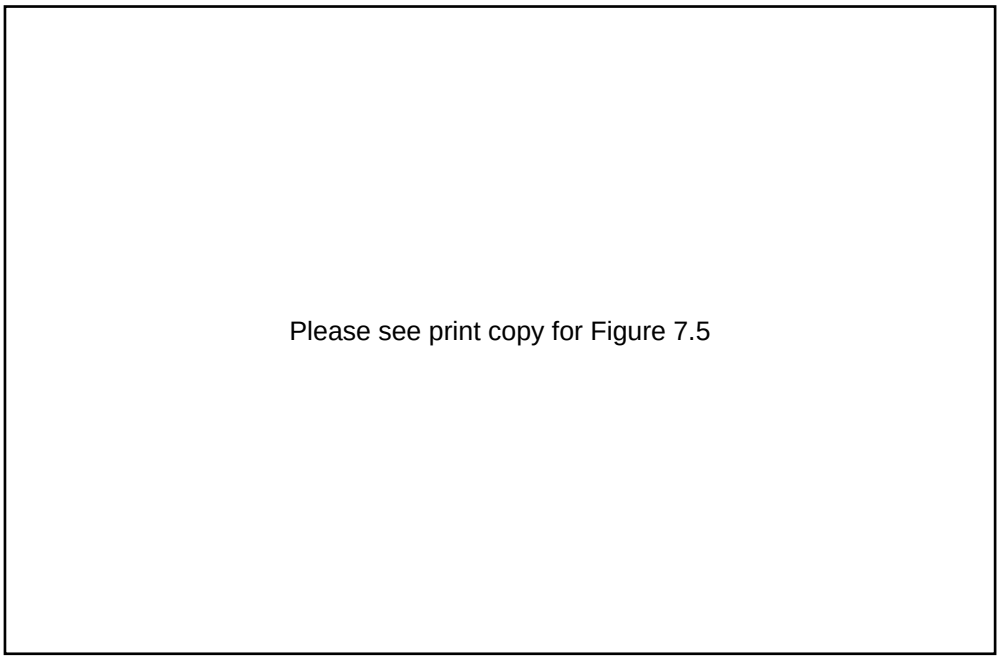

Figure 7.5 Reduction in settlement due to various types of geosynthetics (after Salim, 2004)

7.4.2.4 Design Considerations

Now that the benefits of geosynthetics as a source of reinforcement have been detailed, it is important to consider the optimum in-situ placement location. Past literature reveals that the nearer the reinforcement to the base of a footing (the shallower the depth), the greater the expected added confining pressure and the larger the benefits to the track structure (Raymond, 1992; Raymond and Ismail, 2003). Moghaddas-Nejad and Small (1996) established for pavements that superior performance can be obtained when the reinforcement is placed at the centre of the base layer (70% reduction in deformation) compared to at the base-subgrade interface (40% reduction in deformation). Raymond and Ismail (2003) compared the reinforcement depth to the footing width and concluded that when the ratio of depth to width exceeds 0.5, the reinforcing effect of the geosynthetic is significantly diminished. They identified a ratio of 0.18 – 0.5 as ideal.

However, from a practical perspective, placing the geosynthetic within the upper ballast section will create difficulties relating to maintenance procedures. For this reason, Raymond (1999) suggests that a depth greater than 200 mm and preferably closer to 300 mm would be more suitable, as these depths are not expected to interfere with tamping tines. The studies by Indraratna *et al*. (2002) and Indraratna and Salim (2003) considered the most convenient location to be the ballast-subballast interface, and therefore utilised this position in their experiments. The geosynthetics proved beneficial in improving the substructure characteristics, and it is therefore considered that the ultimate location for any reinforcing agent would probably be at the ballast-subballast boundary.

Lastly, studies have revealed that a greater number of layers of reinforcement will produce superior track behaviour (e.g. Ashmawy *et al*., 1999; Haeri *et al*., 2000; Raymond and Ismail, 2003). All layers need to be reasonably close to the sleeper base for the benefits to be realised. Also, relatively heavy geosynthetics are required to prevent damage during cyclic train loading. Raymond (1999) recommends geosynthetics with a mass per area greater than 500 g/m^2, but recognises that materials approaching 1000 g/m^2 are preferred.

7.4.3 Sleeper Characteristics (Shape, Spacing, Friction)

There are several aspects of sleeper design that can be modified to advance the confining characteristics of the track system. Profillidis (1995) states that the ballast and sleepers work in tandem to transmit transverse (lateral) resistance to the track structure above. One source of such resistance results from sleeper-ballast friction deriving from

the load bearing, crib and shoulder ballast. The degree of transverse resistance offered by the crib ballast depends on the extent of crib filling between sleepers and the level of compaction. Profillidis (1995) states that approximately 30% of the total resistance offered by monoblock prestressed-concrete sleepers results from crib-sleeper friction. Similarly, increased shoulder ballast height or shoulder compaction would also increase the frictional properties at the sleeper extremities, leading to improved lateral stability.

Any efforts made to improve the frictional characteristics at the sleeper-ballast interfaces through sleeper design alterations would also increase the lateral stability of the track. For example, if an alternative 'tapered' or 'wing' shaped sleeper were to be utilised (Figure 7.6), increased resistance to lateral ballast spreading would be achieved. In addition, roughening seating surfaces (Figure 7.7) or incorporating sleeper anchors into track design (particularly on bends, Figure 7.8) are two other methods suggested by Profillidis (1995).

In terms of sleeper spacing and dimensions, it is generally accepted that lateral track stability increases with decreasing sleeper spacing (Raymond and Williams, 1978; Profillidis, 1995, Figure 7.9). Furthermore, it has been reported during field trials in Germany that increasing sleeper lengths by 0.2 m (from 2.4 to 2.6 m) can result in an increase in lateral track resistance of 15-20% (ORE, 1976). Lastly, increasing sleeper weight has also been observed to decrease lateral track deformation, as has the use of concrete sleepers in place of timber sleepers (Profillidis, 1995).

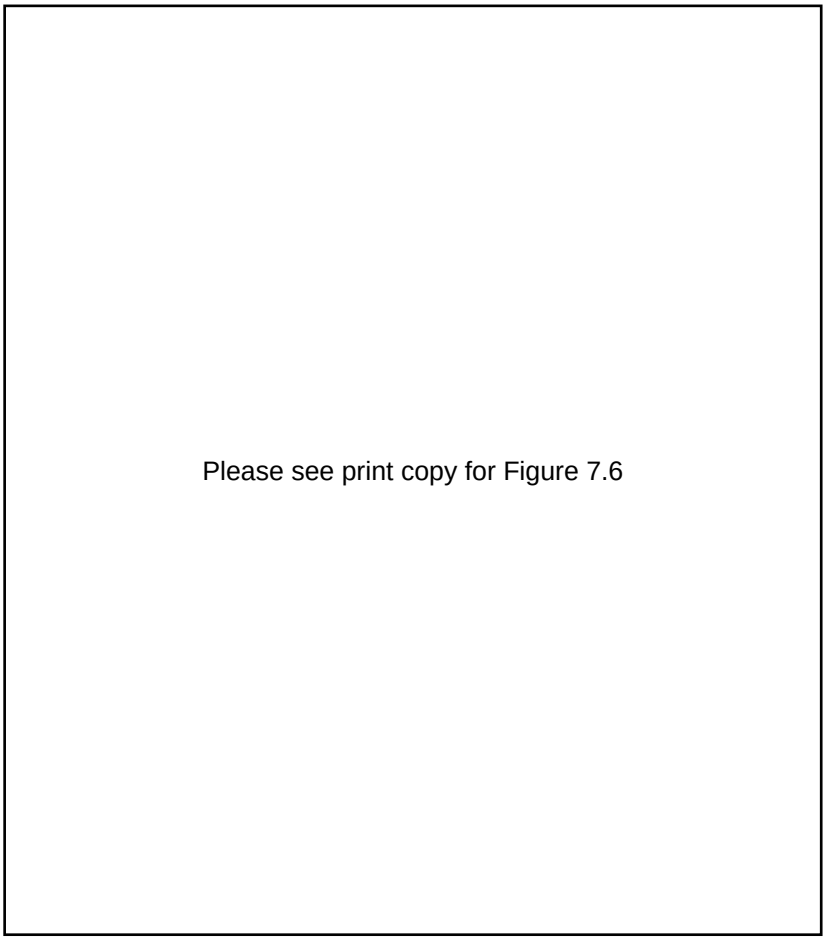

Figure 7.6 Increasing the lateral confining pressure using (a) tapered, or (b) winged sleepers (after Indraratna *et al*., 2005) (not to scale)

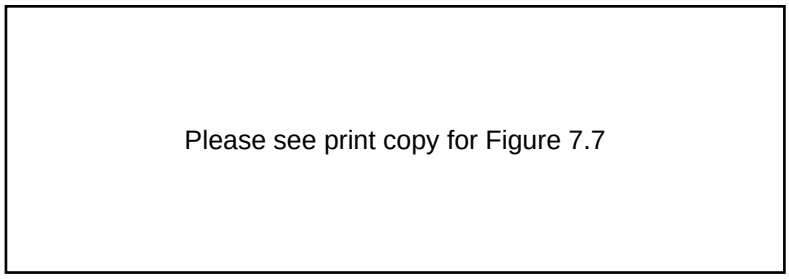

Figure 7.7 Example of roughening of the sleeper base for increased friction between sleeper and ballast (after Profillidis, 1995)

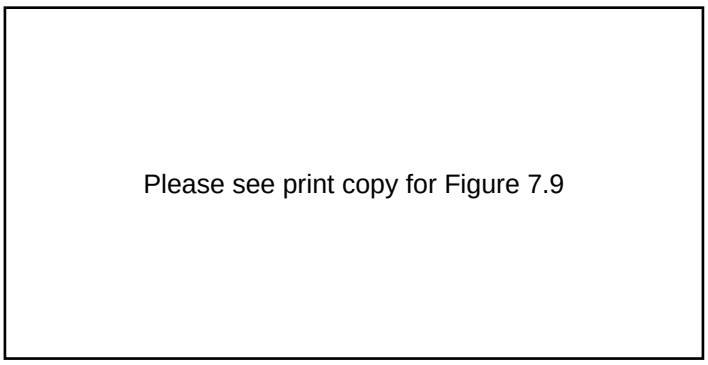

Figure 7.8 Increasing lateral resistance by the incorporation of sleeper anchors (after Profillidis, 1995)

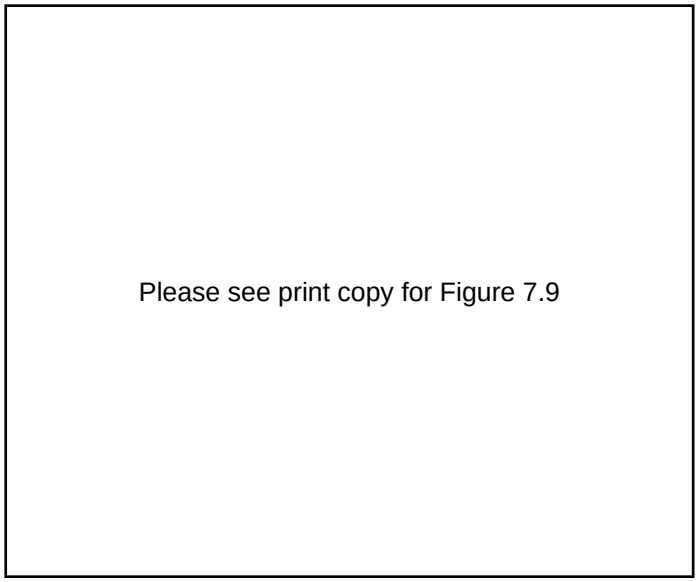

Figure 7.9 Effect of sleeper spacing on the degree of lateral track resistance (after Profillidis, 1995)

7.4.4 Effective Overburden Pressures

Two final sources of in-situ lateral confining pressure are overburden pressures from crib and shoulder ballast, and residual compaction stresses from maintenance procedures and train passage. Assuming an 'at rest' state, any increases in vertical stress caused by greater ballast weight will generate a corresponding increase in horizontal stresses for any particular K_0 value. This can be achieved by:

- increasing the height of the crib and/or shoulder ballast, or
- increasing the degree of compaction (density) of the crib and/or shoulder ballast.

Clearance issues may prevent an extreme increase in shoulder or crib height. However, ensuring that the crib is completely full to the sleeper top and that an adequate shoulder is in place could have a dramatic influence on the magnitude of lateral resistance offered. Figure 7.10 depicts the relative effects of the shoulder height and width on the transverse track resistance of a typical railway line. Evidently, as both the shoulder height and width increase, so too does the confining pressure offered to the load bearing ballast.

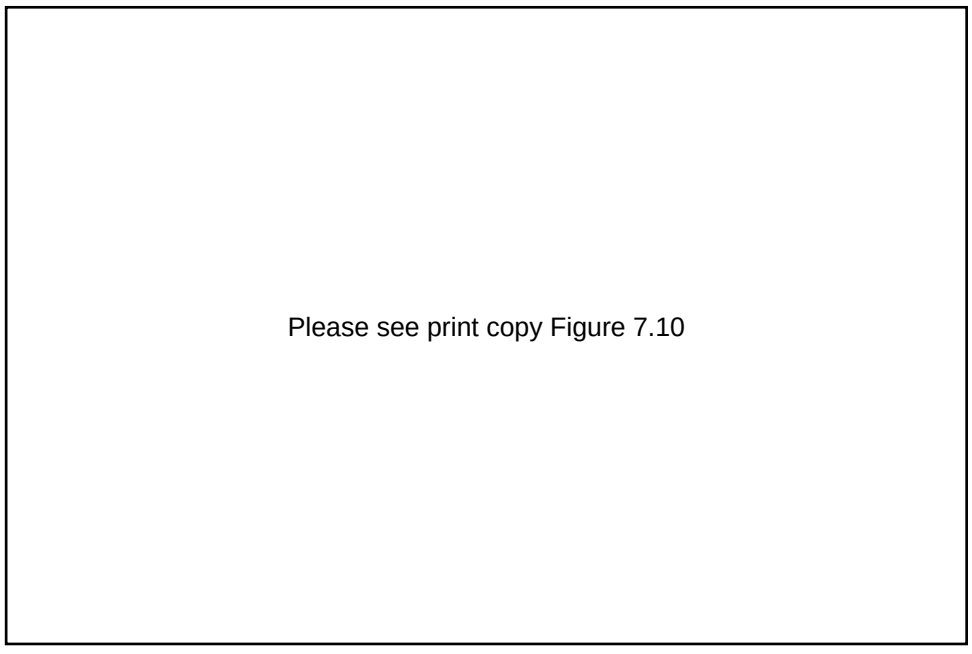

Figure 7.10 Lateral track resistance at the sleeper ends based on the geometrical characteristics of the shoulder ballast (after Profillidis, 1995)

Due to potential clearance issues, perhaps it is more practical for the crib and shoulder ballast to be compacted after maintenance. An example of the potential benefit of crib compaction is illustrated in Figure 7.11. One last technique that could be explored to provide greater overburden is to alter the particle size distribution (PSD) of the crib and/or shoulder ballast. As outlined in Section 2.2.1 (Chapter 2), typical ballast PSD's are relatively uniform, and as such it is difficult to attain a reasonable degree of compaction. However, if an alternative more well graded distribution were employed for the shoulder and crib, a denser aggregate and hence increased overburden could be realised.

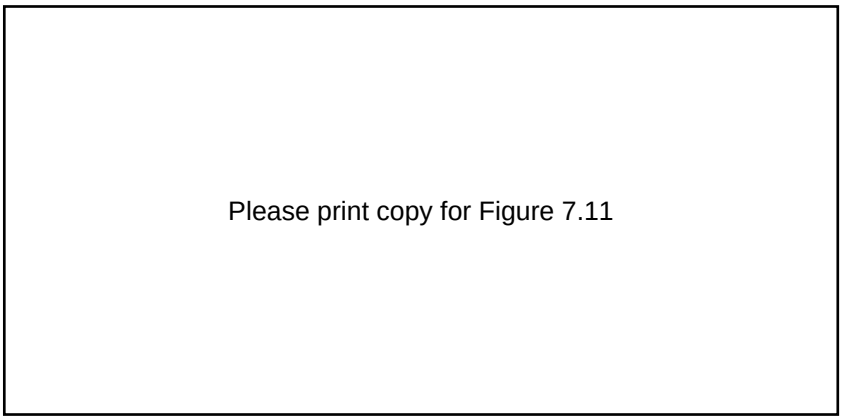

Figure 7.11 Effect of the number of cycles and crib compaction on the level of lateral (transverse) resistance (after Profillidis, 1995)

7.4.5 Summary of Improvement Methods

Table 7.2 compares the four methods described above (lateral restraints, geosynthetics, sleeper characteristics and effective overburden) in terms of the relative effectiveness for in-situ deployment. The various methods are evaluated in terms of costs (installation and maintenance), the extent of potential benefit, and the suitability for railway application. It is thought that the best options for increasing the magnitude of lateral

confinement are the installation of geosynthetics and effective overburden pressure increase via improved ballast density and/or height of the crib and shoulder ballast. These options are preferred due to the relative ease of installation, cheaper costs, greater design simplicity, and overall effectiveness.

Table 7.2 Relative comparison of the various potential methods of increasing the lateral confining pressure

Method	Cost	Extent of Benefit	Railway Suitability
Lateral restraints	High	High	Low
Geosynthetics	Low	Medium	High
Sleeper characteristics	Medium	Low-medium	High
Overburden pressure	Low-medium	Medium	High

7.5 Chapter Summary

This Chapter considered the implications and potential methods associated with altering the effective in-situ ballast confining pressure. Following a summary of the results from Chapters 4 and 5, the consequences and effects of increasing or decreasing lateral confinement were discussed in relation to settlement characteristics, volumetric strain, particle degradation, and resilient modulus. Possible methods of improving the lateral confinement were outlined, and relevant literature was explored to determine the suitability of each method.

The next Chapter provides the conclusions of this research, and also outlines recommendations for future work.

CHAPTER 8

CONCLUSIONS AND RECOMMENDATIONS

8.1 Introduction

Few substructure modifications have been made in recent years to compensate for increasing railway freight. The possibility of modifying track confining pressure as a means of substructure enhancement has been explored using a series of high-frequency, large-scale, cyclic (drained) triaxial tests. Results of this study confirm that confining pressure should be considered as an important design parameter. The following sections provide a précis of the major conclusions obtained regarding the effects of confining pressure, maximum deviator stress magnitude and number of loading cycles on the permanent, resilient, breakage and stepwise loading behaviour of railway ballast. Recommendations for future study are also provided.

8.2 Permanent (Plastic) Deformation Behaviour

(1) The magnitude of vertical (axial) strain ε_a was found to be a function of the applied deviator stress $q_{max,cyc}$ and the degree of lateral confinement σ_3', with ε_a shakedown occurring within 10000 cycles. Specimen 'failure' under constant amplitude cyclic loading was defined by an arbitrary value of ε_a accumulation. A power relationship was used to relate the magnitude of ε_a to σ_3', $q_{max,cyc}$ and N (the number of loading cycles).

(2) Specimens subjected to low σ_3' exhibited dilative behaviour with the degree of volumetric compression ε_v increasing with σ_3'. Dilation occurs mainly within the first 3000 cycles and results from excessive radial strains in combination with large $q_{max,cyc}/p'$ ratios. The evolution of ε_v in compressing specimens continues indefinitely with N for a constant $q_{max,cyc}$.

(3) No definitive relationship between ε_v and $q_{max,cyc}$ was observed. A comparison of ε_v behaviour under static and cyclic loading revealed that cyclically loaded specimens display compressive tendencies for ψ ratios up to about 0.75 ($\psi = q_{max,cyc}/q_{peak,sta}$). Beyond this value, ballast behaviour becomes increasingly dilatant. When $\psi > 1$, specimens can still compress, however, the likelihood of dilation increases with decreasing σ_3' for a particular $q_{max,cyc}$. It was confirmed that cyclically loaded specimens demonstrate a stronger tendency for compression than statically loaded specimens.

(4) Specimen particle size distribution (PSD) has a significant effect on permanent straining characteristics. Significant axial strains and greater volumetric compression is associated with lower C_u gradations. The magnitude of compression for each PSD was identified to be related more to specimen vertical settlement than lateral expansion.

8.3 Recoverable (Resilient) Deformation Behaviour

(1) Resilient strain $\varepsilon_{a,rec}$ data was recorded at a sampling frequency of 590 Hz and filtered to remove electrical noise.

(2) The magnitude of $\varepsilon_{a,rec}$ decreased with each successive loading cycle, resulting in a continual increase in resilient modulus M_R with N up until about 100000 cycles. Beyond this point little change in M_R was observed. The gradual increase in M_R with N was partly attributed to specimen densification from cumulative ε_v. An empirical relationship was derived to link the evolution of M_R to ε_v and N, nevertheless, further research is required to verify the reliability of the equation.

(3) A relationship was developed to relate the expected magnitude of M_R to N, σ_3' and $q_{max,cyc}$. The coefficients of the Brown *et al*. (1975) model were represented as functions of N, thus making it possible to predict M_R for a range of stress conditions at any number of loading cycles.

8.4 Degradation Behaviour

(1) A review of ballast degradation under static loading revealed that particle breakdown increases with confining pressure σ_3'. This behaviour is attributed to the inability of specimens to dilate under higher levels of confinement, and the greater macroscopic stresses that are applied before failure. A new breakage quantification method specific to ballast called the ballast breakage index (BBI) was developed to represent the extent of degradation.

(2) During cyclic triaxial loading, most degradation occurs during the early stages but also accumulates with increasing N due to fatigue. Unlike static loading, there is no direct linear relationship between the magnitude of breakage BBI and σ_3'. Instead, breakage is most significant at high and low σ_3', with minimal breakage obtained at

some intermediate value. Degradation behaviour was subsequently characterised into three distinct zones named the dilatant unstable degradation zone (DUDZ, low σ_3'), the optimum degradation zone (ODZ, intermediate σ_3'), and the compressive stable degradation zone (CSDZ, high σ_3').

(3) DUDZ behaviour ($q_{max,cyc}/p' > 2.5$) is particularly unfavourable in terms of permanent deformation and particle degradation, and should therefore be avoided in-track. The propensity for dilation (and hence DUDZ behaviour) increases with the deviator stress $q_{max,cyc}$ for a particular σ_3'. DUDZ conditions for latite basalt are encountered when $\sigma_3' < 15$, 25 and 50 kPa for $q_{max,cyc} = 230$, 500 and 750 kPa, respectively. The rudimentary requirements for DUDZ behaviour are small σ_3', $\psi > 1$, and specimen dilation. Most degradation in this zone is due to corner breakage.

(4) Specimens within the ODZ ($1.7 < q_{max,cyc}/p' < 2.5$) display slightly compressive behaviour and less particle breakdown. ODZ conditions are encountered within the σ_3' ranges of 15 – 65, 25 – 95, and 50 – 140 kPa, respectively, for $q_{max,cyc}$ magnitudes of 230, 500 and 750 kPa.

(5) The CSDZ ($q_{max,cyc}/p' < 1.7$) is characterised by specimens with reduced particle movement and suppressed dilation, resulting in the introduction of particle splitting and an increase in breakage above ODZ levels.

(6) In essence, the breakage analysis revealed that particle degradation can be minimised if the level of track confinement is increased proportionally with increases in axle load.

(7) Aggregate particle size distribution (PSD) has a significant effect on the expected degree of degradation. Decreased breakage can be expected if the coefficient of uniformity C_u is increased, or if 'vulnerable' particle sizes are removed.

8.5 Stepwise Loading Behaviour

(1) The onset of 'failure' under stepwise (gradually increasing) cyclic loading is suitably defined by a sudden increase in axial and radial strain accompanied by a post-peak reduction in resilient modulus M_R.

(2) Only minimal dilation is observed during the failure process, which generally takes around 10000 loading cycles.

(3) Specimens undergoing stepwise loading failed at ψ ratios equal to 1.37 and 1.51 for $\sigma_3' = 60$ and 120 kPa, respectively, indicating that cyclic loading can enhance the peak strength of ballast.

8.6 Practical Implications

(1) The benefits and pitfalls associated with increasing the degree of lateral ballast confining pressure were identified based on the experimental results from Chapters 4 and 5. It was acknowledged that increased confinement results in reduced ballast

spreading and settlement leading to improved line and level, and greater track stiffness engendering superior ride characteristics. Additional costs associated with the physical application of confinement would be necessary, and in the event of excessive confinement particle degradation may become unacceptable.

(2) This thesis highlights that simple substructure design alterations can be implemented in-track to improve performance and lessen the need for costly maintenance. Four methods of increasing the ballast confining pressure were described, namely the installation of lateral constraints, the use of reinforcing geosynthetics, increased sleeper-ballast friction or altered sleeper characteristics, and increased effective overburden pressure. The level of lateral confinement is a fundamental design criterion for many geotechnical applications, but currently no standards exist in relation to rail tracks. If an appropriate confining pressure is implemented for local in-situ conditions, rail tracks can be improved in terms of degradation and deformation resistance, with enhanced resiliency characteristics.

8.7 Recommendations for Further Study

For a more complete understanding of ballast behaviour under high-speed, drained, cyclic loading, the following topics require more attention:

(1) The experiments reported within this thesis were limited to only one type of aggregate, namely basalt. Further tests should be conducted to extend the theories introduced in this study to other types of materials.

(2) The experimental program was also limited to one testing frequency (20 Hz) and one initial ballast density. Future studies should examine the influence of frequency on ballast behaviour in order to simulate train travel at different speeds. Investigating the effect of the degree of compaction or initial density on ballast performance would also be particularly useful, especially if increased track compaction (as outlined in Chapter 7) were to be employed for substructure enhancement.

(3) A significant amount of experimental work has been conducted on materials such as sands and clays at extremely large confining pressures (>> 1 MPa) under static triaxial loading conditions. Although not directly pertinent to railways, it would be useful to examine the behaviour of coarse materials under much greater stresses (both confining pressure and deviator stress) to gain a better understanding of the degradation and deformation characteristics of granular materials. It would also be interesting to see if the ideas expressed in this thesis, in particular related to the breakage analysis, also apply at considerably larger stress levels.

(4) Future track safety and stability relies on a field trial incorporating some of the strengthening techniques outlined in Chapter 7. For example, the success of geosynthetics in reinforcing the granular layers is best evaluated by in-situ field tests. Similarly, the extent of benefit of increased ballast compaction or increased effective overburden via enhanced shoulder and/or crib height could not be fully realised without a field trial.

(5) The development of analytical and numerical models to simulate the results of this study would be advantageous in predicting cyclic ballast behaviour without having to conduct time consuming and difficult experiments.

REFERENCES

Al-Hussaini, M., (1983). "Effect of Particle Size and Strain on the Strength of Crushed Rock." *5th International Congress on Rock Mechanics*, Melbourne, Australia, pp. E239-243.

Allen, J.J. and Thompson, M.R., (1974). "Resilient Response of Granular Materials Subjected to Time-Dependent Lateral Stresses." *Transportation Research Record*, 510, pp. 1-13.

Allen, J.J., (1973). "The Effects of Non-Constant Lateral Pressures on the Resilient Properties of Granular Materials." Thesis presented to the University of Illinois, in 1973, in partial fulfilment of the requirements for the degree of Doctor of Philosophy.

Alva-Hurtado, J.E. and Selig, E.T., (1981). "Permanent Strain Behavior of Railroad Ballast." *Proceedings of the Tenth International Conference on Soil Mechanics and Foundation Engineering*, Stockholm, Sweden, pp. 543-546.

Alva-Hurtado, J.E., (1980). "A Methodology to Predict the Elastic and Inelastic Behaviour of Railroad Ballast." Report No. OUR80-240D. Department of Civil Engineering, University of Massachusetts, Massachusetts, USA.

American Railway Engineering Association, (1975). *Manual Recommendations, Special Committee on Concrete Ties.* Part 10 Concrete Ties (and Fastenings), AREA Bulletin No. 655.

Anderson, W.F. and Key, A.J., (2000). "Model Testing of Two-Layer Railway Track Ballast." *Journal of Geotechnical and Geoenvironmental Engineering*, 126 (4), pp. 317-323.

Ashmawy, A.K., Bourdeau, P.L., Drnevich, V.P., and Dysli, M., (1999). "Cyclic Response of Geotextile-Reinforced Soil." *Soils and Foundations*, 39 (1), pp. 43-52.

Ashpiz, E.S., Diederich, R., and Koslowski, C., (2002). "The Use of Spunbonded Geotextile in Railway Track Renewal on the St. Petersburg-Moscow Line." *Rail*

International, 33 (11), pp. 14-19.

ASTM (2002). "Standard Test Method for Consolidated Undrained Triaxial Compression Test for Cohesive Soils." ASTM D4767-02.

Baessler, M. and Ruecker, W., (2003). "Track Settlement Due to Cyclic Loading with Low Minimum Pressure and Vibrations." *System Dynamics and Long-Term Behaviour of Railway Vehicles, Track and Subgrade*, Popp, K. and Schiehlen, W., (Editors), Springer, Berlin, pp. 337-356.

Bardet, J.P. and Proubet, J., (1991). "A Numerical Investigation of the Structure of Persistent Shear Bands in Granular Material." *Géotechnique*, 41 (4), pp. 599-613.

Barksdale, R.D. and Itani, S.Y., (1989). "Influence of Aggregate Shape on Base Behavior." *Transportation Research Record*, 1227, pp. 173-182.

Barksdale, R.D., (1972b). *Repeated Load Test Evaluation of Base Coarse Materials*. Georgia Institute of Technology, Atlanta.

Barksdale, R.D., (1972a). "Laboratory Evaluation of Rutting in Base Course Materials." *Proceedings of the 3rd International Conference on Asphalt Pavements*, University of Michigan, pp. 161-174.

Barton, N. and Kjaernsli, B., (1981). "Shear Strength of Rockfill." *Journal of the Geotechnical Engineering Division*, *ASCE,* 107 (GT7), pp. 873-891.

Bernal, J.D. and Mason, J., (1960). "Co-Ordination of Randomly Packed Spheres." *Nature*, 188, pp. 910-911.

Billam, J., (1971). "Some Aspects of the Behaviour of Granular Materials at High Pressures." *Stress-Strain Behaviour of Soils, Proceedings of the Roscoe Memorial Symposium*, pp. 69-79.

Bishop, A.W., (1966). "The Strength of Soils as Engineering Materials." *Géotechnique*, 16, pp. 91-128.

Boominathan, A. and Hari, S., (2002). "Liquefaction Strength of Fly Ash Reinforced with Randomly Distributed Fibers." *Soil Dynamics and Earthquake Engineering*, 22, pp. 1027-1033.

Borden, R.H., Shao, L., and Gupta, A., (1996). "Dynamic Properties of Piedmont Residual Soils." *Journal of Geotechnical Engineering*, 122 (10), pp. 813-821.

Bosserman, B.N, (1981). "Ballast Experiments at FAST." *Proceedings, Facility for Accelerated Testing (FAST) Engineering Conference*, Denver, Colorado, pp. 45-54.

Bowling, A.J., (1980). "Investigations into the Deformability of Rockfill." *Third Australia - New Zealand Conference on Geomechanics*, Wellington, New Zealand, pp. 1-6.

Boyce, J.R., Brown, S.F., and Pell, P.S., (1976). "The Resilient Behavior of a Granular Material under Repeated Loading." *Proceedings Australian Road Research Board*, 8, pp. 8-19.

Broadley, J.R., Johnston, G.D., and Pond, B., (1981). "The Dynamic Impact Factor." *Railway Engineering Conference*, *Sydney*, pp. 87-91.

Brown, G.J., Miles, N.J., and Jones, T.F., (1996). "A Fractal Description of the Progeny of Single Impact Particle Breakage." *Minerals Engineering*, 9 (7), pp. 715-726.

Brown, S.F. and Hyde, A.F.L., (1975). "Significance of Cyclic Confining Stress in Repeated-Load Triaxial Testing of Granular Material." *Transportation Research Board*, Record No. 537, pp. 49-57.

Brown, S.F. and Selig, E.T., (1991). "The Design of Pavement and Rail Track Foundations." *Cyclic Loading of Soils: from Theory to Design*, Blackie and Son Ltd, New York, pp. 249-305.

Brown, S.F., (1974). "Repeated Load Testing of a Granular Material." *Journal of the Geotechnical Engineering Division*, *ASCE,* 100 (GT7), pp. 825-841.

Brown, S.F., Lashine, A.K.F., and Hyde, A.F.L., (1975). "Repeated Load Triaxial Testing of a Silty Clay." *Géotechnique*, 25 (1), pp. 95-114.

Budiman, J.S. and Wibowo, J., (1993). "Effects of Compactor Footprints on the Response of Subgrade Soil." *Transportation Research Record*, 1406, pp. 58-67.

Buonanno, A., Montanelli, F., and Rimoldi, P., (2003). *Preliminary Results from an Instrumented Railways Embankment Reinforced with a Geogrid-Geotextile Geocomposite*. [Online]. Available: www.tenax.net/geosynthetics/tech-doc/tds002.pdf [Accessed 3/10/2003]

Chang, C.S. and Whitman, R.V., (1988). "Drained Permanent Deformation of Sand due to Cyclic Loading." *Journal of Geotechnical Engineering*, 114 (10), pp. 1164-1179.

Charles, J.A. and Watts, K.S., (1980). "The Influence of Confining Pressure on the Shear Strength of Compacted Rockfill." *Géotechnique*, 30 (4), pp. 353-367.

Chou, Y.T., (1977). "Engineering Behavior of Pavement Materials: State of the Art." Report No. AD/A-045 272. US Army Engineering Waterways Experiment Station.

Chrismer, S.M. and Read, D.M., (1994). "Examining Ballast and Subgrade Conditions." *Railway Track and Structure*, *AREA*, pp. 39-42.

Chrismer, S.M., (1985). "Considerations of Factors Affecting Ballast Performance." *AREA Bulletin AAR Research and Test Department Report Number WP-110*, pp. 118-150.

Clarke, C.W., (1957). "Track Loading Fundamentals - 1." *The Railway Gazette, Railway Gazette International*, pp. 45-48.

Coffman, B.S., Kraft, D.G., and Tamayo, J., (1964). "A Comparison of Calculated and Measured Deflections for the AASHO Test Road." *Proceedings, Association of Asphalt Paving Technologists*, pp. 54.

Collins, I.F., and Boulbibane, M., (2000). "Geomechanical Analysis of Unbound Pavements Based on Shakedown Theory." *Journal of Geotechnical and Geoenvironmental Engineering*, 126 (1), pp. 50-59.

Commonwealth of Australia, (1999). "Progress in Rail Reform, Draft Report." Commonwealth of Australia, Canberra.

Coop, M.R., Sorensen, K.K., Bodas Freitas, T., and Georgoutsos, G., (2004). "Particle Breakage During Shearing of a Carbonate Sand." *Géotechnique*, 54 (3), pp. 157-163.

Cundall, P.A., Drescher, A., and Strack, O.D.L., (1982). "Numerical Experiments on Granular Assemblies; Measurements and Observations." *IUTAM Conference on Deformation and Failure of Granular Materials*, Delft, Netherlands, pp. 355-370.

Dahlberg, T., (2001). "Some Railroad Settlement Models - A Critical Review." *Proceedings of the Institution of Mechanical Engineers*, 215 (4) Part F, pp. 289-300.

Daouadji, A., Hicher, P-Y., and Rahma, A., (2001). "An Elastoplastic Model for Granular Materials Taking into Account Grain Breakage." *European Journal of Mechanics A/Solids*, 20, pp. 113-137.

Dehlen, G.L., (1969). "The Effect of Non-Linear Material Response on the Behavior of Pavements Subjected to Traffic Loads." Thesis presented to the University of California, in 1969, in partial fulfilment of the requirements for the degree of Doctor of Philosophy.

Diyaljee, V.A., (1987). "Effects of Stress History on Ballast Deformation." *Journal of Geotechnical Engineering*, 113 (8), pp. 909-914.

Doyle, N.F., (1980). *Railway Track Design: A Review of Current Practice*. Bureau of Transport Economics, Commonwealth of Australia, Canberra.

Drumm, E.C., Boateng-Poku, Y., and Pierce, J.T., (1990). "Estimation of Subgrade Resilient Modulus from Standard Tests." *Journal of Geotechnical Engineering, ASCE*, 116 (5), pp. 774-789.

Duncan, J.M., Williams, G.W., Sehn, A.L., and Seed, R.B., (1991). "Estimation Earth Pressures Due to Compaction." *Journal of Geotechnical Engineering*, 117 (12), pp. 1833-1847.

Earl, R., (1997). "Assessment of Behaviour of Field Soils during Compression." *Journal of Agricultural Engineering Research*, 68, pp. 147-157.

Eberhardt, E., Stimpson, B., and Stead, D., (1999). "Effects of Grain Size on the Initiation and Propagation Thresholds of Stress-Induced Brittle Fractures." *Rock Mechanics and Rock Engineering*, 32 (2), pp. 81-99.

Eisenmann, J., Leykauf, G., and Mattner, L., (1994). "Recent Developments in German Railway Track Design." *Proceedings of the Institution of Civil Engineers, Transportation*, 105, pp. 91-96.

Elliott, R.P. and David, L., (1989). "Improved Characterization Model for Granular Bases." *Transportation Research Record*, 1227, pp. 128-133.

El-Naggar, M., Kennedy, J.B., and Ibrahim, E.M., (1997). "Mechanical Properties of Reinforced Soil." *Composites Part B*, 28B, pp. 275-286.

Fang, Z. and Harrison, J.P., (2002). "Development of a Local Degradation Approach to the Modelling of Brittle Fracture in Heterogeneous Rocks." *International Journal of Rock Mechanics and Mining Sciences*, 39, pp. 443-457.

Feldman, F. and Nissen, D., (2002). "Alternative Testing Method for the Measurement of Ballast Fouling: Percentage Void Contamination." *Conference on Railway Engineering*, Wollongong, Australia, pp. 101-112.

Feng, D.M., (1984). "Railroad Ballast Performance Evaluation." Thesis presented to the University of Massachusetts, in 1984, in partial fulfilment of the requirements for the degree of Doctor of Philosophy.

FIP Commission on Prefabrication, (1987). *Concrete Railway Sleepers*. Thomas Telford, London.

Foun, D. and Martin, M., (2002). "Development of the QR Ballast Specification." *Conference on Railway Engineering*, Wollongong, Australia, pp. 203-212.

Fredlund, D.G., Bergan, A.T., and Wong, P.K., (1977). "Relation Between Resilient Modulus and Stress Conditions for Cohesive Subgrade Soils." *Transportation Research Record*, 642, pp. 73-81.

Freeman, R.B. and Harr, M.E., (2004). "Stress Predictions for Flexible Pavement Systems." *Journal of Transportation Engineering*, 130 (4), pp. 495-502.

Frost, M.W., Fleming, P.R., and Rogers, C.D.F., (2004). "Cyclic Triaxial Tests on Clay Subgrades for Analytical Pavement Design." *Journal of Transportation Engineering*, 130 (3), pp. 378-386.

Gaskin, P.N. and Raymond, G., (1976). "Contribution to Selection of Railroad Ballast." *Transportation Engineering Journal, ASCE*, 102 (TE2), pp. 377-394.

Ghosh, C. and Madhav, M.R., (1994). "Reinforced Granular Fill-Soil System: Confinement Effect." *Geotextiles and Geomembranes*, 13, pp. 727-741.

Goder, D., Kalman, H., and Ullmann, A., (2002). "Fatigue Characteristics of Granular Materials." *Powder Technology,* 122, pp. 19-25.

Grady, D.E. and Kipp, M.E., (1987). "Dynamic Rock Fragmentation." *Fracture Mechanics of Rock*, Atkinson, B. K., (Editor), pp. 429-475.

Haeri, S.M., Noorzad, R., and Oskoorouchi, A.M., (2000). "Effect of Geotextile Reinforcement on the Mechanical Behavior of Sand." *Geotextiles and Geomembranes*, 18 (6), pp. 385-402.

Hagerty, M.M., Hite, D.R., Ullrich, C.R., and Hagerty, D.J., (1993). "One-Dimensional High-Pressure Compression of Granular Media." *Journal of Geotechnical Engineering*, 119, pp. 1-18.

Hardin, B.O., (1985). "Crushing of Soil Particles." *Journal of Geotechnical Engineering*, 111 (10), pp. 1177-1192.

Harris, D., (1992). "Plasticity Models for Soil, Granular and Jointed Rock Materials." *Journal of the Mechanics and Physics of Solids*, 40 (2), pp. 273-290.

Hay, W.W., (1953). *Railroad Engineering*. Wiley, New York.

Hicks, R.G. and Monismith, C.L., (1971). "Factors Influencing the Resilient Response of Granular Materials." *Highway Research Board*, Record No. 345, pp. 15-31.

Hicks, R.G., (1970). "Factors Influencing the Resilient Properties of Granular Materials." Thesis presented to the University of California, in 1970, in partial fulfilment of the requirements for the degree of Doctor of Philosophy.

Hobbs, D.W., (1963). "A Simple Method for Assessing the Uniaxial Compressive Strength of Rock." *International Journal of Rock Mechanics and Mining Sciences*, 1, pp. 5-15.

Hyodo, M., Hyde, A.F.L., Aramaki, N., and Nakata, Y., (2002). "Undrained Monotonic and Cyclic Shear Behaviour of Sand under Low and High Confining Stresses." *Soils and Foundations*, 42 (3), pp. 63-76.

Indraratna, B., and Lackenby, J. Christie D., (2005). "Effect of Confining Pressure on the Degradation of Ballast under Cyclic Loading." *Géotechnique*, 55 (4), pp. 325-328.

Indraratna, B., and Salim, W., (2002). "Modelling of Particle Breakage of Coarse Aggregates Incorporating Strength and Dilatancy." *Proceedings of the Institution of Civil Engineers - Geotechnical Engineering*, 155 (4), pp. 243-252.

Indraratna, B., and Salim, W., (2003). "Deformation and Degradation Mechanics of Recycled Ballast Stabilised with Geosynthetics." *Soils and Foundations*, 43 (4), pp. 35-46.

Indraratna, B., Ionescu, D., and Christie, H.D., (1998). "Shear Behavior of Railway Ballast Based on Large-Scale Triaxial Tests." *Journal of Geotechnical and Geoenvironmental Engineering*, 124 (5), pp. 439-449.

Indraratna, B., Ionescu, D., and Christie, H.D., (2000). "State-of-the-Art Large Scale Testing of Ballast." *CORE 2000, Railway Technology for the 21st Century, Conference on Railway Engineering*, Adelaide, Australia, pp. 24.1-24.13.

Indraratna, B., Ionescu, D., Christie, H.D., and Chowdhury, R.N., (1997). "Compression and Degradation of Railway Ballast Under One-Dimensional Loading." *Australian Geomechanics*, pp. 48-61.

Indraratna, B., Khabbaz, H., Salim, W., Lackenby, J. and Christie, D. (2004). "Ballast Characteristics and the Effects of Geosynthetics on Rail Track Deformation", *International Conference on Geosynthetics and Geoenvironmental Engineering*, *ICGGE*, Bombay, India, pp. 3-12.

Indraratna, B., Salim, W., and Christie, D., (2002). "Improvement of Recycled Ballast Using Geosynthetics". *Proceedings of the 7th International Conference on Geosynthetics*, Nice, France, pp. 1177-1182.

Indraratna, B., Salim, W., Ionescu, D., and Christie, D., (2001). "Stress-Strain and Degradation Behaviour of Railway Ballast Under Static and Dynamic Loading, Based on Large-Scale Triaxial Testing." *Proceedings of the Fifteenth International Conference on Soil Mechanics and Geotechnical Engineering*, Istanbul, pp. 2093-2096.

Indraratna, B., Shahin, M.A., Rujikiatkamjorn, C., and Khabbaz, H., (2005). "Tsunami Affected Coastal Soil Disturbance and Implications on Reconstruction with Special Reference to Low-Cost Dwellings and Rail Tracks". *International Conference on Geotechnical Engineering for Disaster Mitigation and Rehabilitation*. Phoon & Yong (Editors), World Scientific Publishing Company.

Ionescu, D., Indraratna, B., and Christie, H.D., (1998). "Behaviour of Railway Ballast Under Dynamic Loads." *Thirteenth Southeast Asian Geotechnical Conference*, Taiwan, pp. 69-74.

Ishikawa, I. and Sekine, E., (2003). "Dynamic Behaviour of Railroad Ballast in Shaking Table Tests." *Deformation Characteristics of Geomaterials*, Di Benedetto *et al*. (Editors), Swets and Zeitlinger, Lisse, pp. 841-848.

Iwashita, K. and Oda, M., (1998). "Rolling Resistance at Contacts in Simulation of Shear Band Development by DEM." *Journal of Engineering Mechanics*, 124 (3), pp. 285-292.

Iwashita, K. and Oda, M., (2000). "Micro-Deformation Mechanism of Shear Banding Process Based on Modified Distinct Element Method." *Powder Technology*, 109, pp. 192-205.

Iwashita, K. and Oda, M., (2001). "Numerical Simulation of Granular Materials Subjected to Cyclic Loading Under Constant Volume by Modified Distinct Element Method." *Powder and Grains*, Kishino (Editor), Swets & Zeitlinger, Lisse, pp. 251-254.

Jain, V.K. and Keshav, K., (1999). "Stress Distribution in Railway Formation - A Simulated Study." *Proceedings of the 2nd International Symposium on Pre-Failure Deformation Characteristics of Geomaterials*, Torino, Italy, pp. 653-658.

Janardhanam, R. and Desai, C.S., (1983). "Three-Dimensional Testing and Modeling of Ballast." *Journal of Geotechnical Engineering*, 109 (6), pp. 783-796.

Jeffs, T. and Marich, S., (1987). "Ballast Characteristics in the Laboratory." *Conference on Railway Engineering*, Perth, Australia, pp. 141-147.

Jeffs, T. and Tew, G.P., (1991). *A Review of Track Design Procedures, Volume 2-Sleepers and Ballast*. BHP Research Melbourne Laboratories, Melbourne.

Jeffs, T., (1989). "Towards Ballast Life Cycle Costing." *The Fourth International Heavy Haul Railway Conference*, Brisbane, Australia, pp. 439-445.

Jenkins, J.T., Cundall, P.A., and Ishibashi, I., (1989). "Micromechanical Modeling of Granular Materials with the Assistance of Experiments and Numerical Simulations." *Powders and Grains*, Biarez & Gourves, (Editors), Balkema, Rotterdam, pp. 257-264.

John, E.G., (1998). "Simplified Curve Fitting using Spreadsheet Add-Ins." *International Journal of Engineering*, 14(5), pp. 375-380.

Jorenby, B.N. and Hicks, R.G., (1986). "Base Course Contamination Limits." *Transportation Research Record*, 1095, pp. 86-101.

Kalcheff, I.V. and Hicks, R.G., (1973). "A Test Procedure for Determining the Resilient Properties of Granular Materials." *Journal of Testing and Evaluation, ASTM*, 1 (6), pp. 472-479.

Kato, Y., Nakata, Y., Hyodo M., and Murata, H., (2003). "Effect of Particle Characteristics on Drained Shear Properties of Sand." *Deformation Characteristics of Geomaterials*, pp. 707-713.

Kempfert, H-G., Gotschol, A., Hu, Y., and Stocker, T., (2003). "Experimental Investigation and Numerical Modelling of Soils and Ballast under Cyclic and Dynamic Loading." *System Dynamics and Long-Term Behaviour of Railway*

Vehicles, Track and Subgrade, Popp, K. and Schiehlen, W., (Editors). Springer, Berlin, pp. 411-430.

Khedr, S., (1985). "Deformation Characteristics of Granular Base Course in Flexible Pavements." *Transportation Research Record*, 1043, pp. 131-138.

Knutson, R.M. and Thompson, M.R., (1977). "Resilient Response of Railway Ballast." *Transportation Research Record*, 651, pp. 31-39.

Knutson, R.M., (1976). "Factors Influencing the Repeated Load Behavior of Railway Ballast." Thesis presented to the University of Illinois, in 1976, in partial fulfilment of the requirements for the degree of Doctor of Philosophy.

Kou, S.Q., Liu, H.Y., Lindqvist, P.-A., Tang, C.A., and Xu, X.H., (2001). "Numerical Investigation of Particle Breakage as Applied to Mechanical Crushing - Part II: Interparticle Breakage." *International Journal of Rock Mechanics and Mining Sciences*, 38, pp. 1163-1172.

Ladd, R.S., (1978). "Preparing Test Specimens Using Under-Compaction." *Geotechnical Testing Journal*, 1 (2), pp. 16-23.

Lade, P.V., Yamamuro, J.A., and Bopp, P.A., (1996). "Significance of Particle Crushing in Granular Materials." *Journal of Geotechnical Engineering*, 122 (4), pp. 309-316.

Lashine, A.K., (1971). "Some Aspects of the Characteristics of Keuper Marl under Repeated Loading." Thesis presented to the University of Nottingham, in 1971, in partial fulfilment of the requirements for the degree of Doctor of Philosophy.

Lee, K.L. and Farhoomand, I., (1967). "Compressibility and Crushing of Granular Soil in Anisotropic Triaxial Compression." *Canadian Geotechnical Journal*, 4, pp. 68-86.

Lee, K.L. and Seed, H.B., (1967). "Drained Strength Characteristics of Sands." *Journal of the Soil Mechanics and Foundation Division, ASCE*, 93 (6), pp. 117-141.

Lee, W., Bohra, N.C., and Altschaeffl, A.G., (1995). "Resilient Characteristics of Dune Sand." *Journal of Transportation Engineering*, 121 (6), pp. 502-506.

Lees, G. and Kennedy, C.K., (1975). "Quality, Shape and Degradation of Aggregates." *Journal of Engineering Geology*, 8, pp. 193-209.

Lentz, R.W. and Baladi, G.Y., (1981). "Constitutive Equation for Permanent Strain of Sand Subjected to Cyclic Loading." *Transportation Research Record*, 810, pp. 50-54.

Li, D. and Selig, T., (1996). "Cumulative Plastic Deformation for Fine-Grained Substrate Soils." *Journal of Geotechnical Engineering*, 122 (12), pp. 1006-1013.

Li, D. and Selig, T., (1998). "Method for Railroad Track Foundation Design. II: Applications." *Journal of Geotechnical and Geoenvironmental Engineering*, 124 (4), pp. 323-329.

Li, D., (2000). "Deformations and Remedies for Soft Railroad Subgrades Subjected to Heavy Axle Loads." *Advances in Transportation and Geoenvironmental Systems Using Geosynthetics, American Society of Civil Engineers, Geotechnical Special Publication No. 103*, Denver, Colorado, pp. 307-321.

Li, J. and Ding, D.W., (2002). "Nonlinear Elastic Behavior of Fiber-Reinforced Soil Under Cyclic Loading." *Soil Dynamics and Earthquake Engineering*, 22, pp. 977-983.

Liao, C-L, Chang, T-P, and Young, D-H., (1995). "Elasto-Plastic Constitutive Modelling of Granular Assembly." *International Journal of Solids and Structures*, 32 (8-9), pp. 1121-1133.

Lieberenz, K. and Weisemann, U., (2002). "Geosynthetics in Dynamically Stressed Earth Structures of Railway Lines." *Rail International*, 33 (11), pp. 30-39.

Lim, W.L., McDowell, G.R., and Collop, A.C., (2005). "Quantifying the Relative Strengths of Railway Ballasts." *Geotechnical Engineering*, 158 (GE2), pp. 107-111.

Liu, Z., Myer, L.R., and Cook, N.G.W., (1993). "Micromechanics of Granular Materials - Numerical Simulation of the Effects of Heterogeneities." *International Journal of Rock Mechanics and Mining Science & Geomechanics Abstracts*, 30 (7), pp. 1281-1284.

Loret, B., (1982). "Modelization of Sand Behaviour over a Wide Stress Range." *International Symposium on Numerical Methods in Geomechanics*, Dungar, R., Pande, G.N., and Studer, J.A. (Editors), Zurich, pp. 100-109.

Luo, W-K., (1973). "The Characteristics of Soils Subjected to Repeated Loads and their Applications to Engineering Practice." *Soils and Foundations*, 13 (1), pp. 11-27.

Maeda, K. and Miura, K., (1999). "Confining Stress Dependency of Mechanical Properties of Sand." *Soils and Foundations*, 39 (1), pp. 53-67.

Marachi, N.D., Chan, C.K., and Seed, H.B., (1972). "Evaluation of Properties of Rockfill Materials." *Journal of the Soil Mechanics and Foundation Division, ASCE*, 98, pp. 95-114.

Marsal, R.J., (1967). "Large Scale Testing of Rockfill Materials." *Journal of the Soil Mechanics and Foundation Division, ASCE*, 93 (2), pp. 27-43.

Marsal, R.J., (1973). "Mechanical Properties of Rockfill." *Embankment Dam Engineering*, Wiley, New York, pp. 109-200.

McDowell, G.R. and Bolton, M.D., (1998). "On the Micromechanics of Crushable Aggregates." *Géotechnique*, 48 (5), pp. 667-679.

McDowell, G.R. and Harireche, O., (2002). "Discrete Element Modelling of Soil Particle Fracture." *Géotechnique*, 52 (2), pp. 131-135.

McDowell, G.R., Bolton, M.D., and Robertson, D., (1996). "The Fractal Crushing of Granular Materials." *Journal of the Mechanics and Physics of Solids*, 44 (12), pp. 2079-2102.

McGown, A., (1976). "The Properties and Uses of Permeable Fabric Membranes." *Residential Workshop on Materials and Methods for Low Cost Road, Rail and Reclamation Works*, Leura, Australia, pp. 663-708.

Mineral Resources, (2002). *Constructions Materials - Gravel and Crushed Rock*. [Online]. Available: www.quarry.com.au/minres-gravel.htm [Accessed 2002].

Mirghasemi, A.A., Rothenburg, L., and Matyas, E.L., (1997). "Numerical Simulations of Assemblies of Two-Dimensional Polygon-Shaped Particles and Effects of Confining Pressure on Shear Strength." *Soils and Foundations*, 37 (3), pp. 43-52.

Miura, N. and O′Hara, S., (1979). "Particle-Crushing of a Decomposed Granite Soil Under Shear Stresses." *Soils and Foundations*, 19 (3), pp. 1-14.

Moghaddas-Nejad, F. and Small, J.C., (2003). "Resilient and Permanent Characteristics of Reinforced Granular Materials by Repeated Load Triaxial Tests." *Geotechnical Testing Journal*, 26 (2), pp. 152-166.

Moghaddas-Nejad, F. and Small, J.C., (1996). "Effect of Geogrid Reinforcement in Model Track Tests on Pavements." *Journal of Transportation Engineering*, 122 (6), pp. 468-474.

Mohajeri, M. and Towhata, I., (2003). "Stress-Strain Behavior of Compacted Sandy Material under Cyclic Simple Shear." *Soils and Foundations*, 43 (6), pp. 75-89.

Nataatmadja, A. and Tan, Y.L., (2001). "Resilient Response of Recycled Concrete Road Aggregates." *Journal of Transportation Engineering*, 127 (5), pp. 450-453.

Nataatmadja, A., (1989). "Variability of Pavement Parameters under Repeated Loading." Thesis presented to the University of Monash, in 1989, in partial fulfilment of the requirements for the degree of Doctor of Philosophy.

Neil, D.M., (1976). "Railway Design Ballast and Subgrade." *Residential Workshop on Materials and Methods for Low Cost Road, Rail and Reclamation Works*, pp. 637-661.

Ng, T-T. and Dobry, R., (1994). "Numerical Simulations of Monotonic and Cyclic Loading of Granular Soil." *Journal of Geotechnical Engineering*, 120 (2), pp. 388-403.

Norman, G.M. and Selig, E.T., (1983). "Ballast Performance Evaluation with Box Tests." *Bulletin of the American Railway Engineering Association*, 84 (692), pp. 207-239.

Oda, M., (1972). "Deformation Mechanism of Sand in Triaxial Compression Tests." *Soils and Foundations*, 12 (4), pp. 45-63.

Office for Research and Experiments, ORE (1970). *Stresses in Rails, the Ballast and the Formation Resulting from Traffic Loads*. Question D71, Report No. 10, Vols. 1 and 2, International Union of railways, Utrecht, Netherlands.

Office of Research and Experiments, ORE (1965). *Stresses in Rails*. Report No. D71/RP1/E, International Union of Railways, Utrecht, Netherlands.

Office of Research and Experiments, ORE (1974). *Optimum Adaptation of the Conventional Track to Future Traffic*. Question D117, Report No. 5, International Union of Railways, Utrecht, Netherlands.

Office of Research and Experiments, ORE (1969). *Stresses in Concrete Sleepers*. Report D71/RP9/E, International Union of Railways, Utrecht, Netherlands.

Office of Research and Experiments, ORE (1976). *Influence of Various Measures at the Lateral Resistance of an Unloaded Track*. Question D117, Report No. 8, International Union of Railways, Utrecht, Netherlands.

Oldecop, L.A. and Alonso, E.E., (2001). "A Model for Rockfill Compressibility." *Géotechnique*, 51 (2), pp. 127-139.

Olowokere, D.O., (1975). "Strength and Deformation of Railway Ballast Subject to Triaxial Loading." Thesis presented to the Queen's University, in 1975, in partial fulfilment of the requirements for the degree of Doctor of Philosophy.

Ozel, M.R. and Mohajerani, A., (2001). "Resilient Modulus of a Stabilised Fine-Grained Subgrade Soil." *Australian Geomechanics*, 36 (3), pp. 75-86.

Penman, A.D.M., (1978). "The Behaviour of Rockfill Dams." *Geotechnical Engineering*, 9, pp. 105-122.

Ponce, V.M. and Bell, J.M., (1971). "Shear Strength of Sand at Extremely Low Pressures." *Journal of Soil Mechanics and Foundation Engineering*, *ASCE,* 97 (SM4), pp. 625-637.

Profillidis, V.A., (1995). *Railway Engineering*. Avebury Technical, Aldershot.

Profillidis, V.A., (2000). "The Reinforcement Effect of Geotextiles in Railway Subgrades." *Rail International*, 31 (7), pp. 11-14.

Raad, L. and Figueroa, J.L., (1980). "Load Response of Transportation Support Systems." *Transportation Engineering Journal, ASCE*, 106 (TE1), pp. 111-128.

Rada, G. and Witczak, M.W., (1981). "Comprehensive Evaluation of Laboratory Resilient Moduli Results for Granular Materials." *Transportation Research Record*, 810, pp. 23-33.

Ray, S.K., Sarkar, M., and Singh, T.N., (1999). "Effect of Cyclic Loading and Strain Rate on the Mechanical Behaviour of Sandstone." *International Journal of Rock Mechanics and Mining Sciences*, 36, pp. 543-549.

Raymond, G.P. and Davies, J.R., (1978). "Triaxial Tests on Dolomite Railroad Ballast." *Journal of the Soil Mechanics and Foundation Division, ASCE*, 104 (6), pp. 737-751.

Raymond, G.P. and Diyaljee, V.A., (1979). "Railroad Ballast Load Ranking Classification." *Journal of the Geotechnical Engineering Division*, 105 (10), pp. 1133-1153.

Raymond, G.P. and Ismail, I., (2003). "The Effect of Geogrid Reinforcement on Unbound Aggregates." *Geotextiles and Geomembranes*, 21, pp. 355-380.

Raymond, G.P. and Williams, D.R., (1978). "Repeated Load Triaxial Tests on Dolomite Ballast." *Journal of the Geotechnical Engineering Division*, 104 (GT7), pp. 1013-1029.

Raymond, G.P., (1977). "Stresses and Deformations in Railway Track." *CIGGT Report No. 77*-115, Queen's University Press, Ontario, Canada.

Raymond, G.P., (1978). "Design for Railroad Ballast and Subgrade Support." *Journal of the Geotechnical Engineering Division, ASCE*, 104 (GT1), pp. 45-60.

Raymond, G.P., (1979). "Railroad Ballast Prescription: State-of-the-Art." *Journal of the Geotechnical Engineering Division, ASCE*, 105 (GT2), pp. 305-322.

Raymond, G.P., (1985). "Research on Railroad Ballast Specification and Evaluation." *Transportation Research Record 1006 - Track Design and Construction*, pp. 1-8.

Raymond, G.P., (1992). "Reinforced Sand Behavior Overlying Compressible Subgrades." *Journal of Geotechnical Engineering*, 118 (11), pp. 1663-1680.

Raymond, G.P., (1999). "Railway Rehabilitation Geotextiles." *Geotextiles and Geomembranes*, 17, pp. 213-230.

Raymond, G.P., (2002). "Reinforced Ballast Behaviour Subjected to Repeated Load." *Geotextiles and Geomembranes*, 20, pp. 39-61.

Raymond, G.P., Lake, R.W., and Boon, C.J., (1976). "Stresses and Deformations in Railway Track," *CIGGT, Report No. 76-11*, Queen's University Press, Ontario, Canada.

Rhee, S., (1991). "A Study of Resilient Behavior and Constitutive Modeling of Thick Granular Layers for Heavily Loaded Asphalt Pavement." Thesis presented to the Texas A&M, in 1991, in partial fulfilment of the requirements for the degree of Doctor of Philosophy.

Rowshanzamir, M.A., (1995). "Resilient Cross-Anisotropic Behaviour of Granular Base Materials under Repetitive Loading." Thesis presented to the University of New South Wales, in 1995, in partial fulfilment of the requirements for the degree of Doctor of Philosophy.

Sabine, W., Ralf, N., Dawson, A.R., and Wellner, F., (2002). "Deformation Behaviour of Granular Materials under Repeated Dynamic Load." *Environmental Geomechanics*, Monte Verita, Available at www.nottingham.ac.uk/~evzard/ascona2002.pdf

Salim, W., and Indraratna, B., (2004). "A New Elasto-Plastic Constitutive Model for Coarse Granular Aggregates Incorporating Particle Breakage." *Canadian Geotechnical Journal*, 41 (4), pp. 657-671.

Salim, W.M.D., (2004). "Deformation and Degradation Aspects of Ballast and the Role of Geosynthetics in Track Stabilisation." Thesis presented to the University of Wollongong, in 2004, in partial fulfilment of the requirements for the degree of Doctor of Philosophy.

Sammis, C.G. and Ashby, M.F., (1986). "The Failure of Brittle Porous Solids under Compressive Stress States." *Acta Metallurgica*, 34(3), pp. 511-526.

Sawicki, A. and Swidzinski, W., (1995). "Cyclic Compaction of Soils, Grains and Powders." *Powder Technology*, 85, pp. 97-104.

Schmutz, G., (2000). "Ballast and Recycling Spent Ballast." *Rail International*, 31 (7), pp. 2-7.

Schramm, G., (1961). *Permanent Way Technique and Permanent Way Economy, (English Translation by Hans Lange), Otto Elsner Verlagsgessellschaft Darmstadt*.

Schultze, E., (1961). "Elastic Properties of Ballast." *Proceedings of the 5th International Conference on Soil Mechanics and Foundation Engineering*, Paris, France, pp. 323-327.

Scott, J.F., (1985). "Granular Depth Requirement for Railroad Track." *Transportation Research Record 1006 - Track Design and Construction*, pp. 17-22.

Seed, H.B., Mitry, F.G., Monismith, C.L., and Chan, C.K., (1967). "*Factors Influencing the Resilient Deformation of Untreated Aggregate Base in Two Layer Pavements Subjected to Repeated Loading*, " Highway Research Board, Record No. 190.

Seed, R.B. and Duncan, J.M., (1986). "FE Analysis: Compaction-Induced Stresses and Deformations." *Journal of Geotechnical Engineering*, 112 (1), pp. 23-56.

Selig, E.T. and Alva-Hurtado, J.E., (1982). "Predicting Effects of Repeated Wheel Loading on Track Settlement." *Proceedings of the Second International Heavy Haul Railway Conference*, Colorado Springs, pp. 476-487.

Selig, E.T. and Waters, J.M., (1994). *Track Geotechnology and Substructure Management*. Thomas Telford, London.

Shackel, B., (1973b). "The Derivation of Complex Stress-Strain Relations." *Proceedings of the 8th International Conference on Soil Mechanics and Foundation Engineering*, Volume 1, Moscow, Russia, pp. 353-359.

Shackel, B., (1973a). "An Engineering Approach to Defining Three Dimensional Stress-Strain Relationships." *Conference on Stress and Strain in Engineering*, Institute of Engineers, Australia, pp. 26-31.

Shahnazari, H. and Towhata, I., (2002). "Torsion Shear Tests on Cyclic Stress-Dilatancy Relationship of Sand." *Soils and Foundations*, 42 (1), pp. 105-119.

Shahu, J.T., Kameswara Rao, N.S.V., and Yudhbir., (1999). "Parametric Study of Resilient Response of Tracks With a Sub-Ballast Layer." *Canadian Geotechnical Journal*, 36, pp. 1137-1150.

Shenton, M.J., (1974). "Deformation of Railway Ballast Under Repeated Loading Triaxial Tests." *Report RP5, Soil Mechanics Section, British Railway Research Department*, Derby, England.

Shenton, M.J., (1985). "Ballast Deformation and Track Deterioration." *Track Technical Conference*, Thomas Telford Services Ltd, London, pp. 253-265.

Shin, E.C., Kim, D.H., and Das, B.M., (2002). "Geogrid-Reinforced Railroad Bed Settlement due to Cyclic Loading." *Geotechnical and Geological Engineering*, 20, pp. 261-271.

Singh, S.K., (1988). "Relationship Among Fatigue Strength, Mean Grain Size and Compressive Strength of a Rock." *Rock Mechanics and Rock Engineering*, 21, pp. 271-276.

Sitharam, T.G., (1999). "Micromechanical Modeling of Granular Materials: Effect of Confining Pressure on Mechanical Behaviour." *Mechanics of Materials*, 31, pp. 653-665.

Sowers, G.F., Williams, R.C., and Wallace, T.S., (1965). "Compressibility of Broken Rock and the Settlement of Rockfills." *Proceedings of the 6th International Conference on Soil Mechanics and Foundation Engineering*, 2, pp. 561-565.

Standards Australia, (1993a). "Methods of Testing Rocks for Engineering Purposes - Rock Strength Tests - Determination of Point Load Strength Index." AS 4133.4.1 - 1993, Sydney, NSW, Australia.

Standards Australia, (1993b). "Methods of Testing Rocks for Engineering Purposes - Rock Strength Tests - Determination of Uniaxial Compressive Strength." AS 4133.4.2 – 1993, Sydney, NSW. Australia.

Standards Australia, (1995). "Methods for Sampling and Testing Aggregates. Method 6.8.1: Soil Strength and Consolidation Tests - Determination of the Resilient Modulus and Permanent Deformation of Granular Unbound Pavement Materials." AS 1289.6.8.1-1995, Sydney, NSW, Australia.

Standards Australia, (1995a). "Methods for Sampling and Testing Aggregates. Method 23: Los Angeles Value." AS 1141.23 - 1995, Sydney, NSW, Australia.

Standards Australia, (1995b). "Methods for Sampling and Testing Aggregates - Resistance to Wear by Attrition." AS 1141.27 - 1995, Sydney, NSW, Australia.

Standards Australia, (1995c). "Methods for Sampling and Testing Aggregates - Particle Shape, by Proportional Calliper." AS 1141.14 - 1995, Sydney, NSW, Australia.

Standards Australia, (1996). "Aggregates and Rock for Engineering Purposes." AS 2758.7-1996, Sydney, NSW, Australia.

Standards Australia, (1997a). "Railway Permanent Way Material. Part 14: Prestressed Concrete Sleepers." AS 1085.14 -1997, Sydney, NSW, Australia.

Standards Australia, (1997b). "Methods for Sampling and Testing Aggregates. Method 21: Aggregate Crushing Value." AS 1141.21-1997, Sydney, NSW, Australia.

Standards Australia, (1999). "Methods for Sampling and Testing Aggregates - Flakiness Index." AS 1141.15 - 1999, Sydney, NSW. Australia.

Stewart, H.E., (1986). "Permanent Strains from Cyclic Variable-Amplitude Loadings." *Journal of Geotechnical Engineering*, 112 (6), pp. 646-660.

Suiker, A.S.J., (1997). *Fatigue Behaviour of Granular Materials. Part 1 - Constitutive Modelling and Description of Experiments. Tu-Delft Report No. 7-97-119-2*. Delft University of Technology, Netherlands.

Suiker, A.S.J., Selig, E.T., and Frenkel, R., (2005). "Static and Cyclic Triaxial Testing of Ballast and Subballast." *Journal of Geotechnical and Geoenvironmental Engineering*, 131 (6), pp. 771-782.

Sweere, G.T.H., (1990). "Unbound Granular Bases for Roads." Thesis presented to the Delft University of Technology, in 1990, in partial fulfilment of the requirements for the degree of Doctor of Philosophy.

Tanaka, Y., (2003). "Evaluation of Undrained Cyclic Strength of Gravelly Soil by Shear Modulus." *Soils and Foundations*, 43 (4), pp. 149-160.

Tang, C.A., Liu, H., Lee, P.K.K., Tsui, Y., and Tham, L.G., (2000). "Numerical Studies of the Influence of Microstructure on Rock Failure in Uniaxial Compression - Part 1: Effect of Heterogeneity." *International Journal of Rock Mechanics and Mining Sciences*, 37 (4), pp. 555-569.

Tang, C.A., Xu, X.H., Kou, S.Q., Lindqvist, P.-A., and Liu, H.Y., (2001). "Numerical Investigation of Particle Breakage as Applied to Mechanical Crushing - Part 1: Single-Particle Breakage." *International Journal of Rock Mechanics and Mining Sciences*, 38, pp. 1147-1162.

Thom, N.H. and Brown, S.F., (1987). "Effect of Moisture on the Structural Performance of a Crushed-Limestone Road Base." *Transportation Research Record*, 1121, pp. 50-56.

Thom, N.H. and Brown, S.F., (1988). "The Effect of Grading and Density on the Mechanical Properties of a Crushed Dolomitic Limestone." *Proceedings of the 14th Australian Road Research Board Conference*, Part 7, pp. 94-100.

Thompson, M.R., (1989). Report No. FHWA-TS-90-031. National Technical Information Service, Springfield, VA.

Trollope, E.H., Lee, I.K., and Morris, J., (1962). "Stresses and Deformations in Two-Layer Pavement Structures under Slow Repeated Loading." *Australian Road Research Board*, pp. 693.

Tsoungui, O., Vallet, D., and Charmet, J-C., (1999). "Numerical Model of Crushing of Grains Inside Two-Dimensional Granular Materials." *Powder Technology*, 105 (1-3), pp. 190-198.

Ueng, T-S. and Chen, T-J., (2000). "Energy Aspects of Particle Breakage in Drained Shear of Sands." *Géotechnique*, 50 (1), pp. 65-72.

Uzan, J., (1985). "Characterization of Granular Material." *Transportation Research Record*, 1022, pp. 52-59.

Uzan, J., (1999). "Granular Characterization for Mechanistic Pavement Design." *Journal of Transportation Engineering,* 125 (2), pp. 108-113.

Vesic, A.S. and Clough, G.W., (1968). "Behavior of Granular Materials Under High Stresses." *Journal of the Soil Mechanics and Foundation Division, ASCE*, 94 (3), pp. 661-688.

Wong, R.H.C., Chau, K.T., and Wang, P., (1996). "Microcracking and Grain Size Effect in Yuen Long Marbles." *International Journal of Rock Mechanics and Mining Science & Geomechanics Abstracts*, 33 (5), pp. 479-485.

Wu, T.X. and Thompson, D.J., (1999). "The Effects of Local Preload on the Foundation Stiffness and Vertical Vibration of Railway Track." *Journal of Sound and Vibration*, 219 (5), pp. 881-904.

Yamamuro, J.A. and Lade, P.V., (1996). "Drained Sand Behaviour in Axisymmetric Tests at High Pressures." *Journal of Geotechnical Engineering*, 122 (2), pp. 109-119.

Yoder, E.J. and Witczak, M.W., (1975). *Principles of Pavement Design 2nd Edition*. John Wiley and Sons, New York.

Yoo, T.S. and Selig, E.T., (1979). "Field Observations of Ballast and Subgrade Deformations in Track." *Transportation Research Board*, No. 733, pp. 6-12.

Zaman, M., Chen, D-H, and Laguros, J., (1994). "Resilient Moduli of Granular Materials." *Journal of Transportation Engineering*, 120 (6), pp. 967-988.

Zeghal, M., (2004). "Discrete-Element Method Investigation of the Resilient Behavior of Granular Materials." *Journal of Transportation Engineering*, 130 (4), pp. 503-509.

Zicha, J.H., (1989). "High-Speed Rail Track Design." *Journal of Transportation Engineering*, 115 (1), pp. 68-83.

APPENDIX A

DYNAMIC IMPACT FACTORS

This Appendix outlines the two more commonly employed dynamic impact factors (DIF) that are used to account for the dynamic loading aspects of cyclic train loading. Whilst many other DIF currently exist, only the methods proposed by Broadley *et al*. (1981) and ORE (1965) have been considered here.

Broadley *et al*. (1981) studied freight train loading and further developed the statistical impact factor model introduced by Eisenmann (1972). The dynamic impact factor ϕ' represented by Equation A.1 is relevant for train speeds up to 115 km/hr. δ describes the track condition, η is a speed factor, β distinguishes between loaded and unloaded states, and t defines the probability of the maximum allowable rail deflection not being exceeded. Typical values for the parameters in Equation A.1 are tabulated in Table A.1. Once ϕ' has been calculated it is multiplied by the static wheel load and the sleeper-ballast contact pressure is determined according to the procedure given in Section 2.3 (Chapter 2).

$$\phi' = 1 + \delta\eta t\beta \qquad \text{(A.1)}$$

ORE (1965) recorded the forces applied to the rails by locomotives and derived Equation A.2a to calculate the impact factor ϕ'. The variables α' and β' are estimated by Equations A.2b and A.2c, respectively, where V is the vehicle speed in km/hr, d_s is the superelevation deficiency, h is the vertical distance from the rail top to the vehicle centre of mass, and d_h is the horizontal distance between rail centres. Typical values of

β' range from 0.13 to 0.17. Coefficient γ' is found from Equation A.2d and Table A.2. α', β' and γ' are dependent on the vehicle and track characteristics shown in Table A.3.

Table A.1 Recommended values for the parameters of the Broadley *et al*. (1981) dynamic impact factor (Equation A.1)

Please see print copy for Table A.1

$$\phi' = 1 + \alpha' + \beta' + \gamma' \quad \text{(A.2a)}$$

$$\alpha' = 0.04(V/100)^3 \quad \text{(A.2b)}$$

$$\beta' = 2d_s h/d_h^2 \quad \text{(A.2c)}$$

$$\gamma' = \gamma_0 a_0 b_0 \quad \text{(A.2d)}$$

Table A.2 Recommended values of γ_0, a_0, and b_0 for different train speeds for the ORE (1965) impact factor calculation (Equation A.2d)

Please see print copy for Table A.2

Table A.3 Parameters known to influence α', β' and γ' (Equations A.2a – A.2d)

α'	β'	γ'
Vertical track irregularities	Vehicle speed	Vehicle speed
Vehicle speed	Track superelevation deficiency	Track condition
Vehicle suspension characteristics	Location of vehicle centre of gravity	Train maintenance conditions
		Vehicle design

REFERENCES

Broadley, J.R., Johnston, G.D., and Pond, B., (1981). "The Dynamic Impact Factor." *Railway Engineering Conference,* Sydney, pp. 87-91.

Eisenmann, J., (1972). "Germans Gain a Better Understanding of Track Structure." *Railway Gazette International,* 128 (N.8/305).

Office of Research and Experiments (ORE), (1965). *Stresses in Rails*. Report No. D71/RP1/E. International Union of Railways, Utrecht, Netherlands.

APPENDIX B

BREAKAGE QUANTIFICATION METHODS

Several methods have been proposed to quantify the degree of degradation occurring within a granular assembly, and these methods can generally be broken into four categories as shown in Table B.1. Perhaps the three most widely used techniques are those suggested by Marsal (1973), Miura and O′Hara (1979) and Hardin (1985), as described below.

Table B.1 Existing breakage quantification methods

Please see print copy for Table B.1

B.1 Breakage Index B_g (Marsal, 1973)

Marsal (1973) performed large-scale triaxial compression tests on rockfill materials and observed significant amounts of degradation. The breakage index B_g was devised to assist in the design of earth and rockfill dams, where B_g is the percentage by weight of particles that have undergone breakage. To calculate B_g the difference (ΔW_k) between the percentages retained by weight on each sieve size before (W_{ki}) and after (W_{kf}) testing is recorded, and B_g is simply the sum of the positive (or negative) values of ΔW_k, expressed as a percentage. B_g has a lower limit of 0% (no particle breakage) and

theoretical upper limit of 100% (after loading all particles pass the smallest sieve size used). The method is illustrated more succinctly in Figure B.1.

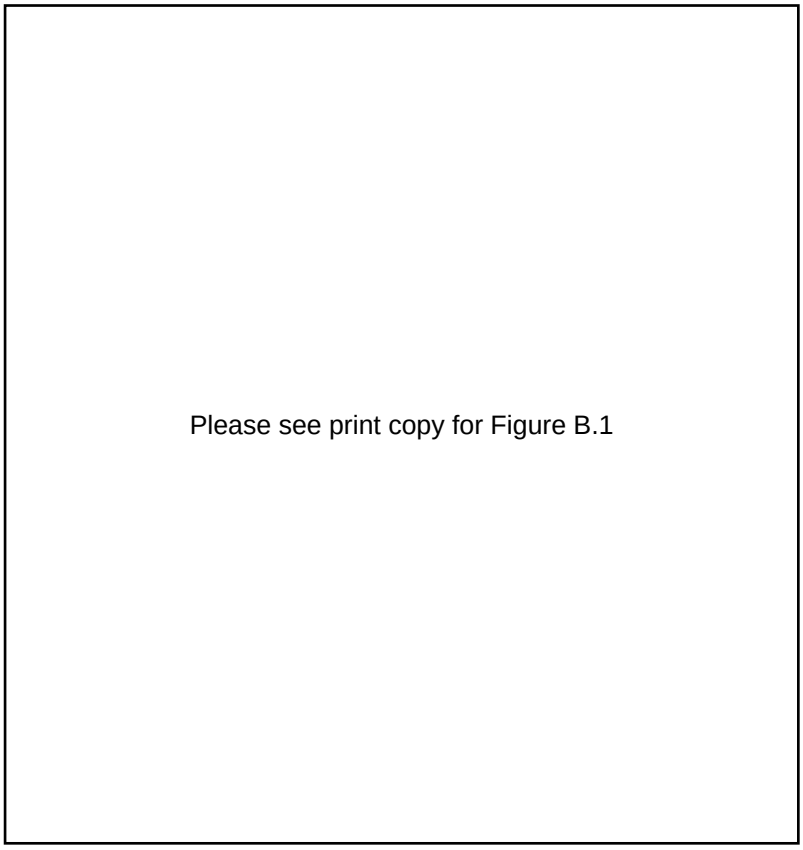

Figure B.1 Calculation of B_g (after Marsal, 1973)

Lade *et al*. (1985) identified that B_g does not accurately portray the amount of breakage when degradation is extensive. Widespread breakage prevents an accurate comparison of the larger sized particles before and after loading, resulting in the significant scatter of results.

B.2 Surface Area Method ΔS (Miura and O′Hara, 1979)

Miura and O′Hara (1979) utilised the increase in overall particle surface area ΔS as a measure of particle crushing for decomposed granite soil. The surface area S of a

granular material can be calculated using Equation B.1, where γ_d is the current dry density of the specimen being tested (g/cm^3) and S_w is the specific surface area (cm^2/g).

$$S = S_w \times \gamma_d \quad \text{(B.1)}$$

To calculate S_w for each particle size fraction, the mean particle diameter d_m is first determined according to Equation B.2, where d_1 and d_2 are the diameters of the largest and smallest particles retained in that fraction. Assuming all the particles are spherical, the specific surface area is then computed from Equation B.3.

$$d_m = \sqrt{(d_1 \times d_2)} \quad \text{(B.2)}$$

$$S_w = SA / (V' \times G_s) \quad \text{(B.3)}$$

SA and V′ are the surface area and volume of a sphere with diameter d_m, respectively, and G_s is the specific gravity of the particles. S_w for each fraction is summed to give the specific surface area for the entire sample. Substitution of $\sum S_w$ into Equation B.1 gives the surface area of the aggregate. The assumption of particle sphericity leads to an underestimation of the surface area, however, the method does provide a good comparison of the surface area before and after loading. The error caused by the assumption of particle shape has been demonstrated to have little effect on the interpretation of results (Miura and O′Hara, 1979).

A.3 Breakage Magnitude B_r (Hardin, 1985)

Hardin (1985) quantified breakage by plotting traditional particle size distribution (PSD) curves (percentage passing versus log of the sieve size) before and after testing. Hardin identified that particles of silt size or smaller (< 0.074 mm) are extremely difficult to break, and therefore serve as a good reference for the magnitude of particle breakage. The potential for breakage (b_p) of a particle of size D can be represented by Equation B.4. Taking into account the large number of particles in a granular assembly, the total breakage potential B_p is given by Equation B.5 and is simply the area between the initial particle size distribution curve and the D = 0.074 mm line, as shown in Figure B.2. During loading a certain degree of crushing takes place, and the area between the initial and final particle size distribution curves is defined as the total breakage B_t (Figure B.3 and Equation B.6), where b_{po} are the original values of b_p, and b_{pl} the values of b_p after loading. Finally, relative breakage B_r is calculated according to Equation B.7 where the total breakage B_t is divided by the potential breakage B_p.

In more simple terms, B_r is simply the area between the two PSD curves before and after loading, divided by the area between the initial PSD curve and the 0.074 mm line.

$$b_p = \log_{10}\left[\frac{D}{0.074}\right] \text{ for } D \geq 0.074 \text{ mm} \tag{B.4}$$

$$B_p = \int_0^1 b_p df \tag{B.5}$$

$$B_t = \int_0^1 (b_{po} - b_{pl}) df \tag{B.6}$$

$$B_r = B_t / B_p \tag{B.7}$$

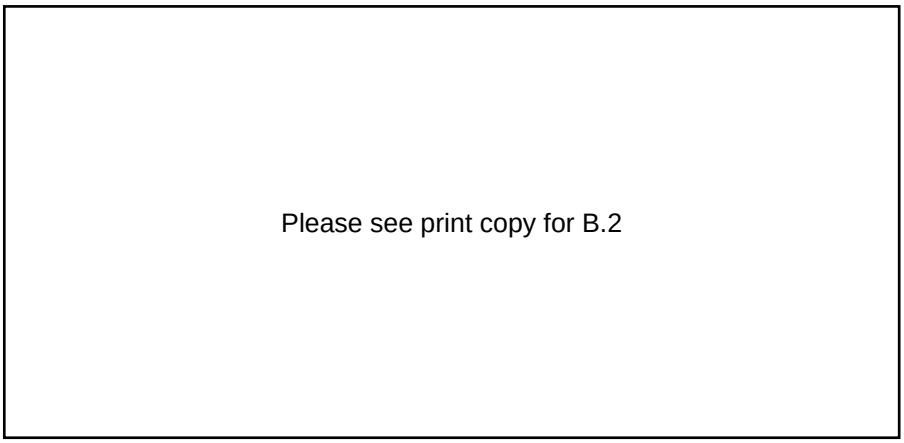

Figure B.2 Breakage potential B_p according to Hardin (1985)

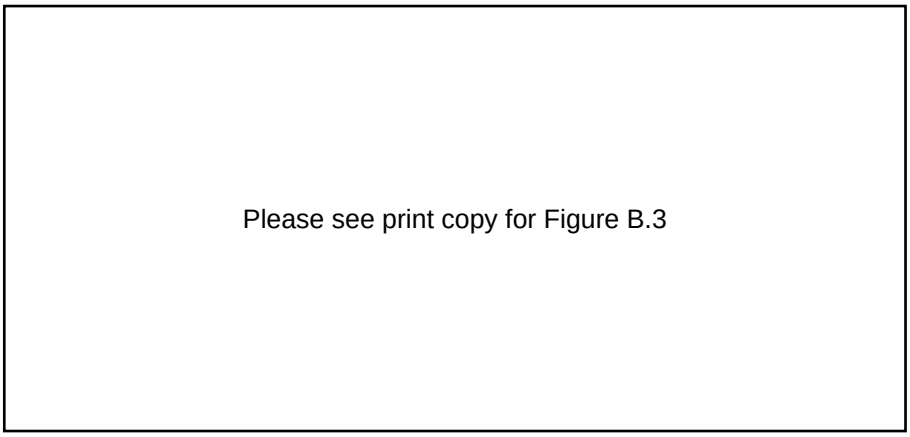

Figure B.3 Total breakage according to Hardin (1985)

REFERENCES

Fukumoto, T., (1992). "Particle Breakage Characteristics of Granular Soils." *Soils and Foundations*, 32(1), pp. 26-40.

Hardin, B.O., (1985). "Crushing of Soil Particles." *Journal of Geotechnical Engineering,* 111 (10), pp. 1177-1192.

Lade, P.V., Yamamuro, J.A., and Bopp, P.A., (1996). "Significance of Particle Crushing in Granular Materials." *Journal of Geotechnical Engineering,* 122 (4), pp. 309-316.

Lee, K.L. and Farhoomand, I., (1967). "Compressibility and Crushing of Granular Soil in Anisotropic Triaxial Compression." *Canadian Geotechnical Journal*, 4 (1), pp. 68-86.

Marsal, R.J., (1973). "Mechanical Properties of Rockfill." *Embankment Dam*

Engineering, Wiley, New York, pp. 109-200.

McDowell, G.R. and Bolton, M.D., (1998). "On the Micromechanics of Crushable Aggregates." *Géotechnique,* 48 (5), pp. 667-679.

McDowell, G.R., Bolton, M.D., and Robertson, D., (1996). "The Fractal Crushing of Granular Materials." *Journal of the Mechanics and Physics of Solids,* 44 (12), pp. 2079-2102.

Miura, N. and O′Hara, S., (1979). "Particle-Crushing of a Decomposed Granite Soil Under Shear Stresses." *Soils and Foundations,* 19 (3), pp. 1-14.

APPENDIX C

PROPERTIES AND CHARACTERISTICS OF THE DYNAMIC ACTUATOR

To meet the specific requirements for dynamic train loading simulation of the railway substructure, a new dynamic actuator, complete with a load cell transducer, two servo valves, an electronic control system, and an integrated data acquisition system (including a data taker and a computer set) were installed as part of the large-scale cylindrical triaxial apparatus at the University of Wollongong. This apparatus was subsequently used to test the response of ballast to high-speed (high frequency) cyclic loading. The dynamic actuator is capable of deviatoric stresses up to 2.1 MPa at a maximum loading frequency of 60 Hz, and thus covers the full range of train speeds and loads expected in-situ.

The basic design specifications for the testing rig are shown in Table C.1 (C. McLellan and Associates, 2002). Motion related characteristics of each test, for example the required loading amplitude and frequency, are entered into the computer program GOUI (Graphical Operator User Interface) as illustrated in Figure C.1. Table C.2 provides descriptions of the fields listed in Figure C.1.

The upper right hand corner of Figure C.1 illustrates typical real-time 'bursts' of load (yellow curve) and position (white curve) data. This data is recorded at a sampling frequency of about 590 Hz (1000 data points in 1.7 seconds) and is consequently used to calculate specimen resilient modulus. The data is saved as an Excel file and later filtered using the Matlab signal processing command '*fir1*' (see Appendix D).

Table C.1 Basic Design Characteristics of the Dynamic Actuator

Hydraulic Power Pack	- Existing 200 Bar/ up to 140 L/min fixed supply pressure
Servo Actuator	- 200 Bar maximum safe working pressure - Design force range to 150 kN - 4″ Bore × 200 mm stroke - Custom designed to suit the application with low friction seals, and built in hydraulic services in the blind end cap
Operating Modes	- Ramped position control (velocity control), with minimum set speed 0.01667 mm/sec, maximum set speed 100 mm/sec - Force override when in position control - Static force control (totally independent of position), with position override if cylinder moves past predetermined position - Dynamic force control, where applied force varies sinusoidally between 2 set levels at a set frequency – control is independent of position, however a position override will occur if the cylinder moves past a predetermined position
Feedback Devices	- 50 000 lb Load cell at 4 mV/V signal sensitivity, amplified to provide 1 – 10 VDC over 0 – 200 kN range - 0 – 200 mm magnetostrictive position transducer, providing 1 – 10 V output signal
Servo Valves	- 2 off 60 L/min rated, very high response type, mechanical feedback

Table C.2 Description of the fields shown in Figure C.1

Function	**Description**
Position SP (mm)	An adjustment to determine where the user wants the actuator positioned
Cylinder Pos FB (mm)	Actual position of the actuator
Cylinder Speed SP (mm/sec)	An adjustment to determine the cylinder speed during position control only
Load Cell FB (kN)	Actual sensed force at the load cell
Lowest Force SP (kN)	An adjustment to enter the minimum required cyclic force
PP Force Range SP (kN)	An adjustment to enter the range of required cyclic force
Min Peak Force FB (kN)	Actual minimum force being detected
Max Peak Force FB (kN)	Actual maximum force being detected
Sine Wave Frequency (Hz)	Desired loading frequency (sinusoidal wave shape)
# of Wave Cycles	Number of loading cycles completed

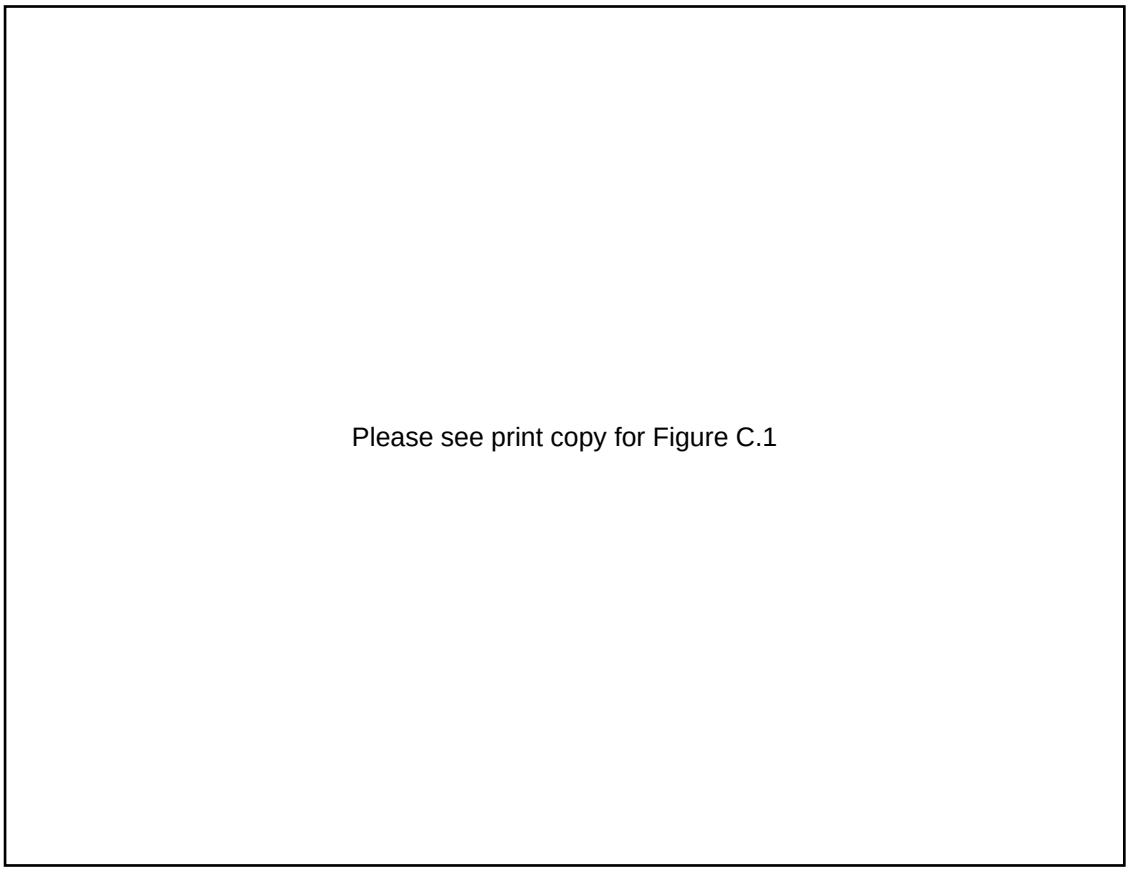

Figure C.1 GOUI screen used to control the movement of the dynamic actuator

REFERENCES

C. McLellan and Associates Pty Ltd, (2002). "Railway Ballast High Frequency Test Rig - Operation and Reference Manual."

APPENDIX D

METHOD OF NOISE REMOVAL FOR THE CALCULATION OF RESILIENT MODULUS

D.1 Introduction

The resilient modulus M_R (Equation 3.5, Chapter 3) governs the elastic behaviour of geomaterials such as ballast after a large number of loading cycles. A reliable assessment of M_R can be achieved when a significantly large number of deviator stress and recoverable strain readings are taken over a relatively short number of loading cycles. GOUI (see Appendix C) is capable of high-speed sampling and has thus been employed for M_R determination.

To calculate M_R for railway ballast 'bursts' of load and position data were recorded at various intervals during each triaxial test (e.g. Figure C.1, Appendix C). Whilst the burst data for load emerged as near perfect sinusoidal waveforms, it was found that the position data fluctuated significantly because of electrical interference that was later determined to be background or white noise. This Appendix outlines the method used to eliminate this noise and the procedure employed to calculate M_R.

D.2 Data Collection and Typical Raw Burst Data

During all the triaxial tests, specimens were subjected to one-way compression loading in which the samples were never unloaded (i.e. the deviatoric load was alternated between two compressive non-zero stress states). There are typically two methods used

to record small strain data, a) LVDT's (or similar devices) attached to the specimen itself (internal measurement), or b) LVDT's (or similar devices) attached to the triaxial shaft (external measurement). The current triaxial arrangement does not allow internal measurement. However, due to the considerable permanent displacements that result from large deviatoric stresses and inaccuracies associated with LVDT's at small strains, the most reliable way to record the required data was via the relative position of the actuator during the loading process. The actuator contains an internal position transducer and always contacts the specimen, therefore the actuator position directly corresponds to the degree of sample deformation as explained in Section 3.6.1 (Chapter 3). The same philosophy is warranted for resilient behaviour.

Even without cyclic loading (i.e. the actuator is fully retracted or in touch with the specimen but stationary) as much as 0.6 mm of actuator movement is often observed as illustrated in Figure D.1. A frequency analysis of this movement (discrete Fourier transform, DFT) is shown in Figure D.2. As the full spectrum of frequencies contributes to the signal in Figure D.1 (from 0 to 300 Hz), the unwanted actuator movement is most likely the result of electrical interference caused by background or white noise.

Figures D.3 and D.4 show typical data 'bursts' for load (deviator stress) and position (resilient strain), respectively, during cyclic loading. GOUI operates under load control, hence the near perfect sinusoidal curve in Figure D.3. The position curve (Figure D.4) represents the deformation response of the specimen to the applied loads, and although a sinusoidal shape is still evident, the data in this form may not give a realistic indication of peak-to-peak resilient strain. Figure D.5 shows the DFT of the data in Figure D.4. The objective of this Appendix is to illustrate the procedure used to remove the data in Figure D.1 from the data in Figure D.4.

Prior to implementing the chosen procedure, simple techniques were undertaken in an attempt to reduce the degree of background noise. This included trying to limit the number of electrical appliances operating in the vicinity of the triaxial cell and electrical insulation of the wires supplying the return signal. When neither of these preventative measures was successful, signal processing was investigated.

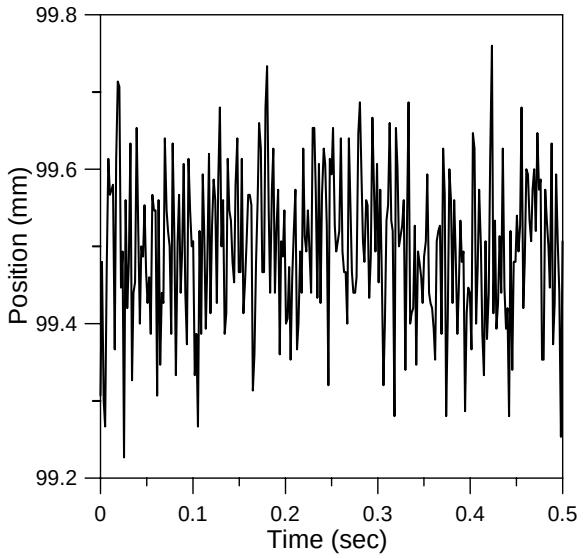

Figure D.1 Typical measured background noise when the actuator is fully retracted or in touch with the specimen but stationary

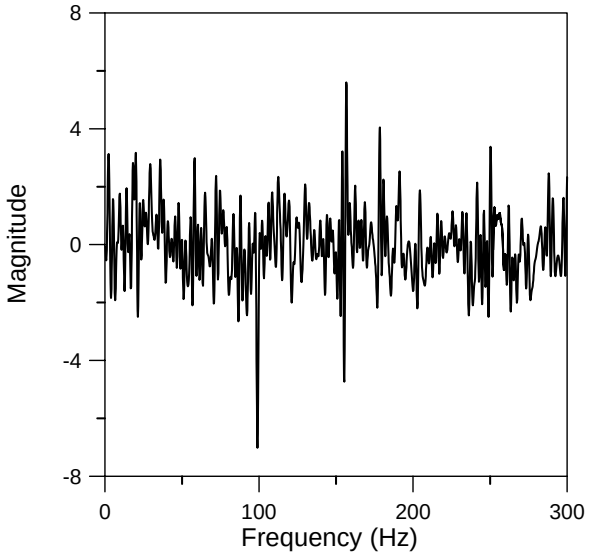

Figure D.2 Discrete Fourier transform of the background noise from Figure D.1, displaying no obvious source of interference

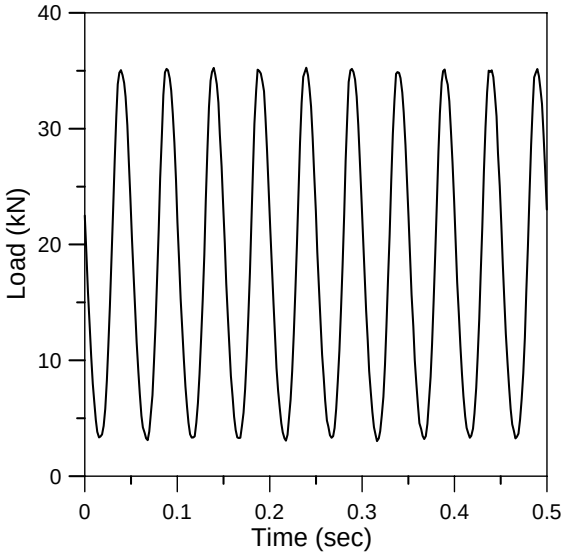

Figure D.3 Typical burst data for deviatoric load

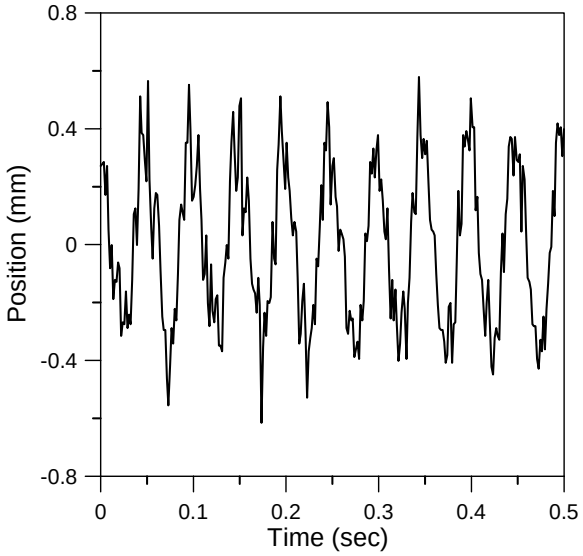

Figure D.4 Typical burst data for position

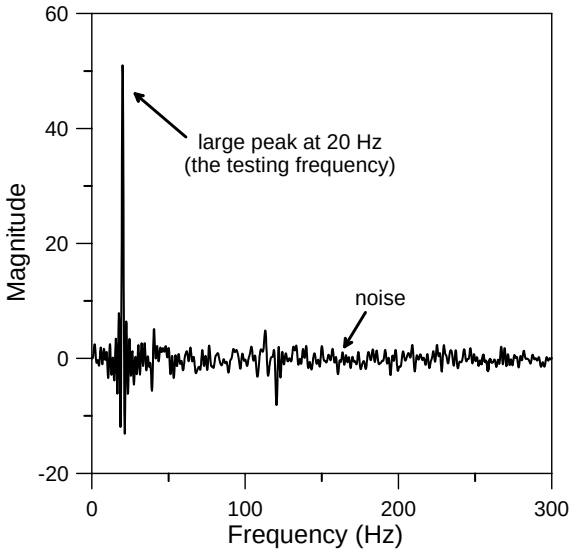

Figure D.5 Discrete Fourier transform of the position data from Figure D.4. A large peak is recorded at the testing frequency of 20 Hz, and background noise is evident at all frequencies

D.3 Filtering using *fir1* in Matlab

fir1 is a finite impulse response filter in Matlab that designs filters in lowpass, highpass, bandpass, and bandstop configurations. Input parameters include time, the data to be filtered (in this case position data), sampling frequency, and frequency cutoffs. The data in Figures D.3 and D.4 was recorded at a loading frequency of 20 Hz, so it was necessary to allow a 'band' of data near 20 Hz to 'pass' through the filter. Data measured at all other frequencies is consequently removed by the filter. The frequency cutoffs in this thesis were chosen as 19 and 21 Hz for all tests conducted at 20 Hz.

D.4 Output ('Filtered') Data

The data from Figure D.4 is filtered and plotted as a function of time in Figure D.6. Clearly the removal of data not directly related to the cyclic loading frequency results in a relatively 'noiseless' sinusoidal curve. Figure D.7 combines the filtered and unfiltered (raw) data for comparison. It is observed that the range of peak and trough values is greatly reduced in the filtered data compared to the raw data, which results in a significantly increased resilient modulus.

D.5 Resilient Modulus Calculation

The specimen behaviour in Figure D.6 is essentially elastic as there is no apparent downward movement in the peaks or troughs with time. The resilient strain is therefore the amplitude of the position curve (in this case approximately 0.7 mm) divided by the initial height of the specimen before loading (resilient strain = 0.7/600 = 0.00117). The

deviator stress can be calculated from Figure D.3 knowing the cross sectional area of the specimen. Finally, the resilient modulus is the deviator stress divided by the recoverable strain.

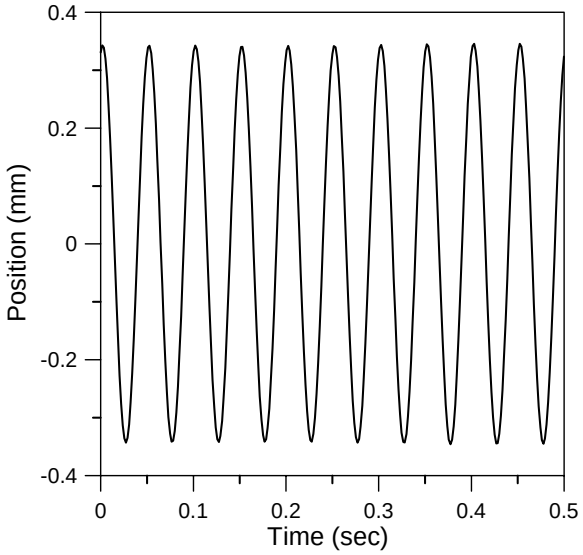

Figure D.6 Filtered position data (originally Figure D.4). All data recorded at frequencies outside of the 19 - 21 Hz band has been excluded

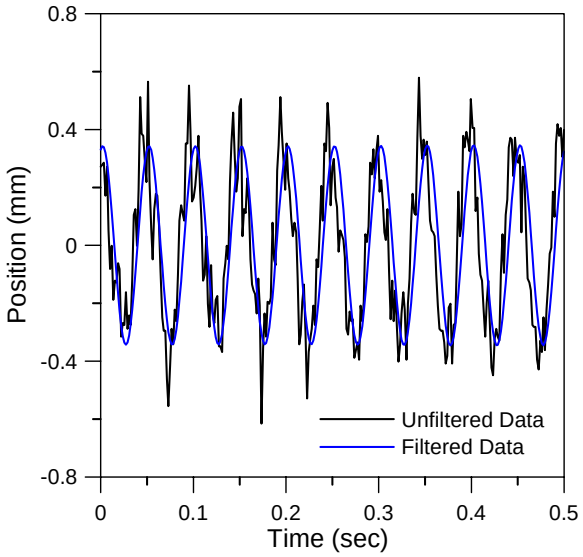

Figure D.7 Effect of filtering on position (resilient strain) data

D.6 Example

The unfiltered and filtered resilient strain and resilient modulus data for the test conducted at $\sigma_3' = 120$ kPa and $q_{max,cyc} = 500$ kPa is shown in Figures D.8 and D.9, respectively. Note that the unfiltered curve in Figure D.8 utilises the absolute minimum and maximum values of position in the calculation of resilient strain (see Figure D.4), hence resulting in the highest possible values of resilient strain (and lowest possible resilient modulus). Also note that the average values of all the recorded peaks and troughs during the 1.7 second interval were used to calculate the resilient strain and resilient modulus magnitudes during each particular burst.

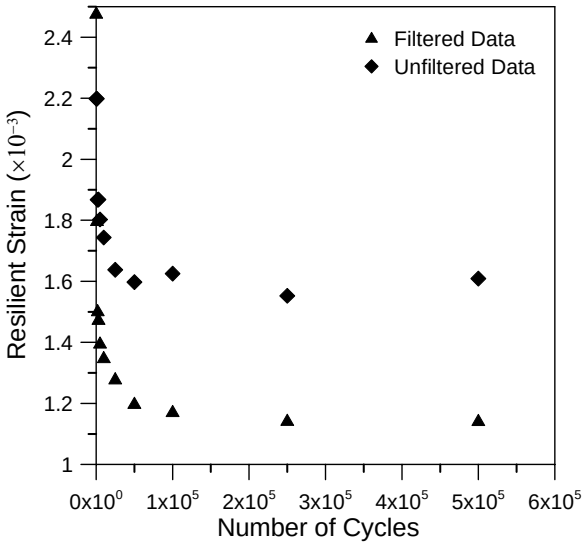

Figure D.8 Effect of filtering on resilient (recoverable) strain for the $\sigma_3' = 120$ kPa and $q_{max,cyc} = 500$ kPa specimen

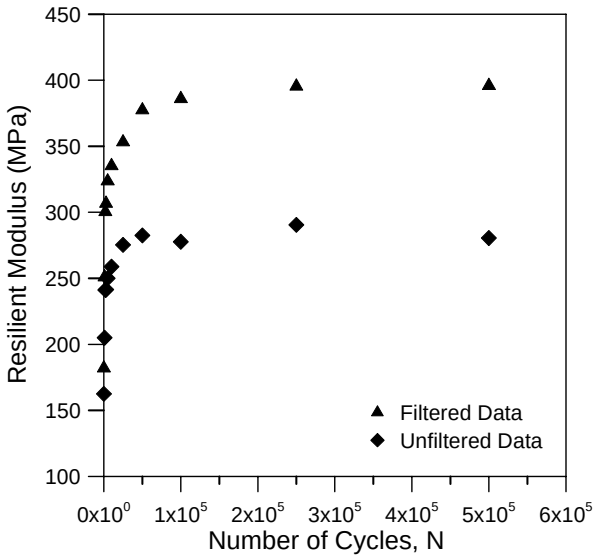

Figure D.9 Effect of filtering on resilient modulus for the σ_3' = 120 kPa and $q_{max,cyc}$ = 500 kPa specimen

APPENDIX E

CURVE FITTING PROCEDURE TO FIND THE RELATIONSHIP BETWEEN RESILIENT MODULUS AND VOLUMETRIC STRAIN

John (1998) detailed a simplified curve fitting technique using the Solver add-in within Microsoft Excel that can be utilised to find a suitable model to relate various experimental parameters. The procedure was used to link the resilient modulus M_R to the volumetric strain ε_v for specimens with constant confining pressure σ_3' and deviator stress magnitude $q_{max,cyc}$. This Appendix outlines the method as summarised by John (1998) and provides a sample calculation for a typical ballast specimen.

The Solver curve fitting procedure outlined by John (1998) is summarised below:

1) Choose an appropriate model/s relating x and y parameters

2) Enter the known x and y values into a spreadsheet

3) Calculate the assumed model based on the known x values (this will give the assumed model y values)

4) Calculate the squared error between the known y values and the assumed model y values

5) Sum the squared errors

6) Using Solver set the squared errors cell to Min

7) Enter the cells to be changed in order to minimise the squared errors cell, and include any constraints

8) Select the Solve button. The curve of best fit based on the chosen model that results in minimal error from the original y data will be calculated.

An example of this procedure for a typical ballast specimen is provided in Table E.1. When the measured and predicted values of M_R from Table E.1 are plotted (Figure E.1), a reasonable degree of correlation is obtained ($R^2 > 0.98$), thus highlighting the suitability of the assumed model and the curve fitting procedure.

Table E.1 Example of the curve fitting procedure outlined in John (1998) for a typical ballast specimen using Equation 4.10

Please see print copy for Table E.1

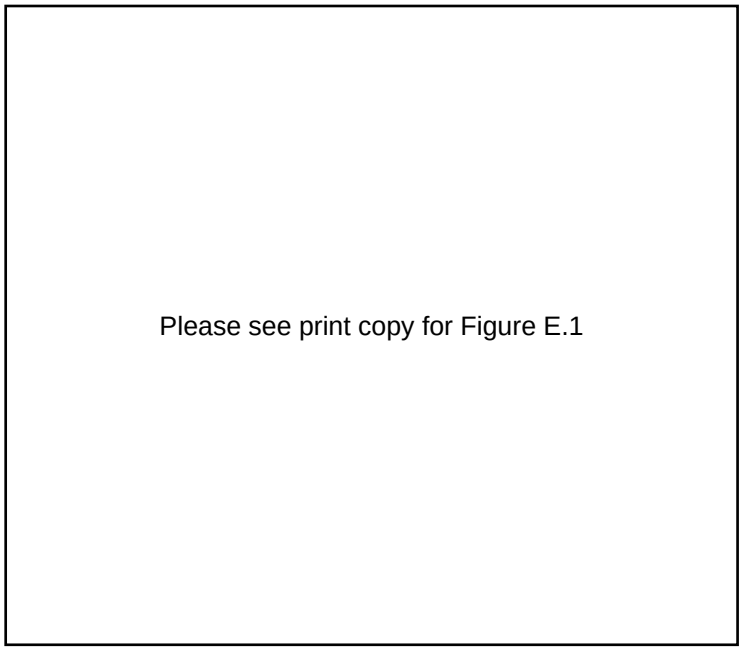

Figure E.1 Comparison of the measured and predicted values of resilient modulus M_R based on Equation 4.10 and the curve fitting technique of John (1998)

REFERENCES

John, E.G., (1998). "Simplified Curve Fitting using Spreadsheet Add-Ins." *International Journal of Engineering,* 14(5), pp. 375-380.